



University of  
**Salford**  
MANCHESTER

**Numerical Investigation into the Effects of Cavities on  
Stability of Slopes and Seepage through Earth Dams under  
Rapid Drawdown Condition**

**Hawraa Hasan Mousa Alateya**

School of Science, Engineering & Environment, University of  
Salford, Salford, United Kingdom

A thesis Submitted in Partial Fulfilment of the Requirements of the  
Degree of Doctor of Philosophy in Civil Engineering

January 2020

# CONTENTS

<b>CONTENTS .....</b>	<b>II</b>
<b>LIST OF TABLES .....</b>	<b>VII</b>
<b>LIST OF FIGURES .....</b>	<b>X</b>
<b>ACKNOWLEDGEMENT.....</b>	<b>XVIII</b>
<b>PUBLICATIONS .....</b>	<b>XIX</b>
<b>NOTATIONS .....</b>	<b>XX</b>
<b>ABBREVIATIONS .....</b>	<b>XXII</b>
<b>ABSTRACT.....</b>	<b>XXIII</b>
<b>CHAPTER ONE: INTRODUCTION .....</b>	<b>1</b>
1.1 Dams .....	1
1.2 Failure mechanisms of earth dams.....	2
1.2.1 Structural Failure .....	3
1.2.2 Seepage Failure.....	4
1.2.3 Hydraulic Failure .....	5
1.3 Seepage through earth dams .....	5
1.4 Statement of cavity problem.....	6
1.5 Slope stability analysis using (PLAXIS 2D) software.....	7
1.6 Significance of the study.....	7
1.7 Study aims and objectives.....	8
1.8 Layout of thesis.....	9
<b>CHAPTER TWO: LITERATURE REVIEW.....</b>	<b>12</b>
2.1 Literature review of seepage analysis .....	12
2.1.1 Equations of flow through porous medium .....	12
2.1.1.1 Darcy’s law .....	13

2.1.1.2 Laplace's equation .....	13
2.1.2 Methods of Seepage Analysis .....	15
2.1.2.1 Numerical methods .....	15
2.1.2.2 Analytical Method .....	18
2.2 Literature review of stability analysis.....	22
2.2.1 Classical stability-analysis methods .....	22
2.2.2 Method of slices .....	23
2.2.2.1 Ordinary method of slices.....	24
2.2.2.2 Bishop's simplified method .....	25
2.2.3 Strength reduction method (SRM).....	27
2.2.4 Numerical studies.....	29
2.2.5 Safety standards .....	36
2.3 Literature review of cavities in soil .....	38
2.4 Conclusion .....	43
<b>CHAPTER THREE: METHODOLOGY .....</b>	<b>44</b>
3.1 Introduction.....	44
3.2 PLAXIS 2D software.....	44
3.3 General properties of the PLAXIS 2D model.....	45
3.2.1 Plane strain.....	45
3.2.3 Elements.....	46
3.2.3.1 15-node triangle .....	46
3.2.3.2 6-node triangle .....	46
3.4 PLAXIS 2D modelling .....	47
3.4.1 Geometry modelling .....	47
3.4.2 Calculations.....	48
3.4.2.1 Mesh creation.....	48
3.4.2.2 Calculations phases.....	49
3.4.2.2.1 Gravity loading .....	49
3.4.2.2.2 Fully-coupled flow-deformation.....	50
3.4.2.2.3 Plastic calculation .....	50
3.4.2.2.4 Safety calculation.....	50
3.5 Seepage theory .....	51

3.5.1 Flow condition .....	53
3.5.2 Boundary condition.....	54
3.6 Staged construction.....	54
3.7 Soil modelling.....	55
3.7.1 MC model .....	55
3.7.1.1 Formulation of the MC model .....	56
3.7.2 HS model .....	57
3.8 2D slope stability analyses.....	59
3.9 Model setup with PLAXIS 2D.....	60
3.10 Study models.....	60
3.10.1 Earth dam model .....	60
3.10.2 Cavity modelling.....	61
<b>CHAPTER FOUR: STABILITY ANALYSIS .....</b>	<b>64</b>
4.1 Introduction.....	64
4.2 Study models.....	65
4.3 Parameters involved in the constitutive modelling.....	65
4.4. Impact of the cavity location.....	66
4.4.1 Impact of the cavity location modelled using the MC model.....	67
4.4.2 Impact of the cavity location modelled using the HS and MC models .....	78
4.5 Impact of cavity shape .....	88
4.5.1 Modelling the earth dam using the MC model .....	88
4.5.2 Modelling the earth dam using the HS and MC models.....	94
4.6 Impact of the cavity diameter .....	99
4.6.1 Modelling the earth dam using the MC model .....	99
4.6.2 Modelling the earth dam using the HS and MC models.....	104
4.7 Impact of the number of cavities .....	108
4.7.1 Impact of the existence of dual cavities modelled using the MC model .....	109
4.7.2 Impact of dual cavities modelled using the HS and MC models.....	115
4.7.3 Impact of three cavities modelled using the MC model .....	120
4.7.4 Impact of three cavities modelled using the HS and MC models.....	126

4.8 Joint impact of the existence of cavities and shear-strength parameters .....	131
4.8.1 Joint impact of the existence of a cavity and the soil's apparent cohesion.....	132
4.8.1.1 Joint impact of the soil's apparent cohesion and cavities modelled using the MC model .....	132
4.8.1.2 Joint impact of the soil's apparent cohesion and cavities modelled using the HS and MC models.....	138
4.8.2 Joint impact of the existence of a cavity and the angle of internal friction ( $\phi$ ) ....	143
4.8.2.1 Joint impact of the angle of internal friction ( $\phi$ ) modelled using the MC model .....	143
4.8.2.1 Joint impact of the angle of internal friction ( $\phi$ ) modelled using the HS and MC models.....	148
4.9 Comparative study .....	153
4.9.1 Joint impact of a cavity's horizontal position and the type of model.....	153
4.9.2 Joint impact of cavity depth and the modelling material.....	158
4.10 Conclusions.....	161
<b>CHAPTER FIVE: SEEPAGE ANALYSIS .....</b>	<b>162</b>
5.1 Introduction.....	162
5.2 Impact of a varying cavity position in the horizontal direction (X) .....	162
5.2.1 Modelling of an earth dam using the MC model .....	163
5.2.2 Modelling of an earth dam using the HS and MC models.....	165
5.3 Impact of cavity depth .....	166
5.3.1 Modelling of an earth dam using the MC model .....	166
5.3.2 Modelling of an earth dam using the HS and MC models.....	168
5.4 Impact of cavity shape .....	171
5.4.1 Modelling of an earth dam using the MC model .....	171
5.4.2 Modelling of an earth dam using the HS and MC models.....	176
5.5 Impact of the number of cavities .....	181
5.5.1 Impact of the existence of dual cavities.....	181
5.5.1.1 Modelling of an earth dam using the MC model.....	181
5.5.1.2 Modelling of an earth dam using the HS and MC models.....	184
5.5.2 Impact of the existence of three cavities.....	186
5.5.2.1 Modelling of an earth dam using the MC model.....	186

5.5.2.2 Modelling of an earth dam using the HS and MC models.....	189
5.6 Comparative study .....	192
5.6.1 Impact of cavities that are situated at the same depth level.....	192
5.6.1.1 Modelling of an earth dam using the MC model.....	192
5.6.1.2 Modelling of an earth dam using the HS and MC models.....	195
5.6.2 Impact of cavities that are situated at different depths .....	199
5.6.2.1 Modelling of an earth dam using the MC model.....	199
5.6.2.2 Modelling of an earth dam using the HS and MC models.....	201
5.6.3 Impact of the type of model using for modelling .....	203
5.7 Conclusions.....	207
<b>CHAPTER SIX: CONCLUSIONS AND RECOMMENDATIONS.....</b>	<b>208</b>
6.1 General overview.....	208
6.2 Impact of a cavity on slope stability of earth dam.....	208
6.2.1 Impact of the horizontal position of the cavity .....	208
6.2.2 Impact of the cavity depth.....	209
6.2.3 Impact of the cavity shape .....	209
6.2.4 Impact of the cavity diameter .....	209
6.2.5 Impact of the number of cavities .....	210
6.2.6 Combined effect of the existence of cavities and shear-strength parameters .....	210
6.2.7 Impact of the type of model.....	211
6.3 Impact of the existence of a cavity on flow rate through earth dam.....	211
6.3.1 Impact of the cavity location (horizontal position and depth) .....	211
6.3.2 Impact of the cavity shape .....	212
6.3.3 Impact of the number of cavities .....	212
6.3.4 Impact of the type of model.....	213
6.4 Recommendations for future work .....	213
<b>REFERENCES.....</b>	<b>214</b>
<b>Appendix A: Model Setup with PLAXIS 2D.....</b>	<b>232</b>
<b>Appendix B: Training Courses.....</b>	<b>244</b>

## LIST OF TABLES

Table 2.1: Safety factor values according to Berisavljević et al., (2015) .....	34
Table 2.2: British Dam Society in 1994 standard .....	36
Table 2.3: Safety standard for earth dam .....	37
Table 2.4: Safety factor according to the (US, 2003) .....	37
Table 2.5: Analytical formulas of seepage flow into circular tunnels .....	40
Table. 3.1: Comparison between the parameters of numerical model and BDS safety standards (1994).....	63
Table 4.1: Input parameters of the MC used in the first series .....	65
Table 4.2: Input parameters of the models used in the second series .....	66
Table 4.3: Coordinates of the locations of cavities in X and Y directions .....	67
Table 4.4: Locations of the cavity under upstream and the corresponding S.F values.....	75
Table 4.5: Locations of the cavity under downstream and the corresponding SF values.....	77
Table 4.6: Locations of the cavity under upstream and the corresponding SF values.....	85
Table 4.7: Locations of the cavity under downstream and the corresponding SF values.....	87
Table 4.8: Locations of the circular cavity and irregular cavity sited under upstream and downstream and the corresponding SF values for the MC model .....	90
Table 4.9: Locations of the circular cavity and irregular cavity sited under upstream and downstream and the corresponding SF values for the MC and HS models.....	96
Table 4.10: The locations and diameters of the cavity and the corresponding SF values for the upstream side .....	101
Table 4.11: The locations and diameters of the cavity and the corresponding SF values for the downstream side.....	102
Table 4.12: The locations and diameters of the cavity and the corresponding SF values for the upstream side .....	106
Table 4.13: The locations and diameters of the cavity and the corresponding SF values for the downstream side.....	108
Table 4.14: Coordinates of cavities' locations for dual-cavity models at the same depth.....	109
Table 4.15: Coordinates of cavities' locations and the corresponding SF values for the dual-cavity models for different depths .....	111

Table 4.16: Coordinates of cavities' locations for dual-cavity models sited under upstream and downstream at the same depth .....	112
Table 4.17: Coordinates of cavities' locations for dual-cavity models sited under upstream and downstream at the different depths .....	114
Table 4.18: Coordinates of cavities locations in X and Y directions for the dual-cavity models sited under upstream .....	115
Table 4.19: Coordinates of cavities' locations and the corresponding SF values for the dual-cavity models sited for different depths.....	117
Table 4.20: Coordinates of cavities' locations for triple-cavity models at the same depth...	121
Table 4.21: Coordinates of cavities' locations and the corresponding SF values for the triple-cavity models for different depths .....	122
Table 4.22: Coordinates of cavities' locations for triple-cavity models sited under upstream and downstream at the same depth .....	123
Table 4.23: Coordinates of cavities' locations for triple-cavity models sited under upstream and downstream at the different depths .....	124
Table 4.24: Coordinates of cavities locations in X and Y directions for the triple-cavity models sited under upstream.....	126
Table 4.25: Coordinates of cavities' locations and the corresponding SF values for the triple-cavity models sited for different depths using the HS and MC models.....	128
Table 4.26: Input and output data showing the impact of soil cohesion and location of cavity on SF values.....	134
Table 4.27: Input and output data showing the impact of soil cohesion and cavity diameter on SF values.....	136
Table 4.28: Input and output data showing the impact of soil cohesion and location of cavity on SF values.....	139
Table 4.29: Input and output data showing the impact of cohesion and cavity diameter on SF values .....	141
Table 4.30: Input and output data showing the impact of the ( $\phi$ ) and location of cavity on SF values .....	144
Table 4.31: Input and output data showing the impact of the ( $\phi$ ) and cavity diameter on SF values .....	146
Table 4.32: Input and output data showing the impact of the ( $\phi$ ) and location of cavity on SF values .....	149
Table 4.33: Input and output data showing the impact of the ( $\phi$ ) and cavity diameter on SF values .....	151



Table 5.1: Coordinates of the locations of cavities in X and Y directions .....	163
Table 5.2: Impact of the depth of a circular cavity beneath the upstream and downstream slopes on the flow rate .....	167
Table 5.3: Impact of the depth of a circular cavity beneath the upstream and downstream slopes on the flow rate .....	170
Table 5.4: Comparison between the impact of the presence of a circular cavity and an irregular cavity on flow rate.....	172
Table 5.5: Comparison between the impact of the presence of a circular cavity and an irregular cavity on flow rate.....	178
Table 5.6: The coordinates of cavities' locations in X and Y directions for dual-cavity models .....	182
Table 5.7: The input and output data showing the effect of presence of two cavities on flow rate .....	183
Table 5.8: The input and output data showing the effect of presence of two cavities on flow rate .....	185
Table 5.9: The coordinates of cavities locations in X and Y directions for triple-cavity model .....	187
Table 5.10: The input and output data showing the effect of presence of three cavities on flow rate .....	188
Table 5.11: The input and output data showing the effect of presence of three cavities on flow rate .....	191

## LIST OF FIGURES

Figure 1.1: Failure mechanisms for earth dams (USBR, 2001).....	10
Figure 1.2: Images of cavities with various sizes and location in soil of AL-Najaf city/ Iraq (Aziz, 2008) .....	10
Figure 1.3: Possible cavities underneath Mosul Dam, mostly close to the reservoir side (from SIGIR, 2007 report) .....	11
Figure 2.1: Description diagram for Schaffernak solution .....	19
Figure 2.2: Description diagram for Casagrande solutions (1937).....	20
Figure 2.3: Description diagram for Dupuit's solution.....	20
Figure 2.4: The slip surface and forces acting on slice (Fredlund and Krahn, 1977).....	25
Figure 2.5: Values of $M_i(\theta)$ (after Janbu, 1973).....	26
Figure 2.6: The slip surface and forces acting on a typical slice (Lambe and Whitman, 1969) .....	27
Figure 2.7: Section A, a geometrical model of the dam body. The zones are: (1) core, (2) fine filter, (3) coarse filter, (4) rockfill, (5) foundation consisting of till.....	35
Figure 2.8: SF values for section A according to Toromanovic et al., (2016).....	35
Figure 3.1: The coordinate system (PLAXIS, 2018).....	45
Figure 3.2: Position of nodes and stress points in triangular soil elements (PLAXIS, 2018) .	47
Figure 3.3: The finite element mesh in PLAXIS 2D for study model.....	62
Figure 3.4: Geometry of the considered earth dam model.....	62
Figure 3.5: The geometry of the cavity.....	63
Figure 3.6: A scheme of the shapes of the cavities.....	63
Figure 4.1: SF vs location of a cavity under upstream using the MC model.....	68
Figure 4.2: Maximum values of total displacement vs location of a cavity under upstream using the MC model.....	68
Figure 4.3: Contour of total displacement for the impact of a cavity's position under upstream using the MC model.....	69
Figure 4.4: SF vs location of a cavity under downstream at a depth of 1m using the MC model.....	71

Figure 4.5: Maximum values of total displacement vs location of a cavity under downstream at a depth of 1m using the MC model.....	71
Figure 4.6: Contour of total displacement for the impact of a cavity's position under downstream using the MC model .....	72
Figure 4.7: Comparison between the impact on the SF of a cavity existing under the upstream and downstream slopes using the MC model .....	73
Figure 4.8: Comparison between the impact on the maximum values of the total displacement of a cavity existing under the upstream and downstream using the MC model .....	74
Figure 4.9: SF vs location of a cavity situated under upstream using the MC model for depths Y= 1m, 2m, 3m, 4m.....	75
Figure 4.10: Impact of cavity depth on the maximum of total displacement for a cavity situated under upstream at positions X2 using the MC model .....	76
Figure 4.11: SF vs location of a cavity for depths (Y=1m to Y=4m) under downstream using the MC model .....	77
Figure 4.12: Impact of cavity depth on the maximum of total displacement for a cavity situated under downstream at positions X2 using the MC model .....	78
Figure 4.13: SF vs location of a cavity under upstream using the HS and MC models .....	79
Figure 4.14: Maximum values of total displacement vs location of a cavity under upstream using the HS and MC models .....	79
Figure 4.15: Contour of total displacement for the impact of a cavity's position under upstream using the HS and MC models.....	80
Figure 4.16: SF vs location of a cavity under downstream using the HS and MC models .....	81
Figure 4.17: Maximum values of total displacement vs location of a cavity under downstream using the HS and MC models .....	82
Figure 4.18: Contour of total displacement for the impact of a cavity's position under downstream using the HS and MC models.....	83
Figure 4.19: Comparison between the impact on the SF of a cavity being present under upstream and downstream using the HS and MC models .....	84
Figure 4.20: Comparison between the impact on the maximum values of the displacement of a cavity's presence under upstream and downstream using the HS and MC models.....	84
Figure 4.21: SF vs location of a cavity for depths (Y=1m to Y=4m) situated under upstream using the HS and MC models .....	86
Figure 4.22: Contour of total displacement for the effect of cavity depth under upstream using the HS and MC models .....	86
Figure 4.23: SF vs location of a cavity for depths (Y=1m to Y=4m) situated under downstream using the HS and MC models.....	87

Figure 4.24: Impact of cavity depth on the maximum of total displacement for a cavity situated under downstream at positions X2 using the HS and MC models .....	88
Figure 4.25: Comparison between the impact of the presence of a circular cavity and an irregular cavity sited under upstream on the displacement values using the MC model.....	89
Figure 4.26: The impact of the presence of a circular and an irregular cavity under upstream on the SF using the MC model for depths (Y=1m to Y=4m) .....	91
Figure 4.27: Comparison between the impact of the presence of a circular cavity and an irregular cavity sited under downstream on the displacement values using the MC model....	92
Figure 4.28: The impact of the presence of a circular and an irregular cavity under downstream on the SF using the MC model for depths (Y=1m to Y=4m) .....	93
Figure 4.29: Comparison between the impact of the presence of a circular cavity and an irregular cavity under upstream on the displacement values using the HS and MC models...	94
Figure 4.30: The impact of the presence of a circular and an irregular cavity under upstream on the SF using the HS and MC models for depths (Y=1m to Y=4m).....	95
Figure 4.31: Comparison between the impact of the presence of a circular cavity and an irregular cavity under downstream on the displacement values using the HS and MC models .....	97
Figure 4.32: The impact of the presence of a circular and an irregular cavity under downstream on the SF using the HS and MC models for depths (Y=1m to Y=4m).....	98
Figure 4.33: Impact of cavity's diameter on the FS of upstream using MC model for different positions and depths: (a) Y= 1m, (b) Y= 2m, (c) Y= 3m .....	100
Figure 4.34: Impact of cavity's diameter on the FS of downstream using MC model for different positions and depths: (a) Y= 1m, (b) Y= 2m, (c) Y= 3m.....	103
Figure 4.35: Impact of cavity's diameter on the FS of upstream using the HS and MC models for different positions and depths: (a) Y= 1m, (b) Y= 2m, (c) Y= 3m .....	105
Figure 4.36: Impact of cavity's diameter on the FS of downstream using the HS and MC models for different positions and depths: (a) Y= 1m, (b) Y= 2m, (c) Y= 3m .....	107
Figure 4.37: Example cavity arrangement for models with two cavities sited at the same depth (L3).....	110
Figure 4.38: Impact on the SF for models with two cavities sited at a depth of 1m using the MC model .....	110
Figure 4.39: Impact on the SF of the existence of two cavities at different positions and depths using the MC model .....	111
Figure 4.40: Comparison between the impact on the SF of two cavities situated under upstream and downstream using the MC model.....	113
Figure 4.41: Comparison between the impact on the SF of two cavities sited under upstream and downstream at various depths using the MC model .....	113

Figure 4.42: Typical cavity arrangement for models with two cavities sited at the different depths (L2).....	114
Figure 4.43: Comparison between the impact on the SF of the depth of two cavities within the same model using the MC model.....	115
Figure 4.44: Impact on the SF of the existence of two cavities for models with cavities sited at a depth of 1m using the HS and MC models .....	116
Figure 4.45: Impact on the SF of the existence of two cavities at different positions and depths using the HS and MC models.....	117
Figure 4.46: Comparison between the impact on the SF of two cavities situated at the same depth under upstream and downstream using the HS and MC models .....	118
Figure 4.47: Comparison between the impact on the SF of two cavities situated under upstream and downstream at various depths using the HS and MC models .....	119
Figure 4.48: Comparison between the impact on the SF of the depth of two cavities within the same model using the HS and MC models .....	120
Figure 4.49: Impact on SF of the presence of three cavities at different positions and depth Y= 1m using the MC model .....	121
Figure 4.50: Impact on the SF of the existence of three cavities at different positions and depths using the MC model .....	122
Figure 4.51: Comparison between the impact on the SF of three cavities at the same depth situated under upstream and downstream using the MC model .....	124
Figure 4.52: Comparison between the impact on the SF of three cavities at different depths situated under upstream and downstream using the MC model .....	125
Figure 4.53: Comparison between the effect on the SF of a change in depth for triple-cavity models using the MC model .....	126
Figure 4.54: Impact on SF of the presence of three cavities at different positions and depth Y= 1m using the HS and MC models .....	127
Figure 4.55: Impact on SF of the existence of three cavities at different positions and depths using the HS and MC models .....	128
Figure 4.56: Comparison between the impact on the SF of three cavities being situated under upstream and downstream using the HS and MC models .....	129
Figure 4.57: Comparison between the impact on the SF of three cavities at various depths being situated under upstream and downstream using the HS and MC models.....	130
Figure 4.58: Comparison between the effect on the SF of a change in depth for triple-cavity models using the HS and MC models.....	131
Figure 4.59: Joint impact on SF of the cavity position and soil cohesion using the MC model .....	133

Figure 4.60: Joint impact of the cavity depth and soil cohesion on the SF using the MC model for the positions of cavity: (a) X1, (b) X2, (c) X3 .....	135
Figure 4.61: Joint impact of cavity diameter and soil cohesion on the SF using the MC model for the positions of cavity: (a) X1, (b) X2, (c) X3 .....	137
Figure 4.62: Joint impact on SF of the cavity position and soil cohesion using the HS and MC models .....	138
Figure 4.63: Joint impact of the cavity depth and soil cohesion on the SF using the HS and MC models for the positions of cavity: (a) X1, (b) X2, (c) X3 .....	140
Figure 4.64: Joint impact of cavity diameter and soil cohesion on the SF using the HS and MC models for the positions of cavity: (a) X1, (b) X2, (c) X3 .....	142
Figure 4.65: Joint impact of the cavity position and the ( $\phi$ ) on SF using the MC model.....	143
Figure 4.66: Joint impact of the cavity depth and the ( $\phi$ ) on the SF using the MC model for the positions of cavity: (a) X1, (b) X2, (c) X3 .....	145
Figure 4.67: Joint impact of cavity diameter and the ( $\phi$ ) on the SF for the positions of cavity: (a) X1, (b) X2, (c) X3 .....	147
Figure 4.68: Joint impact of the cavity position and the ( $\phi$ ) on SF using the HS and MC models .....	148
Figure 4.69: Joint impact of the cavity depth and the ( $\phi$ ) on the SF using the HS and MC models for the positions of cavity: (a) X1, (b) X2, (c) X3.....	150
Figure 4.70: Joint impact of cavity diameter and the ( $\phi$ ) on the SF using the HS and MC models for the positions of cavity: (a) X1, (b) X2, (c) X3.....	152
Figure 4.71: Joint impact of the cavity position and the type of model on the SF of upstream for the presence of a cavity: (a) circular, (b) irregular .....	154
Figure 4.72: Impact of the cavity position and the type of model on the maximum of the total displacement of upstream for the cavity's presence: (a) a circular cavity, (b) an irregular cavity.....	155
Figure 4.73: Joint impact of the cavity position and the type of model on the SF of downstream for the presence of a cavity: (a) circular cavity, (b) irregular cavity.....	156
Figure 4.74: Impact of the cavity position and the type of model on the maximum of the total displacement of downstream for the cavity's presence: (a) a circular cavity, (b) an irregular cavity.....	157
Figure 4.75: Joint impact on stability of the type of model and the cavity's horizontal position under upstream: (a) Y= 1m, (b) Y= 2m, (c) Y= 3m, (d) Y= 4m .....	159
Figure 4.76: Joint impact on stability of the type of model and the cavity's horizontal position under downstream: (a) Y= 1m, (b) Y= 2m, (c) Y= 3m, (d) Y= 4m.....	160

Figure 5.1: Flow rate vs location of a circular cavity beneath upstream using the MC model .....	164
Figure 5.2: Flow rate vs location of a circular cavity beneath downstream using the MC model.....	164
Figure 5.3: Flow rate vs location of a circular cavity beneath upstream using the HS and MC models .....	165
Figure 5.4: Flow rate vs location of a circular cavity under downstream using the HS and MC models .....	166
Figure 5.5: Flow rate vs location of a circular cavity beneath the upstream at various depths using the MC model.....	167
Figure 5.6: Flow rate vs location of circular cavities beneath downstream at various depths using the MC model.....	168
Figure 5.7: Flow rate vs location of a circular cavity at various depths beneath upstream using the HS and MC models .....	169
Figure 5.8: Flow rate vs location of a circular cavity at various depths beneath downstream using the HS and MC models .....	171
Figure 5.9: Comparison between the impact of a circular cavity and an irregular cavity under upstream on the flow rate using the MC model for depths (Y=1m to Y=4m) .....	173
Figure 5.10: Comparison between the impact of a circular cavity and an irregular cavity under downstream on the flow rate using the MC model for depths (Y=1m to Y=4m) .....	175
Figure 5.11: Comparison between the impact of a circular cavity and an irregular cavity under upstream on the flow rate using the HS and MC models for depths (Y=1m to Y=4m) .....	177
Figure 5.12: Comparison between the impact of a circular cavity and an irregular cavity under downstream on the flow rate using the HS and MC models for depths (Y=1m to Y=4m).....	180
Figure 5.13: Flow rate vs location of cavities for models with dual cavities situated at a depth of 1m using the MC model .....	182
Figure 5.14: Flow rate vs location of cavities for models with dual cavities at various depths using the MC model.....	183
Figure 5.15: Flow rate vs location of cavities for models with dual cavities at a depth of 1m using the HS and MC models .....	184
Figure 5.16: Flow rate vs location of cavities for models with dual cavities at various depths using the HS and MC models .....	186
Figure 5.17: Flow rate vs location of cavities for models with three cavities at a depth of 1m using the MC model.....	187

Figure 5.18: Flow rate vs location of cavities for models with three cavities at various depths using the MC model.....	189
Figure 5.19: Flow rate vs location of cavities for models with three cavities at a depth of 1m using the HS and MC models .....	190
Figure 5.20: Flow rate vs location of cavities for models with three cavities at various depths using the HS and MC models .....	191
Figure 5.21: Comparison between the effect of the cavity's presence under upstream and downstream for depths (Y=1m to Y=4m) using the MC model.....	193
Figure 5.22: Comparison between the effect on flow rate of the presence of two cavities located under upstream and downstream, for different positions and at a depth of 1m using the MC model .....	194
Figure 5.23: Comparison between the effect on flow rate of the presence of three cavities located under upstream and downstream, for different positions and at a depth of 1m using the MC model .....	195
Figure 5.24: Comparison between the effect of the cavity's presence under upstream and downstream on flow rate for depths (Y=1m to Y=4m) using the HS and MC models .....	197
Figure 5.25: Comparison between the effect on flow rate of the presence of two cavities located under upstream and downstream for different positions and at a depth of 1m using the HS and MC models .....	198
Figure 5.26: Comparison between the effect on flow rate of the presence of three cavities located under upstream and downstream, for different positions and at a depth of 1m using the HS and MC models .....	199
Figure 5.27: Comparison between the effect on flow rate of the presence of two cavities located under upstream and downstream, for different positions and depths using the MC model.....	200
Figure 5.28: Comparison between the effect on flow rate of the presence of three cavities located under upstream and downstream, for different positions and depths using the MC model.....	201
Figure 5.29: Comparison between the effect on flow rate of the presence of two cavities located under upstream and downstream, for different positions and depths using the HS and MC models.....	202
Figure 5.30: Comparison between the effect on flow rate of the presence of three cavities located under upstream and downstream, for different positions and depths using the HS and MC models.....	203
Figure 5.31: Impact of the type of mode on flow rate for cavities present under upstream using the HS and MC models for depths: (a) Y=1m, (b) Y=2m, (c) Y=3m, (d) Y=4m.....	204
Figure 5.32: Impact of the type of mode on flow rate for cavities present under downstream for depths: (a) Y=1m, (b) Y=2m, (c) Y=3m, (d) Y=4m .....	206





## ACKNOWLEDGEMENT

All praise belongs to Allah for providing me with the patience and strength to go on and complete this task.

This thesis is submitted in partial fulfilment of the requirements for the PhD degree at the University of Salford. This work has been conducted at the school of Computer, Science and Engineering under the supervision of Dr Alireza Ahangar Asr.

I would like to offer my gratitude to my supervisor, Dr Alireza Ahangar Asr, the person who has given me the opportunity to study the PhD at the University of Salford. He has guided me with how good research is done. I am thankful to him for his guidance, support, motivation, and encouragement through my PhD.

I would like to thank my office colleagues in the school of Computer, Science and Engineering for their continued support and encouragement during my degree.

Special thanks to my colleagues in the Civil Engineering Department of the Kufa University especially Dr Khawla Shubber, For valuable advice, discussions and support.

I acknowledge the financial support from the Iraqi Ministry of Higher Education and Scientific Research, Iraqi Cultural Attache in London and the University of Kufa in Iraq. I owe to them for the scholarship and thank you for the trust which is given to me to complete my PhD.

My deepest thanks to my family who their support and understanding have been a strong driving force throughout my work. Thank you all.

## PUBLICATIONS

- 1- Al-Ateya, H., & Ahangar Asr, A. (2017). Numerical investigation into the effect of cavity size and location on stability of earth dams. Proceedings of the 25th UKACM Conference on Computational Mechanics. pp. 199-202.
- 2- Al-Ateya, H., & Ahangar Asr, A. (2017). Effect of Location of Cavities on Stability Analysis of Slopes. CSE 2017 Annual PGR Symposium.
- 3- Alateya, H., & Ahangar Asr, A. (2018). NUMERICAL ANALYSIS OF INFLUENCE OF CAVITIES ON SEEPAGE THROUGH EARTH DAMS. Proceedings of the 6th European Conference on Computational Mechanics (ECCM 6) 7th European Conference on Computational Fluid Dynamics (ECFD 7), Glasgow, UK.
- 4- Alateya, H., & Ahangar Asr, A. (2019). The Joint Influence of Cavities Presence and Rapid Drawdown Condition on Discharge Rate through Earth Dams. Proceedings of the 2019 UKACM Conference City, University of London
- 5- The Manuscript “Numerical investigation into the stability of earth dam slopes considering the effects of cavities” Engineering Computations Journal, and has been reviewed. (2019). (accepted)

## NOTATIONS

<b><u>Sample</u></b>	<b><u>Definition</u></b>
$E_{50}^{ref}$	Reference modulus of primary loading in standard drained triaxial test, kPa
$E_{ode}^{ref}$	Reference modulus of primary loading in drained oedometer test, kPa
$E_{ur}^{ref}$	Reference modulus of unloading /reloading in drained triaxial test
$H_i$	Vector of nodal heads
$k_x$	Hydraulic conductivity in the X-direction, (L/T)
$k_y$	Hydraulic conductivity in the Y-direction, (L/T)
$k_z$	Hydraulic conductivity in the Z-direction, (L/T)
$N_i$	Matrix of shape functions
$\nu_{ur}$	Poisson ratio of unloading and re-loading
$v_x$	Velocity in the X-direction (L/T)
$v_y$	Velocity in the Y-direction (L/T)
$v_z$	Velocity in the Z-direction (L/T)
$\gamma_w$	Unit weight of water (F/L <sup>3</sup> )
$\tau$	Shear stress, kPa
$\phi$	Angle of internal friction (degree)
$\sigma$	Normal effective stress, kPa
$\Psi$	Flow function
$c$	Cohesion of the soil, kPa
$D$	Cavity diameter(cm)
$d$	Average diameter of soil particles (L)
$D$	Depth of the tunnel (m)
$d$	Length drainage path (m)
$D$	Pile diameter (m)
$d$	Reduction in free surface (L)
$d$	Depth of water above ground surface (m)
$e$	Element
$h$	Total head (L)
$H$	Dam height (m)
$h_1$	Water height at the top of the dam (L)
$h_1$	Upstream head (L)
$h_2$	The water heights at the bottom of the dam (L)

$i$	Hydraulic gradient
$K$	Coefficient of permeability (L/T)
$k_c$	Coefficient of permeability for the core (L/T)
$k_d$	Coefficient of permeability for the dam (L/T)
$L$	Cavity location (m)
$l$	Length of flow path (L)
$n$	Number of elements
$N$	Shape function
$p$	Hydrostatic pressure (F/L <sup>2</sup> )
$p^{ref}$	Reference stress, kPa
$q$	quantity of seepage (L <sup>3</sup> /T)
$Q$	Seepage of the dam without a core (L <sup>3</sup> /T)
$Q_1$	Seepage of dam with a core (L <sup>3</sup> /T)
$R$	Radius of tunnel (m)
$Re$	Reynolds number
$s$	Distance along the flow line (L)
$s$	Length scaled along the phreatic surface (m)
$S$	Shear strength, kPa
$u$	Pore water pressure, kPa
$\nu'$	Poisson's ratio
$V_s$	Discharge velocity (L/T)
$X$	Cavity position (m)
$X$	Distance between the pile and cavity (m)
$Y$	Cavity depth (m)
$Z$	Elevation of head (L)
$\alpha$	Downstream slope angle (degree)
$\beta$	Downstream slope angle (degree)
$\gamma$	Unit weight of soil (kN/m <sup>3</sup> )
$E'$	Young's modulus, kPa
$\lambda^*$	Modified compression index
$\mu$	Coefficient of viscosity (F/L.T)
$\rho$	Fluid density (F/L <sup>3</sup> )
$\Phi$	Fraction angle (degree)
$\Psi$	Dilation angle (degree)

## ABBREVIATIONS

<b><u>Sample</u></b>	<b><u>Definition</u></b>
BDS	British Dam Society
FE	Finite Element method
HS	Hardening Soil model
MC	Mohr-Coulomb model
NRCS	Natural Resources Conservation Service
SF	Safety Factor
SRM	Strength reduction method
ULDC	Urban Levee Design Criteria
USACE	United States Army Corps of Engineers
USBR	United State Department of Interior Bureau of Reclamation

## ABSTRACT

The stability of dams and natural slopes is a significant and interesting issue and one of the key challenges in the civil engineering field. Cavities forming under earth structures are problematic in the field of geotechnical engineering and may lead to structural damage and loss of life and property.

This thesis presents a numerical investigation to evaluate the stability of earth dams and seepage through them, considering the combined impact of the presence of cavities in the subsoil and rapid-drawdown conditions. The current work aims to examine the influence of several parameters related to the cavity – such as the location (varying in X and Y directions), shape and diameter of the cavity, and the number of cavities – on the flow rate and the slope stability of the earth dam. The joint effects on stability of cavities and the strength parameters of slopes (soil cohesion and angle of internal friction) were also investigated and analysed parametrically. A numerical simulation was conducted to analyse seepage and slope stability (by calculating the safety factor [SF] against stability) considering the impact of cavities, using the finite element-based PLAXIS 2D software. This study includes two main stages of analysis. The first was performed employing the Mohr-Coulomb (MC) model to model the slope material and the subsoil. However, in the second stage, the Hardening Soil (HS) and MC models were employed to model the slope material and subsoil, respectively.

It is concluded that the presence of cavities under the upstream slope impacts both slope stability and the flow rate through the earth dam dramatically, which causes a considerable decrease in the SF and a notable increase in the flow rate: the SF decreased significantly to 0.715, and this value does not satisfy the minimum limit (1.2–1.3) set by the codes of practice for the stability of dam slopes under rapid-drawdown conditions. The existence of a cavity greatly influences the seepage and stability of the slopes on the upstream side; the SF decreased noticeably by 64.9%, compared to 11.9% on the downstream side, while the flow rate increased to  $459.8 \times 10^{-3} \text{m/day}$ , as opposed to  $2.572 \times 10^{-3} \text{m/day}$  for a cavity-free model. In addition, the location of a cavity in the X direction has more influence on slope stability and seepage than its location in the Y direction, as the SF and flow rate increase or decrease only slightly when changing the cavity depth. Increasing the cavity diameter resulted in a significant reduction in SF values no matter where the cavity was located, either horizontally or vertically. The existence of two or three cavities at the same depth has more of an influence on the slope's stability compared to them existing at different depths within the same model. Slope stability in the earth dam during rapid-drawdown conditions increases with an increase in the soil cohesion and friction angle; however, these increases are

insignificant compared to the major effects of the cavities on the stability. This influence is even bigger if the cavities are positioned in locations with the maximum effect on stability (at critical horizontal positions). Based on what has been concluded from the simulation related to the effect of cavity shape, this proves that the cavity's horizontal position has more influence on the dam's stability and the flow rate than its shape. It is found that using the MC model or HS model has a similar impact on the dam's stability and, no matter where these cavities are found under the upstream or downstream slope, the type of model used does not reduce the cavity's influence when it exists in crucial positions. It is concluded that the horizontal position of the cavity is the factor that has the most influence on slope stability and seepage.

To summarize, the results of this thesis – obtained through executing numerical analyses – could help to give a better understanding and provide a clearer view of the influence of the presence of cavities in the foundations of slopes and earth dams.



## CHAPTER ONE: INTRODUCTION

### 1.1 Dams

Of the various large-scale engineering projects undertaken by the construction industry, dam construction involves particularly heavy and complex challenges. Earth and rockfill dams have become far more common than other types of dams since 1980. The reasons for this growth in popularity include the fact that the method of construction for earth and rockfill dams doesn't require advanced technology; it utilizes cheap raw soil materials and subsurface materials; and it doesn't require a valley of a particular shape. Furthermore, the geometric design of embankment dams varies depending on the borrow materials from the soil, subsurface conditions, and the type of construction (PS and Balan, 2014). Consequently, a feasible design can lead to a significant reduction in construction time, materials used, and costs (Hasani et al., 2013; Gutierrez et al., 2003). The first man-made dam was constructed sometime around 3,000 to 5,000 years ago. Whenever it was built, that first dam was almost certainly an irrigation dam (Garg, 1984; Narita, 2000).

A dam is a barrier that prevents or constrains water flow to create a reservoir upstream for a number of possible purposes, such as to supply water for irrigation, for human consumption or industrial use; to generate electricity; navigability; and flood control. Dams may be constructed to achieve one or more of the above purposes (Arora, 2002). When choosing the type of the earth dam, many factors must be considered, including topography, foundation conditions, potential environmental impacts, available construction facilities, and the results of any studies on the socio-economic impacts of the dam. For a dam to be feasible, it should: be built from locally available materials; maintain stability under all foreseeable loading and operating conditions; be sufficiently watertight to maintain seepage at an acceptable level; and feature appropriate outlet works to prevent overtopping of the dam crest (Ismail et al., 2012; Zeidan, 1993).

Depending on the structure and materials used, dams are categorized as embankment dams, gravity dams and barrage dams, with several subtypes. The two main types of embankment dams are earth-filled dams and rock-filled dams. Embankment dams constitute about 85% of all dams built (Elshemy et al., 2002). Earth dams are simple structures that use their own significant weight to guard against sliding and overturning (Jansen et al., 1988). An earth dam is constructed of soil materials (sand, loam, clay and so on), with a trapezoidal or

approximately trapezoidal cross-section. Earth dams are frequently used because of their ease of construction and maintenance. They have significant importance since they are considered to be one of the cheapest means of administering large volumes of water. Presently, earth dams are the most prevalent type of dam (Al-Jorany, 1996).

## 1.2 Failure mechanisms of earth dams

The failure of earth structures such as earth dams or natural slopes is one of the most important problems in geotechnical engineering, with the potential to cause significant damage to infrastructure and heavy loss of life in regions affected by earth structures' failure. The consequences of failure are often significant, in spite of the small size of the dam (Jiang, 1999; Kwon and Moon, 2006; Yanmaz and Gunindi, 2008; Hsu et al., 2011; Maula and Zhang, 2011). For example, the 1963 failure of the Vajont Dam in Italy caused 2,600 deaths; the 1976 failure of the Teton Dam in America caused 100 deaths and estimated economic losses of 1 billion USD; and the 1993 failure of the Gouhou Dam in China caused 300 deaths. An earth dam failure can be defined as an incidence of excessive erosion or the deformation of a dam body's "embankment," which may cause an uncontrollable release of reservoir water or be detrimental to appurtenant structures. To estimate the safety of a dam and the potential for failure, possible failure mechanisms must be recognized, which can be graded into three main categories: structural failure, seepage failure and hydraulic failure (USBR, 2001), as shown in Figure (1.1). Dam failures may take place as a result of several scenarios, such as the instability of the structure of the dam, seepage through the body of the dam or its foundations, seismic effects and the rapid-drawdown condition (Zeidan et al., 2017). A statistical analysis of 534 dam failures from 43 countries prior to 1976 indicated that earth-rock dam failures accounted for the largest proportion of all dam failures and included 49% caused by overtopping, 28% due to seepage in the dam body, and 29% resulting from seepage into the dam foundations (Maula and Zhang, 2011). Dam failures can be classified into three main categories: (1) Hydraulic: 40% (2) Seepage: 30% (3) Structural failures: 30% (Punmia and Lal, 1992). "The most common causes of dam failure are leakage and piping (35%), overtopping (25%), spillway erosion (14%), excessive deformation (11%), sliding (10%), gate failure (2%), faulty construction (2%) and earthquake instability (2%)" (Lukman et al., 2011). Investigations performed by Garg (1984) indicated that around 40%, 25% and 35% of failures are imputed to hydraulic, structural and seepage failures respectively. Sherard et al. (1963) conducted a vast survey on the reasons for dam failures and reported that the failure of earth dams may be caused by overtopping; action of earthquake forces;

embankment and foundation piping; embankment sliding, cracks and differential settlement; sliding during construction; wave action; damage as a result of the solution of some materials in water; damage caused by animals; and damage caused by surface drying.

### 1.2.1 Structural Failure

The main type of structural failure is a shear failure, which leads to sliding soil mass along the slopes of a dam. Every soil mass with a slope at one end is subjected to shear stresses on internal surfaces or failure planes in the soil mass near the slope. This is a result of gravitational forces that exert a downward force on the soil mass adjoining the slope. Multiple analytical techniques and models have been formulated to determine the critical slip surface and the associated factor of safety. These techniques include the Ordinary Method of Slices (Noori and Ismaeel, 2011).

Earth dams are sensitive engineering structures that require design and successful construction and need continual analysis of their stability. The stability of a slope is a significant issue for dam designers before, during and after construction. A slight change in the safety factor can lead to a big change in the cost of construction, create the need for expensive repair work or imperil public safety (Khabbaz et al., 2012). The critical periods in the dam's life that must be assessed from the viewpoint of shear failure are: the crucial phase for the upstream side at the end of construction and during rapid drawdown conditions, whilst the stability of the downstream side must be ensured at the end of construction and during the steady-state phase (Jalil, 2011; Fathani and Legono, 2010).

The structural failure types for earth dams are steady-state, seismic and the rapid-drawdown condition. Steady-state failure takes place on the downstream side beneath case of steady-state seepage for reservoir water, which may happen due to an increase in the pore water pressure in the dam. Seismic failure occurs due to the influence of horizontal earthquake forces on the soil mass, which leads to parts of the embankment or foundations being liquefied in a phenomenon called liquefaction. The phenomenon causes an increase in the driving force with a decrease in soil resistance, which leads to sliding soil mass along the slopes of the dam (USBR, 2001). The third type of failure is rapid drawdown. Stability analysis under the rapid drawdown condition is a significant consideration in the design of dams. This type of failure takes place as a result of the reservoir water level reducing speedily after a long duration of being raised to the normal operating level for a dam or in the levees condition, during a prolonged flood. During a flooding season, the reservoir water level raises. Often, such floodwater can vanish in a relatively short duration of time. In such

conditions, the supporting water load is quickly removed from the upstream slope, but the pore water pressure within the dam's body does not have enough time to dissipate, thus it remains high, leading to an undrained unloading condition in which the total stresses reduce with the increasing shear stresses within the dam's body (Singh and Varshney, 1995; Reddi, 2003; Kerkes and Fassett, 2006; VandenBerge, 2014). According to (Elshemy et al., 2002), structural failures amount to about 25% of dam failures.

### **1.2.2 Seepage Failure**

Seepage through earth dams is one of the main factors in the failure of earth dams (Hasani et al., 2013). Groundwater flow exerts a significant influence on the deformation of soils, rocks, and geotechnical structures, potentially threatening their stability. Seepage control is thus vital for maintaining the safety and stability of the dam engineering works (Fipps et al., 1986; Yang et al., 2010; Siddappa et al., 2007). Two main problems arise from seepage through earth dams. The first problem is estimating the quantity of seepage, which is frequently a major economic issue for storage dams (Aboelela, 2016). The second problem is concerned with the stability of the embankment of a dam against water flow through or under an embankment that can carry fine soil particles to the surface at the downstream slope. The gradual removal of soil particles from a mass leads to the development of cavities. Also, cracks can be created as a result of differential settlement within the earth embankment. Such cavities and cracks can form channels of water to flux through the dam, causing the erosion of the dam from the inside out. This phenomenon is known as "piping" (USBR, 2001). Piping failure is one of the main causes of the failure of embankment dams. Because internal erosion can take place as a result of normal operations, it may be more dangerous on a dam than the effect of floods and earthquakes (Fell et al., 2003).

Some of the primary factors that contribute to seepage include high permeability of the substrate; cracks and fissures; and uneven settlement, which causes gaps or cracks either in the soil or between the soil and the structure of the dam. Excessive seepage can be managed with: the use of low-permeability soil layers; the provision of core walls in the earth structure; or the construction of cut-off walls in the foundations. The use of upstream blankets and the extension and widening of seepage channels can also assist in reducing the quantity of seepage (Khattab, 2010). According to (Foster and Fell, 1999), 25% of all dam failures occurred due to fine granules being washed out of the dam body or foundations. Seepage failures account for more than 35% of all earth dam failures (Elshemy et al., 2002). Some examples of seepage failures include the Fontenelle Dam (the USA, 1964) and the

Walter F. George Dam (the USA, 1970) (Rice, 2007). Carsington Dam (England, 1981) failed in 1981 due to stability failure (Davey and Eccles, 1983), with large cracks emerging in the dam body, although disaster was averted. Around 30% of dam failure was found to have been due to seepage failure, namely, piping and sloughing (Middlebrooks, 1953). Seepage flow through a dam's body or foundation constitutes more than one third of earth dam failures (Varshney, 1973; Subuh, 2002).

### **1.2.3 Hydraulic Failure**

Dams are designed with principal and emergency spillways to control the maximum reservoir elevation and prevent the reservoir from flowing over the top of the dam, or "overtopping." When the spillways are not adequately designed, or if they become obstructed and cease to function, overtopping may occur (USBR, 2001). Overtopping can cause considerable amounts of erosion on the slope side of a dam, which can affect the dam's stability. Furthermore, overtopping is one of the most significant causes of dam failure. The International Commission on Large Dams (ICOLD, 1973), reports that around 35% of failures resulted from overtopping. According to (Costa, 1985), overtopping causes around 34% of all earth dam failures.

## **1.3 Seepage through earth dams**

Seepage is one of the significant factors that contribute to the failure of earth dams (Cedergren, 1967), taking place as a result of the difference in the water levels of the upstream and downstream faces of earth dams (Selim, 1947). The groundwater flow depends on the type of flow, the soil media, liquid properties, hydraulic gradient, and the boundary conditions (Arslan & Mohammad, 2011).

Seepage is unavoidable in earth dams; however, it is especially necessary to control seepage through earth dams (Fell et al., 1992; Fredlund et al., 1994). Seepage flow may cause the softening and sloughing of slopes as a result of pore water pressure developing, which causes a reduction in the soil's resistance leading to shear failure (Punima, 1981; Sachpazis, 2014). To prevent seepage failure, the flow of water through the body of the dam and its foundations must not be so large in quantity as to defeat the purpose of the dam, nor at a pressure high enough to cause erosion and piping. This implies a number of things. Firstly, it necessitates the limiting of the amount of seepage through the dam body and foundations. Secondly, the seepage line should be kept well within the downstream face of the structure to rule out

saturation and the resultant sloughing. Thirdly, seepage water that makes it through the structure or foundations should not be permitted to remove any particle, as this is another cause of piping. The driving force of water seepage depends on the pressure gradient, while the opposing force of the structure arises from the strength properties of the material. Lastly, no seepage of water from the upstream to the downstream face should be tolerated. This water seepage may take place via conduits, at the location of joints between earth and concrete sections of the structure, or through cavities made by aquatic creatures.

(Fattah et al., 2017) Seepage analysis is fundamental to the design of an earth dam to compute the water losses of the reservoir, assess the pore water pressure distribution, and define the location of the free surface that is utilized in the stability analysis (Sherard et al., 1963).

#### **1.4 Statement of cavity problem**

The existence of cavities in soils is a significant area of interest within the field of geotechnical engineering. It is one of the most serious soil-related problems since cavities might result in damage to structures and the loss of life. In particular, when cavities exist under hydraulic structures, these cavities can form channels for water movement that extend and then collapse when they reach a critical size (Culshaw and Waltham, 1987).

Cavities that exist under the structures are classified into two types: natural and artificial. Natural cavities may be created due to the extinction of some seas or water areas or as a result of the chemical action in soils or rock including limestone, salt, dolomite and gypsum, because these materials can dissolve under the influence of water movement (Badie and Wang, 1984). Water passing through soils and rock carries with it some soft particles. The gradual removal of soil particles leads to the development of cavities of various shapes and sizes. (Aziz, 2008) reported cavities in sandy soil ranging from 100 mm to 3000 mm, as shown in Figure (1.2). Moreover, the movement of water through cracks and faults leads to the expansion of those cracks and faults, creating cavities that are often irregular in form and subject to collapse when they amount to a critical size (Terzaghi and Peck, 1967). Exact investigations to locate the site of cavities and voids close to the surface represents one of the most important factors, as these cavities could form channels for the movement of water. It is also important to know the properties of materials that fill cavities and the surrounding area, where cavities may be filled with dry air or partially or totally filled with water or soft sediment (Vogelaar, 2001; Styles et al., 2005). The failure of structures built on such soils is likely to happen as a result of the generation of cavities before or after the application of load.

The existence of cavities is one of the challenges of designing and constructing structures such as earth dams. Man-made cavities might be occurred due to the creation of sewer networks, tunnelling, drilling the canals, mining or extraction of raw materials and outputs from some factories (Badie and Wang, 1984). Both natural and artificial cavities must be considered in the design and construction the structures (Crapps, 2010; Zaynal, 2004).

Another cause of serious stability issue is the presence of geological problems in the dam foundations. The existence of problematic materials beneath a dam might cause serious stability issues. This occurred underneath the St. Francis Dam in 1928, where the substrate lost strength, leading to dam collapse. Bedrock dissolution was blamed, which was also held as a factor in the collapse of the Tbilisi Dam in the USSR (Nedriga and Dem'yanova, 1986; Salih, 2013). Likewise, the foundation of the Mosul Dam is very poor from a geological standpoint, due to the large water reservoir and the associated movement of groundwater leading to the dissolution of gypsum and anhydrite in the foundations and abutments (Kelley et al., 2007). From the report of SIGIR (2007), there exist caves of various sizes and shapes underneath the Mosul Dam, especially in the mid-line under the centre of the dam, and close to the upstream area underneath the reservoir (see Figure 1.3).

## **1.5 Slope stability analysis using (PLAXIS 2D) software**

Recently, techniques in the field of seepage analysis and slope stability analysis for earth dams have witnessed significant progress by using software. One of these pieces of software is PLAXIS 2D, which is a two-dimensional finite element software utilized to execute deformation, stability and flow analysis for different types of geotechnical applications.

## **1.6 Significance of the study**

The stability of slopes and earth dams and seepage analysis are important aspects of geotechnical engineering, and research and studies related to the influence of the existence of cavities in the subsoil of hydraulic structures are very rare. This study provides a numerical assessment of the stability of earth dams are constructed on soil containing cavities or cavities may create within it over time. In this study, research was conducted to investigate this phenomenon in depth using PLAXIS 2D software. Cavities were created and situated at various depths from the soil surface and at different distances from the dam's centreline under both sides of the dam. The overall investigation aims to get a better estimation of the

effects of cavities on slope stability and seepage through the earth dams. It is hoped that the outcomes acquired from this research will contribute to avoiding or reducing the risks caused by the existence of cavities in soils.

## 1.7 Study aims and objectives

The aim of this study is to:

To study the stability of slopes of an earth dam constructed on foundations containing cavities. The study aims to include all the relevant parameters that can contribute significantly to give a better insight and to ensure the safety of the structures based on such soils.

The key objectives of the current study are as follows:

1. To use finite element software PLAXIS 2D to develop an earth dam model to examine and estimate the effects of cavity existence on stability and seepage through earth dam
2. Numerical study of the effects of the presence of cavities in the foundation of earth dams on the slope stability under rapid drawdown conditions.
3. To evaluate the effects of the presence of a single cavity under the base of an earth dam in terms of location, diameter, number and shape on slope stability.
4. To study and understand the impact of the existence of cavities in the subsoil of earth dams on the quantity of seepage through earth dams during rapid drawdown.
5. To assess the flow rate passing through an earth dam built on subsoil containing cavity in terms of the impact of location, shape, and the number of cavities using the developed PLAXIS model.
6. To study the influence of the presence of more than one cavity on the quantity of seepage and slope stability of earth dams.
7. To implement the developed PLAXIS 2D model to simulate the influence of material properties (cohesion of soil and angle of internal friction) on the stability of slopes of earth dams considering the presence of cavities in the base.
8. To conduct a parametric analysis on model outcomes to find the most and least effective cavity parameters on stability and seepage phenomena.



## **1.8 Layout of thesis**

This introduction presents an overview of dams; provides some background information regarding dam failure issues; and describes the importance of this study, the aims and objectives and the layout of the dissertation.

Chapter two presents a brief review of the literature concerning the subject, which includes a summary of the theories of slope stability analysis and seepage analysis for earth dams and previous research on the influence of cavities.

Chapter three is devoted to the methodology of the present numerical research. This chapter presents an overview of PLAXIS 2D software, modelling with PLAXIS 2D, describing constitutive modelling executed in the software and a description of the study model.

Chapter four presents the numerical results achieved using the PLAXIS 2D software and discussions regarding the influence of the existence of cavities on the slope stability of earth dams.

Chapter five presents the numerical results achieved using the PLAXIS 2D software and discussions regarding the influence of the existence of cavities on seepage passing through earth dams.

Chapter six presents conclusions drawn from the present study and provides recommendations for future research.

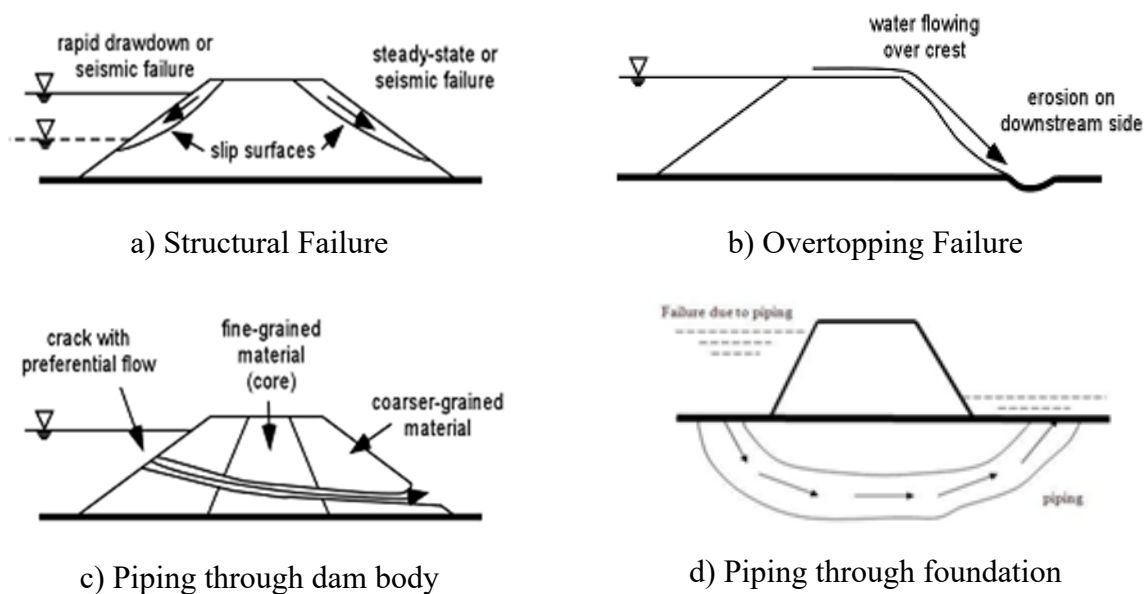


Figure 1.1: Failure mechanisms for earth dams (USBR, 2001)

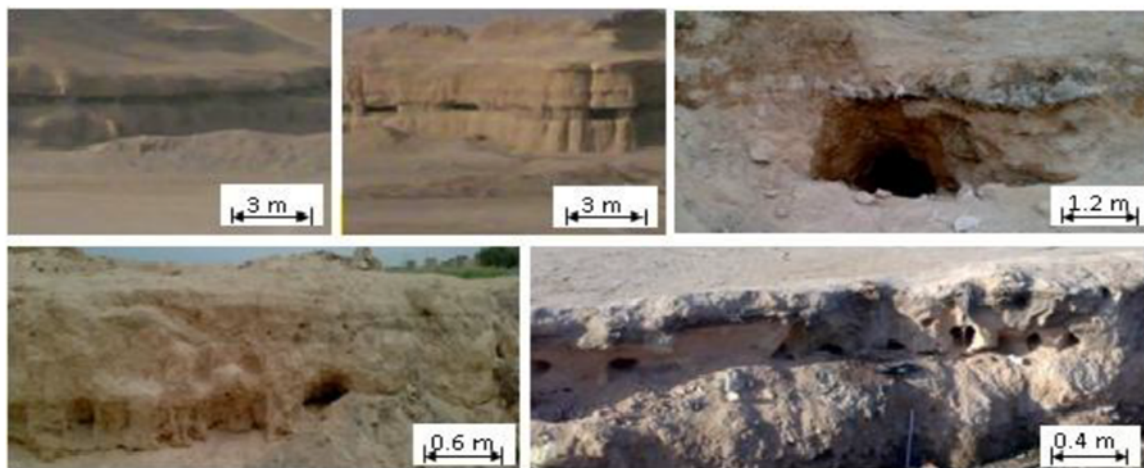


Figure 1.2: Images of cavities with various sizes and location in soil of AL-Najaf city/ Iraq (Aziz, 2008)

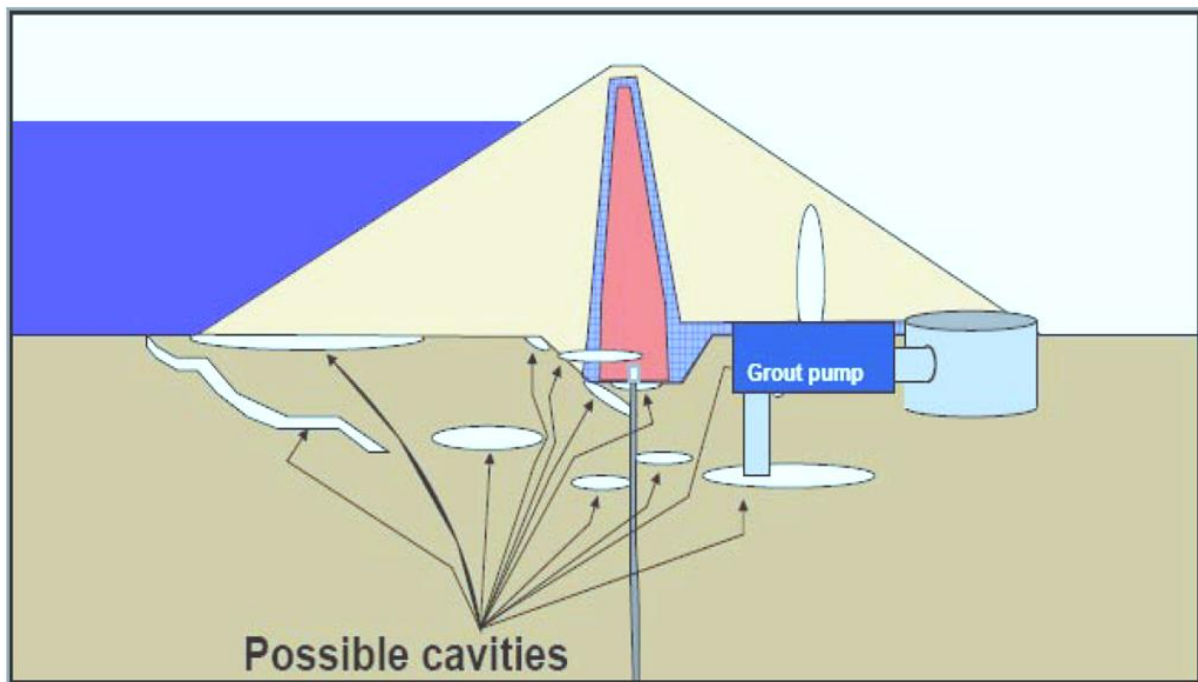


Figure 1.3: Possible cavities underneath Mosul Dam, mostly close to the reservoir side (from SIGIR, 2007 report)

## CHAPTER TWO: LITERATURE REVIEW

This chapter presents the general concepts, substantial background and theory on which stability and seepage analyses rely. The literature review offered in the coming sections is related to previous studies on seepage through dams and cavities, and also slope-stability analysis.

### 2.1 Literature review of seepage analysis

Many studies have tackled seepage analysis since Darcy (1856), as mentioned in Harr (1962), who suggests the primary law of flow through porous media by conducting a series of tests in a vertical pipe full of sand. The seepage flow relies on many factors, which include the flow type, soil media, characteristics of flowing liquid, hydraulic gradient and boundary conditions (Arslan and Mohammad, 2011). Water flows as a result of the hydraulic head gradient; it flows in the direction of the reduction of potential energy due to variations in elevation and pressure. The hydraulic head or total head ( $h$ ) is a general measure for potential energy;  $H$  includes the velocity head, pressure and elevation head. The velocity head is small compared to the pressure and elevation head; consequently, the total head is equal to the sum of the pressure head and elevation of head, and can be expressed as follows:

$$h = p/\gamma_w + Z \quad 2.1$$

where  $h$  is the total head,  $p$  is the hydrostatic pressure ( $F/L^2$ ),  $\gamma_w$  is the unit weight of water ( $F/L^3$ ); and  $Z$  is the elevation head (L) (Elshemy et al., 2002; Zeidan, 1993).

#### 2.1.1 Equations of flow through porous medium

The quantity of seepage is associated with the velocity, pressure, and viscosity of the fluid that flows through the soil. The fluid parameters are unidentified variables that may change from one site to another, also from one time to another (Harr, 1962).

### 2.1.1.1 Darcy's law

The flow of water in soils is generally ruled by Darcy's law that can be applied to determining the rate of the quantity of seepage. The "Darcy's law of seepage" establishes a linear relationship between the seepage velocity and hydraulic head gradient. This law, which is a simple consequence of viscous flow neglecting inertia effects, can be generalized to a two-dimensional situation (Carthy, 1982).

$$V_s = ki \quad 2.2$$

$$\text{or} \quad V_s = -k \frac{dh}{ds} \quad 2.3$$

where:  $V_s$  is the seepage velocity of fluid in porous media (L/T);  $K$  is the hydraulic conductivity, (L/T);  $i$  is the hydraulic gradient ( $= -dh/ds$ );  $h$  is the piezometric head; and  $s$  is the distance along the flow line (L).

Darcy's law is applicable to the flow through porous media in two and three dimensions. Equation 2.3 is valid when the value of the Reynolds number is taken equal to or less than one, and the flux is laminar (Harr, 1962):

$$\text{Re} = \frac{V_s d \rho}{\mu} \leq 1 \quad 2.4$$

where  $V_s$  is the flow velocity (L/T);  $d$  is the average diameter of soil particles (L);  $\rho$  is the fluid density (F/L<sup>3</sup>); and  $\mu$  is the coefficient of viscosity (F/L.T).

### 2.1.1.2 Laplace's equation

The components of seepage velocity for three-dimensional flow based on Darcy's law are as follows (Craig, 2004):

$$v_x = -k_x \frac{\partial h}{\partial x} \quad 2.5a$$

$$v_y = -k_y \frac{\partial h}{\partial y} \quad 2.5b$$

$$v_z = -k_z \frac{\partial h}{\partial z} \quad 2.5c$$

where  $v_x, v_y, v_z$  are the velocity components in the x, y and z directions, respectively; and  $K_x, k_y, k_z$  are the hydraulic conductivity in the x, y and z directions, respectively. The net volume of water flowing per unit of time in or out of an element of the soil must be equal to the change per unit of time of the volume of water in that element to ensure the continuity (Terzaghi et al., 1996).

$$\frac{\partial v_x}{\partial x} + \frac{\partial v_y}{\partial y} + \frac{\partial v_z}{\partial z} = 0 \quad 2.6$$

Equation 2.6 becomes

$$k_x \frac{\partial^2 h}{\partial x^2} + k_y \frac{\partial^2 h}{\partial y^2} + k_z \frac{\partial^2 h}{\partial z^2} = 0 \quad 2.7$$

For isotropic and homogeneous soil, the permeability of soil is equal in all directions of flow, thus this means:

$$k_x = k_y = k_z = k$$

Therefore, Equation 2.7 can be written as:

$$\frac{\partial^2 h}{\partial x^2} + \frac{\partial^2 h}{\partial y^2} + \frac{\partial^2 h}{\partial z^2} = 0 \quad 2.8$$

Equation 2.8 is called Laplace's equation.

For two-dimensional seepage analysis, the equation of flow is as follows:

$$\frac{\partial^2 h}{\partial x^2} + \frac{\partial^2 h}{\partial y^2} = 0 \quad 2.9$$

## 2.1.2 Methods of Seepage Analysis

Several methods have been evolved to analyse the seepage in soils as numerical, analytical and experimental solutions. These methods require a general model depicting the phenomena of seepage, including soil characteristics and the boundary conditions, to utilize the calculated pore water pressure, flow distribution and quantities of seepage. In general, Laplace's equation represents a mathematical base for many methods, which are applied to obtain exact or approximate solutions (Lambe and Whitman, 1969). Experimental models have been used to determine the flow rate, pore water pressure and phreatic surface; however, most of the experimental methods are applicable for simple geometry, and homogeneous and linear soils, but these methods become difficult to apply to complicated geometries and, non-homogeneous and nonlinear soils (Billstein et al., 1999).

Many studies were conducted using diverse geophysical methods to monitor water seepage through and under earth dams, including resistance-based methods, space potential, radar and temperature (Johansson and Dahlin, 1996; Panthulu et al., 2001; Boleve et al., 2011).

Panthulu et al. (2001) used geophysical methods that consider it important to map seepage pathways and watch the alterations of seepage over time, allowing technically and economically effectual remedial measures to be put in place. In this study, electrical methods were used for delineating seepage zones for two saddle dams in India, which are based on a heterogeneous rock. The electrical resistivity method was utilized to determine zones appropriate for seepage; furthermore, the self-potential (SP) method was utilized to determine air-leakage paths. The SP measurements show negative anomalies of  $10 \pm 20$  volts in amplitude, indicating a drop-in seepage, which is in conjunction with the leakage measurements taken by the project authorities.

### 2.1.2.1 Numerical methods

In recent years, as a result of the appearance of several difficulties during the application of experimental and analytical methods, and the fact that computer systems have evolved significantly, the computer software adopting numerical methods have been utilized extensively for modelling different seepage conditions in embankments. The numerical methods that are utilized widely in the field of computational mechanics include the FE method, the finite-difference method, the finite-volume method, the numerical manifold method, the meshless method and the boundary element method (Bathe and Khoshgoftaar,

1979; Lam and Fredlund, 1984; Li et al., 2003; Jie et al., 2004; Zheng et al., 2005; Jiang et al., 2010; Bear and Verruijt, 2012; Abhilasha and Antony Balan, 2013). Many software packages that are based on numerical solution techniques – such as PLAXIS (2D and 3D), MODFLOW, SEEP/W, ANSYS, PDEase2D and SVFLUX – are used to conduct analysis of seepage through embankment dams (Abhyankar and Bhole, 2011).

The finite element (FE) method is a technique that is utilized broadly in design, and in the numerical analysis of linear, nonlinear, and two- and three-dimensional problems in nearly all fields of engineering. In recent decades, the FE method, coupled with the growing capabilities of computers, has become a very robust and useful technique for solving complicated problems in civil engineering (Newmark, 1965). It has been adopted widely by many software packages for analysing seepage and stability for earth dams, which include PLAXIS (2D and 3D), ANSYS, SNAIL, FLAC (2D and 3D), GeoStudio and CLARA-W.

Since 1970s, the FE technique – combined with the fast development in digital computers – has become a robust tool for resolving complicated water problems (Chandrakant and Johan, 1977; Rushton and Redshaw, 1979; Singh, 2008).

Zienkiewicz and Taylor (1977) were the first to use the FE method to resolve Laplace's equation for the condition of steady seepage. Many studies have been conducted utilizing the FE approach to simulate seepage through embankments (Papagianakis and Fredlund, 1984; Lam et al., 1987; Potts and Zdravkovic, 1999; Subuh, 2002; Jairy, 2010; Ismaeel and Noori, 2011; Navas, and López-Querol, 2013).

Uromeihy and Barzegari (2007) investigated the properties of the geological engineering of the ground of Chapar-Abad Dam to estimate the seepage flow and to choose an appropriate system of waterproofing before the construction of the dam. The dam is situated in Iran, and in the construction stage, it had a height of 45m. PLAXIS 2D software was used to analyse the problem of seepage through the ground, and in-situ tests were used to evaluate the soil-permeability values. The outcomes of PLAXIS 2D can simulate the water seepage under the core of the dam when waterproofing is inserted at various depths, which aids the design of the depth of the grout curtain. Based on the data obtained from monitoring the site, PLAXIS 2D modelling and experimental methods, an appropriate waterproofing system could be chosen and designed for the Chapar-Abad Dam.



Kamanbedast and Shahosseini (2011) assessed three methods that could be used to reduce seepage through an earth dam and selected the best method. Karkheh earth dam was selected as the study case. This assessment was conducted using Seep/w software. The methods used to reduce seepage were concrete blankets, upstream cover and saturation conditions (with filter and drain). It was found that using concrete blankets led to a significant decrease in the seepage rate.

Kirra et al. (2015) analysed seepage and stress at Walter F. George Dam in the USA by utilizing the FE software GeoStudio. The surface of the phreatic flow, the distribution of pore water pressures and the change in the total head of the dam were analysed. The model was used to simulate the seepage of the dam for various conditions of operation. It is proved that dam design is unsafe against the failure of seepage. It proposes using a concrete diaphragm wall to improve the dam design and to limit the problem of seepage. In addition, it concludes that conducting an accurate simulation for existing and failed dams are necessary.

Sazzad et al. (2015) presented a numerical study to estimate the impact of seepage through dams with various measurements and conditions. Various geometric models of dams were used for this, and then a comparison was done between the numerical and analytical outcomes. The SEEP/W software was applied to examine the seepage. It is shown that the shape and size of the net have a slight impact on seepage. The flow-rate values gained using SEEP/W are similar to those gained from the analytical method used by Casagrande (1937) and Stello (1987), if the angles upstream and downstream are similar to a homogeneous earth dam. Furthermore, the angles of the upstream and downstream slopes do not impact seepage in the case of providing mud pulp, while it increases when increasing the angles of slopes for a dam without a clay core. It is noticed that there is a significant decrease in flow rate for a model with an existing clay core. The difference in the flow-rate values between a pervious and impervious base is lower if the core is not supplied, and the seepage is considered to be independent of the permeability of base. Finally, the core shape has a considerable impact on the flow, where a trapezoidal core shape is the best option.

Irzooki (2016) used SEEP/W software to obtain a new empirical formula to calculate the quantity of seepage passing through a homogenous earth dam with an existing horizontal toe drain. Karkheh earth dam was selected as the study case. SEEP/W is a part of the FE software package GeoStudio. The analyses were conducted considering three different slopes for both the upstream and downstream sides, three different lengths of horizontal toe drain, three

different free boards, three different widths of the crest and three different dam heights. The quantity of flow was defined for each stage of analysis. The results indicate that – by increasing the angle of the upstream and downstream slopes, the water depth of the reservoir and the length of the drain – the quantity of seepage increases. Moreover, the outcomes also reveal that the quantity of seepage reduces as the crest width and the height of the free board also reduce. It an empirical formula was developed to calculate the rate flow through an earth dam with a horizontal drain. The length of the horizontal drain is the variable with the most influence on the quantity of seepage; however, the angle of the upstream slope is the least influential variable.

Abdulsattar et al. (2017) simulated the seepage through KHASA-CHAI dam for three different water levels for the reservoir and considering the effect of the existence of upstream filter. The numerical analysis was made using SEEP/W software to determine whether the dam is safe against boiling failure. The height of the zoned dam is 58m, and the water levels studied are as follows: the maximum water level is 49.17m, the half-filled condition has a water level of 33.81m and the minimum water level is at 18.43m. It is deduced that the presence of a core results in a significant decrease in the quantity of seepage. The existence of a filter has little influence on increasing the quantity of seepage; however, it has a considerable influence on reducing the exit gradient.

### 2.1.2.2 Analytical Method

The analytical methods depend on the solution of differential equations employing simplifying presumptions to solve the seepage equations in porous medias. These presumptions are appropriate under particular conditions, and thus their field of application is limited by problems related to geometry and boundary conditions (Fakhari and Ghanbari, 2013). Analytical solutions can be used to estimate seepage through earth dams, but most of these methods need suppositions and have the ability to solve simple problems of seepage only.

Schaffernak (1917) proposed Equation 2.10 and Equation 2.11 to compute the discharge rate through a homogenous embankment positioned on an impervious subsoil, as displayed in Figure 2.1.

$$q = k l \sin \beta \tan \beta \quad 2.10$$

$$l = \frac{d}{\cos \beta} - \sqrt{\frac{d^2}{\cos^2 \beta} - \frac{H^2}{\sin^2 \beta}} \quad 2.11$$

where  $\beta$  is the downstream slope angle,  $d$  the length drainage path (m), and  $H$  is the height of water in the reservoir (m).

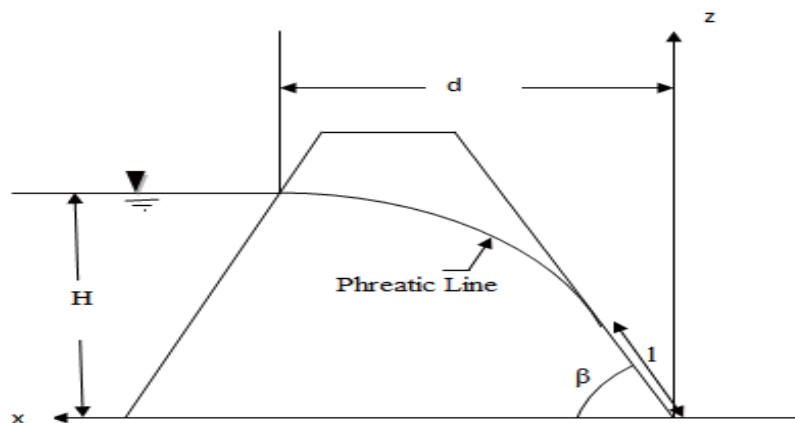


Figure 2.1: Description diagram for Schaffernak solution

Casagrande (1937) assumed the hydraulic gradient ( $dz/dx$ ) equals to ( $dz/ds$ ) to estimate the quantity of seepage through the embankment dam by assuming that the hydraulic slope  $dz/dx$  equals to  $dz/ds$  as follows:

$$q = k l \sin^2 \alpha \quad 2.12$$

where,

$$l = s - \sqrt{s^2 - \frac{h^2}{\sin^2 \alpha}} \quad 2.13$$

$$s = \sqrt{d^2 + h^2}, \quad d = b - 0.7\Delta \quad 2.14$$

where  $s$  is the length scaled along the phreatic surface (m),  $h$  is the downstream water height (m),  $b$  is the width of core floor,  $\alpha$  is the downstream slope angle and  $\Delta$  is as displayed in Figure 2.2.

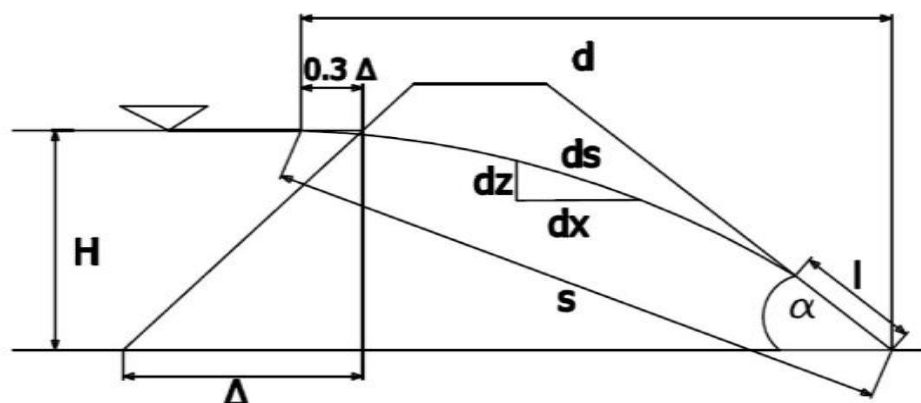


Figure 2.2: Description diagram for Casagrande solutions (1937)

In 1963 Dupuit supposed that the hydraulic gradients have identical slopes of free surface. At that time, the rate of seepage for every vertical section of the dam was calculated using Darcy's law, based on Equation 2.15.

$$q = k \frac{h_1^2 - h_2^2}{2l} \quad 2.15$$

where  $k$  is the hydraulic conductivity,  $l$  is the length of flux path, and  $h_1$  and  $h_2$  are the water heights at the upstream and downstream of dam, respectively, as displayed in Figure 2.3.

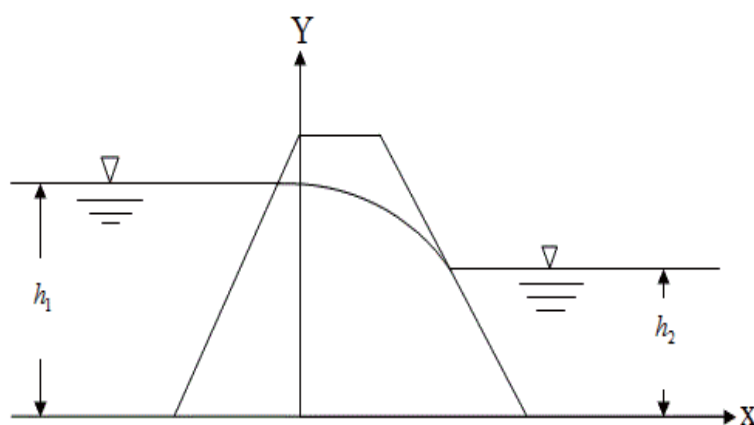


Figure 2.3: Description diagram for Dupuit's solution

Fu and Sheng (2009) presented a numerical model for analysing the unsteady seepage flow through an earth dam. A set of laboratory tests were carried out on seepage flux through a dam, considering unsteady conditions for verifying the authenticity and the precision of the numerical model. A comparison with analytical solutions was made to assess the performance of the numerical model. The results identified that the authenticity and the precision of the model were sufficient to address a seepage problem in complicated conditions. It was also shown that the method of specifying the seepage surface through the description of saturation is normal, reasonable and workable in de facto applications. This method provides a comparatively simple computing system compared to conventional methods.

Rezk and Senoon (2011) proposed an analytical solution based on an experimental study conducted previously to locate the fall in the phreatic surface in every zone of the core. The effect of core permeability and the decline of the phreatic surface for all seepage rates for flow through the embankment were examined. Comparisons indicate that the phreatic surface obtained from an analytical solution is quite close to that gained from using an experimental method at the first zone (upstream), through and after the core. The results indicate that relative seepage ( $Q_1/Q$ ) rises as the relative permeability ( $k_c/k_d$ ) increases, while the relative drop ( $d/h_1$ ) reduces as the ( $k_c/k_d$ ) increases. Where  $Q$  is the seepage of the dam without a core,  $Q_1$  is the seepage of dam with a core,  $k_c$  is the coefficient of permeability for the core,  $k_d$  is the coefficient of permeability for the dam,  $d$  is the reduction in free surface owing to core, and  $h_1$  is the upstream head.

Aboelela (2016) used the analytical solutions that were evaluated previously to assess the hydraulic performance of the control measures of seepage quantity through earth dams. The control methods included flat slopes, drainage systems at the toe, and a catch drain in the tail water. The results indicate that the control measures used had a significant impact on the seepage characteristics of earth dams established on previous subsoils.

## 2.2 Literature review of stability analysis

The stability of slopes is an important consideration in the design and construction of earth dams, rockfill dams, retaining walls and excavations, from safety and cost points of view. One of the main reasons for slope failure is the failure of the soil mass located beneath the slope, which is called a “slide”. It involves the downward and outward movement of the entire mass of soil that participates in a failure (Terzaghi et al., 1996). Generally, the most significant factors that the stability of slopes rely on are (1) slope geometry, (2) soil slope properties, and (3) the internal and external forces impacting on the slope (Pham et al., 2013; Hammouri et al., 2008). The selection of the slope stability analysis method requires the collection of field information and failure observations, which give a clear understanding of the failure mechanism for slopes.

The influences that must be considered for a slope-stability analysis of an earth dam are as follows:

- External loads, such as the self-weight of the body, the surcharge and forces resulting from serial construction.
- Seepage forces resulting from a steady or transient flux of water (Li and Desai 1983).

### 2.2.1 Classical stability-analysis methods

The limit equilibrium method has been utilized widely by researchers and designers to perform the stability analysis of slopes. The fundamental assumption for this method is based on the shear strength of the soil along the potential failure surface as governed by the Mohr-Coulomb (MC) failure (USA, 2003):

$$S = c + \sigma \tan \varphi \quad 2.16$$

where  $S$  is the shear strength,  $c$  is the cohesion of the soil,  $\varphi$  is the angle of internal friction and  $\sigma$  is the normal stress.

The limit equilibrium method assumes that the shear strength of the soil is partly mobilized along a assumed failure surface, which is likely to be a straight line or any other non-uniform surface. According to this method, the safety factor (SF) is the proportion of shear strength ( $S$ ) to the shear stress ( $\tau$ ):

$$SF = \frac{S}{\tau} \quad 2.17$$

The SF in Equation 2.17, which is presented by (Bishop, 1955), is determined as a proportion of the total shear strength available to total shear strength mobilized (Spencer, 1967). In the case of saturated soils, Equation 2.17 becomes the following:

$$S = c + (\sigma - u) \tan \phi \quad 2.18$$

where  $(\sigma - u)$  is effective stress, and  $u$  is the pore water pressure

The driving force (shear stress) resulting from the soil weight acts to move the soil mass down the slope, while the resisting force resulting from soil shear strength along the base of soil mass (on the slip surface) acts to keep the soil mass in place. If the driving force is bigger than the resisting force, the soil mass will slip along the base, causing the slope failure (USBR, 2001). The term SF indicates the closeness to potential failure for a given soil mass. The SF is defined as the proportion of the actual resisting force or moment to the minimum driving force or moment required to cause failure (Bishop, 1955; Abramson et al., 2002). Accordingly, an SF value that is greater than 1 denotes that a slope is stable, an SF value that is less than 1 indicates a failure, and an SF value of 1 means that the slope is theoretically on the brink of failure.

### 2.2.2 Method of slices

The method of slices is used widely to analyse slope stability. It includes a number of methods such as Bishop's simplified, Fellenius, Spencer, Morgenstern-Price and Sarma method. In the method of slices, the assumed failure surface is circular. The soil mass above the failure surface is partitioned into a series of vertical slices while considering the equilibrium of the slices and holding the supposition that the base of all slices is a straight line. The number of slices required depends on the soil properties and the geometry of the slope. Most software utilize a method of slices because of their ability to address slopes with complicated geometries, changing soil and water cases and the effect of external boundary forces. Consequently, these methods are the most popular for analysing slope stability (Al-Bataineh, 2006). The method of slices is considered to be a perfect method for determining exact solutions for any shape of failure (Whitman and Bailey, 1967).

### 2.2.2.1 Ordinary method of slices

This method is also known as the Fellenius' method; it is the easiest method of slices to apply. The soil mass above the failure surface is partitioned into a number of vertical slices. The resultant of forces acting on any slice is found by taking into account the mechanical equilibrium for the slices. The method assumes that the resultant forces acting on each slice is parallel to its base, whereby the interslice forces are ignored (Fellenius, 1936). Nevertheless, the resultant forces on the left and right of a slice are not unequal and not collinear, since Newton's third law is not satisfied by this method (Fredlund and Krahn, 1977).

This permits a simple static equilibrium computation, considering the weight of the soil, along with the shear and normal stresses along the plane of failure.

The thickness of the soil block is  $b$ . The slices on the left and right experience normal forces  $E$ , and shear forces  $S$  and  $S$ ; the weight of the slice produces force  $W$ . The pore water pressure and reactions of the base balance the normal and shear forces,  $N$  and  $T$ , respectively, as shown in Figure 2.4.

For the ordinary method of slices, the resultant vertical and horizontal forces are as follows:

$$\sum F_v = 0 = W - N \cos \alpha - T \sin \alpha \quad 2.19$$

$$\sum F_h = 0 = kW + N \sin \alpha - T \cos \alpha \quad 2.20$$

where  $k$  is a linear factor that specifies the rise in the horizontal force with the depth of the slice. Solving for  $N$  gives the following:

$$N = W \cos \alpha - kW \sin \alpha \quad 2.21$$

Next, the method assumes that each slice can rotate about a centre of rotation and that a moment of balance about this point is also needed for equilibrium. A balance of moments for all the slices taken together gives the following, as cited in (Fredlund and Krahn, 1977):

$$\sum M = 0 = \sum_j (W_j x_j - T_j R_j - N_j f_j - kW_j e_j) \quad 2.22$$

where  $j$  is the index of a slice;  $x_j$ ,  $R_j$ ,  $f_j$  and  $e_j$  are the moment arms; and loads on the surface have been ignored. The moment equation can be utilized to find a solution for the shear forces at the interface, after replacing the term for the normal force:



$$\sum_j T_j R_j = \sum_j [W_j x_j - (W_j \cos \alpha_j - kW_j \sin \alpha_j) f_j - kW_{jej}] \quad 2.23$$

Applying Terzaghi's strength theory and transforming the stresses into moments, the equation can be written as follows:

$$\sum_j \tau l_j R_j = l_j R_j \sigma'_j \tan \phi' + l_j R_j c' = R_j (N_j - u_j l_j) \tan \phi' + l_j R_j c' \quad 2.24$$

SF is the proportion of the maximum moment from Terzaghi's theory to the assessed moment:

$$SF = \frac{\sum_j \tau l_j R_j}{\sum_j T_j R_j} \quad 2.25$$

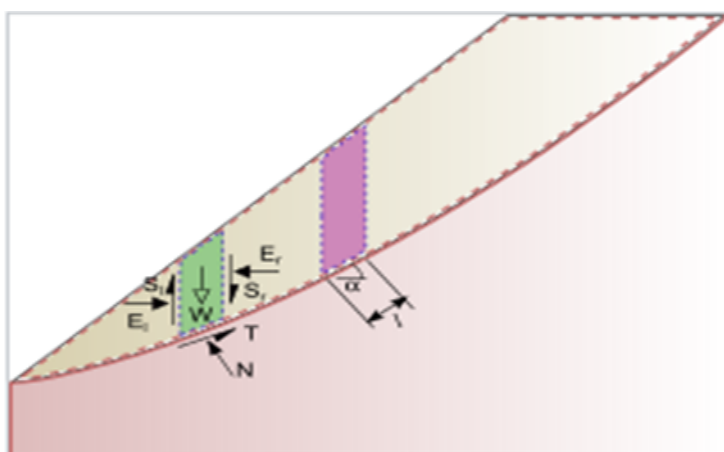


Figure 2.4: The slip surface and forces acting on slice (Fredlund and Krahn, 1977)

### 2.2.2.2 Bishop's simplified method

Bishop (1955) suggests a more accurate solution to the slice's method, which supposes that the resultant of the interslice forces acting on each slice has a horizontal line of action, and the interslice shear forces are ignored. According to the simplified method, the SF can be computed from the following:

$$SF = \frac{\sum_{i=1}^{i=n} [c' \Delta X_i + (W_i - U_i \Delta X_i) \tan \theta'] [1/M_i(\theta)]}{\sum_{i=1}^{i=n} W_i \sin \theta_i} \quad 2.26$$

where:

$$M_i(\theta) = \cos \theta_i \left( 1 + \frac{\tan \theta_i \tan \theta'}{SF} \right) \quad 2.27$$

where  $c'$  and  $\theta'$  are effective shear strength parameters for the soil at the base of the slice;  $n$  is the number of slices;  $W_i$  is the weight of the slice;  $\theta_i$  is the slope of the slice;  $u_i$  is the average of pore water pressure at the bottom of the slice (where  $u_i = h_i \times \gamma_w$ );  $h_i$  is the height of water in the piezometer placed at the bottom of the slice; and  $\gamma_w$  is the unit weight of water.

There is less than a 5% error in the value of the SF obtained by this approach (Whitman and Bailey, 1967). Bishop's simplified and Fellenius methods are non-stringent approaches, and can satisfy some of the equilibrium conditions and be used to make some simplified suppositions (Zhu et al., 2003; Abramson et al., 2002).

Equation 2.26 can be solved using the trial-and-error method; the value of  $M_i(\theta)$  can be obtained from Figure 2.5. The two aforementioned methods (the ordinary method and Bishop's simplified method) are displayed in Figure 2.6, which shows the differences between the two methods.

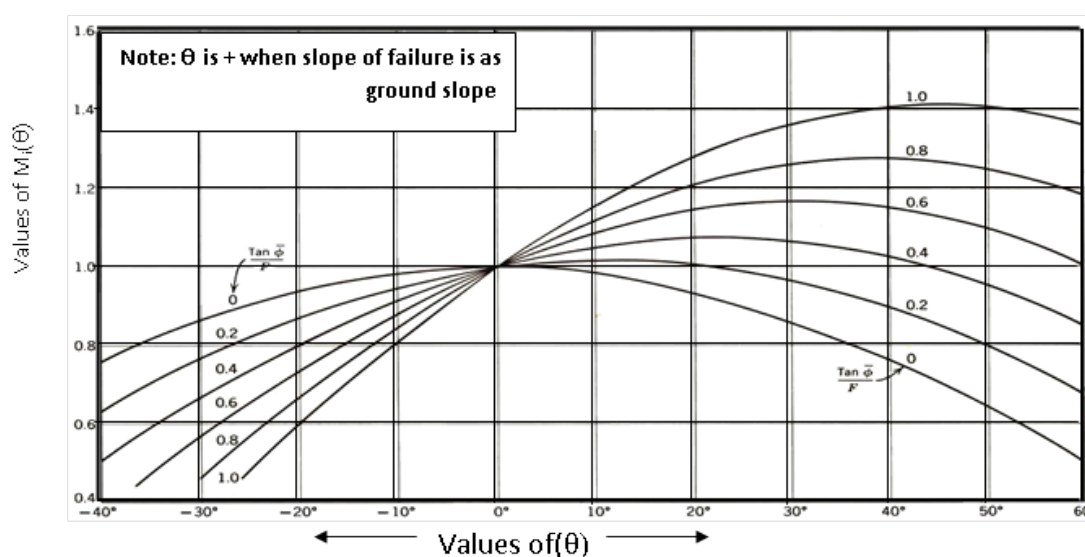


Figure 2.5: Values of  $M_i(\theta)$  (after Janbu, 1973)

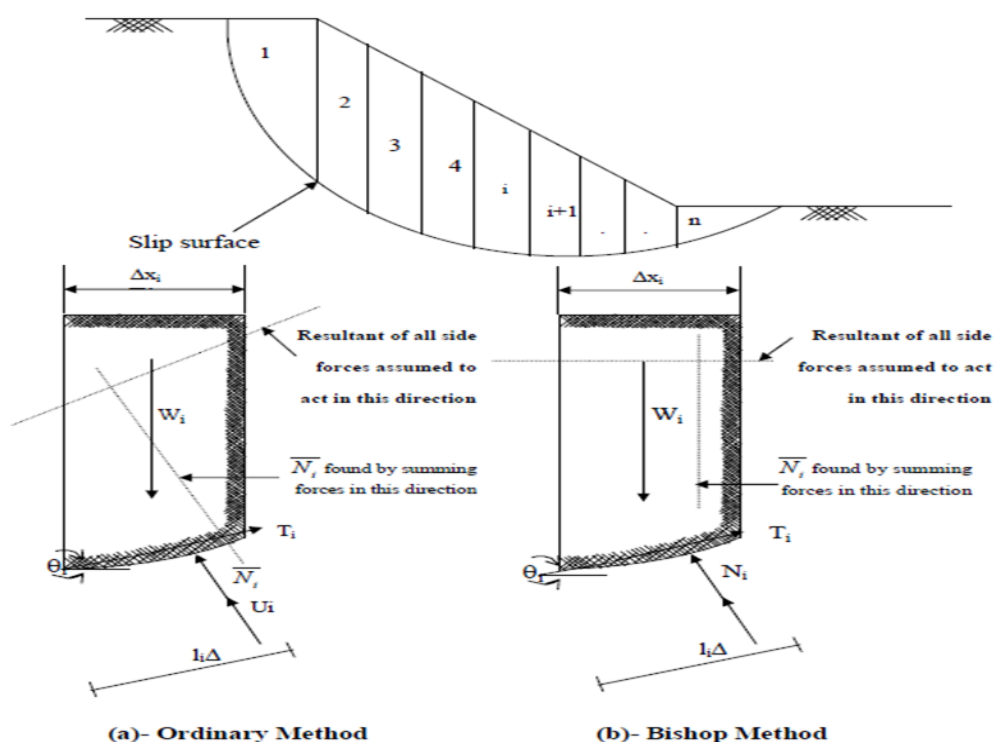


Figure 2.6: The slip surface and forces acting on a typical slice (Lambe and Whitman, 1969)

### 2.2.3 Strength reduction method (SRM)

Since 1975, the SRM has been applied to analyse slope stability by Zienkiewicz et al. (1975) and then has been used by (Naylor, 1981; Ugai and Leshchinsky, 1995; Erxiang, 1997; Dawson et al., 1999; Griffiths and Lane, 1999; Zheng et al., 2005) and others. SRM and the limit equilibrium method are the most extensively utilized approaches for analysing slope stability. In fact, both approaches have some constraints in practice. In the case of using the limit equilibrium method, several assumptions are required regarding the conditions between slices of soil/rock. However, SRM needs repeated calculations and does not provide the slide surface directly (Li et al., 2014). The SRM is characterized by (i) its ability to prophesy deformations and stresses of supporting elements at failures, such as piles and geotextiles; (ii) it does not need any assumptions to be made regarding the distribution of shear force between slices; (iii) it is appropriate to numerous complicated states, and can provide information such as pressures, pore water pressures and movements (Wei et al., 2009); and (iv) in the SRM, the critical sliding surface can be found automatically from decreasing the shear strength and it is not essential to determine the shape of the slide surface at first (Cheng et al., 2007). Thus, this method normally sets a SF equal to or somewhat lower than that set by the limit

equilibrium technique (Sun et al., 2014). This method has been utilized in many geotechnical software packages, such as PLAXIS 2D, SNAIL and FLAC 2D (Zhang, 2005). This technique is used in the FE method to calculate the SF for slopes (Dawson et al., 1999; Griffith and Lane, 1999). By decreasing the index of shear strength progressively, the  $c$  value is divided at the same time by a parallel reduction coefficient, which results in a new series of strength-index. This calculation is done numerous times until a critical state failure of the slope is reached, and, at this time, the slope's SF is brought into use (Huang et al. (2008) and Wei (2008)).

The SF is defined as the reduction of soil shear strength until the slope reaches a critical failure state and equals the proportion of soil strength to the reduction of soil strength at the critical failure state (He and Zhang 2012).

In elastic-plastic FE method, a numerical analysis based on the concept of strength reduction, for a point in a domain – according to the general definition of the Bishop safety coefficient, and considering the shear strength – the MC failure criteria is expressed as follows (He and Zhang 2012):

$$S = c + \sigma \tan \varphi \quad 2.28$$

where  $c$  is the cohesion of the soil and  $\varphi$  is the angle of shearing resistance. The factor of safety of the specified shear plane of this point is this:

$$SF = \frac{S}{\tau} = \frac{c + \sigma \tan \varphi}{\tau} \quad 2.29$$

Assuming that the shear failure of soil does not take place, the real shear stress in soils and the maximum shear strength are equal; that is, the following is true:

$$\tau = \tau_{fm} = \frac{S}{SF} = \frac{c + \sigma \tan \varphi}{\tau} = C_m + \sigma \tan \varphi m \quad 2.30$$

Thus, the reduction in the real shear stress in soil can be considered to be the fold reduction shear strength index, which is as follows:

$$C_m = \frac{c}{F} \phi m = \arctan \frac{\tan \phi}{F} \quad 2.31$$

The fold reduction factor  $F$  was given a temporary value, based on strength reduction theory; the fold reduction shear strength indices were then obtained; and  $F$  was altered constantly till the calculation became divergent.

The factor of shear strength reduction rises incrementally until a collapse happens. At this instant, the shear strength reduction factor becomes the global minimal SF, which has the same meaning as an SF defined in the limit equilibrium method.

#### 2.2.4 Numerical studies

The numerical-modelling studies provide an improved view of the performance of slopes and failure mechanisms related to water-level variation. In addition, these studies are not too expensive compared to the other types of study. However, it is difficult for numerical studies to analyse reliably every detail of the method and failure mechanism (Jia et al., 2009).

FE modelling has been utilized extensively to examine the impact of the variation of water levels adjoining slopes on the slopes' stability. Many investigations have been conducted regarding the effect of rapid drawdown on slopes' stability (Griffiths and Lane, 1999; Lane and Griffiths, 2000; Rinaldi et al., 2004; Zhang et al., 2005; Luo et al., 2005; Zhan et al., 2006; Khassaf et al., 2013; Khalil, 2012; Vandenberghe, 2014).

Huang (1996) presented a numerical method to simulate the stability of an earth dam when the reservoir is full. Firstly, the trial-and-error method was applied to obtain the piezometric heads at various points of a dam. Secondly, the FE analysis was applied using a cap model to model the soil of dam. This study was performed considering the Liyuetan reservoir in Taiwan as a case study. The outcome of the numerical analysis shows that the SF is sufficient, and the dam is safe with respect to sliding.

Duncan (1996) provided an inclusive review of slope analysis using the FE approach and limit equilibrium method. The results of the comparison between field measurements and an FE analysis identify that the measured deformations are less than the computed deformations. Lane and Griffiths (2000) used the FE method to assess the stability of slopes under drawdown conditions to produce operating schemas for conditions that must apply to real structures.

Tran (2002) studied numerically the stability of a homogeneous earth dam using PLAXIS 2D software. The stability analysis of the dam was executed in a staged construction to assess the behaviour of the stress-strain, consolidation and shear failure. The height of the studied dam is 20m, with a crest width of 7m, and an inclination of upstream and downstream of 1V: 3H. The construction of the dam included 5 stages with each stage of five-month consolidation. The dam is modelled for analysis before the impoundment, thus the water level was assumed at the ground surface. It was revealed that the SF reduces progressively as the stages of construction advance from the first staged construction to the final stage as calculated:  $SF_{1st\ stage} = 2.055$ ,  $SF_{2nd\ stage} = 1.345$ ,  $SF_{3rd\ stage} = 1.121$ ,  $SF_{4th\ stage} = 1.018$  and  $SF_{5th\ stage} = 1.010$ . Reducing the development of excess pore pressure in the dam's body is, therefore, a very significant factor in the construction of earth dams.

Aryal (2006) performed a study to analyse the stability of a natural slope. The SF was calculated using some of the approaches in GeoStudio software – (i) the ordinary method, (ii) Bishop's simplified method, (iii) Janbu's simplified method, (iv) Morgenstern-Price method – and (v) PLAXIS 2D for various conditions of groundwater. According to this study, the SF values obtained from both software packages are similar. The SF for wet conditions is equal to (i) 1.192, (ii) 1.353, (iii) 1.234 and (iv) 1.36 and (v) 1.27 for the respective approaches, while the SF for dry conditions is equal to (i) 1.39, (ii) 1.55, (iii) 1.41, (iv) 1.55 and (v) 1.45 for the respective approaches.

Berilgen (2007) presented a study to estimate the slope stability under rapid-drawdown conditions, considering the effect of the permeability of the soil, drawdown rate, drawdown proportion and loading cases. The Hardening Soil (HS) model was selected to model the soil behaviour using PLAXIS 2D software. It shows that the developed displacement value in the embankment is affected by its hydraulic conductivity and drawdown rate greatly, and the displacement manner appears to be largely indicative of the slip surface. Moreover, it was concluded that it is vital to consider the pore pressures resulting from the stress and their dissipation, as well as the pore pressures resulting from leakage in the fine soils.

Hammouri et al. (2008) performed a comparative study to analyse slope stability using the limit equilibrium method and the FE method. Three different models were considered, using homogeneous and non-homogeneous slopes, taking account of the impacts of rapid drawdown, undrained clay soils and the crack position. FE software PLAXIS 2D and limit equilibrium software SAS-MCT were employed to simulate the stability. A comparison was

made between the SF and the critical slip surfaces gained using both approaches. It is found that the shape and location of the critical slip surface are roughly comparable for the two methods, excluding the case where undrained clay soil was used for modelling the slope, for which the FE method was unable to define the critical slip surface.

Xu et al. (2009) analysed the slope stability of the Shangzhuang earth dam using an FE approach. The FE analyses were executed by means of ABAQUS and GEO/SLOPE software. It is a homogeneous earth dam. The height of the dam is 31.75m and the width of the crest is 6.0m. The inclination of the upstream slope is 1:2.5 and that of the downstream slope is 1:3.0. A stability analysis was conducted during the reduction of the water level from the flood water level of 117.60m to the level of 104.92m. It was demonstrated that the FE approach can readily simulate complicated boundary conditions and overcome the shortcomings of the limit equilibrium approach. It was shown that rapid drawdown causes a reduction in stability of the slope. Accordingly, the monitoring of the dam should be strengthened in drawdown conditions for the water level in the reservoir to prevent the slope failure.

Jia et al. (2009) presented a large-scale experimental model to simulate slope performance when it undergoes a rise in water level followed by a drop in water level. The dimensions of the model were as follows: 15m long, 6m high and 5m wide, and the inclinations of both the sides were 1 Vertical: 1 Horizontal. The control system for the water level has been improved to allow the simulation of the rise and abrupt drop in the water level. Based on the results, the drawdown of the water level outside the slope resulted in a considerable delay in dissipation of the pore water pressures inside the slope, with a large settlement occurring at the slope crest. The findings give a better understanding of the physical behaviour and failure mechanism for both a saturated and unsaturated slopes exposed to water-level variations.

Keyvanipour et al. (2012) used PLAXIS 2D to analyse the behaviour of Bar (Hussein Abad) dam. The constitutive models MC and HS were utilized for the stress-strain analysis. The simulation of the dam was performed during the first impounding. This study was based on the devices data of the bar dam, which is of 35.5m high. In general, it is shown that the HS model is better able to predict the behaviour of the dam to determine the dam's stability during construction and thereafter. Also, the difference between the results of the HS model and the devices findings is lower than the difference between the devices results and the

results of the MC model. It is also shown that the efficiency of PLAXIS 2D to model the behaviour of the dam construction is agreeable.

Khabbaz et al. (2012) performed a comparative study to simulate the stability of a heterogeneous slope using the limit equilibrium and FE methods. The limit equilibrium program SLOPE/W and the FE program PLAXIS 2D were utilized in this comparison. It was demonstrated that the SF obtained from SLOPE/W is 1.1% less than that obtained from PLAXIS 2D for the drained analysis, in which the SF amounted to 1.936 and 1.958, respectively. It was also shown that the locations and shapes of the sliding surfaces are roughly congruent for both approaches. Furthermore, it was found that the elastic modulus has little impact on the SF values. However, dam-geometry and soil-shear parameters have a significant impact on stability.

López-Acosta et al. (2013) studied the safety of levees numerically using the PLAXFLOW and PLAXIS 2D programs to undertake transient-seepage and stability analyses, under rapid-drawdown conditions. The effects of hydraulic conductivity, drawdown proportion, drawdown rate and material properties were examined, using MC and HS as constitutive models. As shown in this study, the slope stability in the conditions of partial and total saturation is impacted mainly by the permeability of the soil and the rate of the drawdown of the water. The condition of rapid drawdown takes place when the water level in the reservoir drops faster, compared to dissipation of the water pore pressure, which is caused by the drawdown. It was noted that the SF decreases with the increasing the drawdown ratio  $L/H$ , where  $L$  is the water level in the reservoir after the drawdown at each stage of the drawdown, and  $H$  is the dam height.

Athania et al. (2015) executed a numerical study to analyse the stability and seepage of an earth dam for steady-state and transient conditions using FE software PLAXIS 3D. The effect of Young's modulus ( $E$ ) and the angle friction on the stability were considered in these analyses. The slope stability was examined for different conditions, which involved the following: the full water level of a reservoir (steady state), rapid-drawdown conditions over 5-and 10-day periods, slow-drawdown conditions over a 50-day period and low water level (steady state). The results imply that the maximum displacement at the crest decreases when increasing the value of Young's modulus, and the change in the angle of internal friction has a vital effect on achieving the criteria of total stability. The results also reveal that the SF values obtained using PLAXIS 3D are more dependable than the ones obtained by using the



limit equilibrium method, and dam stability decreased enormously under rapid-drawdown conditions.

Shivamant et al. (2015) conducted a numerical study to analyse the slope stability of a dyke utilizing the limit equilibrium and FE approaches. FE (PLAXIS 2D) software and limit equilibrium method (SLOPE/W) software were adopted to realize this aim. The stability was estimated after the end construction phase, after the sedimentation of ash at the base, and with empty and rapid-drawdown conditions. It is found that the dyke is safe for the three conditions studied; in addition, the obtained SF value utilizing PLAXIS 2D is lower than that obtained from SLOPE/W. According to the results, rapid-drawdown conditions are the most crucial.

Farshidfar and Nayeri (2015) applied the strength reduction technique utilizing PLAXIS 2D software to analyse slope stability and calculate the SF and deformations. The results obtained from applying this approach were compared with those obtained from using a finite-difference approach. It was concluded that applying the strength reduction technique gives a satisfactory outcome. As the slope angle increases, the SF decreases, and the slopes are damaged further. The slope becomes more stable when the angle of internal friction of the slope is increased. The results of the FE method and the finite-difference method are similar. Finally, the shear strength reduction technique forecast the deformations that happened over time.

Abbas (2015) used the GeoStudio SLOPE/W and SEEP/W software to analyse slope stability and seepage of Al-Fada dam. SLOPE/W applies the Bishop method to analyse slope stability; however, SEEP/W is based on the FE method and simulates seepage through the dam. The SF was computed for different probable slip surfaces. To analyse the slope stability of the dam, four water-level cases were considered as follows:

Case 1: Operational case with the maximum water level of 174.00 masl; SF = 1.516.

Case 2: Drawdown with the minimum water level of 166.90 masl; SF= 1.565.

Case 3: Dry case – the final stage of construction; SF= 1.787.

Case 4: Downstream is dry; SF= 1.893.

It was shown that the slope stability of the Al-Fada earth dam is perfect under all of the aforementioned water-level cases.

Berisavljević et al. (2015) carried out an investigation to assess the ability of limit equilibrium and FE methods to define the critical failure surface and determine the minimum value of the SF for four slopes. The analyses were done using the limit equilibrium method software (BGSLOPE and SLIDE) and FE-method software PLAXIS 2D. It was identified that the results obtained from both techniques are similar, provided they are applied properly using suitable software. The values of the SF gained from the analysis are presented in Table 2.1.

Table 2.1: Safety factor values according to Berisavljević et al., (2015)

Method	Safety Factor (SF)			
	Slope 1	Slope 2	Slope 3	Slope 4
BGSLOPE (Bishop)	1.289	2.248		
BGSLOPE (Maksimovic, optimized)	1.236	2.107	1.696	
SLIDE (optimized)			1.691	1.879
PLAXIS ( $\varphi = \psi$ )	1.249	2.126	1.712	1.900
PLAXIS ( $\psi = 0$ )	1.236	2.102	1.690	1.884

Majeed (2015) simulated the seepage and stability of Hassan Kanosh Dam in Iraq numerically. In this study, three software packages were employed to analyse the stability and seepage, which are based on the FE method. SIGMA/W software was utilized to analyse the stresses and deformations of the earth dam, SEEP/W software was used to calculate the flow rate, while the SF values were calculated using SLOPE/W software. The analysis was conducted considering the critical conditions of a dam, which include full-reservoir, empty-reservoir and rapid-drawdown conditions, as well as investigating the effect of seismic forces. It was shown that the dam is safe for potential loading and operational conditions. All the critical slip surfaces passed through the dam shell, which indicates that this zone represents the weakest zone within the dam.

Fattah et al. (2015) studied the behaviour of a earth dam under the rapid drawdown of the reservoir's water level. The FE software GeoStudio was employed in this study. The earth was analysed at staged construction. The dam stability was simulated during rapid-drawdown conditions for various water levels in the reservoir. Dau Tieng Reservoir, which is a homogeneous earth dam, was the chosen case study. The dam height is 31m, with a crest

width of 10m. The upstream and downstream slopes range from 1:3 to 1:4.5 and from 1:3 to 1:4, respectively. It was concluded that the stability of the upstream slope reduces significantly when the water level drops to less than 1/3 of the dam height.

Toromanovic et al. (2016) presented a study to assess the stability of a hydropower earth dam in Northern Sweden. PLAXIS 2D software was used to calculate the SF and to assess the deformations for three sections of the dam. Three cross-sections have been selected for the analyses; A, B and C, section A is shown in Figure 2.8. The results were compared with those obtained using SLOPE/W software. The results indicate that the size of the deformations is satisfactory, and the SF is acceptable for safety-standards requirements. The results of the numerical analysis can be used to determine the warning values for dam stability. The results gained from the analysis are shown in Figures 2.7 and 2.8.

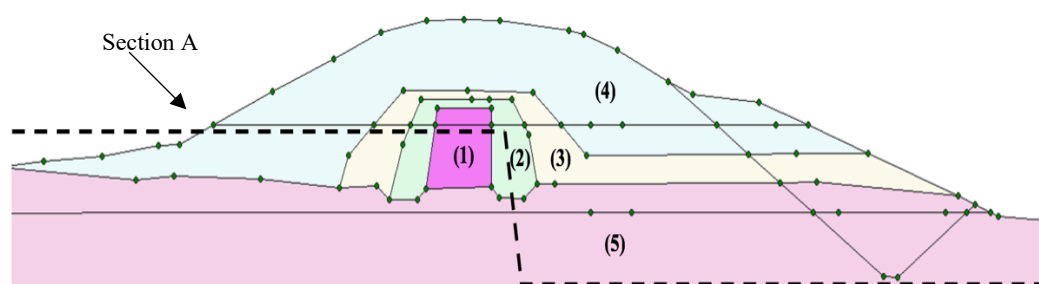


Figure 2.7: Section A, a geometrical model of the dam body. The zones are: (1) core, (2) fine filter, (3) coarse filter, (4) rockfill, (5) foundation consisting of till.

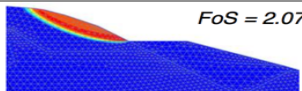
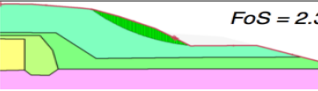
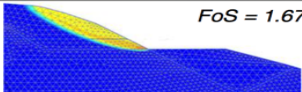
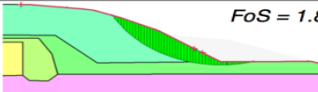
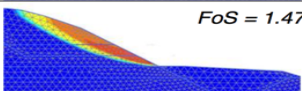
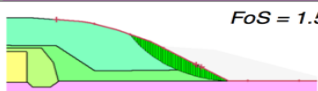

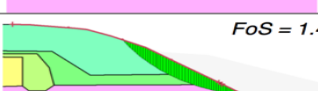

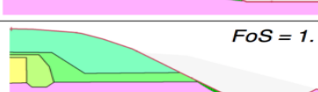
Excavation phase	PLAXIS	SLOPE/W
1	 $FoS = 2.07$	 $FoS = 2.35$
2	 $FoS = 1.67$	 $FoS = 1.82$
3	 $FoS = 1.47$	 $FoS = 1.55$
4	 $FoS = 1.37$	 $FoS = 1.45$
5	 $FoS = 1.19$	 $FoS = 1.15$

Figure 2.8: SF values for section A according to Toromanovic et al., (2016)

Fattah et al. (2017) employed the SEEP/W and SLOPE/W FE programs to simulate slope stability and seepage through an earth dam. Al-Wand earth dam in Iraq was selected as the case study to undertake the analysis for various cases of drawdown; the water level was emptied within three periods (11 days, 3 days and 1 day). The results showed that drawdown conditions caused a linear decrease in the pore water pressure at all points within the embankment; the flux rate through the downstream slope reduced linearly with time; and the SF reduced slightly during the short period after the water level in the reservoir reduced rapidly, and then began to rise.

Zhang et al. (2004) and Hu et al. (2005) carried out studies involving experiments with physical models, give clear and improved insights into the modes and mechanisms of failure related to the variations in water level in the neighbourhood of the slope. In general, these studies are expensive to implement and few of these studies have been conducted.

### 2.2.5 Safety standards

The geometrical parameters of the considered earth dam model were selected according to the recommendations of British Dam Society in 1994, as shown in Table 2.2.

Table 2.2: British Dam Society in 1994 standard

Geometrical parameters	Geometrical study model parameters	Specification limits
Crest width	6m	Minimum 2m
Upstream slope	1:2.5	Minimum 1:2.5
Downstream slope	1:2.5	Minimum 1:2
Free board	3m	Minimum free board 1.5

The design and safety assessment of embankment dams must comply with the standards suggested in codes and safety regulations issued by the accredited establishments. Among the many safety regulations for dams; the USBR (2011); NRCS (2005); ULDC (2012) criteria are considered to be the basic criteria used for extensive verification in this study. Table 2.3 identifies the safety standards for the SF in different operating situations.

Table 2.3: Safety standard for earth dam

Establishment	Loading condition	Stress parameter	SF
BDS, 1994	End of Construction	Total and Effective stress	1.3-1.5
	Steady seepage case	Effective stress	1.3-1.5
	Rapid drawdown	Total stress	1.2-1.3
USACE, 2003	End of Construction	Total stress	1.3
	Steady seepage case	Effective stress	1.5
	Rapid drawdown	Total stress	1.2
NRCS, 2005	End of Construction	Total and Effective stress	1.4
	Steady seepage case	Total and Effective stress	1.5
	Rapid drawdown	Total and Effective stress	1.2
USBR, 2011	End of Construction	Total and Effective stress	1.3
	Steady seepage case	Effective stress	1.5
	Rapid drawdown	Effective stress	1.3
ULDC, 2012	Steady seepage case	Effective stress	1.5
	Rapid drawdown	Effective stress	1.2

The minimum limits for the SF according to the (US, 2003) criteria with regard to the stability of the upstream and downstream slopes are displayed in Table 2.4.

Table 2.4: Safety factor according to the (US, 2003)

Loading condition	Minimum SF	Slopes
End of Construction	1.3	Upstream and Downstream
Steady seepage case	1.5	Downstream
Rapid drawdown	1.1-1.3	Upstream

## 2.3 Literature review of cavities in soil

During the last few decades, many studies have been fulfilled to simulate ground water flow and assess the stability of dams and natural slopes. The research projects that are concerned with analysing the effect of cavities on seepage through hydraulic structures are still very limited. There are no systematic studies related to the issue of the influence of cavities on the stability of earth dams. Some of the available literature pertaining to this topic investigates the effect of gypsum rock and gypseous soil on the stability of dams built of them. Some of them are concerned with the influence of the existence of tunnels on the seepage problem, whereas others relate to the effect of cavities on the performance and stability of other geotechnical applications, such as piles. The dams constructed on gypsum substrates are likely to suffer from the continuous weakening of their foundations, with the risk of failure gradually increasing due to the formation and growth of cavities in various shapes and sizes. Cavities in the foundations of dams can cause comprehensive failure within the body of gypsum rock, which, in turn, weakens the foundations of dams, along with landing and the generation of sinkholes in the surrounding areas (Maximovich and Meshcheryakova, 2009). Consequently, several studies have been conducted to examine the effect of the dissolution of dissolvable substrates, such as gypsum, which is considerable for the stability of dams.

Salih (2013) developed new procedures to estimate the influence of dissolution on the mechanical properties of gypsum substrates, in order to analyse the issues of stability under dams constructed on gypsum substrates. The research adopted Mosul Dam as a study case, which has suffered serious problems associated with the dissolution of gypsum and cavity formation.

A large number of reservoirs around the world have been adversely impacted by gypsum karstification, and this demonstrates that seepage under the dam site is the most common problem (Cooper and Calow, 1998). The effect on dams' safety of the dissolution of soluble substrates is investigated in some studies – such as (Calcano and Alzura, 1967; James and Lupton, 1978; Calvino et al., 1981; Yilmaz, 2001; Dreybrodt et al., 2002; Romanove et al., 2003; Shafiei et al., 2008)– which conclude that the dissolution of soluble substrates may cause problems associated with the stability of dams built on such a substance; for example, increasing seepage rates and the formation of caverns/cavities.

Polubarinova and Kochina (1962) derived the following approximate formula to assess the seepage for a horizontal tunnel in a completely saturated, homogeneous medium.

$$q = \frac{2\pi K(d - \varphi_0)}{\ln\left(\frac{2D}{R}\right)} \quad 2.32$$

where  $K$  is the hydraulic conductivity,  $R$  is the radius of tunnel,  $D$  is the depth of the tunnel's centreline,  $\varphi_0$  is the hydraulic head at the tunnel circumference and  $d$  is the depth of water above ground surface (cited by Lei, 1999).

Goodman et al. (1965) derived an approximate formula for the steady inflow rate along the length of a tunnel that is located under a lake or large river, which counts the lake or river as an infinite source of water.

$$Q_L = 2\pi KH_0 / \ln(2D/R) \quad 2.38$$

where  $Q_L$  is the inflow per unit length of tunnel,  $H_0$  is the water head above the tunnel,  $D$  is the distance from the bed of the lake to the center of tunnel,  $R$  is the radius of tunnel and  $K$  is the hydraulic conductivity.

Lei (1999) developed an analytical formula founded on the Polubarinova-Kochina formula (1962) for hydraulic head, the flow function and the in-flux rate of a 2D steady water flow close to a horizontal tunnel. The state considered is a tunnel existing in a wholly saturated, homogeneous and isotropic soil, and where a fixed hydraulic head state is reached around the tunnel circumference; the exact formula of steady inflow for tunnel is:

$$Q = \left( \frac{2\pi KH_0}{\ln\left(\frac{H_0}{R} + \sqrt{\left(\frac{H_0}{R}\right)^2 - 1}\right)} \right) \quad 2.39$$

where  $Q$  is the groundwater discharges,  $K$  is the coefficient of permeability,  $R$  is the radius of tunnel and  $H_0$  is the head of water above the tunnel.

Farhadian et al., (2012) researched the validity of several analytical equations referred to in Table 2.5, which were used to calculate the quantity of seepage into tunnels for different values of  $R/H$  (where  $R$  is the radius of tunnel and  $H$  is the head of water above the tunnel), by utilizing regression analysis. It was confirmed that the  $R/H$  rate has an impact on the precision of the analytical procedures used to compute the quantity of seepage into tunnels.

Table 2.5: Analytical formulas of seepage flow into circular tunnels

Authors	formulas
Goodman (1965)	$Q = 2\pi K \frac{H_0}{\ln\left(\frac{2D}{R}\right)}$
Freeze and Cherry (1979)	$Q = \frac{2\pi k H_0}{\ln\left(\frac{2H_0}{R}\right)}$
Heuer (1991)	$Q = \frac{2\pi k H_0}{\ln\left(\frac{2D}{R}\right)} \cdot 1/8$
Lei (1999)	$Q = 2\pi k \frac{H_0}{\ln\left(\frac{H_0}{R} + \sqrt{\left(\frac{H_0}{R}\right)^2 - 1}\right)}$
El-Tani (1999)	$Q = 2\pi k \frac{1 - 3\left(\frac{R}{2H_0}\right)^2}{\left[1 - \left(\frac{R}{2H_0}\right)^2\right] \ln\left(\frac{2H_0}{R} - \left(\frac{R}{2H_0}\right)^2\right)}$
Karlsruud (2001)	$Q = 2\pi k \frac{H_0}{\ln\left(\frac{2H_0}{R} - 1\right)}$
Lombardi (2002)	$Q = 2\pi k \frac{H_0}{\ln 2H_0/R [1 + 0.4\left(\frac{R}{H_0}\right)^2]}$

Several researchers have investigated the performance of footings resting on soil with cavities/voids. (Atkinson and Potts, 1977; Wang and Baus, 1980; Baus and Wang, 1983; Wang and Badie, 1985; Azam et al., 1991; Jao and Wang, 1998; Tahmasebipoor et.al. 2012) report that the existence of voids in the soil beneath the footing can cause instability in the foundation and thus damage the whole structure, and the collapse of soil under the loaded footing would be in the form of a wedge in the primary vacuum.

Khattab and Khalil (2009) used PLAXIS 2D and PLAXIS 3D software to study the effect of the existence of a cavity on the performance of the foundation. The influence of parameters such as horizontal location, depth, shape, size and the sectional area of a single cavity beneath the foundation base on the displacement and the distribution of stress was evaluated in this search. The results showed that the size and shape of the cavity influenced the displacement and stress concentration below the foundation for the chosen cavity sections (circular, elliptic, loaf, and square) when conducting both 2D and 3D analysis.

Lee et al. (2014) studied the effect of square voids on the stability of a surface strip footing located on undrained clay. PLAXIS 2D was used to calculate the factors for the vertical bearing capacity of footing for different geometrical and material variables such as the horizontal position of the void, the void's depth, the distance between the two voids, non-



homogeneity and the rigidity of soil. This study presents design charts to calculate the factors for vertical bearing capacity as a function of the width and height of voids, the vertical and horizontal distance between the footing and voids, and the distance between the two voids.

Jayamohan et al. (2015) carried out a numerical investigation using PLAXIS 2D to improve the bearing capacity of a strip footing situated over a weak, clayey soil containing circular voids by adding a reinforced foundation bed. A series of laboratory-scale load tests were performed to validate the finite element analysis results. Based on the experimental and numerical results, it was concluded that the influence of the void is significant when it is situated within a critical depth and critical eccentricity. It was also showed that the behaviour of load-settlement behaviour improved considerably with the addition of the foundation bed and the reinforced foundation bed. It was noted that there is a great concentration of stress near the void.

Lavasan et al. (2016) conducted a parametric study to examine the bearing capacity of a strip foundation built on soil containing twin circular voids using PLAXIS 2D software. This study involved some parameters related to the location of voids such as depth, position and eccentricity in addition to examining the effect of the size of footing/voids. It was shown that there is a critical horizontal distance between cavities and a critical depth at which the effects of cavities weaken the ultimate capacity of the foundation.

Al-Jazaairry and Sabbagh (2017) examined the effect of circular cavities on the behaviour of a strip footing subjected to an inclined load. An numerical study was conducted using PLAXIS 2D to estimate the failure of a strip footing situated over soil containing cavities. The study involved many cases; in all cases, the results indicated that there is a critical depth under the foundation where cavities have a minimal effect on the foundation. The results imply that this simulation could be used to analyse the load-carrying capacity of soil with a cavity. Moreover, the results demonstrate that the load-carrying capacity varies with the varying location and size of the cavities, and the depth of footing, when cavities are located above the critical depth. The results can be utilized to design a shallow foundation situated on this type of soil.

Many researchers have performed numerical and experimental investigations to study the influences of cavities or tunnels on the bearing capacity of piles (Mroueh and Shahrour,

2002; Cheng et al., 2004; Aziz et al., 2012; Ng and Lu, 2013; Basile, 2014). The results reveal that the impact of the existence of cavities or tunnels near a piled foundation in weak soil is could be problematic in the field of civil engineering.

Al-Taie et al. (2007) performed a laboratory study to examine the performance of horizontally loaded piles in soil containing circular cavities. A test device was manufactured for testing and cavities were simulated using a simple technique. The results imply that there is a conjoint influence between the number of cavities and their position on the performance of the pile; the influence of the cavities fades when the value of  $X/D$  is greater than 8, where  $X$  is the distance between the pile and cavity, and  $D$  is the pile diameter.

Maatooq et al. (2014) conducted an experimental investigation of the interaction between a circular cavity and an adjoining sheet pile embedded in a sandy soil. The investigation derived an expression that could be utilized to calculate the quantity of seepage considering the spacing between the sheet pile wall and the cavity centreline, located at the upstream and downstream zones, and the spacing between the cavity centreline and water level.

## 2.4 Conclusion

Numerous examples from the body of relevant literature have been reviewed with a view to establish the present level of knowledge in the field regarding the issues of stability and seepage through earth dams. A considerable amount of literature, both experimental and theoretical, has been published in this field of study; however, existing studies and research regarding the issues of stability and seepage through hydraulic structures, considering the impact of the existence of cavities, are very limited. It has been found that a large volume of research associated with the study of the seepage and stability were conducted on slopes and earth dams constructed on soils without the presence of cavities. More specifically, to the best knowledge of the author, the influence of the presence of cavities on the stability of the slopes and earth dams has not yet been investigated nor established. This chapter provided an overview of cavities and the reasons for their formation; seepage; factors affecting the stability of slopes and dams; the most important laws and theories related to slope stability and the seepage through slopes; and the effects, both hazardous and not, resulting from the existence of cavities. Therefore, this study is an attempt to investigate the impact of the presence of cavities on the slope stability of earth dams and on the seepage through these dams.

## CHAPTER THREE: METHODOLOGY

### 3.1 Introduction

Numerical methods are used to obtain approximate solutions when analytical solutions cannot be developed. With the advances in the field of geotechnics numerical modelling, numerical methods have become the methods most widely employed for analysing slope stability and water flow. In this chapter, an introduction to the PLAXIS 2D software used in the present study is presented, which includes an overview of the software, the general properties of the PLAXIS 2D model and two-dimensional (2D) modelling with PLAXIS 2D, presenting the constitutive models executed in the software and a description of the study model.

### 3.2 PLAXIS 2D software

PLAXIS 2D is a powerful and modernized finite element (FE) software package designed to simulate in 2D the problems of stability, deformation and groundwater flow in soil and rock mechanics. The evolution of the program started in 1987 at Delft University of Technology (Kahlström, 2013). Three subprograms constitute PLAXIS 2D: the calculation program, the output program and the input program. Since soil is a multi-stage material, specific methods are required to deal with hydrostatic and non-hydrostatic pore water pressures. To accurately simulate this extraordinary non-linear behaviour of soils and rocks, improvements have been made in PLAXIS 2D (PS and Balan, 2013). PLAXIS 2D consists of a set of constitutive models, which vary in complexity and the fields of applicability; it can calculate stresses and strains, and failure conditions; and it allows the creation of an entire automatic mesh based on the triangulation principle (Tahmasebipoor et al., 2012). It is used extensively (Brinkgreve et al., 2018) in various geotechnical-engineering applications – such as embankments, foundations, reservoir geomechanics and excavations. PLAXIS 2D software provides certain benefits from its soil stability or seepage calculations, compared to other similar kinds of geotechnical software (Wei et al, 2011).

### 3.3 General properties of the PLAXIS 2D model

Generating a geometry model is the first step in creating a 2D FE model. The geometry model is generated in the x-y plane of the global coordinate system, as shown in Figure 3.1, while the z-direction is the out-of-plane direction (cited by (Brinkgreve et al., 2018)). In the global coordinate system, the positive z-direction is towards the user. The compressive stresses and forces, which include pore pressure, are considered to be negative in all of the output data, while tensile stresses and forces are considered to be positive. Figure 3.1 shows the 3D Cartesian coordinate system, which forms the basis of the stresses, despite PLAXIS 2D is being a 2D software package. The out-of-plane stress is identified as  $\sigma_{zz}$  in a plane-strain analysis. The tangential direction is z, the axial coordinate is y and the radial coordinate is x in an axisymmetric analysis. The hoop stress is  $\sigma_{zz}$ , whereas the radial stress is  $\sigma_{xx}$  in this condition (Brinkgreve et al., 2018).

#### 3.2.1 Plane strain

It is preferred that this model is used for geometries with uniform cross-sections, and conformable stress cases and loading schema over a specific length perpendicular to the cross-section in the z-direction. The forces per unit length in the out-of-plane direction (z-direction) are regarded as the calculated forces resulting from given displacements in a plane-strain analysis (see Figure 3.1). Strains and displacements are supposed to be zero in the z-direction. Nevertheless, normal stresses in the z-direction are taken fully into account (Brinkgreve et al., 2018).

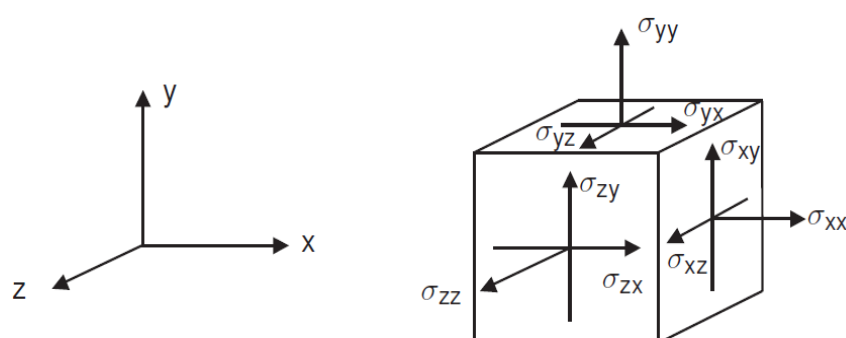


Figure 3.1: The coordinate system (PLAXIS, 2018)

### 3.2.3 Elements

The analysis carried out by PLAXIS 2D is either axisymmetric or plane strain with 6-node or 15-node triangular elements, as shown in Figure 3.2. The FE analysis is conducted in PLAXIS 2D by dividing the continuum into distinguished elements with nodes. For any problem, the unknowns within a specific group of boundary conditions must match the freedom degree, with separate values for each node (Brinkgreve et al., 2018). In this study, a freedom degree is associated with the displacement components. Every line element is split into three nodes, which are appointed displacement values, and which are involved in the six-node triangles, while the line of five points constructs a 15-node triangle (Brinkgreve et al., 2018).

#### 3.2.3.1 15-node triangle

One of the default elements is the 15-node triangle. A fourth-order interpolation for displacements is offered by the 15-node triangle and twelve Gauss points (stress points) are involved in the numerical integration. The soil element type chosen here is compatible with the type of element for structural elements and interfaces automatically. It is a very accurate element. High-quality stress findings are obtained for complicated problems using the 15-node triangle; for instance, to calculate the collapse for incompressible soils (Nagtegaal et al., 1974; Sloan, 1981; Sloan & Randolph, 1982). It is suggested that the 15-node triangle is used in axisymmetric analysis specifically. The use of 15-node triangles requires high memory consumption and more time in calculation and operation performance (Brinkgreve et al., 2018).

#### 3.2.3.2 6-node triangle

A second-order interpolation for displacements is provided by the 6-node triangle, and its numerical integration includes three Gauss points. The soil type chosen here should have automatic compatibility with the type of element used for structural elements and interfaces. It is a somewhat delicate element, and good findings are obtained in the standard deformation analyses provided that the number of elements used is adequate. Nevertheless, the axisymmetric models should be treated with caution, as should cases in which (possible) failure can play a role, such as analysing safety through a  $\phi$ - $c$  reduction or the calculation of bearing capacity. Using 6-node elements can cause the overprediction of failure or safety

factors (SF). For such instances, it is recommended that 15-node elements are used (Brinkgreve et al., 2018).

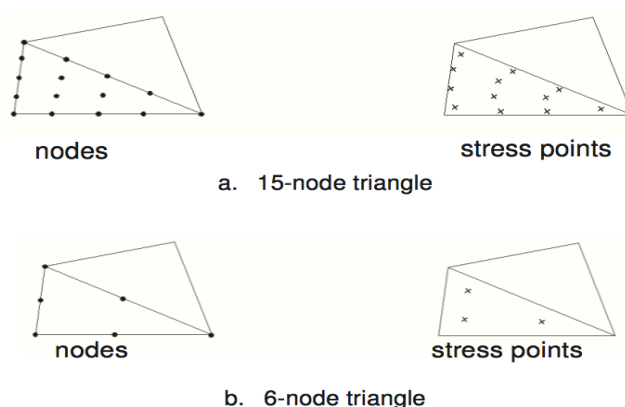


Figure 3.2: Position of nodes and stress points in triangular soil elements (PLAXIS, 2018)

### 3.4 PLAXIS 2D modelling

There are five modes in PLAXIS 2D that are used to complete the modelling process, namely soil, structures, mesh, flow conditions and staged construction. These five modes involve both Geometry and Calculation modes.

#### 3.4.1 Geometry modelling

The geometry modes are used to define the geometric configuration of the project, which are as follows:

**Soil:** The soil mode defines the soil stratigraphy, the initial conditions of the soil layers and the generic water levels.

**Structures:** The structures mode gives the definition of the geometric entities, along with the structural elements and forces in the project.

In general, the creation of a 2D geometry model in the x-y plane, and the definition of the material properties and boundary conditions are essential for performing an FE analysis utilizing the PLAXIS 2D software. The geometry model is a combination of points, lines and surfaces. When defining multiple boreholes to identify the soil stratigraphy at various positions, PLAXIS 2D will provide an automatic interpolation between boreholes, and it can derive the location of the soil layers from the borehole information. The upper and lower boundaries of the soil layers can differ through boreholes, which makes it possible to identify the non-horizontal soil layers with a non-uniform thickness (Brinkgreve et al., 2018).

### 3.4.2 Calculations

Once the geometry-modelling process is finished, the calculations stage starts, which comprises creating the mesh and defining the construction stages. Practically, a project is sectioned into phases. In a similar way, the program conducts the calculation process by dividing it into phases. Each calculation phase is partitioned into a number of computational steps. This procedure is essential because the behaviour of soil is non-linear, which needs loadings to be applied in small ratios. Nevertheless, in many cases, it is adequate to define the situation that must be reached at the end of a calculation stage. The sub-division into suitable load steps is performed by using automatic procedures in PLAXIS 2D. The flow conditions and staged construction modes define the construction stages. The stress field at the beginning of the initial geometry configuration, by means of Gravity loading or the K0 procedure, is always the first calculation stage. After that, the following calculation stages can be specified. The selection of the type of calculation must be done in every phase. In the calculation mode of the input program, the calculation operations are specified, which are as follows:

**Mesh:** In the mesh mode, the geometry model is disassembled and converted to a mesh of FEs.

**Flow conditions:** This mode defines and modifies the user specified.

**Staged construction:** In the staged construction mode, the calculation for the project is done (Brinkgreve et al., 2018).

#### 3.4.2.1 Mesh creation

To carry out FE calculations, the geometry has to be split into FEs after the definition of the complete geometry model. Mesh is the term used for a composition of FEs. To achieve exact numerical results, the mesh should be adequately fine. On the contrary, to avoid prolonged calculation times, very fine meshes should not be used. The PLAXIS 2D software allows the automatic generation of FE meshes in a variety of sizes, such as very coarse, coarse, medium, fine and very fine. A robust triangulation procedure is the basis for the creation of the mesh. The soil stratigraphy – along with all structural elements, loads and boundary conditions – is taken into consideration in the process of mesh creation (Brinkgreve et al., 2018).



### 3.4.2.2 Calculations phases

The FE calculations are divided into different sequential calculation phases. Every phase of the calculation corresponds with a specific loading or construction stage. The construction mode defines the construction stages. The calculation type of a phase must be defined as the first step for PLAXIS 2D analysis. The initial stress state of the soil is generated through the choices available in the initial phases, which are the K0 procedure and Gravity loading. The only option that can be utilized to carry out groundwater flow analysis is the Groundwater flow. The choices available to conduct deformation analysis are Dynamic, Fully coupled flow-deformation, Consolidation, Plastic, and Safety. There are nine phases of calculation in the safety analysis of earth dams. The dam is constructed in the first phase. The reservoir is filled to the required water level (standard) in the second phase. A steady-state groundwater flow calculation is used to calculate the water pressure distribution in such cases. Both the third and fourth phase begin from the standard position. A coupled flow-deformation calculation is used in both situations as calculation type. The fifth calculation stage also begins from the initial phase and considers the long-term behaviour of the dam (when the water level is low in the reservoir), which uses the steady-state flow calculation to compute the water pressure distribution. The phi-c reduction method is used to calculate the safety factor (SF) of the dam for all four water pressure cases. The current study considers the following cases (Brinkgreve et al., 2018):

- Water level stays at 12m (long-term condition).
- Water level falls rapidly from 12m to 4m.
- Water level falls slowly from 12m to 4m.
- Water level stays at 4m (long-term condition). See Figure 1 in Appendix A.

#### 3.4.2.2.1 Gravity loading

Gravity loading is one of the plastic calculations used to define the initial stresses of the subsoil in the initial stage. The generation of the initial stresses relies upon the unit weight of the soil. The computed initial in situ stresses should be compared to the soil investigation reports to make sure that the correct values are generated for the initial stresses. For this stage, a steady-state flow calculation is used to calculate the water pressure distribution (Brinkgreve et al., 2018).

### 3.4.2.2.2 Fully-coupled flow-deformation

This calculation approach is utilized to carry out the third and fourth phases, which begin after the initial phase (e.g. the reservoir water level at 12m and then the water level is depressed to 4m). There are distinct differences in the time periods in which this is done (i.e. there are various speeds of water level lowering: rapid drawdown and slow drawdown). A fully coupled flow-deformation analysis is performed in the case of needing to analyse the simultaneous development of deformations and pore pressures in saturated and partially saturated soils due to the time-dependent alterations of the hydraulic boundary conditions. The analysis of the fully coupled flow-deformation considers the behaviour of the unsaturated soil and the suction in the unsaturated area above the phreatic level (Brinkgreve et al., 2018).

### 3.4.2.2.3 Plastic calculation

The fifth calculation is performed when the water level in the reservoir is low (the long-term behaviour). This calculation phase is utilized to conduct an analysis of elastic-plastic deformation, where the time is not taken into consideration in the change of pore pressure. The plastic calculation is suitable for most of the applications of practical geotechnical. Though a time interval can be defined, the time influences are not considered by a plastic calculation unless the Soft Soil Creep model is utilized (Brinkgreve et al., 2018).

### 3.4.2.2.4 Safety calculation

This type is the choice available in PLAXIS 2D to estimate SF. Till the structure fails, this approach performs the successive reduction of the shear strength parameters –  $\tan \phi$  and  $c$  – of the soil, along with the tensile strength.

At a certain stage in the analysis, the values of strength parameters are expressed by the total multiplier  $\Sigma Msf$ :

$$\Sigma Msf = \frac{\tan\phi_{input}}{\tan\phi_{reduced}} = \frac{C_{input}}{C_{reduced}} = \frac{S_{u,input}}{S_{u,reduced}} = \frac{Tensile\ strength_{input}}{Tensile\ strength_{reduced}} \quad 3.1$$

S represents the shear strength. The parameters' subscript 'reduced' means the reduced values implied in the analysis, while the strength parameters' subscript 'input' means the properties introduced in the material sets. When the calculation begins to place all material

strengths at their input values, the  $\Sigma Msf$  is set to 1.0. The ‘load advancement number of steps’ procedure is used to carry out safety calculations. The increment of the strength reduction of the first calculation step is specified through the incremental multiplier  $Msf$ . Until the completion of every step, the successive reduction of the strength parameters is done automatically. A fully developed failure mechanism must occur after the final step, and this should be closely monitored. The SF in such a situation is given by the following:

$$SF = \frac{\text{available strength}}{\text{strength at failure}} = \text{value of } \Sigma Msf \text{ at failure} \quad 3.2$$

The SF that is traditionally utilized in soil mechanics is the ratio of real strength to the minimum strength needed for equilibrium. As the stress-dependent stiffness behaviour and hardening effects are not included in the analysis, these models will act as a standard Mohr-Coulomb (MC) model in reality when utilizing the safety calculation combined with advanced soil models. In such a situation, the starting stresses are used at the beginning of the calculation phase to estimate the stiffness. It is kept the same until the completion of the calculation phase. The SFs achieved from the strength-reduction method chosen for the safety calculation are similar to those obtained using the traditional slip-circle analysis (Brinkgreve et al., 2018).

### 3.5 Seepage theory

PLAXIS 2D has specific advantages regarding the stability calculation of soil or seepage calculation over other geotechnical programs (Wei et al, 2011). PLAXIS comprises engineering creation tools and automatic settings to permit efficient and accurate analysis of geotechnical problems with minimal training (PS and Balan, 2014).

In PLAXIS 2D, the theory of groundwater percolation is principally dependant on the percolation theory of FEs. Darcy’s law describes the flux in porous media, considering the vertical flux inside the x-y plane:

$$q_x = -k_x \frac{\partial \phi}{\partial x}; q_y = -k_y \frac{\partial \phi}{\partial y} \quad 3.3$$

where  $q$  is the seepage rate. The acquired permeability and groundwater head gradient are used to calculate the flow rate. The head can be defined as follows:

$$\phi = y - \frac{p}{\gamma_w} \quad 3.4$$

where  $y$  is the vertical location and exemplifies the negative pore water pressure. In the case of the steady-state flow, the terms of persistent application are as follows:

$$\frac{\partial q_x}{\partial x} + \frac{\partial q_y}{\partial y} = 0 \quad 3.5$$

Equation 3.3 expresses the total amount of water flowing into the unit body total water per unit of time and is equal to the outflow (cited by Qizhi et al., 2017). After finishing the simulation of the discrete objects, the conformable groundwater head is utilized in any position within cell to define the values of the node cell:

$$\phi = (\xi, \eta) = N\varphi^e \quad 3.6$$

where  $N$  is the shape function, and  $\xi$  and  $\eta$  show the local coordinates. According to Equation 3.6, the flow rate depends on the groundwater head gradient. The gradient matrix can be specified. It is necessary to introduce the reduction function in Darcy's law to characterize saturated soil and unsaturated soil:

$$q_x = -K^r k_x \frac{\partial \phi}{\partial x}; q_y = k_y \frac{\partial \phi}{\partial y} \quad 3.7$$

The reduction function value beneath the saturation line is equal to 1, while the value up the phreatic line is equal to -1. The function value is lessened to  $10^{-4}$  in the transition region above the phreatic line. In the transition region, the logarithmic function has a linear relationship:

$$\lg K^r = - \frac{4p}{p_k} \quad 3.8$$

where  $p$  is the head pressure and  $p_k$  is the head pressure where the reduction function decreases to the head pressure of  $10^{-4}$  (F/L<sup>2</sup>). In PLAXIS 2D, the default is 0.7m (with the selected unit of length has nothing to do), (cited by Qizhi et al., 2017). The proportion of flux

is expressed as follows:

$$q = -K^r RB \phi^e \quad 3.9$$

The flux from the node ratio is gained by integrating the node traffic:

$$Q^e = - \int B^T q dV \quad 3.10$$

where  $B^T$  represents the transfer matrix. The next formula applies at the unit level:

$$Q^e = K^e \phi^e; K^e = \int K^r B^T RB_q dV_0 \quad 3.11$$

On a global level, all units of contributions are superimposed, and boundary conditions are applied (groundwater flow and head loss), which take the form of  $n$  unknown quantities of  $n$  equations (cited by Qizhi et al., 2012):

$$Q = K\phi \quad 3.12$$

where  $K$  is a global traffic matrix, and  $Q$  comprises the boundary conditions specified as flux losses.

### 3.5.1 Flow condition

In general, effective stress analysis is utilized in PLAXIS. It is known that the total stress is the sum of the effective stress,  $\sigma'$ , and active pore pressures,  $p_{active}$ .

$$\sigma = \sigma' + p_{active} \quad 3.13$$

where  $p_{active}$  is the active pore pressure, which is represented as the effective saturation  $S_{eff}$ ,  $p_{water}$  is times the pore water pressure.

$$p_{active} = S_{eff} \cdot p_{water} \quad 3.14$$

There is variation between the pore water pressure and active pore pressure when the value of the saturation degree is lower than unity. PLAXIS 2D can simulate the behaviour of saturated soil beneath the phreatic level and partly saturated soil above the phreatic level.

Additionally, pore pressure is divided into steady-state pore pressure,  $p_{steady}$ , and excess pore pressure,  $p_{excess}$ :

$$p_{water} = p_{steady} + p_{excess} \quad 3.15$$

Excess pore pressure occurs due to stress alterations in undrained materials (Brinkgreve et al., 2018).

### 3.5.2 Boundary condition

The determination of which boundaries are ‘open’ and which are ‘closed’ is termed the flow boundary conditions of a phase. The position of the flow of water into or out of the soil is defined by the flow boundary conditions in a groundwater flow or fully coupled flow-deformation analysis. Thus, in such situations, the entire pore pressure is affected (Brinkgreve et al., 2018).

### 3.6 Staged construction

Staged construction loading is chosen in PLAXIS 2D for performing stability analysis. The time interval of the calculation phase should be considered prior to the specification of the construction stage. The unit of time is used to express the time interval. The load advancement ultimate level procedure is used to conduct staged construction by calculating a total multiplier ( $\Sigma M_{stage}$ ). The multiplier begins at zero and is supposed to attain the final level of 1.0 at the end of some specific cases (Brinkgreve et al., 2018). Nevertheless, it may be necessary to divide the staged construction operation into more than one calculation phase and to assign a moderate value for  $\Sigma M_{stage}$ . This is widely applied for embankments that are built quickly, such as upstream constructions. The slow loading during staged construction greatly dissipates the load-induced pore pressures (Vick, 1990).

### 3.7 Soil modelling

The behaviour of soil is very complex and differs greatly under various loading conditions. Basically, soil behaves in an elasto-plastic manner. No constitutive model can fully depict the complicated behaviour of various soils under various loading cases. There are specific limitations and benefits to all models, depending upon their particular application (Levasseur et al., 2014). At present, the constitutive soil models can be roughly divided into three categories: elastic models (e.g. the elastic model and Duncan-Chang [DC] model), elastic-ideal plastic models (e.g. the MC model and the Drucker-Prager [DP] model), and strain hardening elastoplastic models (e.g. the Modified Cam Clay [MCC] model and Hardening Soil [HS] model). Although the most commonly used is the MC model, the most significant applications in soil-nature simulations are the MCC model and the HS model (Zhonghua and Weidong, 2010; Feng and Po, 2011). The mathematical framing for the soil defines deformations in soils resulting from alterations in the present stress conditions. PLAXIS 2D includes various simple and advanced models that vary in their ability to model the mechanical behaviour of soils and rocks. The relationship of stress and strain in the material forms the basis of the design of all the models. The constitutive models include the MC, Modified Cam Clay, HS, HS with small-strain stiffness, Soft Soil, Soft Soil Creep, and Jointed Rock models (Brinkgreve et al., 2018). However, within the scope of the current study, two of the most widely used constitutive models have been adopted to model the behaviour of soil materials, namely the MC and HS models, and these are presented in the next sections of this chapter.

#### 3.7.1 MC model

In the case where the soil undergoes alterations of stress or strain, its behaviour becomes non-linear. In the PLAXIS 2D software, the advanced soil models comprise some such characteristics. The MC model is a linear elastic-perfectly plastic model, which is simple and commonly used; the initial estimation of soil behaviour can be done by using the MC model. The linear elastic portion of it is dependent on Hooke's law, while the perfectly plastic portion is dependent on the MC failure criterion. The simplicity of this model enables it to be used in numerous studies; also, it does not require many parameters. Irreversible strains are associated with the concept of plasticity. Therefore, to assess plastic points, a subordinate of stress-strain capitulation is inserted as a phase in a prime stress environment. Apparently, few points in the surrender level have fully flexible behaviour. According to this model, the strain

and the rate of strain are constituted from elastic and plastic parts. This means the following is true:

$$\underline{\dot{\sigma}}^e = \underline{D}^e \dot{\epsilon}^e = \underline{D}^e (\dot{\epsilon} - \dot{\epsilon}^P) \quad 3.16$$

Plastic strains are based on the ratio of a derived surrender function to stresses, as per plasticity theory (Hill,1950), where plastic strains can be deemed to be vectors columnar to the surrender level. The relation between the rates of effective stress and effective strain can be achieved based on this:

$$\underline{\dot{\sigma}} = \left( \underline{D}^e - \frac{\alpha}{a} \underline{D}^e \frac{\partial g}{\partial \underline{\sigma}} \frac{\partial f^T}{\partial \underline{\sigma}} \underline{D}^e \right) \underline{\dot{\epsilon}} \quad 3.17$$

In this equation  $d = \frac{\partial g}{\partial \underline{\sigma}} \underline{D}^e \frac{\partial f^T}{\partial \underline{\sigma}}$

Moher- Coulomb surrender standard has been according to main stresses and comprises of a hexahedron cone in major stress environment can be shown as a general equation;

$$f_{(i,j,k)} = \frac{1}{2} \left| \left[ \dot{\sigma}_{(j,k,i)} - \dot{\sigma}_{(k,i,j)} \right] \right| + \frac{1}{2} \left| \left[ \dot{\sigma}_{(j,k,i)} + \dot{\sigma}_{(k,i,j)} \right] \right| \sin \phi - c \cos \phi \leq 0 \quad 3.18$$

where k, j and i are 2, 3 and 1, respectively; while  $\phi$  and C are the cohesion and soil fraction degree.

The  $\Psi$  parameter is the dilatation angle, which can be modelled using its aid volume strain for saturated soils.

### 3.7.1.1 Formulation of the MC model

The mechanical behaviour of soils has been formulated with different degrees of accuracy. In PLAXIS 2D, the MC failure criterion can be used to interpret the soil behaviour at failure; this is the model that is used in this research. Five parameters are required to create an MC model: cohesion (c), the angle of internal friction ( $\phi$ ), Young's modulus (E), Poisson's ratio ( $\nu$ ) and the angle of dilatancy ( $\psi$ ). The formulation of the MC model is based on Coulomb's friction law, and consists of six yield functions (Brinkgreve et al., 2018):

$$f_{1a} = \frac{1}{2} (\sigma'_2 - \sigma'_3) + \frac{1}{2} (\sigma'_2 + \sigma'_3) \sin \phi - c \cos \phi \leq 0 \quad 3.19$$



$$f_{1b} = \frac{1}{2} (\sigma'_3 - \sigma'_2) + \frac{1}{2} (\sigma'_3 + \sigma'_2) \sin\phi - c \cos\phi \leq 0 \quad 3.20$$

$$f_{2a} = \frac{1}{2} (\sigma'_3 - \sigma'_1) + \frac{1}{2} (\sigma'_3 + \sigma'_1) \sin\phi - c \cos\phi \leq 0 \quad 3.21$$

$$f_{2b} = \frac{1}{2} (\sigma'_1 - \sigma'_3) + \frac{1}{2} (\sigma'_1 + \sigma'_3) \sin\phi - c \cos\phi \leq 0 \quad 3.22$$

$$f_{3a} = \frac{1}{2} (\sigma'_1 - \sigma'_2) + \frac{1}{2} (\sigma'_1 + \sigma'_2) \sin\phi - c \cos\phi \leq 0 \quad 3.23$$

$$f_{3b} = \frac{1}{2} (\sigma'_2 - \sigma'_1) + \frac{1}{2} (\sigma'_2 + \sigma'_1) \sin\phi - c \cos\phi \leq 0 \quad 3.24$$

where  $\phi$  and  $c$  are the parameters of the plastic model. “The condition  $f_i = 0$  for all yield functions (where  $f_i$  is used to denote each individual yield function) represents a fixed hexagonal cone in principal stress space” (cited by (Brinkgreve et al., 2018)). Six plastic potential functions can be defined for the MC model, as follows:

$$g_{1a} = \frac{1}{2} (\sigma'_2 - \sigma'_3) + \frac{1}{2} (\sigma'_2 + \sigma'_3) \sin\psi \quad 3.25$$

$$g_{1b} = \frac{1}{2} (\sigma'_3 - \sigma'_2) + \frac{1}{2} (\sigma'_3 + \sigma'_2) \sin\psi \quad 3.26$$

$$g_{2a} = \frac{1}{2} (\sigma'_3 - \sigma'_1) + \frac{1}{2} (\sigma'_3 + \sigma'_1) \sin\psi \quad 3.27$$

$$g_{2b} = \frac{1}{2} (\sigma'_1 - \sigma'_3) + \frac{1}{2} (\sigma'_1 + \sigma'_3) \sin\psi \quad 3.28$$

$$g_{3a} = \frac{1}{2} (\sigma'_1 - \sigma'_2) + \frac{1}{2} (\sigma'_1 + \sigma'_2) \sin\psi \quad 3.29$$

$$g_{3b} = \frac{1}{2} (\sigma'_2 - \sigma'_1) + \frac{1}{2} (\sigma'_2 + \sigma'_1) \sin\psi \quad 3.30$$

The angle of dilatancy,  $\psi$ , is the third plasticity parameter. “This parameter is required to model positive plastic volumetric strain increments (dilatancy) as actually observed for dense soils.” (cited by (Brinkgreve et al., 2018)).

### 3.7.2 HS model

In 1999, in the framework of the elasticity theory, the HS model was established by (Schanz et al., 1999). Rowe’s stress-dilatancy theory (1962) is the foundation for describing the plastic strain behaviour of this model. The elastic and plastic strains are calculated based on the stiffness of the surface tension, and this stiffness differs for the initial loading/unloading

(Obrzud, 2010). This model is an advanced model and is used to simulate the behaviour of various kinds of soil, whether they are soft or stiff (Schanz, 1998). The exposure of the soil to the fundamental deviatoric loading leads to a decrease in its hardness and the development of irreversible plastic strains concurrently. A hyperbola is used to approximate the identified relation between the axial strain and the deviatoric stress in the specific situation of a drained triaxial test. This relation was first developed by Kondner (1963) and utilized subsequently in a popular hyperbolic model (Duncan & Chang, 1970). However, the HS model largely replaces the hyperbolic model: firstly, by utilizing the plasticity theory instead of elasticity theory; secondly, by incorporating soil dilatancy; and, thirdly, by considering the yield cap. The HS model is a more appropriate alternative, as it considers plasticity theory, allows the entry of dilatation parameters, and considers soil hardness in relation to stress and strain. In consolidation conditions, the feature of this model relating soil hardness to stress is expressible as follows:

$$E_{oed} = E_{ode}^{ref} (\sigma / p^{ref})^m \quad 3.31$$

It is assumed that  $m = 1$  for soft soils, which is close to reality.

$$E_{ode}^{ref} = P^{ref} / \lambda^* \quad 3.32$$

$$\lambda^* = \lambda / (1 + e_0) \quad 3.33$$

where  $p^{ref}$  is the reference stress and  $\lambda^*$  is the modified compression index. Similarly, the flexibility ratio for unloading and reloading can be related to the modified inflation ratio of  $K^*$ :

$$E_{ur}^{ref} = 3P^{ref} (1 - 2v_{ur}) / K^* \quad 3.34$$

$$K^* = K / (1 + e_0) \quad 3.35$$

where  $v_{ur}$  is the Poisson ratio of unloading and re-loading.

The influence of soil movement or secondary subsidence that happens significantly in the long term is not considered in this model.

The friction angle ( $\Phi$ ), cohesion ( $c$ ) and dilation angle ( $\Psi$ ) are used to define the limited stress status for the MC model. However, in the HS model three different inputs, the three-axis loading ( $E_{ode}$ ), hardness of three-axis unloading ( $E_{ur}$ ), and the hardness of oedometer loading are used to describe the soil stiffness more precisely. The major difference of the MC model to the HS model is that the HS model is subject to stress and considers the hardness. This means that the hardness increases with pressure in all cases; i.e. as the pressure increases, so does the hardness. Hence, the estimate for each of the three hardness values associated with the reference stress is 100kPa (Mollaei et al., 2015). The capability to simulate hardening behaviour is the most significant characteristic of the HS model (Schanz and Vermeer 1998). Moreover, there is greater flexibility in modelling using the HS model and it uses more input parameters (Keyvanipour et al., 2012).

### 3.8 2D slope stability analyses

2D techniques are employed in evaluating slope stability in the case where plane strain is presumed, which supposes that the slip surface is infinitely wide, and hence the three-dimensional (3D) effects are insignificant because of the infinite width of the sliding mass. In reality, slopes are not infinitely wide and the 3D effects impact slope stability (Duncan, 1992). In addition, 3D analyses are considered more accurate in terms of their ability to make calculations using the 3D nature of model (Griffiths and Marquez, 2007). On the other hand, some cases do not require 3D analysis as those issues can be resolved through simple assumptions in 2D analyses (Zebarjadi Dana et al., 2018). 2D methods remain the most widely used methods in slope stability analysis, despite the limitations of these 2D methods. The main reason for this obvious omission is that 2D analysis is convenient for assessing slope stability because it gives a conservative estimate of the SF (a lower SF), as proved in many studies: (Duncan, 1992; Cheng et al., 2005; Nian et al., 2012; Leong and Rahardjo, 2012; Stark and Eid, 1998; Chaudhary et al., 2016; Hungr, 1987; Zheng et al., 2011; Arellano and Stark, 2000; Lam and Fredlund, 1993; Eid et al., 2006; Cavoundis, 1987). Anagnosti (1969) introduced the first 3D technique for analysing slope stability and calculating the 3D SF. A comparison of the traditional 2D analyses and this method showed that a 3D SF can be 50% greater than a 2D SF. According to (Lefebvre and Duncan, 1971), the variations in estimates are caused by 2D analyses overlooking the end effects. Duncan (1996) stated that the difference between the SF obtained from both analyses does not exceed 15%. (Cavoundis,

1987) reported that the 2D SF is less than the 3D SF, and 3D methods may include simplified assumptions that ignore significant sides, giving a ratio of 2D SF to 3D SF that is greater than 1. 2D analysis can be used instead of 3D analysis when the difference between them is small (Zheng et al., 2011).

In comparison to the 3D analysis, in the 2D slope stability analysis it is easier to construct the model and complete the simulation in a relatively shorter time, (Shen and Karakus, 2013; Wines, 2016), while the 3D stability analyses require harder and more complex data input (Leong and Rahardjo, 2012). However, there are also several benefits of using 3D analyses, which include the utilization of more-realistic geometry, boundary conditions, groundwater conditions and in situ stress conditions. These aspects help to enhance the authenticity of the analysis results and gives an efficient viewpoint on the issue and possible failure mechanism. These are the basic differentiators between 2D and 3D analyses (Griffiths and Marquez, 2007; Wines, 2016; Shen and Karakus, 2013).

In recent decades, the 2D techniques have been accepted increasingly in the analysis of slopes (Griffiths and Lane, 1999; Cheng et al., 2007).

### **3.9 Model setup with PLAXIS 2D**

The steps for the model setup in PLAXIS 2D software are described in appendix A.

### **3.10 Study models**

A model of an earth dam and a cavity were conducted using PLAXIS 2D finite element software in order to simulate the slope stability and seepage through earth dams, considering the impact of the existence of cavities coupled with rapid-drawdown conditions.

#### **3.10.1 Earth dam model**

A model of an earth dam was created by means of PLAXIS 2D with an assumption of plane-strain conditions. A fine FE mesh was selected for modelling the soil embankment and the subsoil. An appropriate mesh for the required calculation accuracy was selected by refining the mesh until the outcomes did not differ considerably by refining further. Since the calculation time is significant in conducting the analyses, this procedure ensures selecting mesh with adequate accuracy to conduct the calculations in the least possible time

(Brinkgreve et al., 2018). The FE mesh used is displayed in Figure 3.3. The mesh was created with 15-node triangular elements. This element gives a fourth-order interpolation for displacements, and it includes 12 numerical integration stress points. Higher-quality stress analysis results can be produced by using 15-node triangle elements compared to 6-node (Brinkgreve et al., 2018). The earth-dam model was composed of 356 soil elements, 3005 nodes and 4272 stress points, with the average element size equal to 1.168m. The earth-dam model is 15m from the crest to the subsoil, the dam crest width is 6m and the depth of subsoil is 20m. The upstream and downstream slopes are inclining 1:2.5 (vertical: horizontal). All geometric dimensions of the dam model were assumed in accordance with the recommendations of the British Dam Society (BDS) (1994), as shown in Table 1. Water could flow through all boundaries, except at the bottom boundary of the model (Brinkgreve et al., 2018). The initial reservoir water level was assumed to be at a height of 12m from the ground surface (high water level); thereafter, it was speedily reduced to a level of 4m (low water level) over 5 days to simulate rapid-drawdown conditions. The geometry of the earth dam model is depicted in Figure 3.4.

### 3.10.2 Cavity modelling

Cavities were modelled using PLAXIS 2D software as ideal holes without any lining and created by extracting elements from the soil mass in the FE model (the 2D tunnel model was created using PLAXIS in Structures mode to create model cavities). The tunnel's cross section consists of lines and arcs, which are provided optionally, with features such as lining, facades, load, specified displacement, boundary flow conditions, etc. PLAXIS 2D provides three options for the tunnel shape: free, circular, and full or half-tunnel. Within the scope of the present study, the free and circular shapes were selected to simulate the effect of both irregularly shaped and circular cavities on slope stability and seepage through simulated earth-dam models (Brinkgreve et al., 2018). The steps of the cavity model setup in PLAXIS 2D software are described in appendix A. Figure 3.5 shows the geometry of the cavity with details of parameters, while Figure 3.6 shows the shapes of the cavities used in the study.

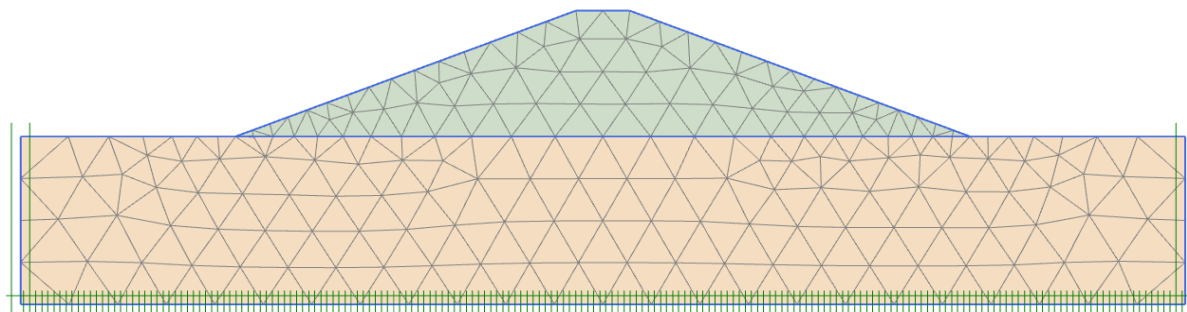


Figure 3.3: The finite element mesh in PLAXIS 2D for study model

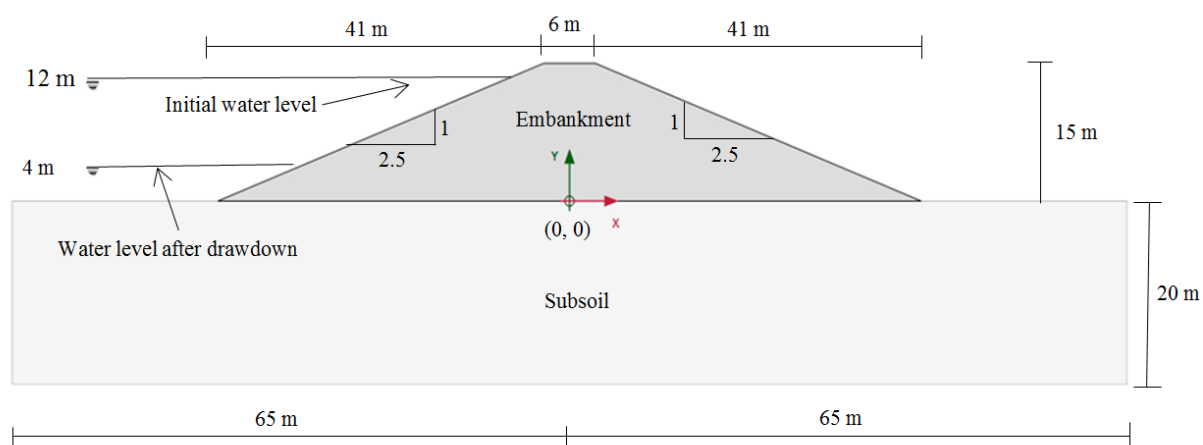


Figure 3.4: Geometry of the considered earth dam model

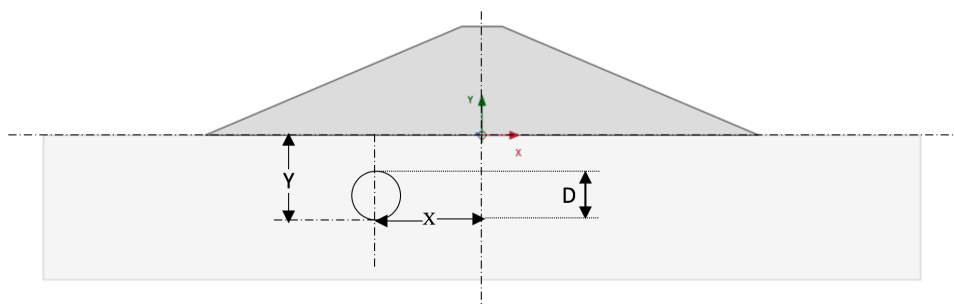


Figure 3.5: The geometry of the cavity

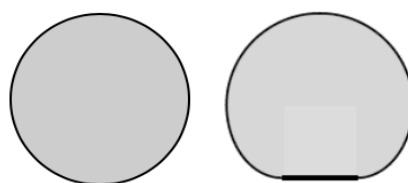


Figure 3.6: A scheme of the shapes of the cavities

Table. 3.1: Comparison between the parameters of numerical model and BDS safety standards (1994)

Parameters	Earth dam model	Safety standard	Case of dam safety
Crest width	3.0m	Minimum 2.0m	Agreeable
Upstream slope	1:2.5	Minimum 1:2.5	Agreeable
Downstream slope	1:2.5	Minimum 1:2	Agreeable
Free board	3m	Minimum free board 1.5m	Agreeable

## CHAPTER FOUR: STABILITY ANALYSIS

### 4.1 Introduction

This chapter includes the numerical analyses and results that were performed to simulate the impact of the existence of cavities in the subsoil of an earth dam on the stability of its slopes. PLAXIS 2D was used to develop models and analyse the slope stability while considering rapid-drawdown conditions.

In this study, two main series of analyses were conducted. In the first, the earth dam was modelled using the Mohr-Coulomb (MC) model; whereas, in the second, the embankment and subsoil were modelled using the Hardening Soil (HS) and MC models, respectively. The study involved two primary sections. For the first section, which is to study the effects of the existence of cavities on the slope stability of an earth dam, the following geometric parameters of the cavity are considered:

- Cavity position (X): This is the horizontal distance between the cavity's centreline and the earth dam's centreline.
- Cavity depth (Y): This is the vertical distance between the embankment's base and the cavity's centreline
- Cavity shape: Most research works carried out in various geotechnical engineering fields have paid great attention to studying the effect of circular cavities (Al-Jazaairry, 2017; Jayamohan et al., 2015; Tahmasebipoor et al., 2012). However, in fact, the cavities might be formed in different sizes and irregular forms under the ground surface (see Figure 1.1). Consequently, this study involves an attempt to assess the influence of the existence of both irregular and circular cavities on the stability of earth dams.
- Cavity diameter (D): This is the diameter of the cavity. According to Aziz (2008), cavities can form in various shapes and sizes underground, and their sizes range between 10cm and 300cm. Accordingly, cavities with diameters of 20cm, 60cm and 100cm were adopted.
- The number of cavities: The impact of the existence of more than one cavity on the slope stability of the earth dam is studied. It is worth mentioning that most research in the various geotechnical engineering applications has addressed the influence of a single cavity (Khattab and Khalil, 2009).



The second section involves an evaluation to the joint impact of the existence of cavities and the embankment's shear-strength parameters (cohesion and the angle of internal friction) on stability.

## 4.2 Study models

The stability analyses were conducted utilizing the numerical models (earth dam and cavities) developed in PLAXIS 2D, as previously presented in section 3.6.

## 4.3 Parameters involved in the constitutive modelling

Due to the fact that critical slip surfaces pass into the body of the dam (embankment), both constitutive models MC and HS were utilized for modelling the embankment, however, the subsoil was modelled using the MC model in all analyses. Table 4.1 presents the input parameters of the MC model implemented in PLAXIS 2D modelling, while Table 4.2 shows the input parameters of the HS model.

Table 4.1: Input parameters of the MC used in the first series

Parameters	Embankment	Subsoil	Unit
Model	Mohr-Coulomb	Mohr-Coulomb	
Drainage type	Drained	Drained	
$\gamma$ unsaturated	16.0	17.0	kN/m <sup>3</sup>
$\gamma'$ saturated	20.0	21.0	kN/m <sup>3</sup>
$v'$	0.33	0.3	
$C'$	25	5.0	kN/m <sup>2</sup>
$\psi, \phi'$	0, 22.5	5.0, 35.0	Degree
$k_x, k_y$	1E-4	0.01	m/day
$E'$	2.0E4	5.0E4	kN/m <sup>2</sup>

Table 4.2: Input parameters of the models used in the second series

Parameters	Embankment	Subsoil	Unit
Model	Hardening Soil	Mohr-Coulomb	
Drainage type	Drained	Drained	
$\gamma$ unsaturated	16.0	17.0	kN/m <sup>3</sup>
$\gamma$ ' saturated	20.0	21.0	kN/m <sup>3</sup>
$v$ '	0.33	0.3	
$C$ '	25	5.0	kN/m <sup>2</sup>
$\psi, \phi$ '	0, 22.5	5.0, 35.0	Degree
$k_x, k_y$	1E-4	0.01	m/day
$E_{50}^{ref}$	25.0E3		kN/m <sup>2</sup>
$E_{ode}^{ref}$	25.0E3		kN/m <sup>2</sup>
$E_{ur}^{ref}$	75.0E3		kN/m <sup>2</sup>

#### 4.4. Impact of the cavity location

The horizontal and vertical impact of the existence of cavities on stability was analysed in this study. In order to assess the impact of a cavity's horizontal position, fifteen positions in the subsoil of the upstream and downstream sides of the earth dam were selected. These positions were randomly distributed to cover the embankment base. The coordinates of the hypothetical horizontal positions of cavities as listed in Table 4.3. To simulate the impact of cavity depth, four hypothetical depths under both sides of the dam model were chosen;  $Y=1\text{m}, 2\text{m}, 3\text{m}$  and  $4\text{m}$ . The stability analyses carried out considered the existence of a single circular cavity of 60cm diameter.

Table 4.3: Coordinates of the locations of cavities in X and Y directions

Cavity location	Cavity depth (Y), m	The coordinates of position in X-axis (X), m	
		Upstream side	Downstream side
L1	1	0	0
L2	1	-8	+8
L3	1	-17	+17
L4	1	-20	+20
L5	1	-24	+24
L6	1	-28	+28
L7	1	-35	+35
L8	1	-40	+40

#### 4.4.1 Impact of the cavity location modelled using the MC model

Analyses were done using the MC model to model the earth dam considering the creation of a cavity at a depth of 1m beneath the upstream and downstream sides. The coordinates of the horizontal positions of cavities as detailed in Table 4.3.

Figure 4.1 illustrates the effect of the horizontal position of a cavity on upstream stability, which is expressed by the values of the safety factor (SF), whereas Figure 4.2 shows the impact on the values of maximum total displacement. As revealed in these figures, the existence of a cavity reduces the stability of the upstream slope noticeably: the SF decreased from 2.036 for models without a cavity to 0.715 for models with a cavity at location L2 (-8, -1), respectively. Also, the value of the maximum displacement increased from 24.91mm to 29.46mm for the same models. This behaviour is due to the decreasing strength of the subsoil because of the presence of the cavity, as well as a possible intersection between the cavity and the slope-failure surfaces, incurring further weakness, as shown in Figure 4.3. It is clear that the stress-concentration area started to expand within the sliding mass concentrated above the cavity at location L2 (-8, -1), where the horizontal distance from the dam's centreline increased to its end (from L2 (-8, -1) to L8 (-40, -1)). Consequently, the SF values increased from 0.715 to 1.966, while the displacement values decreased from 29.46mm to 24.83mm for models with cavity at locations L2 and L8, respectively (see Table 2 for the details of the positions). It is worth mentioning that the SF value for the model with a cavity at L2 is less than the minimum acceptable value (1.2–1.3), thus the dam is considered to be unsafe according to the criterion for the stability of an earth dam during rapid-drawdown conditions (NRCS, 2005; USBR, 2011; ULDC, 2012).

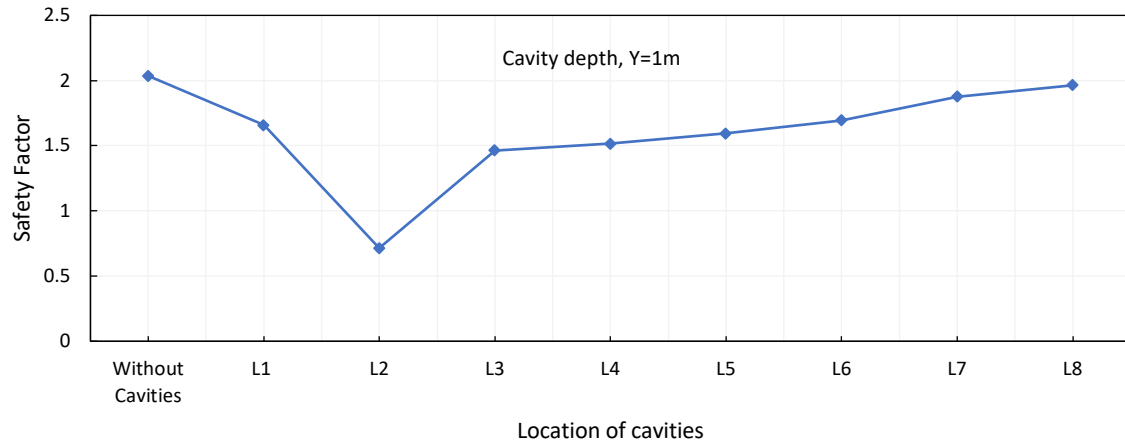


Figure 4.1: SF vs location of a cavity under upstream using the MC model

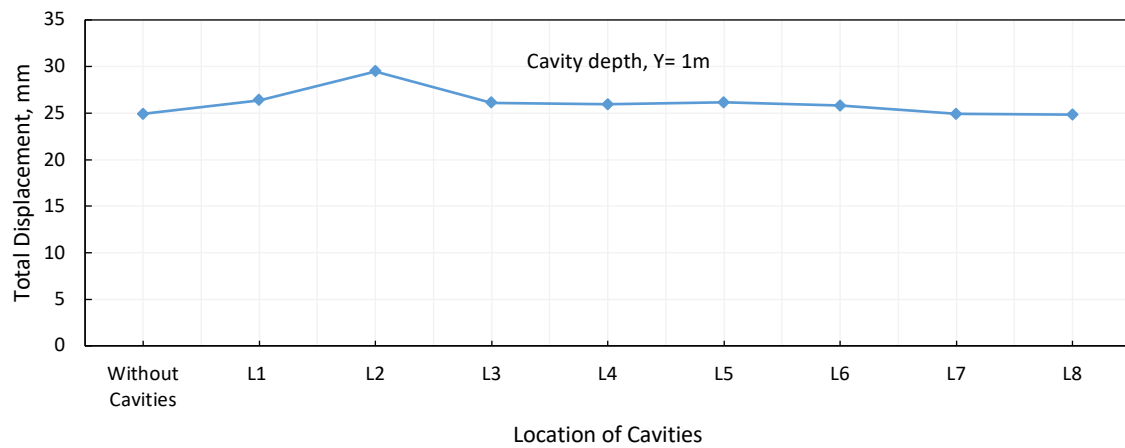


Figure 4.2: Maximum values of total displacement vs location of a cavity under upstream using the MC model

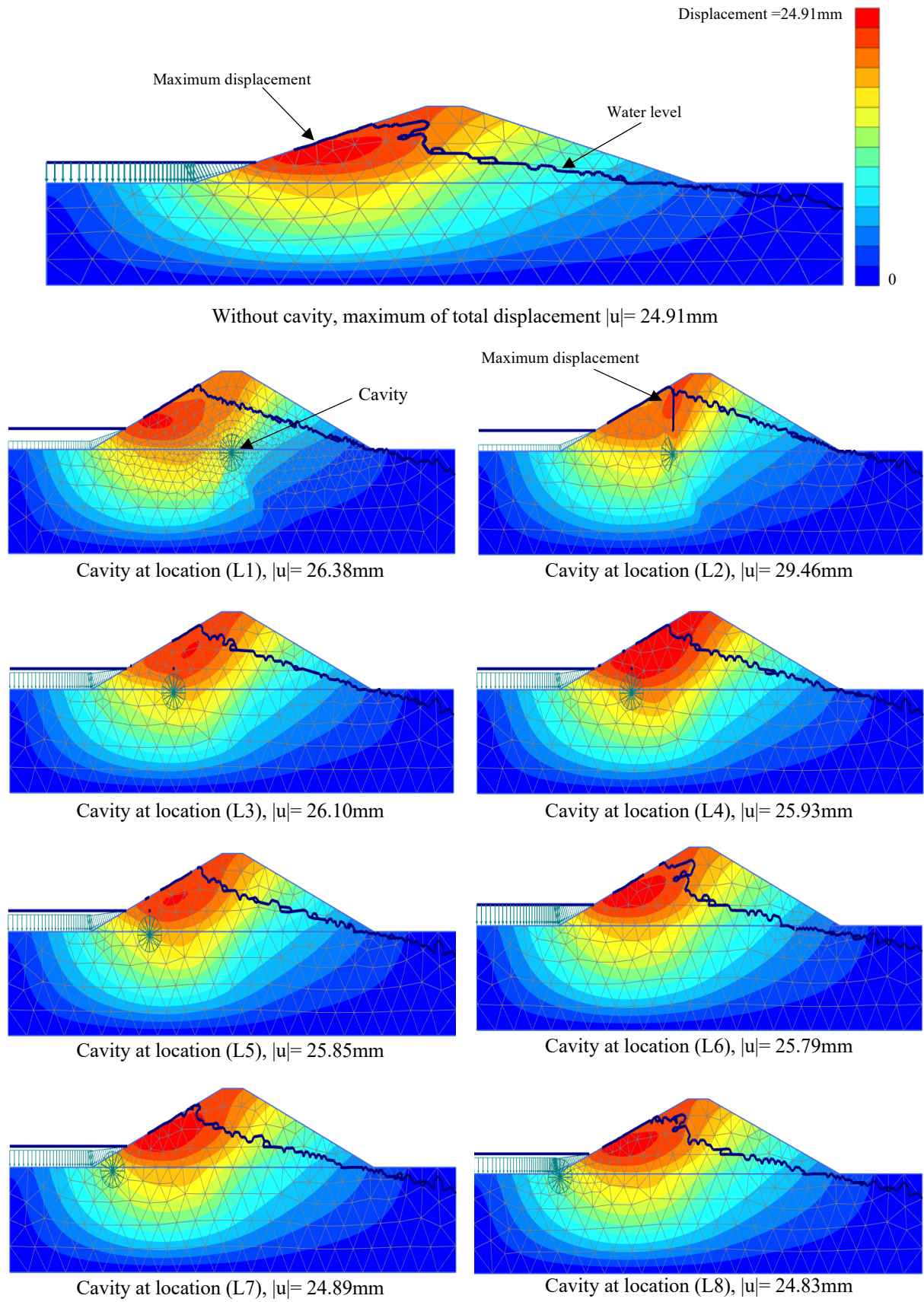


Figure 4.3: Contour of total displacement for the impact of a cavity's position under upstream using the MC model

Figure 4.4 and Figure 4.5 indicate the effects of a cavity's position under the downstream side on the SF and total displacement values; refer to Table 4.3 for details of the positions. It should be noted that the existence of a cavity decreases the stability of the dam: the SF decreased from 2.036 for the model without a cavity to 1.794 and 1.837 for models with cavity locations L2 (8, -1) and L8 (40, -1), respectively. It should also be mentioned that the SF values remained larger than the minimum value specified (1.2–1.3) according to the slope-stability criterion mentioned previously. This suggests that the earth dam is more stable or safer under rapid-drawdown conditions when a cavity is situated under the downstream side as opposed to the upstream side, where the presence of a cavity could damage stability significantly. This behaviour may be attributed to the fact that the cavity is further away from potential failure surfaces, as shown in Figure 4.4. The maximum displacement values increased from 24.91mm for a cavity-free model to 25.61mm (by 2.8%) for a model with a cavity at location L2, then decreased slightly towards the end of the earth dam, where it is 24.93mm at location L8. Figure 4.6 shows the displacement values and slip surfaces for the impact of a cavity's position under the downstream side.

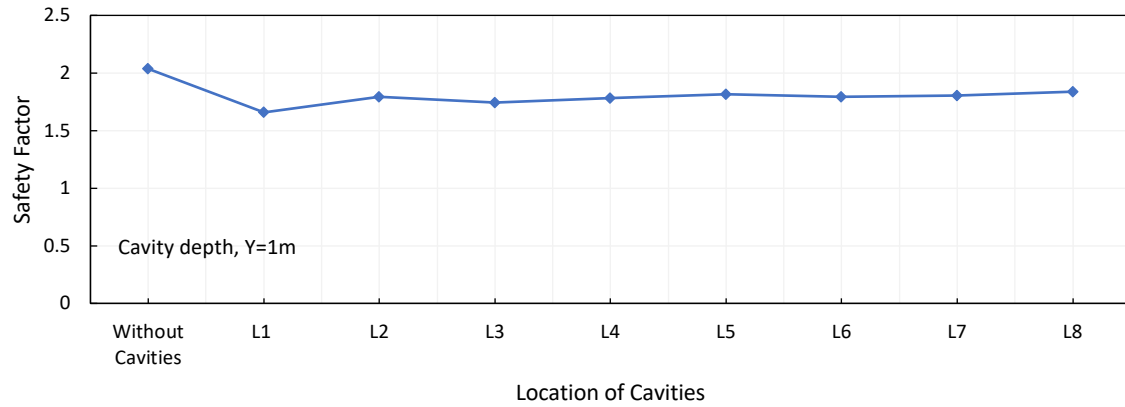


Figure 4.4: SF vs location of a cavity under downstream at a depth of 1m using the MC model

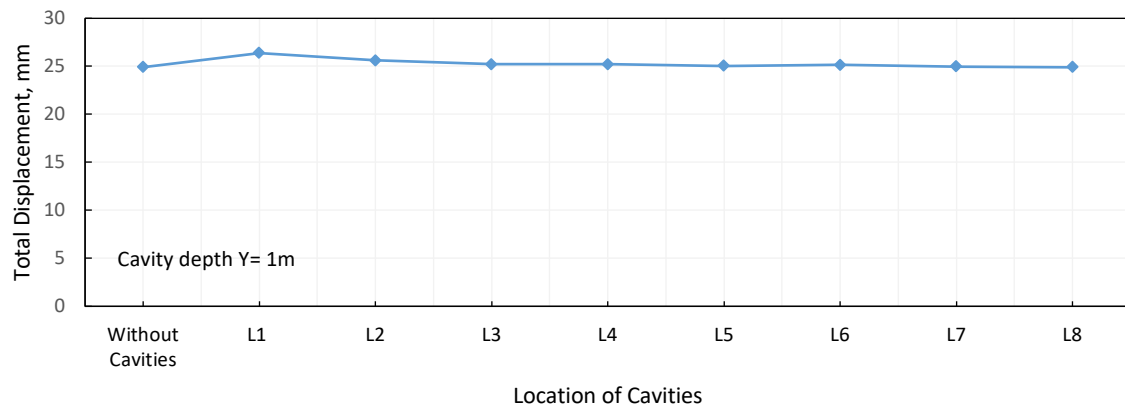


Figure 4.5: Maximum values of total displacement vs location of a cavity under downstream at a depth of 1m using the MC model

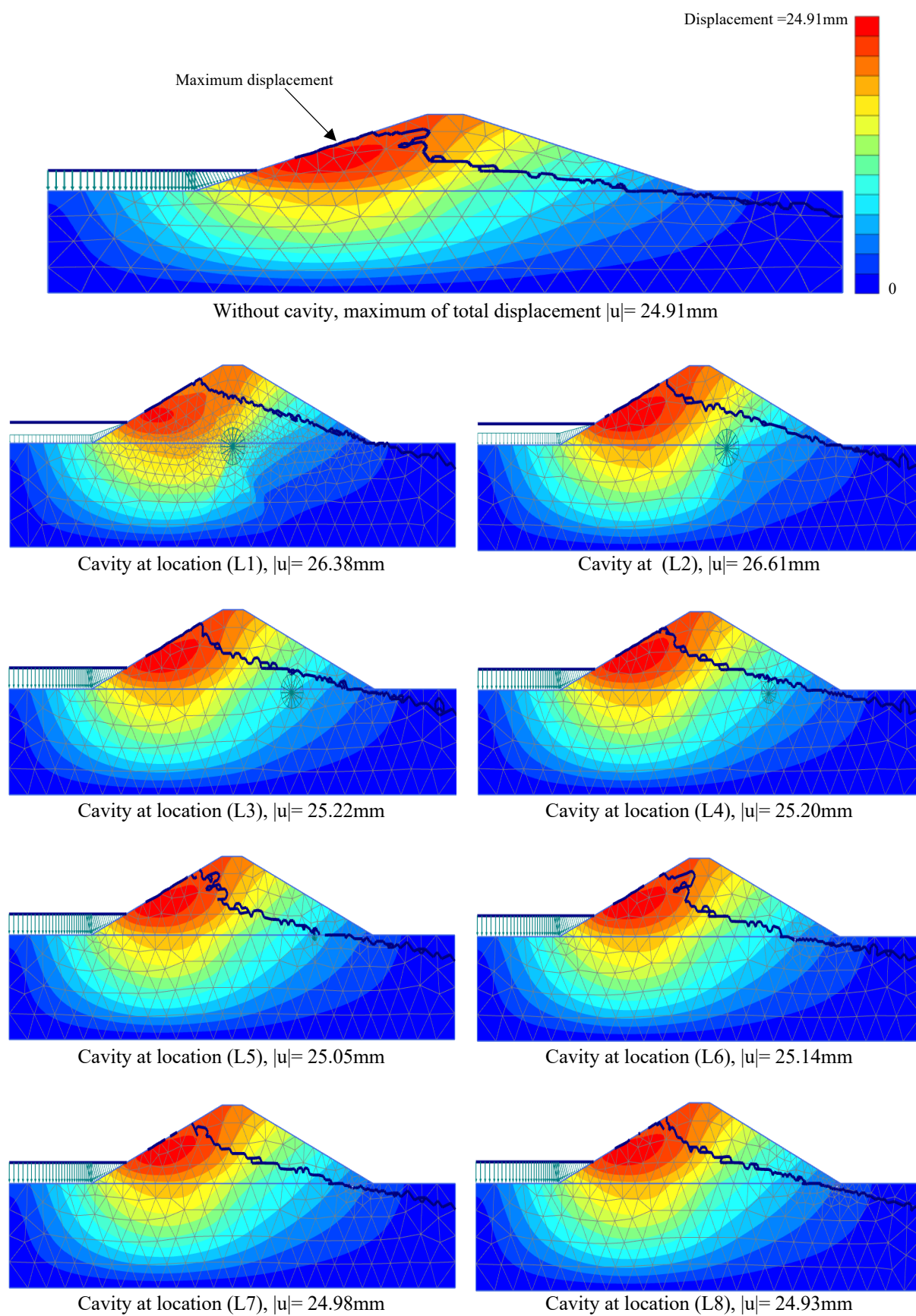


Figure 4.6: Contour of total displacement for the impact of a cavity's position under downstream using the MC model



Figure 4.7 reveals the results of a comparison between the impact on the SF of a cavity existing under the upstream and downstream sides, while Figure 4.8 reveals a similar comparison for their impact on the displacement values. It appears that the existence of a cavity along with a rapid drop in the reservoir's water level greatly influences the stability of the slopes on the upstream side; however, this impact is not as significant on the downstream side of the dam. It has been remarked that the SF values decreased significantly by about 64.9% at location L2(-8, -1) on the upstream side, compared to 11.9% on the downstream side at location L2(8, -1), but the values of the displacement increased by about 18.3% on the upstream side, compared to 2.8% on the downstream side. This is because of the combined impact of the existence of a cavity and the condition of the rapid drawdown of the reservoir's water. It is known that the rapid drawdown is one of the most serious conditions on the stability of the upstream side (Fathani and Legono, 2011). In rapid-drawdown conditions, the countervailing water pressure of upstream decreases, which leads to a reduction in upstream stability. The soil inside the dam's body remains saturated, and the flow begins towards the upstream. Seepage and hydrodynamic pressures create downward forces that negatively affect stability and lead to critical conditions in the upstream side (Fattah and Hassan, 2017). Accordingly, it can be deduced that the risks to stability due to a cavity existing beneath the upstream side increase during rapid-drawdown conditions. According to Figure 4.7, the SF values for models with cavity locations L7 and L8 under downstream are smaller than those values for the upstream side, where the SF amounted to 1.805 and 1.837 for L7 and L8 on the downstream side, respectively, compared to 1.876 and 1.966 for L7 and L8 for the upstream side, respectively. This behaviour may be due to the proximity of the cavity's position to the default water level.

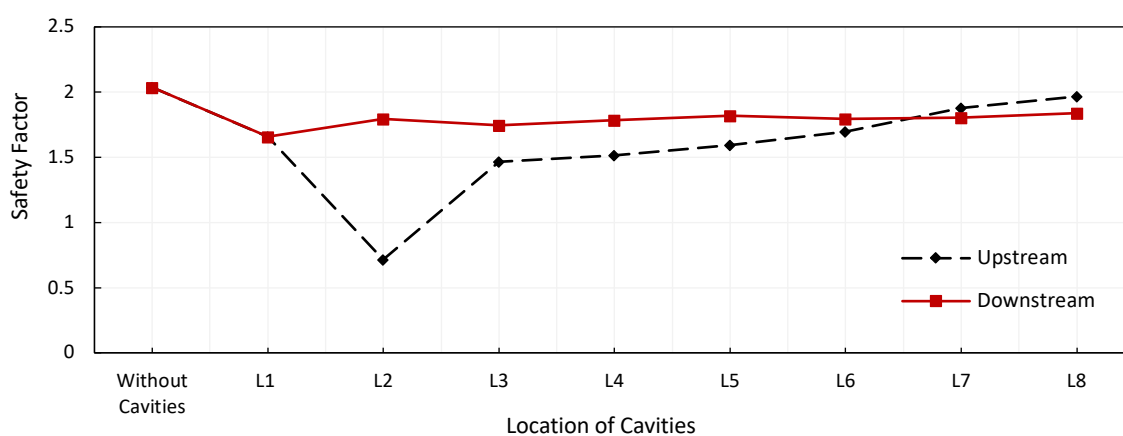


Figure 4.7: Comparison between the impact on the SF of a cavity existing under the upstream and downstream slopes using the MC model

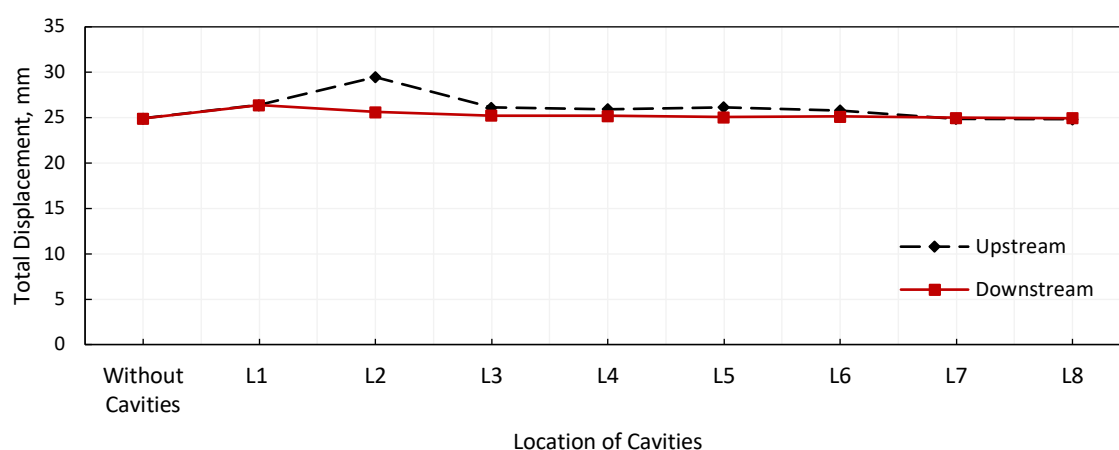


Figure 4.8: Comparison between the impact on the maximum values of the total displacement of a cavity existing under the upstream and downstream using the MC model

The impact of cavity depth on the SF values for the models of a cavity under upstream are illustrated in Figure 4.9. The detail of the cavity's location and corresponding SF values are outlined in Table 4.4. The results show that cavity depth influences slope stability slightly. The SF values fluctuated somewhat (increasing or decreasing) as the cavity depth increased for the models created for all locations, with the exception of locations L2 and L5. The SF value increased from 0.715 to 1.028 as the cavity depth increased from 1m to 4m for position X2; however, it decreased significantly from 1.594 to 1.173 at locations L5 (-24, -1) and L5 (-24, -2). For example, the SF values for the models containing cavity locations (-17, -1), (-17, -2), (-17, -3) and (-17, -4) are 1.463, 1.416, 1.452 and 1.491, respectively. Table 4.4 shows the SF values that relate to the depth-effect analysis. Figure 4.10 shows an example of the change in the contour of total displacement with the change of the cavity's depth for the models of a cavity situated at position X2 under upstream. According to this figure, the displacement values decreased gradually with an increasing cavity depth. The displacement values decreased from 29.46mm to 25.94mm with increasing depth to 4m. This behaviour could be because, as the depth increases, the cavity is no longer in the zone influenced by the stress distribution. This could also mean that the presence of a cavity creates potential weaknesses in the soil; however, if the cavity is located outside of the stress zone of influence or nearer to the boundary of the stress bulb, these effects could be negligible.

Table 4.4: Locations of the cavity under upstream and the corresponding S.F values

Cavity location	Coordinates of position in X-axis, m	SF			
		Cavity depth, m			
		Y= 1m	Y= 2m	Y= 3m	Y= 4m
Without cavities		2.036			
L1	0	1.658	1.638	1.647	1.662
L2	-8	0.715	0.751	0.791	1.028
L3	-17	1.463	1.416	1.452	1.491
L4	-20	1.516	1.447	1.458	1.464
L5	-24	1.594	1.173	1.489	1.492
L6	-28	1.694	1.602	1.577	1.593
L7	-35	1.876	1.789	1.690	1.694
L8	-40	1.966	1.923	1.949	1.987

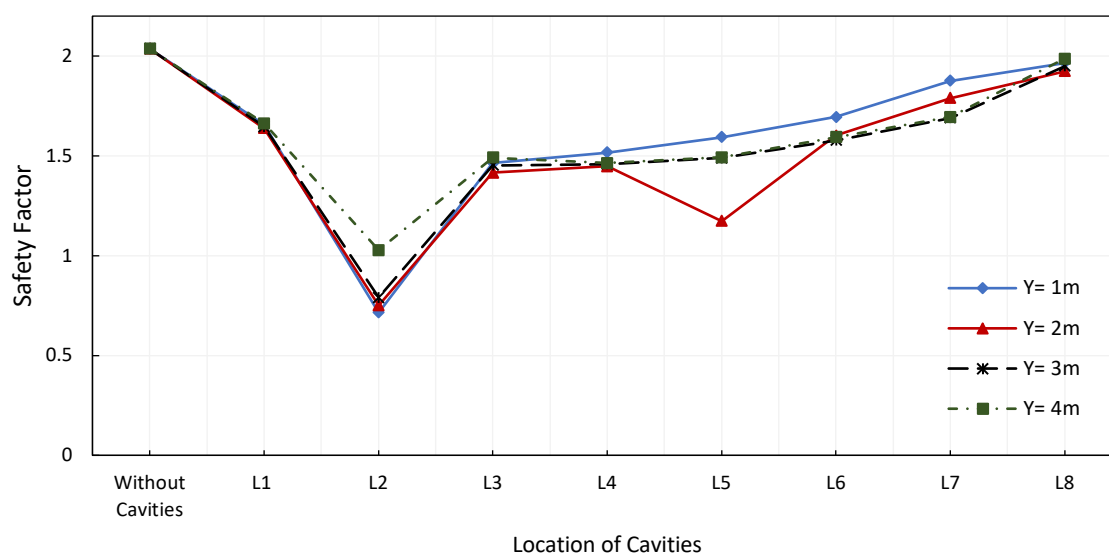


Figure 4.9: SF vs location of a cavity situated under upstream using the MC model for depths Y= 1m, 2m, 3m, 4m

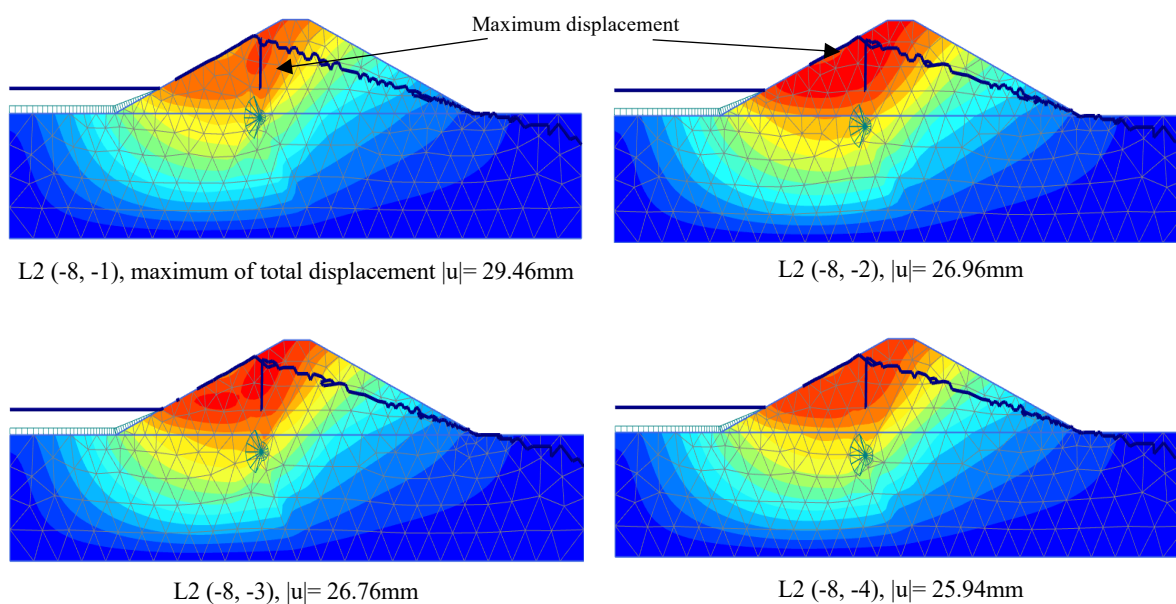


Figure 4.10: Impact of cavity depth on the maximum of total displacement for a cavity situated under upstream at positions X2 using the MC model

Figure 4.11 demonstrates the impact of cavity depth on the stability for models with a cavity situated beneath downstream. As in the upstream analysis, it should be noted that, by increasing the cavity depth, the SF values fluctuate for all models. The SF increased from 1.794 to 1.826 when the cavity depth was increased from 1m to 4m for models with a cavity at position (X2= 8m), whereas, the displacement value reduced slightly from 25.61mm to 25.94mm. With respect to the other horizontal positions (X3–X8), the SF values decreased when the cavity depth was increased from 1m to 2m, and then increased when the depth was increased to 4m. For example, the SF values decreased from 1.743 to 1.712 and then increased to 1.793 for locations L3 (17, -1), (17, -2) and (17, -4), respectively. Table 4.5 gives the SF values that relate to the depth-effect analysis. An example of the effect of the cavity depth on the contour of the total displacement for models situated at position X2 below downstream are as given in Figure 4.12. It is clear from this figure that, by increasing the cavity depth, the displacement values dropped slightly, as the displacement values dropped from 25.61mm to 25.48mm for models with cavity locations (8, -1) and (8, -4), respectively. This could be due to the presence of the cavity coinciding with the weakest potential slip surfaces, inducing a further drop in the SF.

Table 4.5: Locations of the cavity under downstream and the corresponding SF values

Cavity location	Coordinates of position in X-axis, m	SF			
		Cavity depth, m			
		Y= 1m	Y= 2m	Y= 3m	Y= 4m
Without cavities		2.036			
L1	0	1.658	1.638	1.647	1.662
L2	+8	1.794	1.796	1.820	1.826
L3	+17	1.743	1.712	1.733	1.793
L4	+20	1.785	1.740	1.748	1.753
L5	+24	1.817	1.769	1.703	1.724
L6	+28	1.796	1.638	1.643	1.676
L7	+35	1.805	1.677	1.556	1.755
L8	+40	1.837	1.684	1.637	1.673

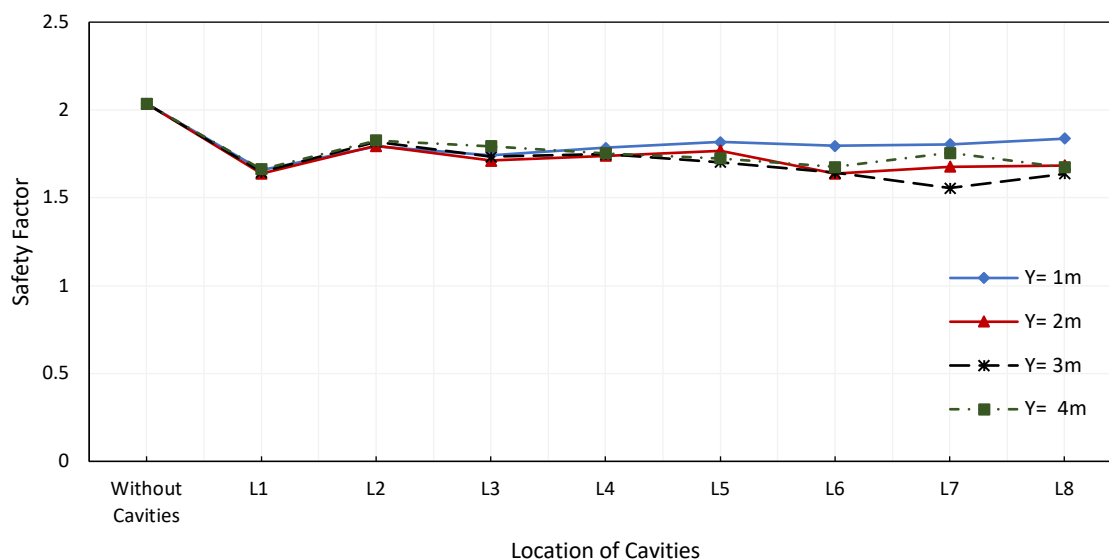


Figure 4.11: SF vs location of a cavity for depths (Y=1m to Y=4m) under downstream using the MC model

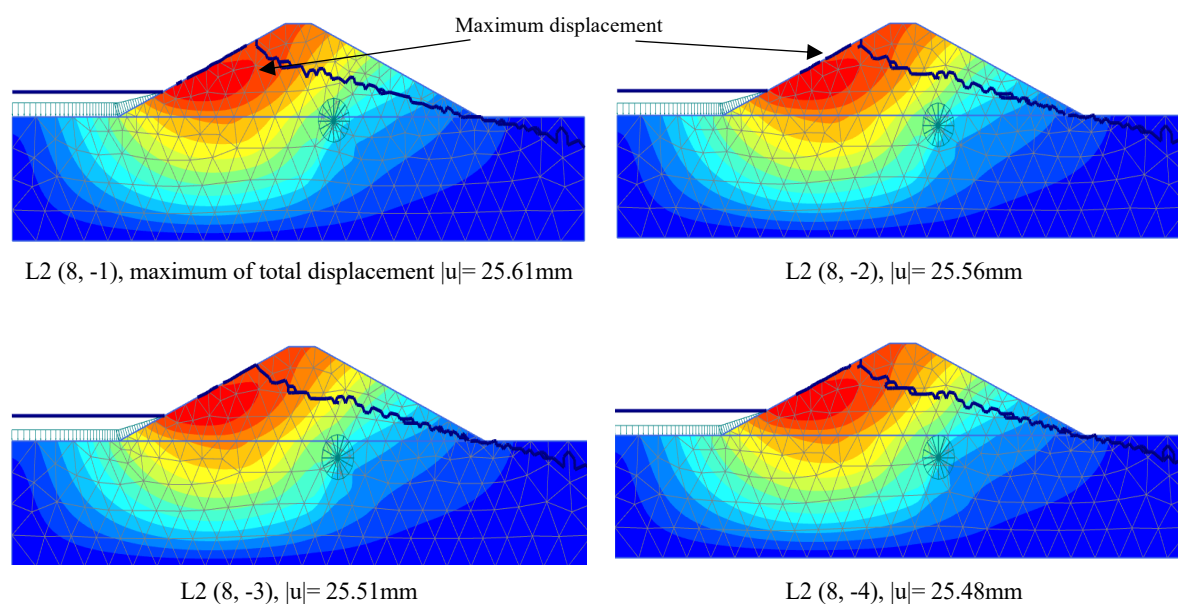


Figure 4.12: Impact of cavity depth on the maximum of total displacement for a cavity situated under downstream at positions X2 using the MC model

#### 4.4.2 Impact of the cavity location modelled using the HS and MC models

The HS and MC models were employed for modelling the earth dam in this section. The impact of the existence of a circular cavity was evaluated, while adopting the same horizontal positions as detailed in Table 4.3. Each cavity was situated at a depth of 1m.

Figure 4.13 illustrates the impact of the horizontal position of a cavity on upstream stability, while Figure 4.14 shows their effect on the maximum values of total displacement. It can be seen that the existence of a cavity decreases significantly the stability of the earth dam. The SF values reduced from 1.982 for a cavity-free model to 0.727 for one with a cavity situated at location L2 (-8, -1); in contrast, the values of displacement increased from 26.48mm to 37.17mm for the same models. This behaviour can be attributed to a decrease in the subsoil strength as a consequence of the presence of a cavity, and a possible intersection of the cavity locations and potential failure surfaces of the slope. Moreover, in a rapid drawdown of the reservoir water level, deformations occur in the upstream slope, and there is an abrupt drop in the effective stress values due to the soil in the embankment remaining saturated without the time required for the drainage of water from the upstream slope, and without an equal dissipation in the excess pore water pressures (Tran, 2004). It should be noted that the SF values did not satisfy the minimum limits (1.2-1.3) set by the codes of practice for the stability of dam slopes in rapid-drawdown conditions when the cavity was positioned at location L2 (NRCS, 2005; USBR, 2011; ULDC, 2012). It is obvious that by increasing the

horizontal distance between a cavity's position and the centreline of the dam, the SF values increased from 0.727 to 1.867, and the displacement values decreased from 32.73mm to 27.22mm for models with cavity locations L2 (-8, -1) and L8 (-40, -1), respectively. This behaviour is due to the cavity being located away from the potential failure surface as a result of increasing the horizontal distance from centreline of the dam towards the end of the dam's base, as shown in Figure 4.15. It can be concluded from the results that the presence of a cavity has a greater impact on the SF values compared to the displacement values. The change in the SF values is equal to 63.3%, compared to 40.3% for the displacement values at location L2.

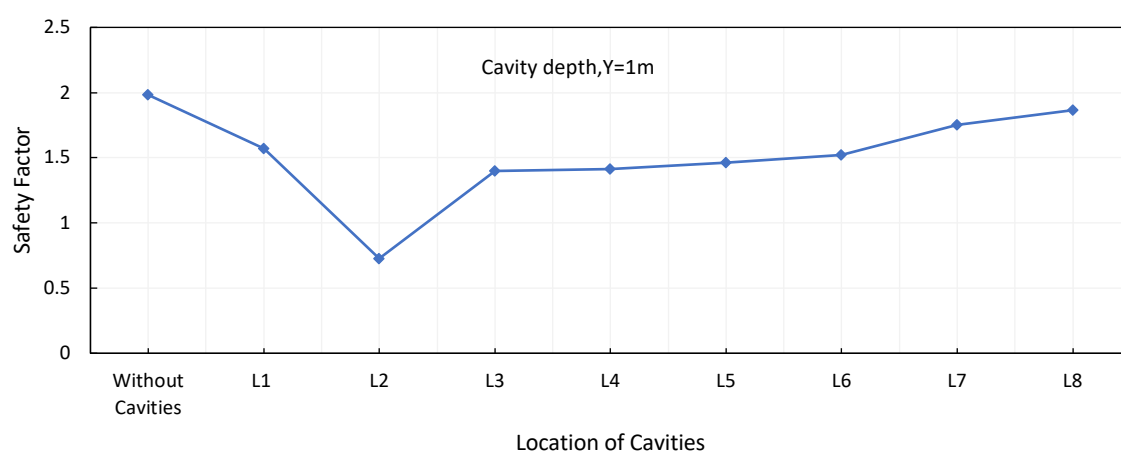


Figure 4.13: SF vs location of a cavity under upstream using the HS and MC models

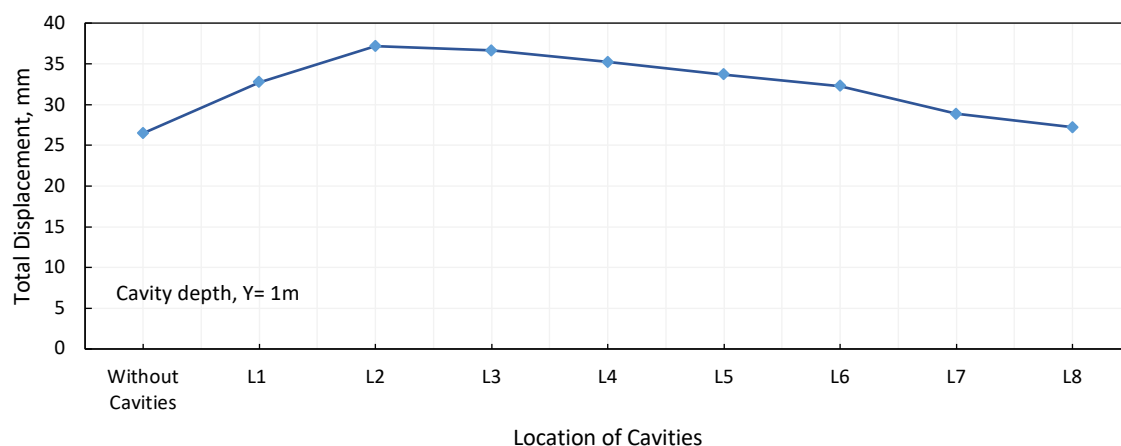


Figure 4.14: Maximum values of total displacement vs location of a cavity under upstream using the HS and MC models

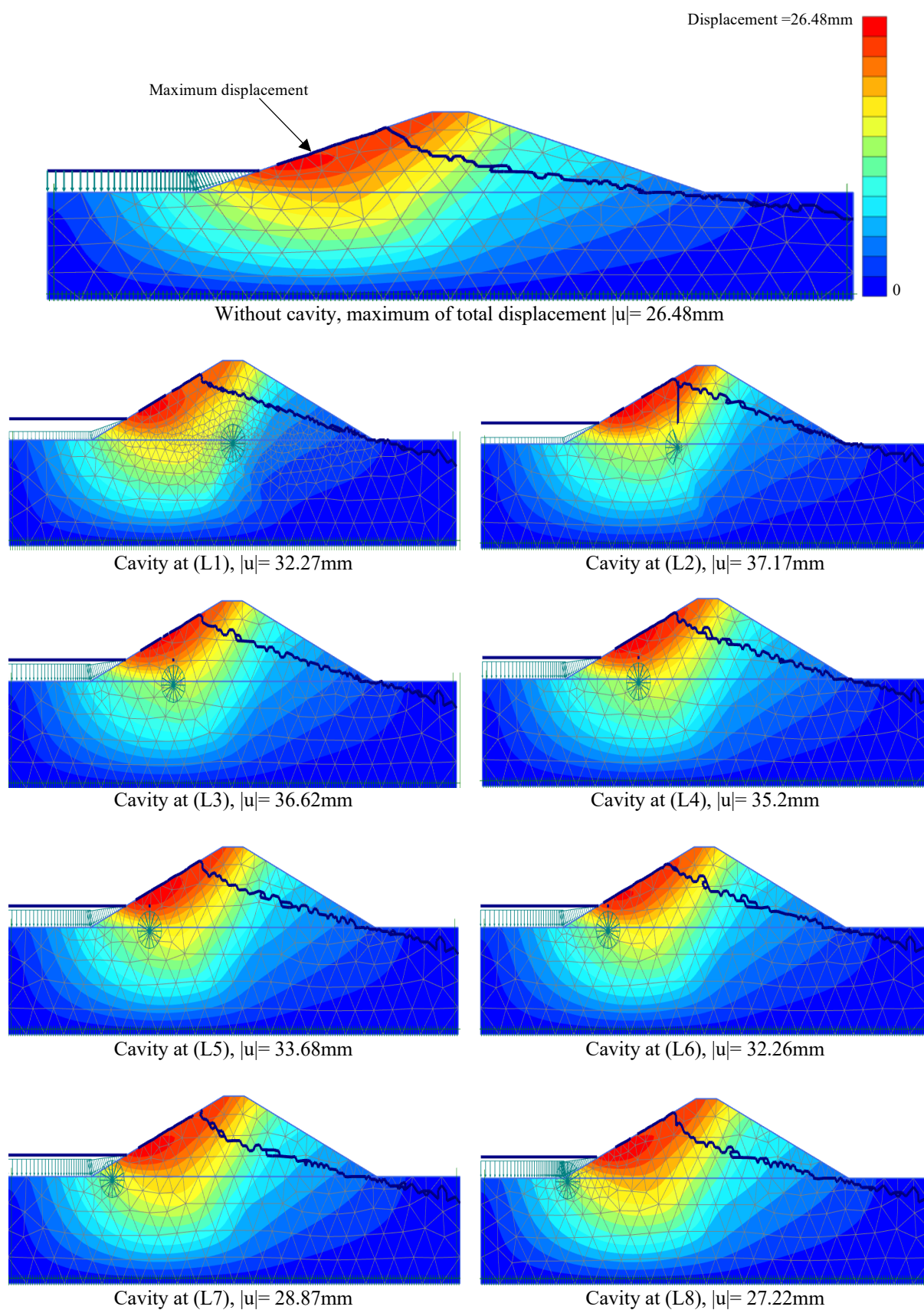


Figure 4.15: Contour of total displacement for the impact of a cavity's position under upstream using the HS and MC models



Figure 4.16 and Figure 4.17 reveal the impact on the SF and displacement values of the cavity's horizontal position for a cavity situated under the downstream, while Figure 4.18 shows the contour of the maximum total displacement for the impact of the cavity. In general, the SF values decrease with the presence of a cavity: these values decreased from 1.982 for a cavity-free model to 1.781 for an earth-dam model with a cavity situated at L2 (8, -1), with an increase in the total displacement from 26.48mm to 28.71mm. However, it is clear that the SF values still satisfy the minimum limits specified by the codes of practice for earth-dam stability during rapid-drawdown conditions (1.2–1.3). This indicates that the earth dam used in this research remains safe in rapid drawdown conditions. The SF values increased as the cavity's position moved away from the centreline of the earth dam towards the end of the dam base: these values ranged from 1.571 to 1.852 for models with cavity locations L1 (0, -1) and L8 (40, -1), respectively, as expected. In addition, the maximum displacement values decreased from 32.73mm to 26.0mm for locations L1 and L8, respectively. The reason for this behaviour may be the increase in the distance between the cavity's positions and the potential failure surfaces. As a cavity moves away from the centreline of the earth dam, it does not intersect with failure surfaces, as demonstrated in Figure 4.18.

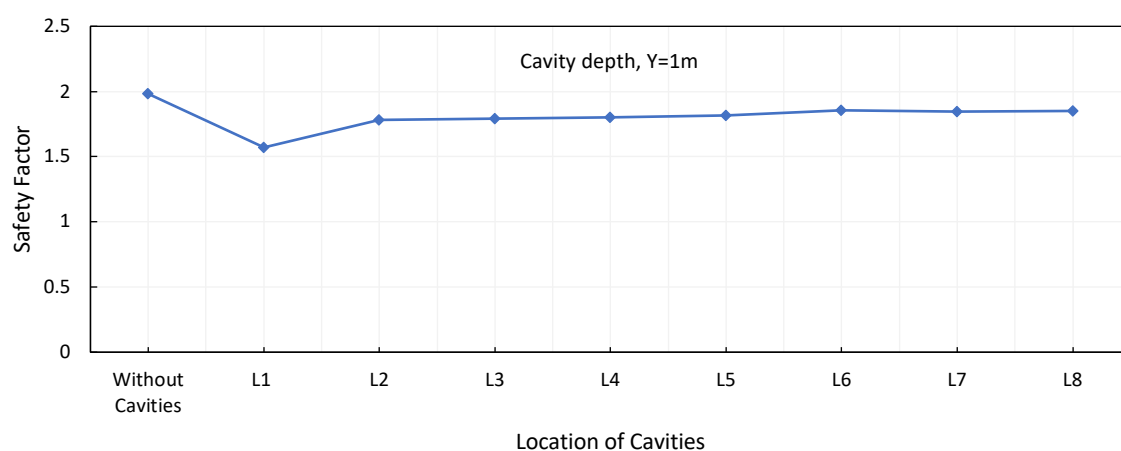


Figure 4.16: SF vs location of a cavity under downstream using the HS and MC models

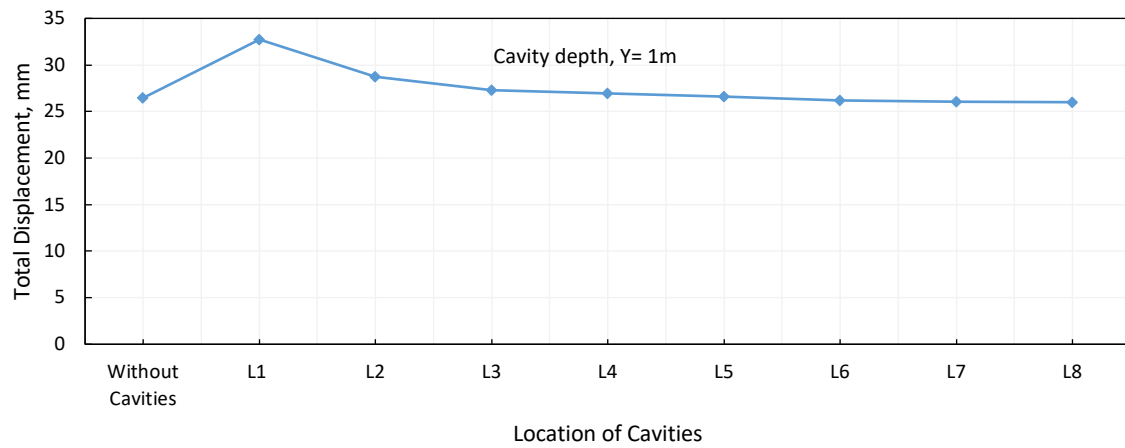


Figure 4.17: Maximum values of total displacement vs location of a cavity under downstream using the HS and MC models

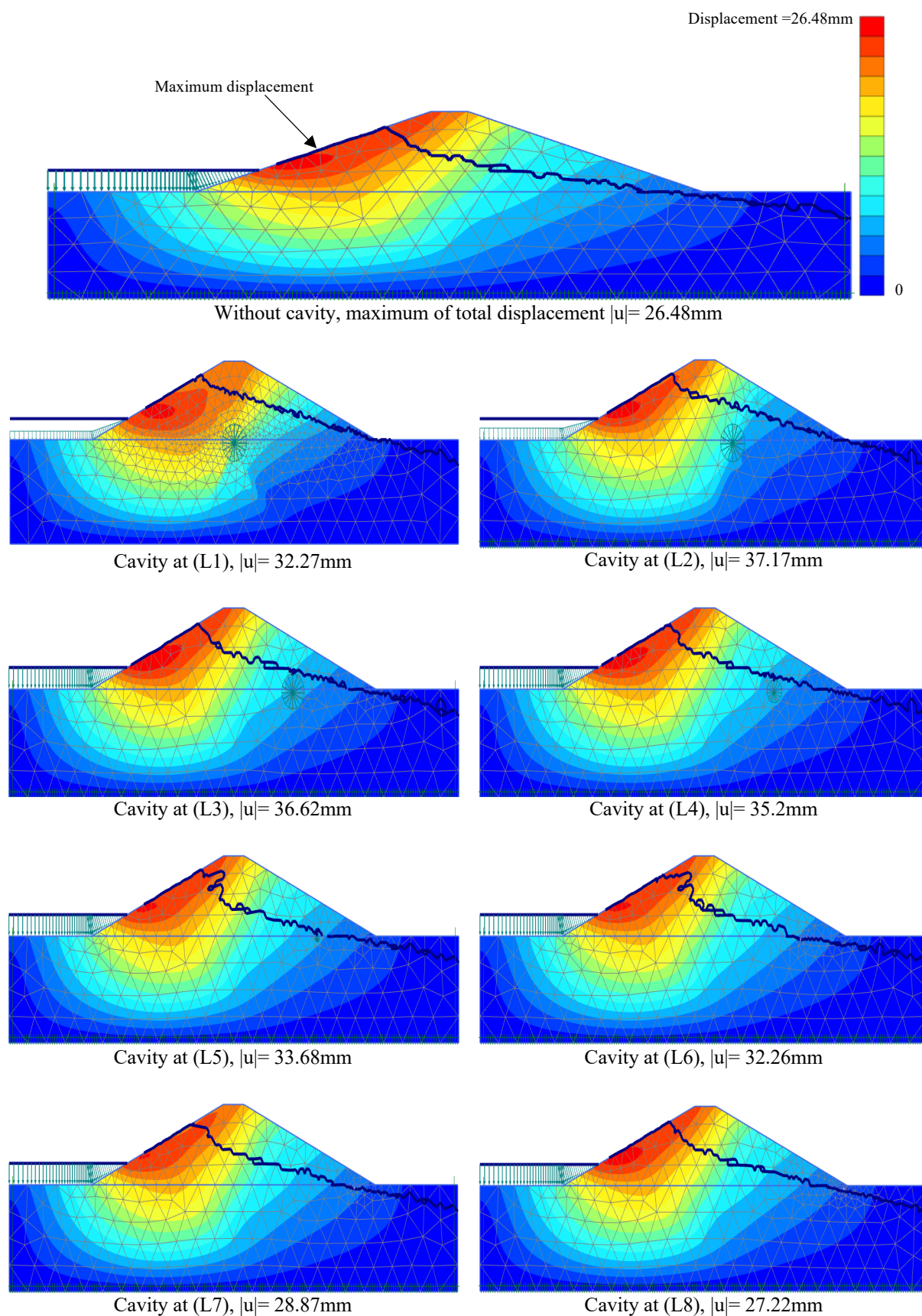


Figure 4.18: Contour of total displacement for the impact of a cavity's position under downstream using the HS and MC models

Figure 4.19 and Figure 4.20 indicate that a rapid reduction in the water level with a cavity present has a significant impact on the stability of the upstream side compared to the downstream side. For the upstream side, it appears that the SF values decrease considerably from 1.982 to 0.727 (which is equivalent to 63.3%) for a cavity-free model to the ones with a cavity at location L2, respectively; this is in contrast to the downstream side of the dam model, where the SF value decreases from 1.982 to 1.781, which is equivalent to 10.1%. Conversely, the displacement value increased from 26.48mm to 37.17mm (which is equivalent to 40.3%) from a cavity-free model to the ones with a cavity under upstream cavity at location L2,, respectively, compared to 28.71mm (which is equivalent to 8.4%) for the downstream side.

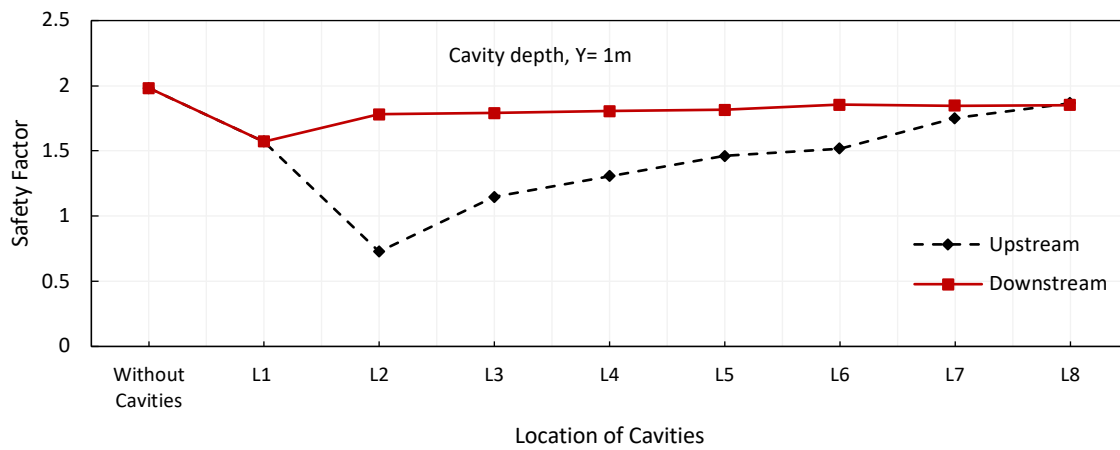


Figure 4.19: Comparison between the impact on the SF of a cavity being present under upstream and downstream using the HS and MC models

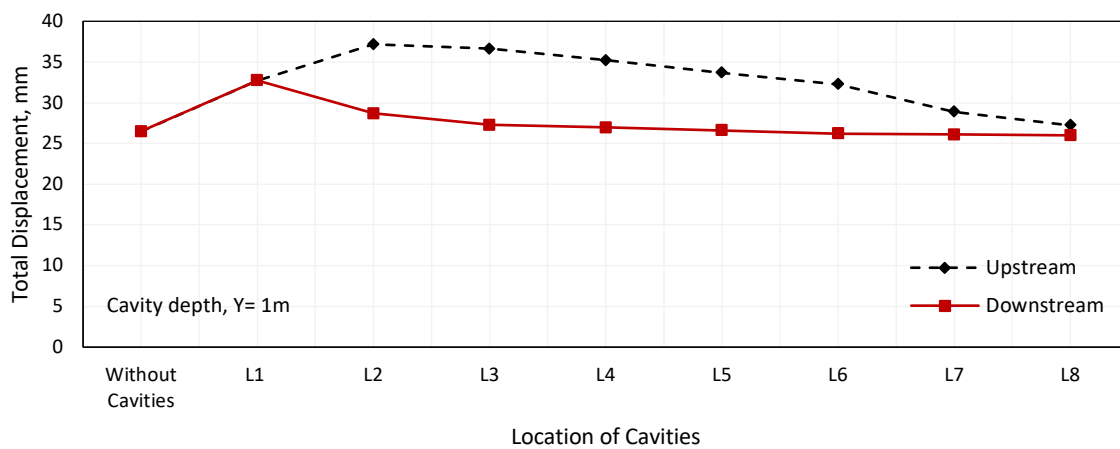


Figure 4.20: Comparison between the impact on the maximum values of the displacement of a cavity’s presence under upstream and downstream using the HS and MC models

In order to assess the impact of cavity depth on the stability of the upstream and downstream slopes, a set of locations (varying in position vertically and horizontally) were selected, as explained in the MC model analysis.

The impact of a cavity depth situated beneath the upstream on its stability is revealed in Figure 4.21 and Table 4.6. It can be concluded from these results that the variation in a cavity's depth has a minor effect on slope stability. Generally, the SF values fluctuate slightly (increasing or decreasing) as the cavity depth increases for all models with a cavity, except for models with cavity location L1, L2 and L6. In these locations, a continuous increase in SF is observed as the cavity depth increases from 1m to 4m. For example, the SF values increased from 0.727 to 1.053 for cavity locations L1(-8, -1) and L1(-8, -4), respectively. Figure 4.22 shows the effect of depth for a cavity situated under the upstream slope on the contour of total displacement. It seems that the displacement values drop somewhat when the cavity depth is increased; it dropped from 37.17mm to 36.63mm for models with cavity locations L1(-8, -1) and L1(-8, -4), respectively. This behaviour can be attributed to the fact that the cavity begins to move away from the area affected by the stress distribution as the cavity depth increases. Furthermore, this could denote that a cavity generates weaknesses in the soil; however, these effects could be insignificant if the cavity is situated outside of the stress area of influence or closer to the boundary of the stress bulb, as is clearly shown in Figure 4.22.

Table 4.6: Locations of the cavity under upstream and the corresponding SF values

Cavity location	Coordinates of position in X-axis, m	SF			
		Cavity depth, m			
		Y= 1m	Y= 2m	Y= 3m	Y= 4m
	Without cavities	1.982			
L1	0	1.571	1.574	1.586	1.598
L2	-8	0.727	0.738	0.767	1.053
L3	-17	1.398	0.876	1.347	1.366
L4	-20	1.411	1.418	1.454	1.458
L5	-24	1.461	1.162	1.485	1.542
L6	-28	1.519	1.525	1.532	1.580
L7	-35	1.752	1.606	1.622	1.692
L8	-40	1.867	1.803	1.816	1.862

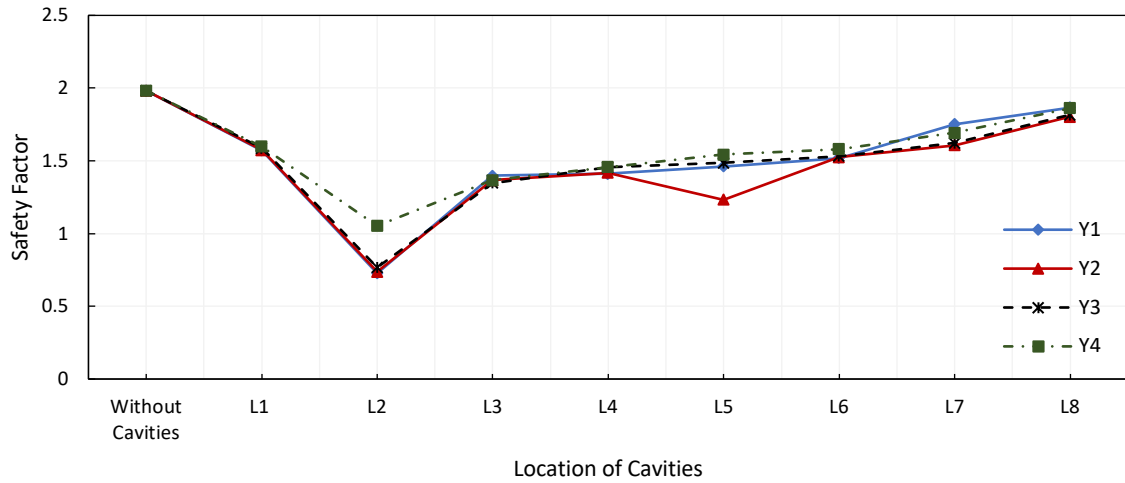


Figure 4.21: SF vs location of a cavity for depths (Y=1m to Y=4m) situated under upstream using the HS and MC models

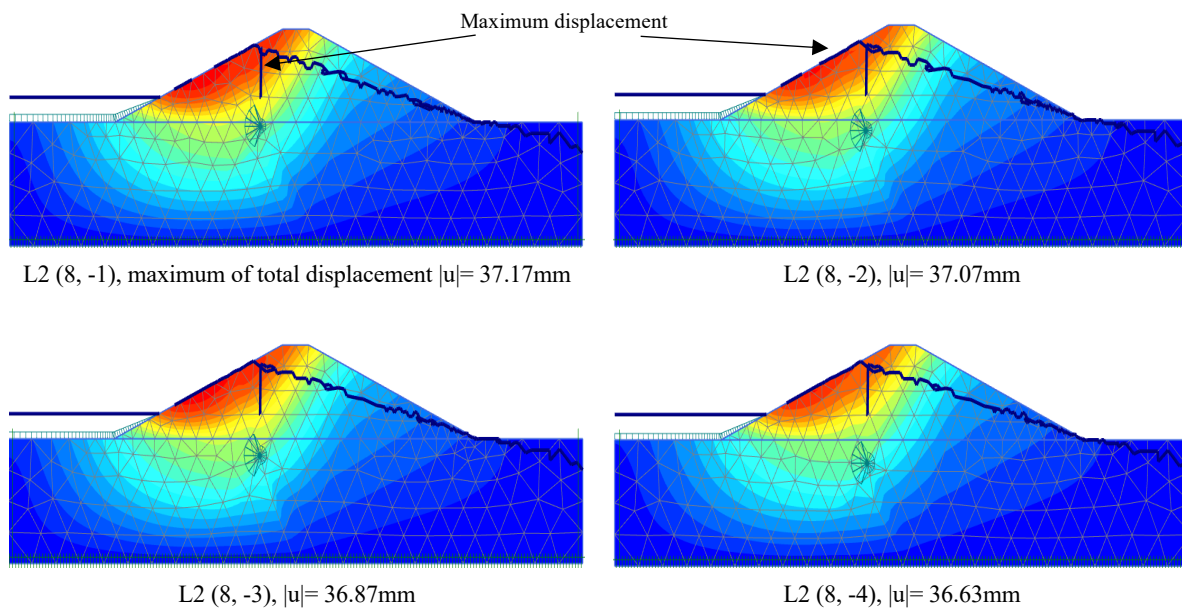


Figure 4.22: Contour of total displacement for the effect of cavity depth under upstream using the HS and MC models

Figure 4.23 and Table 4.7 illustrate the impact of the depth of a cavity sited under the downstream side on the stability. Similar to the upstream results presented previously, it is obvious that slope stability is affected (decreasing or increasing) by increasing the cavity depth. The SF values decreased as the cavity depth was increased from 1m to 2m; afterwards, the SF values rose when the depth was increased to 4m for locations L3, L4 and L6. However, there was a continuous decrease in the SF value when the depth was increased to

3m, and then it increased as the depth was increased to 4m. For example, the SF value decreased from 1.781 to 1.762 at locations L2 (8, -1) and L2 (8, -3), respectively; afterwards, it increased to 1.767 at location L2 (8, -4). With respect to positions X3, X4, X6 and X8, the SF value reached its lowest value at a depth of 2m, where these values are 1.753, 1.749, 1.68 and 1.678, respectively. Figure 4.24 shows an example of the effect of cavity depth on the displacement values for the cavity located at position X2. According to this figure, the cavity depth affects the displacement slightly; it decreased from 28.71mm to 26.51mm when the depth was increased from 1m to 4m.

Table 4.7: Locations of the cavity under downstream and the corresponding SF values

Cavity location	Coordinates of position in X-axis, m	SF			
		Cavity depth, m			
		Y= 1m	Y= 2m	Y= 3m	Y= 4m
	Without cavities	1.982			
L1	0	1.571	1.574	1.586	1.598
L2	+8	1.781	1.767	1.762	1.767
L3	+17	1.790	1.753	1.758	1.761
L4	+20	1.804	1.749	1.755	1.798
L5	+24	1.816	1.760	1.720	1.740
L6	+28	1.855	1.680	1.697	1.706
L7	+35	1.847	1.720	1.648	1.685
L8	+40	1.852	1.678	1.643	1.676

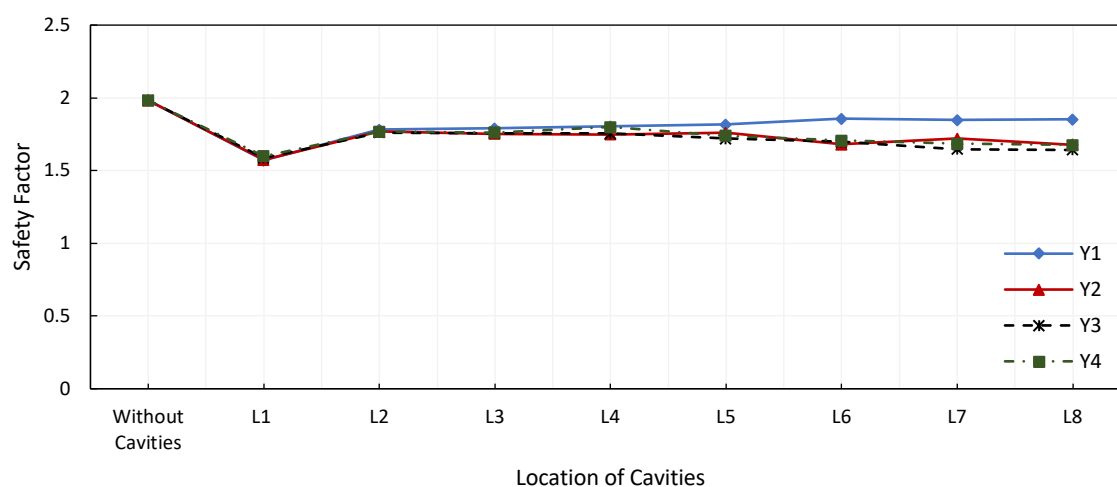


Figure 4.23: SF vs location of a cavity for depths (Y=1m to Y=4m) situated under downstream using the HS and MC models

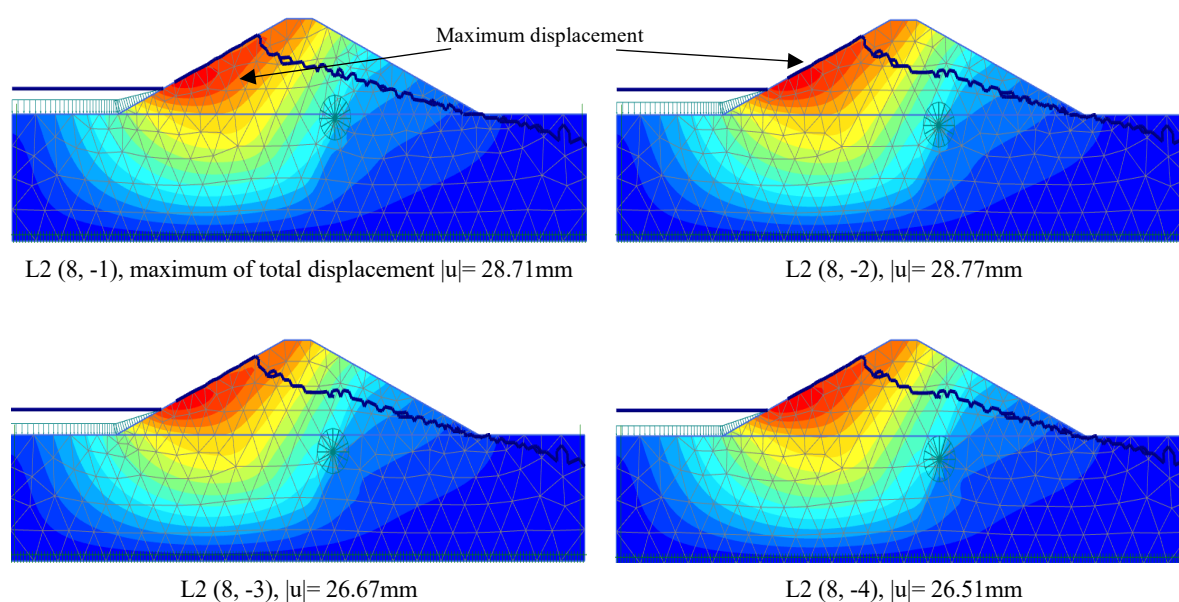


Figure 4.24: Impact of cavity depth on the maximum of total displacement for a cavity situated under downstream at positions X2 using the HS and MC models

## 4.5 Impact of cavity shape

In order to assess the impact of the cavity's shape on the stability of earth dams, a comparison was carried out of the impact of the existence of a circular and an irregular cavity under each side. The comparisons were made using PLAXIS 2D and were under drawdown conditions. In these analyses, a model of a single cavity with a diameter of 60cm was created in several horizontal positions and depths.

### 4.5.1 Modelling the earth dam using the MC model

All stability simulations at this stage were conducted using the MC model to model the earth dam. Various horizontal and vertical cavity locations were considered in the analyses, as detailed in Table 4.8.

Figure 4.25 and Figure 4.26 show a comparison between the impact of a circular cavity and the impact of an irregular cavity under upstream on the displacement values and SF. A similar impact on the displacement values was observed due to the existence of both types of cavity under upstream. Generally, the displacement values for models with an irregular cavity are somewhat greater than for those with a circular cavity; except for location L5 (-24, -1), where it is of 26.13mm for a circular-cavity model, compared to 25.98mm for ones with an irregular-cavity model. The maximum displacement value is of 29.46mm (which is



equivalent to 18.3%) for a circular-cavity model, compared to 30.06mm (which is equivalent to 20.6%) for an irregular-cavity model with a cavity at location L2 (-8, -1). The stability analysis results are summarized in Table 4.8. It is clear that the existence of both types of cavity has a similar effect on dam stability. The SF values were close to each other, irrespective of vertical and horizontal changes in the location of the cavity. Overall, the SF values for irregular-cavity models are smaller. For example, for position X2, the SF is 0.715, 0.751, 0.791 and 1.028 for circular-cavity models with a cavity at depths of 1m, 2m, 3m and 4m, respectively, in contrast to 0.688, 0.686, 0.748 and 0.964 for an irregular-cavity model with a cavity at the same respective depths. The maximum drop in the SF is 64.9% for a circular-cavity model, as opposed to 66.2% for an irregular-cavity model at location L2 (-8, -1). The results reveal an exception at location L5 (-24, -2), where the SF is equal to 1.173 for a circular-cavity model, compared to 1.505 for an irregular-cavity model.

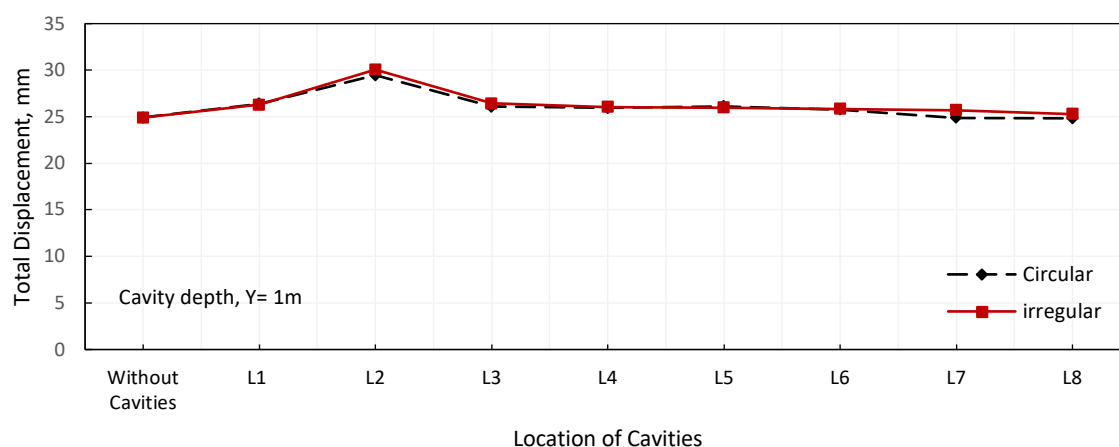


Figure 4.25: Comparison between the impact of the presence of a circular cavity and an irregular cavity sited under upstream on the displacement values using the MC model

Table 4.8: Locations of the circular cavity and irregular cavity sited under upstream and downstream and the corresponding SF values for the MC model

L	X, m	SF, Upstream							
		Cavity depth, m							
		Y= 1m		Y= 2m		Y= 3m		Y= 4m	
		Circular	Irregular	Circular	Irregular	Circular	Irregular	Circular	Irregular
Without Cavities		2.036							
L1	0	1.658	1.661	1.638	1.571	1.647	1.636	1.662	1.639
L2	-8	0.715	0.688	0.751	0.686	0.791	0.748	1.028	0.964
L3	-17	1.463	1.391	1.416	1.373	1.452	1.434	1.491	1.452
L4	-20	1.516	1.478	1.447	1.439	1.458	1.454	1.464	1.468
L5	-24	1.594	1.504	1.173	1.505	1.489	1.546	1.492	1.560
L6	-28	1.694	1.690	1.602	1.549	1.577	1.559	1.593	1.586
L7	-35	1.876	1.797	1.789	1.733	1.690	1.752	1.694	1.785
L8	-40	1.966	1.959	1.923	1.884	1.949	1.895	1.987	1.926
SF, Downstream									
L1	0	1.658	1.661	1.638	1.591	1.647	1.636	1.662	1.639
L2	+8	1.794	1.758	1.796	1.777	1.82	1.792	1.826	1.858
L3	+17	1.743	1.727	1.712	1.713	1.733	1.715	1.793	1.751
L4	+20	1.785	1.774	1.740	1.706	1.748	1.732	1.753	1.741
L5	+24	1.817	1.793	1.769	1.753	1.703	1.766	1.724	1.773
L6	+28	1.796	1.764	1.638	1.612	1.643	1.660	1.676	1.669
L7	+35	1.805	1.839	1.677	1.664	1.556	1.641	1.755	1.773
L8	+40	1.837	1.884	1.684	1.689	1.637	1.675	1.673	1.693

(L) : Location of cavity (x, y); (X): The coordinates of the cavities' positions in X-axis

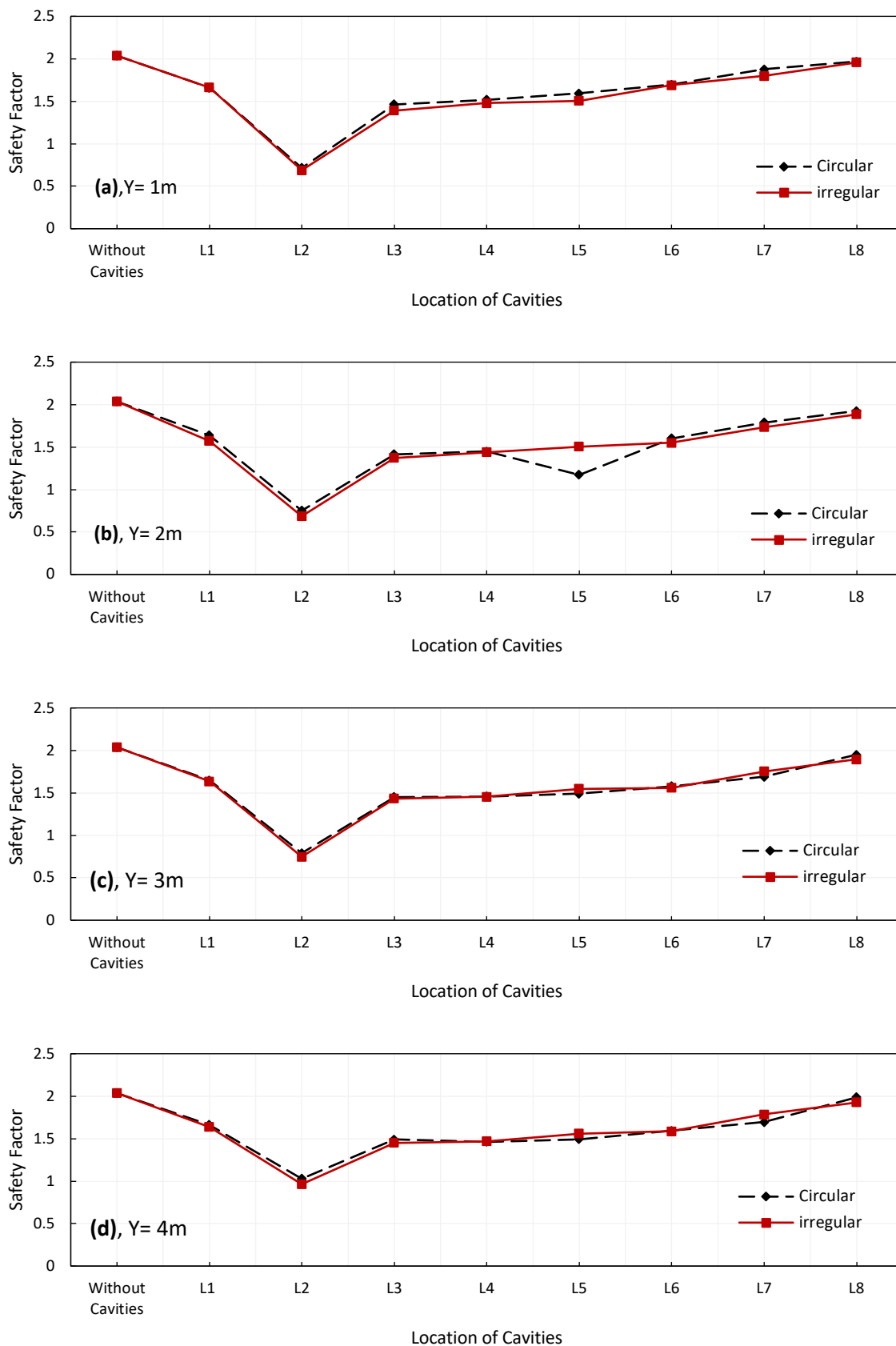


Figure 4.26: The impact of the presence of a circular and an irregular cavity under upstream on the SF using the MC model for depths (Y=1m to Y=4m)

A comparison between the impact of the existence of a circular cavity and an irregular cavity under the downstream slope on the displacement values and SF is demonstrated in Figure 4.27 and Figure 4.28. The coordinates of the cavity's position in the X and Y directions for each model, and the corresponding the SF values are listed in Table 4.8. Similar to the upstream-side results presented previously, the results indicate that the displacement values for irregular-cavity models are slightly bigger than those values for circular-cavity models for most models; however, for locations L1, L7 and L8, the displacement values for irregular-cavity models are smaller. The maximum displacement value is 26.38mm (which is equivalent to 5.9%) for a circular-cavity model, as opposed to 26.3mm (which is equivalent to 5.5%) for an irregular-cavity model with a cavity at location L1 (0, -1). As shown in Figure 4.28, the existence of an irregular cavity influences stability in a similar way to a circular cavity, where the cavity exists horizontally or vertically. Moreover, the results show that the SF values obtained by using irregular-cavity models are smaller than those obtained by using circular-cavity models and remained higher than the minimum recommended value for slope stability under rapid-drawdown conditions. This observation is applicable to most cavity models, except for those models with cavity locations such as (35, -1), (40, -1), (24, -3), (28, -3), (35, -3), (40, -3) and (24, -4). For example, the SF is 1.805 for a circular-cavity model, compared to 1.839 for an irregular-cavity model with a cavity at location L7 (35, -1).

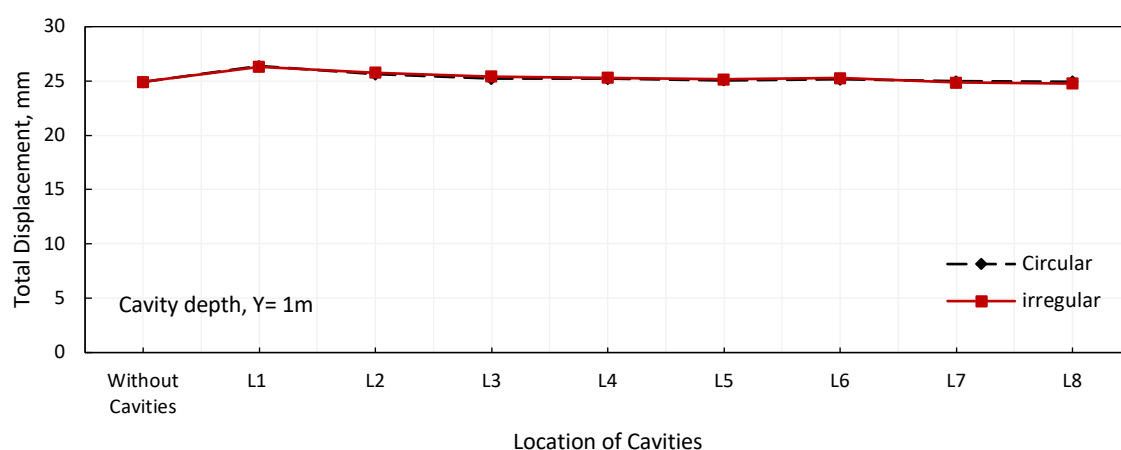


Figure 4.27: Comparison between the impact of the presence of a circular cavity and an irregular cavity sited under downstream on the displacement values using the MC model

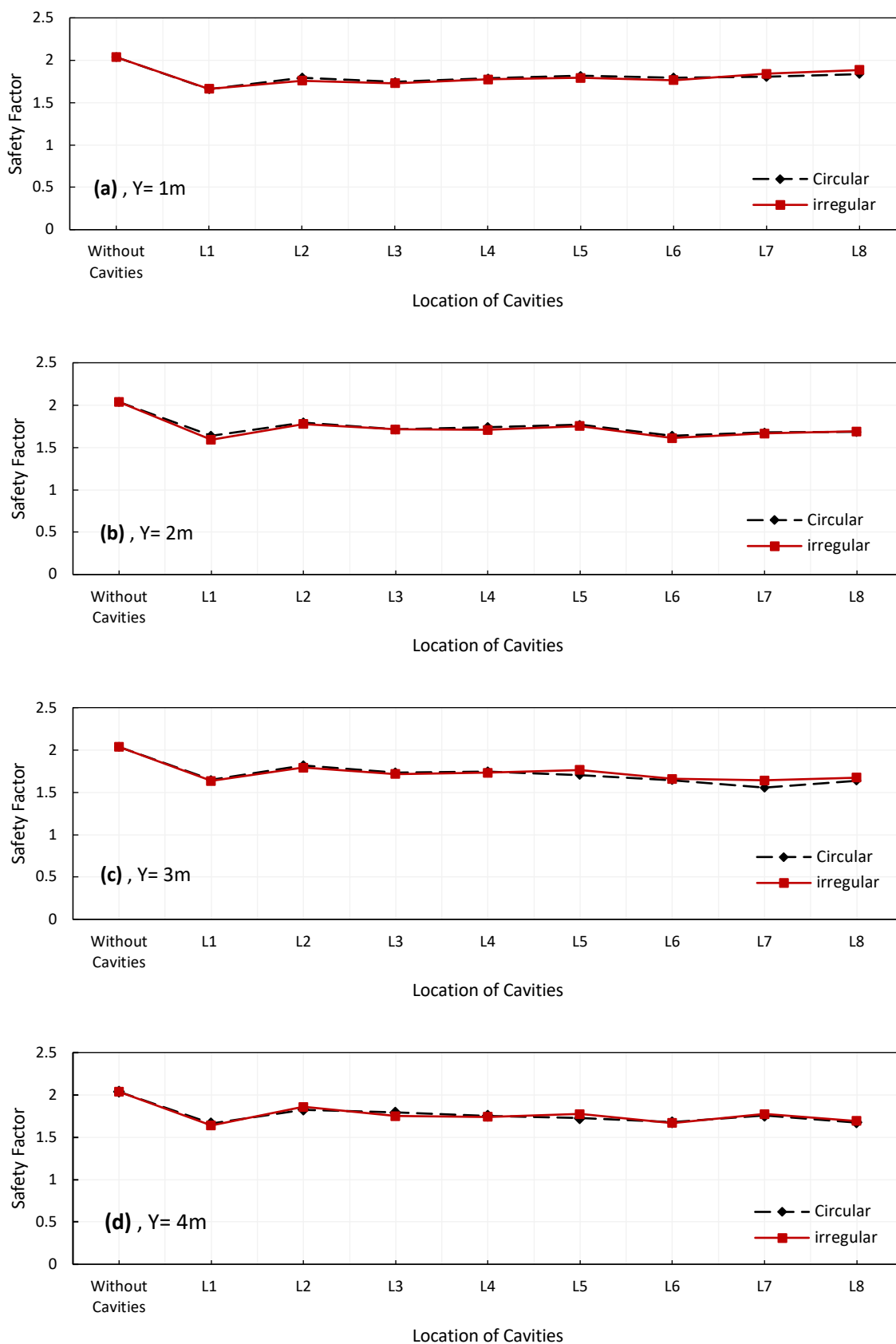


Figure 4.28: The impact of the presence of a circular and an irregular cavity under downstream on the SF using the MC model for depths (Y=1m to Y=4m)

### 4.5.2 Modelling the earth dam using the HS and MC models

A series of comparisons were done to simulate the effects of the presence of an irregular-shaped cavity on slope stability by using the MC and HS models to model the embankment and subsoil. A cavity was generated in various horizontal positions and depths, as detailed in Table 4.9.

Figure 4.29 shows the displacement values for models with a circular or an irregular cavity under the upstream slope versus the cavity's location. It should be noted that the irregular-cavity models recorded displacement values a little greater or less than those for circular-cavity models. The maximum displacement value was recorded at location L2 (-8, -1) for both cavity-type models; it is 37.17mm (which is equivalent to 40.3%) for a circular-cavity model, compared to 37.54mm (which is equivalent to 41.7%) for an irregular-cavity model. A comparison between the influence of the presence of a circular and an irregular cavity positioned under upstream on the SF values is illustrated in Figure 4.30. A summary of the locations and results obtained results are itemized in Table 4.9. It can be concluded that the cavity shape has an insignificant influence compared to the cavity's horizontal position. This observation is applicable to all models no matter where the cavity was situated horizontally or vertically. At cavity locations (-8, -1), (-8, -2), (-8, -3) and (-8, -4), the SF values are 0.727, 0.738, 0.767 and 1.053 for circular-cavity models, respectively, compared to 0.692, 0.845, 0.866 and 1.114, respectively, for irregular-cavity models. Generally, it can be observed that there is a slight difference (increasing or decreasing) between the SF values for circular-cavity and irregular-cavity models, except for a cavity at location L3 (-17, -1), where the SF is 1.398 for a circular-cavity model compared to 1.580 for an irregular-cavity model.

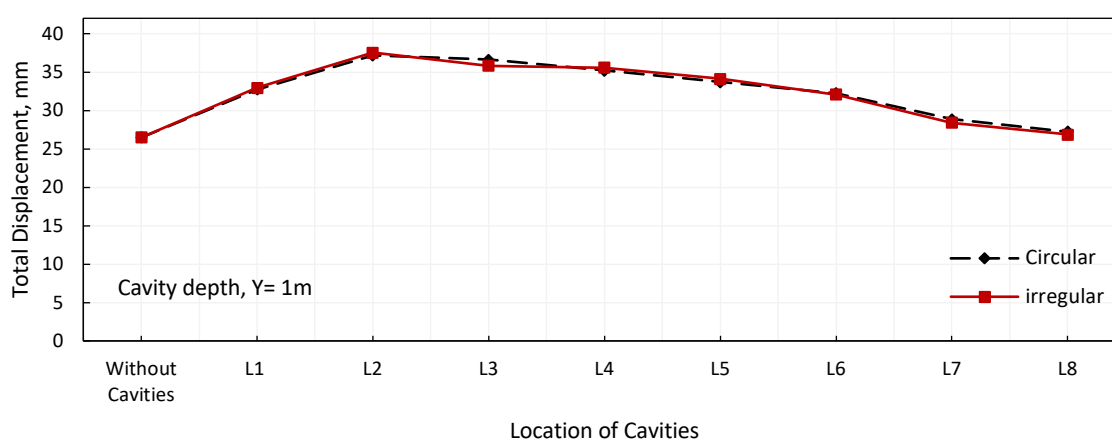


Figure 4.29: Comparison between the impact of the presence of a circular cavity and an irregular cavity under upstream on the displacement values using the HS and MC models

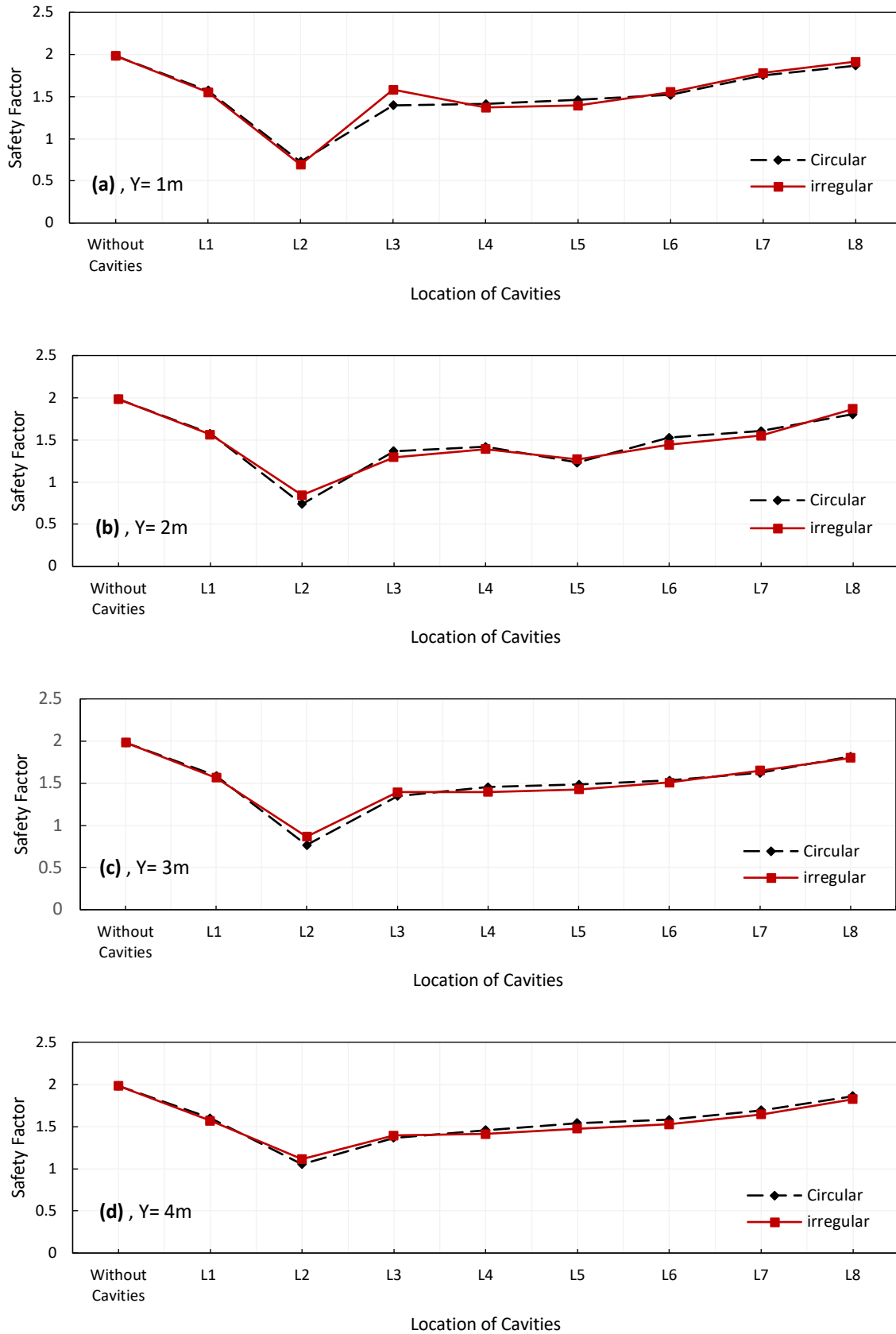


Figure 4.30: The impact of the presence of a circular and an irregular cavity under upstream on the SF using the HS and MC models for depths (Y=1m to Y=4m)

Table 4.9: Locations of the circular cavity and irregular cavity sited under upstream and downstream and the corresponding SF values for the MC and HS models

L	X, m	SF, Upstream							
		Cavity depth, m							
		Y= 1m		Y= 2m		Y= 3m		Y= 4m	
		Circular	Irregular	Circular	Irregular	Circular	Irregular	Circular	Irregular
Without Cavities		1.982							
L1	0	1.571	1.552	1.574	1.562	1.586	1.567	1.598	1.569
L2	-8	0.727	0.692	0.738	0.854	0.767	8.866	1.053	1.114
L3	-17	1.398	1.580	1.366	1.293	1.347	1.394	1.366	1.394
L4	-20	1.411	1.370	1.418	1.392	1.454	1.398	1.458	1.412
L5	-24	1.461	1.395	1.232	1.271	1.485	1.427	1.542	1.476
L6	-28	1.519	1.554	1.525	1.441	1.532	1.508	1.580	1.525
L7	-35	1.752	1.780	1.606	1.551	1.622	1.651	1.692	1.644
L8	-40	1.867	1.911	1.803	1.867	1.816	1.801	1.862	1.825
Safety Factor, Downstream									
L1	0	1.571	1.552	1.574	1.562	1.586	1.567	1.598	1.569
L2	8	1.781	1.753	1.767	1.750	1.762	1.718	1.767	1.725
L3	17	1.790	1.769	1.753	1.718	1.758	1.705	1.761	1.733
L4	20	1.804	1.770	1.749	1.723	1.755	1.758	1.798	1.789
L5	24	1.816	1.786	1.76	1.732	1.72	1.687	1.740	1.693
L6	28	1.855	1.837	1.68	1.680	1.697	1.692	1.706	1.703
L7	35	1.847	1.896	1.72	1.681	1.648	1.686	1.685	1.711
L8	40	1.852	1.846	1.678	1.639	1.643	1.659	1.676	1.666

(L) : Location of cavity (x, y); (X): The coordinates of the cavities' positions in X-axis

The displacement values for models with a circular cavity and for models with an irregular cavity under the downstream side and the corresponding cavity positions are shown in Figure 4.31. It is obvious from this figure that the displacement values are a little larger for irregular-cavity models than those for circular-cavity models; however, there are exceptions at locations L7 and L8. The maximum increase percentage of displacement is 24.4% for an irregular-cavity model below the dam's centreline, as opposed to 23.6% for a circular-cavity model.



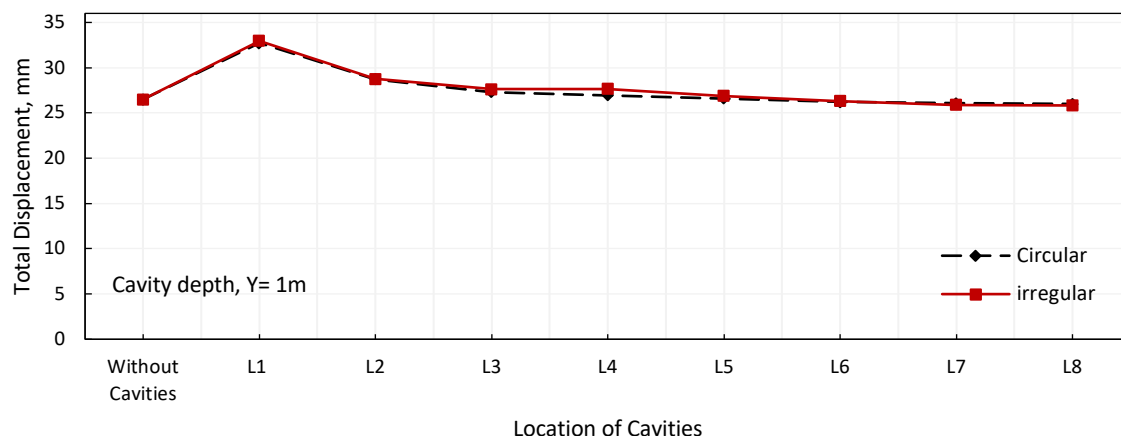


Figure 4.31: Comparison between the impact of the presence of a circular cavity and an irregular cavity under downstream on the displacement values using the HS and MC models

Figure 4.32 compares the impact on the stability of the existence of an irregular cavity with the existence of a circular cavity under the downstream slope. The details of the cavity's location and calculated SF values are outlined in Table 4.9. These being similar to the results for the downstream side obtained using the MC model, it can be deduced that the presence of an irregular cavity has a similar effect to the presence of a circular cavity for the majority of models. The obtained SF from all analyses are higher than the minimum approved values for slope stability under drawdown conditions (1.2–1.3); therefore, it can be concluded that the studied earth-dam model is stable. The lowest SF value recorded was 1.552 for an irregular-cavity model, compared to 1.571 for a circular-cavity model with a cavity at location L1 (0, -1). As mentioned in the previous analyses, the SF values are somewhat bigger for circular-cavity models than for irregular-cavity models for most locations considered, with an exception at L7. In cavity locations (35, -1), (35, -2), (35, -3) and (35, -4), the SF values amounted to 1.847, 1.72, 1.648 and 1.685, respectively, for circular-cavity models, compared to 1.896, 1.681, 1.686 and 1.711, respectively, for irregular-cavity models.

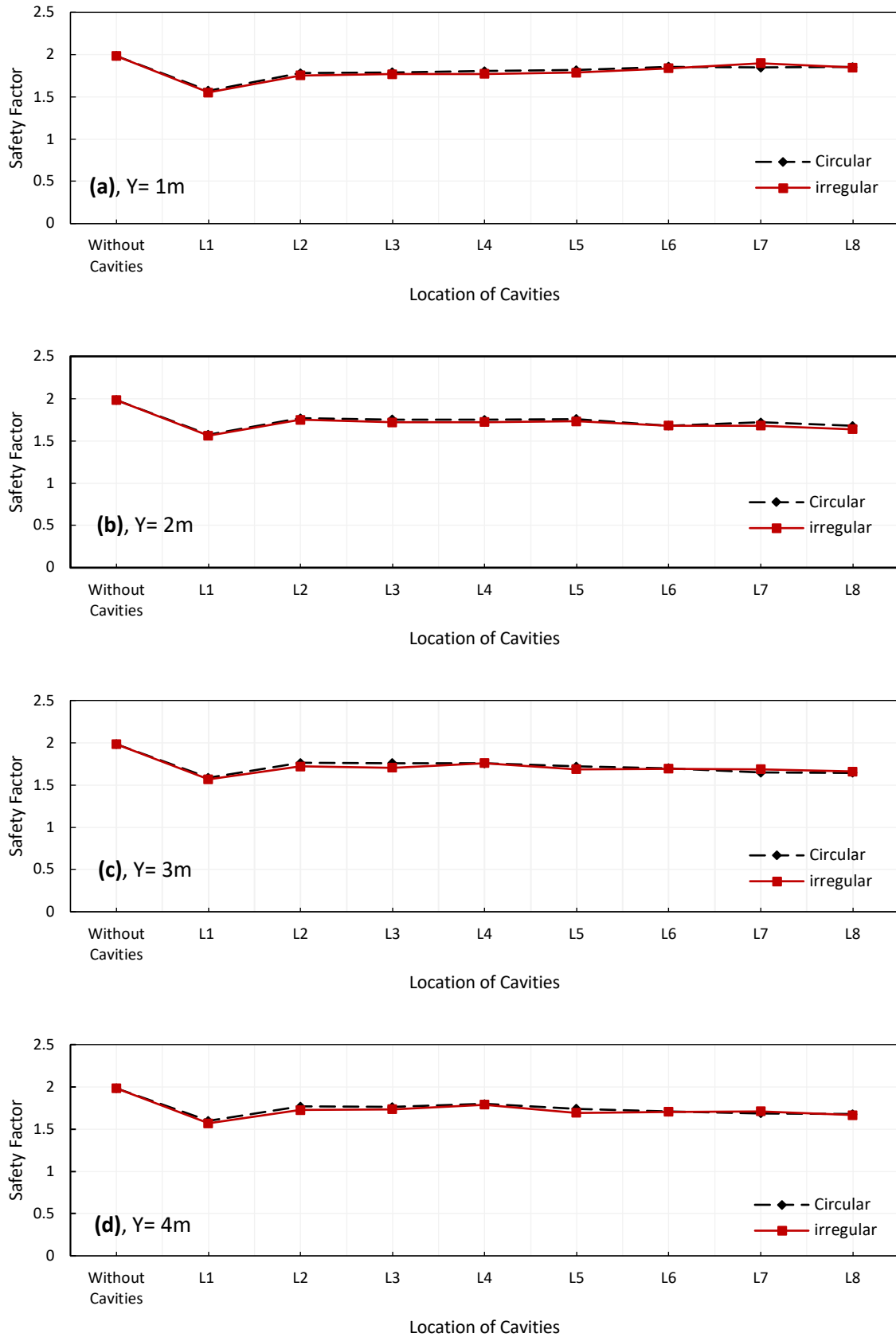


Figure 4.32: The impact of the presence of a circular and an irregular cavity under downstream on the SF using the HS and MC models for depths (Y=1m to Y=4m)

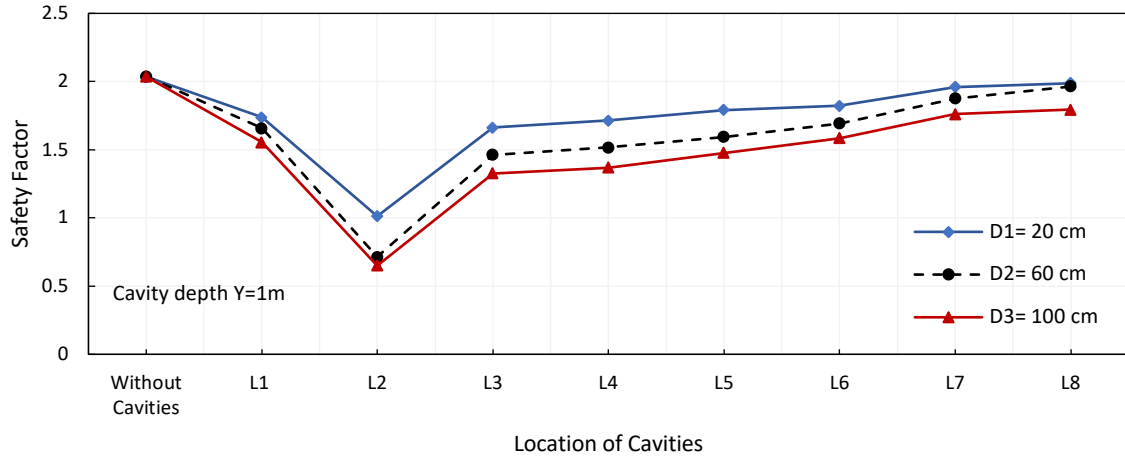
Based on what was concluded from the simulation related to the effect of cavity shape, this proves that the cavity's horizontal position is more influential on the dam's stability than its shape. In addition, the values of SF and displacement which obtained from the application of the two shapes, in general, are close to each other. Therefore, to simplify the modelling process, a circular-cavity model was adopted to simulate the impact of cavity diameter, the number of cavities and the joint impact of cavities and the embankment's shear-strength parameters on a slope's stability.

## 4.6 Impact of the cavity diameter

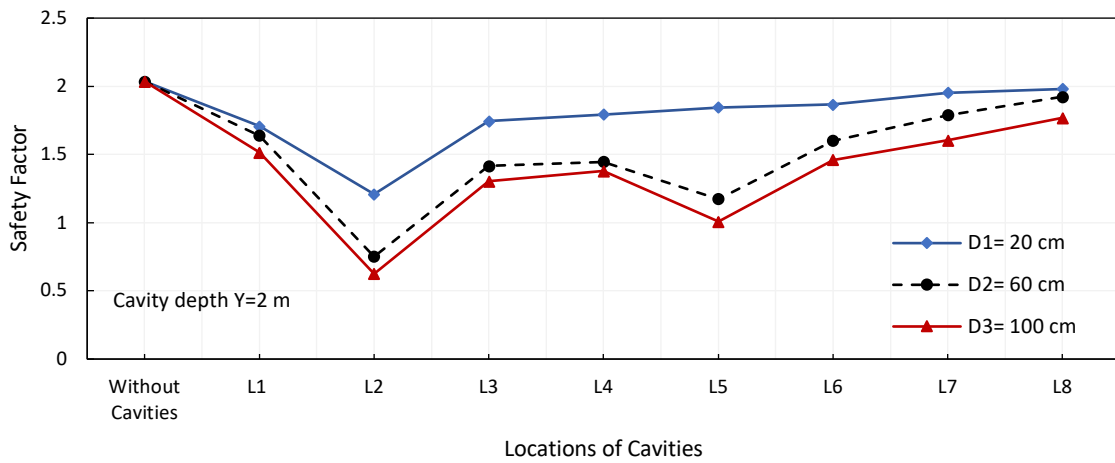
In this subsection, the results of the investigation of the impact of the cavity diameter on the stability of an earth dam under rapid-drawdown conditions are presented. Various diameters of cavity were assumed ( $D= 20\text{cm}$ ,  $60\text{cm}$  and  $100\text{cm}$ ). The cavity was created in different horizontal positions, as listed in Table 4.3, and at different depths ( $Y= 1\text{m}$ ,  $2\text{m}$  and  $3\text{m}$ ).

### 4.6.1 Modelling the earth dam using the MC model

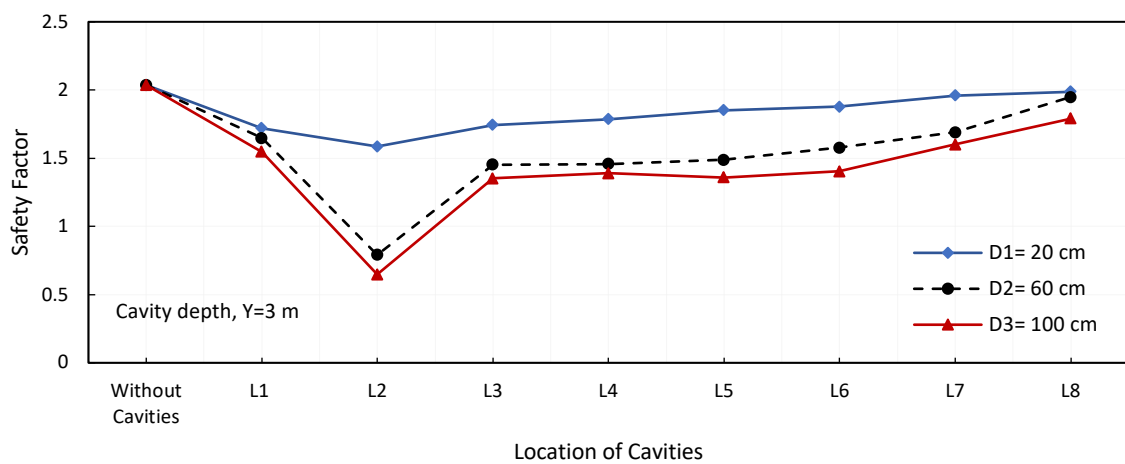
Figure 4.33 and Table 4.10 illustrate the combined impact of the cavity's location and its diameter on the stability of the upstream side. The MC model was used to model the embankment and the subsoil of the earth dam. It is clear that the cavity diameter affects the stability of the dam significantly as the cavity diameter increases from  $20\text{cm}$  to  $100\text{cm}$ . This behaviour was observed in all models, regardless of where the cavity was situated horizontally or vertically. This may indicate the fact that increasing a cavity's diameter also increases the probability of it intersecting with critical sliding surfaces. For example, the SF values dropped from  $1.013$  to  $0.65$  and from  $1.586$  to  $0.648$  as the cavity diameter increases from  $20\text{cm}$  to  $100\text{cm}$  for models with a cavity situated at L2 (-8, -1) and L2 (-8, -3), respectively, whereas the displacement values increased from  $29.46\text{mm}$  to  $31.76\text{mm}$  and from  $24.90\text{mm}$  to  $31.58\text{mm}$  for the same models, respectively. In addition, further increasing the cavity diameter makes the earth dam unstable when the cavity is situated in location L2 (-8, -3), L3 (-17, -2) and L5 (-24, -2), where the SF values are equal to or smaller than the values recommended by the codes of practice for earth-dam stability under rapid-drawdown conditions (1.2–1.3) (NRCS, 2005; USBR, 2011; ULDC, 2012). Table 4.10 details the cavity locations and corresponding SF values.



(a)



(b)



(c)

Figure 4.33: Impact of cavity’s diameter on the FS of upstream using MC model for different positions and depths: (a) Y= 1m, (b) Y= 2m, (c) Y= 3m

Table 4.10: The locations and diameters of the cavity and the corresponding SF values for the upstream side

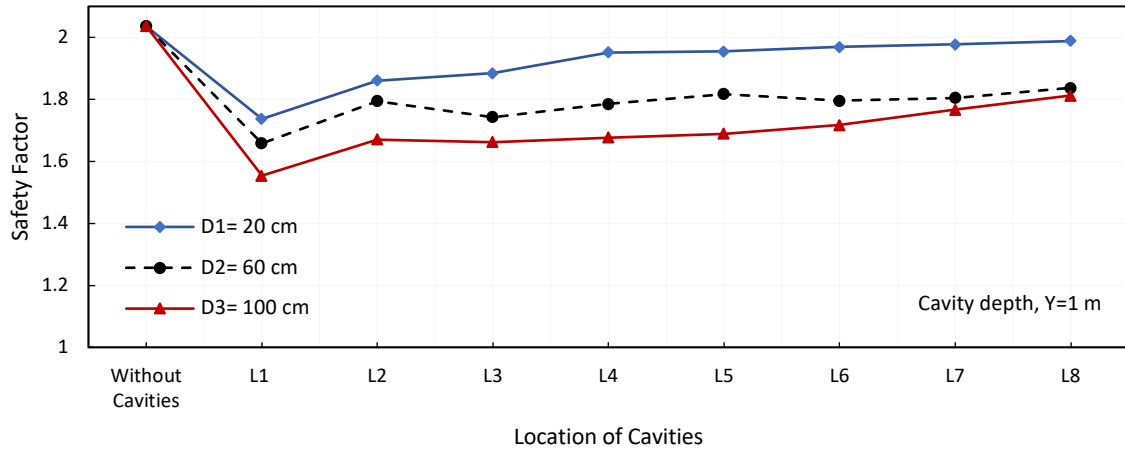
Cavity location	Coordinates of position (X), m	Cavity depth (Y), m	SF		
			Diameter of cavity, cm		
			20	60	100
Without cavities			2.036		
L1	0	1	1.737	1.658	1.554
		2	1.706	1.638	1.515
		3	1.721	1.647	1.546
L2	-8	1	1.013	0.715	0.650
		2	1.209	0.751	0.625
		3	1.586	0.791	0.648
L3	-17	1	1.663	1.463	1.326
		2	1.745	1.416	1.303
		3	1.743	1.452	1.351
L4	-20	1	1.714	1.516	1.368
		2	1.793	1.447	1.378
		3	1.786	1.458	1.389
L5	-24	1	1.791	1.594	1.478
		2	1.845	1.173	1.007
		3	1.831	1.489	1.358
L6	-28	1	1.821	1.694	1.585
		2	1.867	1.602	1.460
		3	1.877	1.577	1.404
L7	-35	1	1.961	1.876	1.760
		2	1.952	1.789	1.604
		3	1.960	1.690	1.600
L8	-40	1	1.988	1.966	1.795
		2	1.981	1.923	1.767
		3	1.989	1.949	1.790

The joint effect of cavity's location and its diameter on the SF values for models containing a cavity beneath the downstream slope, as shown in Figure 4.34 and Table 4.11. Similar to the results for the upstream side presented previously, it appears that increasing the cavity diameter from 20cm to 100cm results in decreasing the SF as expected, regardless of changes in the cavity's location, either horizontally or vertically. For instance, the SF decreased from 1.861 to 1.671 and from 1.845 to 1.623 for models with a cavity at location L2 (8, -1) and L2 (8, -3), respectively; and, for these locations, the displacement values increased from

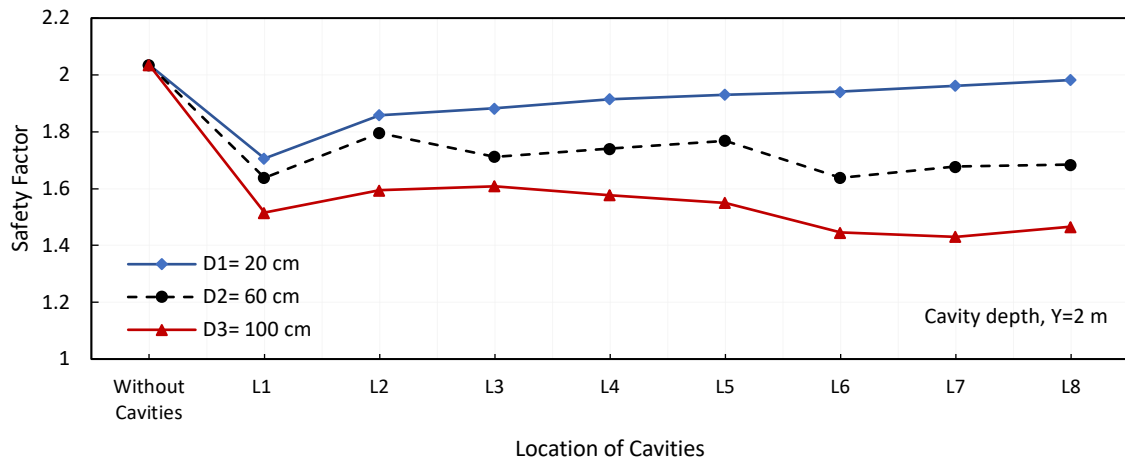
25.61mm to 24.57mm and from 25.66mm to 24.72mm, respectively. The smallest SF value obtained, however, is 1.430; this belongs to the model with a cavity of diameter 100cm at location L7 (35, -2), which is greater than the minimum value stipulated by the codes of practice for the stability of dam slopes during rapid-drawdown conditions (1.2–1.3). This is in contrast to the behaviour of the upstream slope. The results indicate that, although increasing the diameter of a cavity below the downstream slope caused a lower SF, the impact was not sufficient to cause failure.

Table 4.11: The locations and diameters of the cavity and the corresponding SF values for the downstream side

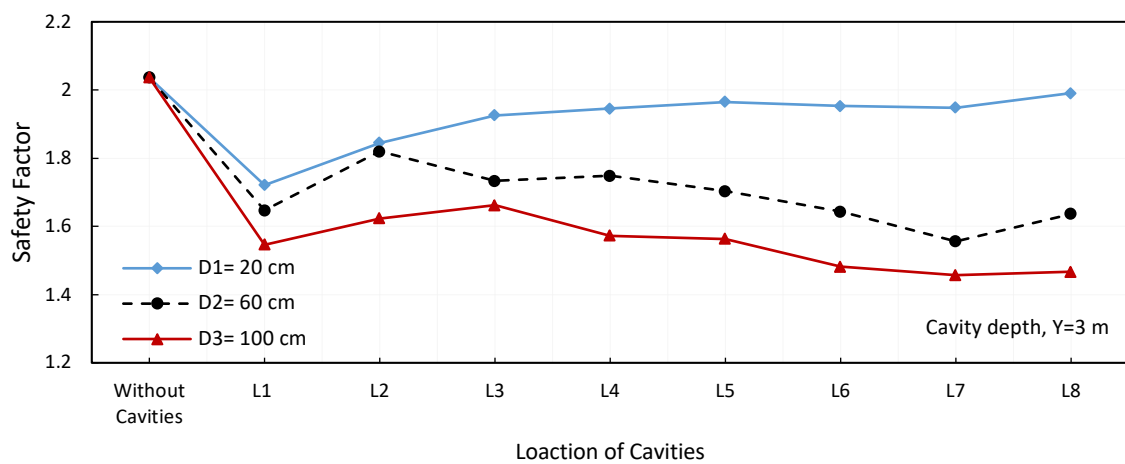
Cavity location	Coordinates of position (X), m	Cavity depth (Y), m	SF		
			Diameter of cavity, cm		
			20	60	100
Without cavities			2.036		
L1	0	1	1.737	1.658	1.554
		2	1.706	1.638	1.515
		3	1.721	1.647	1.546
L2	8	1	1.861	1.794	1.671
		2	1.859	1.796	1.594
		3	1.845	1.820	1.623
L3	17	1	1.884	1.743	1.662
		2	1.882	1.712	1.608
		3	1.926	1.733	1.662
L4	20	1	1.951	1.785	1.677
		2	1.915	1.740	1.577
		3	1.945	1.748	1.573
L5	24	1	1.955	1.817	1.689
		2	1.931	1.769	1.550
		3	1.965	1.703	1.563
L6	28	1	1.969	1.796	1.717
		2	1.941	1.638	1.445
		3	1.953	1.643	1.482
L7	35	1	1.977	1.805	1.767
		2	1.962	1.677	1.430
		3	1.948	1.556	1.457
L8	40	1	1.989	1.837	1.812
		2	1.982	1.684	1.466
		3	1.990	1.637	1.467



(a)



(b)



(c)

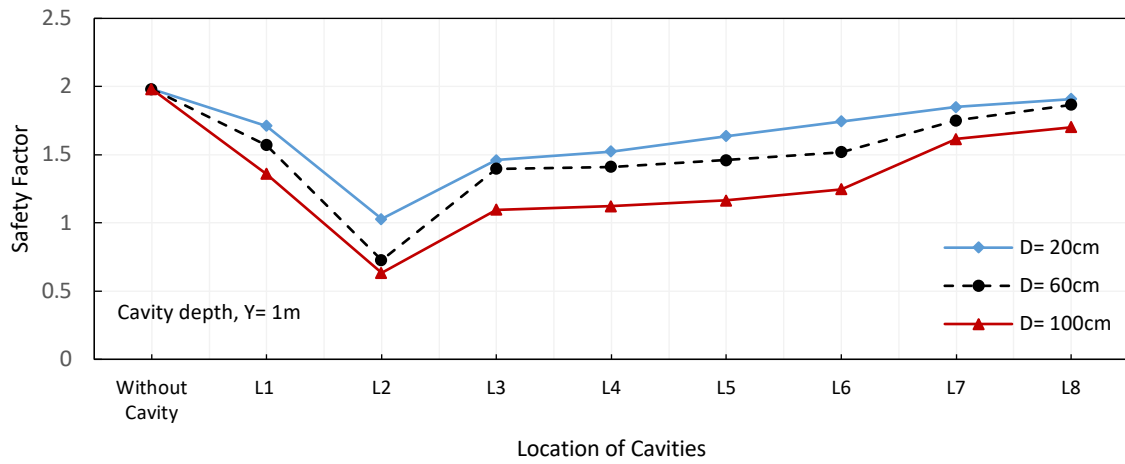
Figure 4.34: Impact of cavity’s diameter on the FS of downstream using MC model for different positions and depths: (a) Y= 1m, (b) Y= 2m, (c) Y= 3m

#### 4.6.2 Modelling the earth dam using the HS and MC models

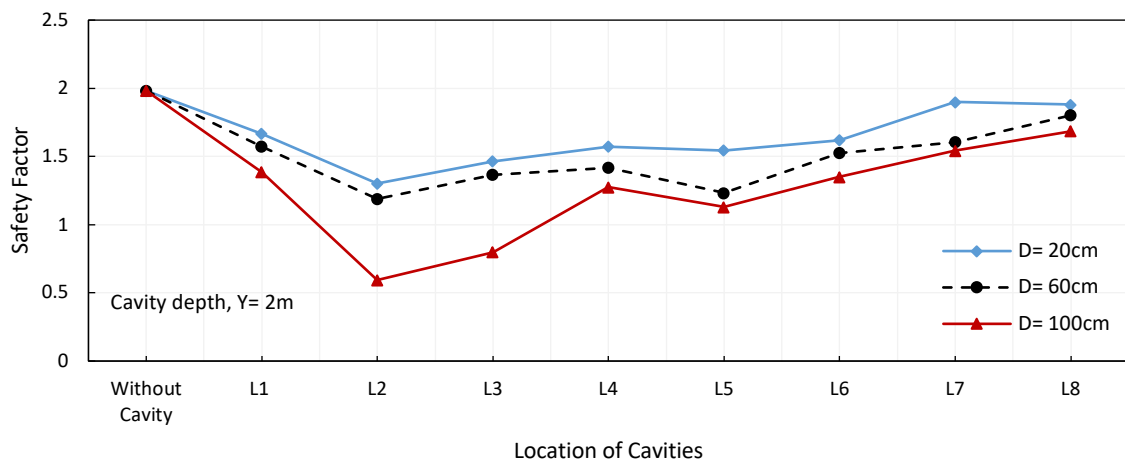
In the second analysis, the HS and MC models were used to model the embankment and subsoil. Each modelled cavity's location and diameter are as given in the first part of the analysis of the impact of cavity diameter.

Figure 4.35 reveals the SF values versus the cavity's location for models with a cavity situated under the upstream side. Table 4.12 identifies the input parameters and the PLAXIS 2D output. According to the results, it can be observed that the stability of the earth dam reduces considerably when there is an increase in cavity diameter from 20cm to 100cm. This impact has been observed for all models, regardless of the change in the location of cavity vertically and horizontally. For example, the SF values dropped from 1.030 to 0.634 and from 1.374 to 0.927 as the cavity diameter increased from 20cm to 100cm for models with cavity locations (-8, -1) and (-8, -3), respectively; however, the displacement values increased from 37.17mm to 39.46mm and from 28.83mm to 35.21mm, respectively, for the same models. It is important to mention that the percentage decrease for the SF varies according to the cavity's position. For instance, the SF dropped by 64.6% for a model with a cavity at location L2 (-8, -1), compared to 10.7% for the ones with a cavity at location L8 (-45, -1) when increasing the cavity diameter( refer to Table 4.12 for details of the SF values). The results prove that the increase in cavity diameter for a cavity situated at locations L2 to L6 made the earth-dam model unstable, where the SF values dropped below the minimum stipulated values (1.2–1.3).

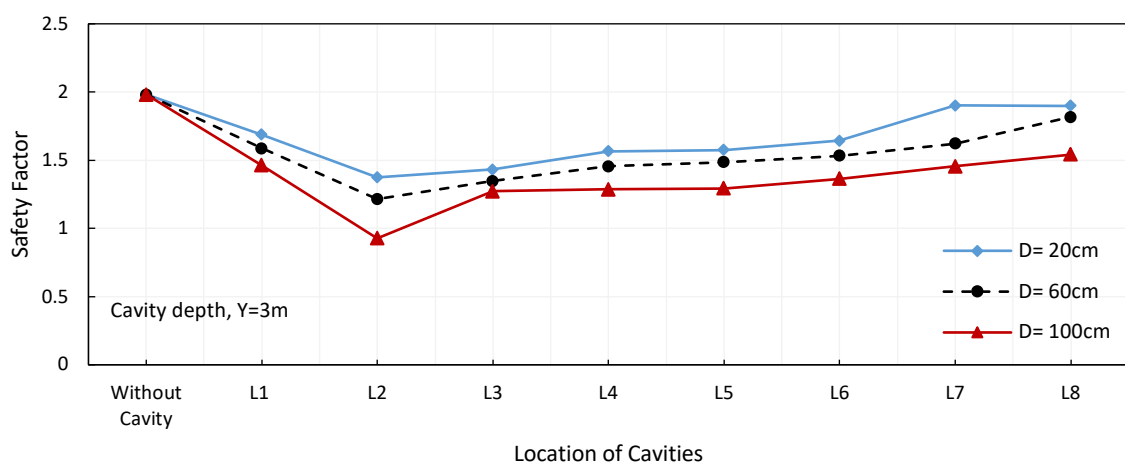




(a)



(b)



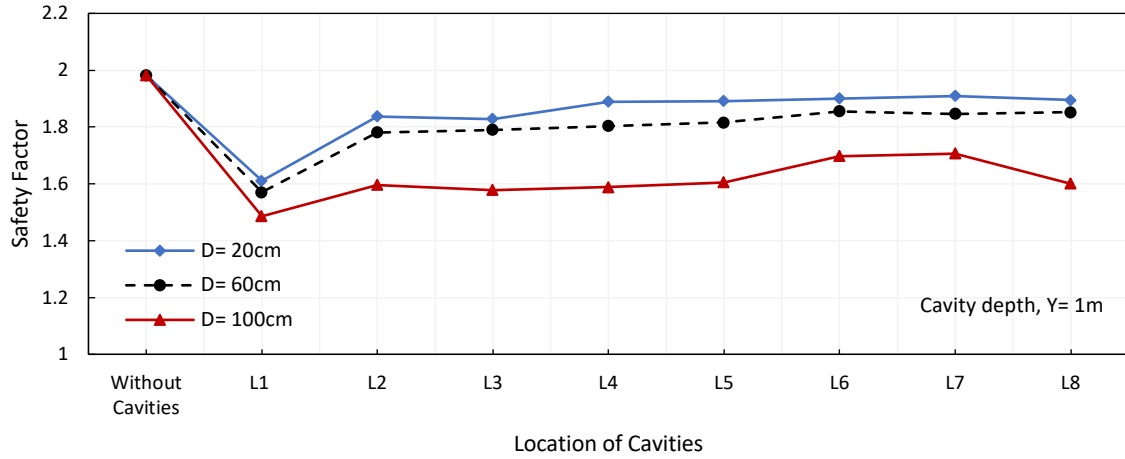
(c)

Figure 4.35: Impact of cavity’s diameter on the FS of upstream using the HS and MC models for different positions and depths: (a) Y= 1m, (b) Y= 2m, (c) Y= 3m

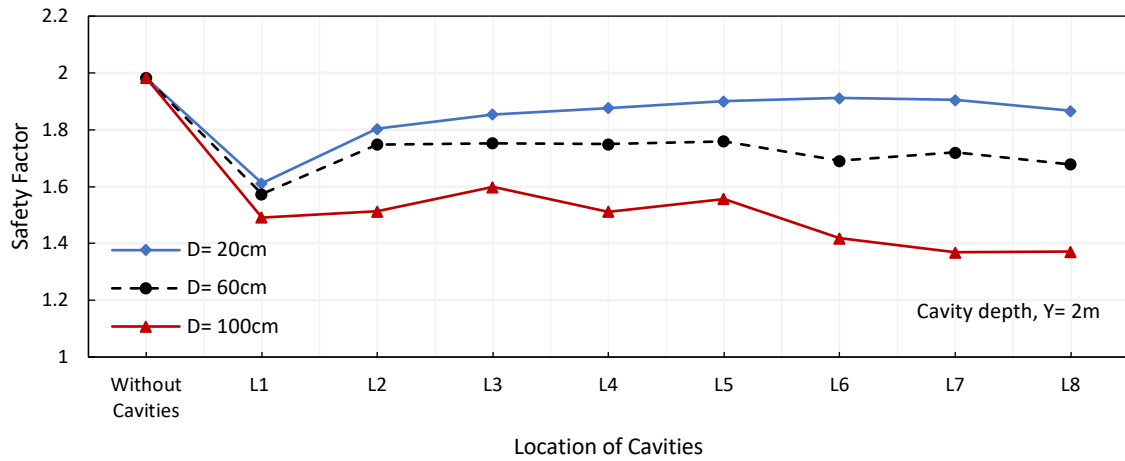
Table 4.12: The locations and diameters of the cavity and the corresponding SF values for the upstream side

Cavity location	Coordinates of position (X), m	Cavity depth (Y), m	SF		
			Diameter of cavity, cm		
			20	60	100
Without cavities			1.982		
L1	0	1	1.711	1.571	1.360
		2	1.666	1.574	1.385
		3	1.687	1.586	1.461
L2	-8	1	1.030	0.727	0.634
		2	1.302	1.189	0.594
		3	1.374	1.215	0.927
L3	-17	1	1.460	1.398	1.096
		2	1.464	1.366	0.798
		3	1.432	1.347	1.273
L4	-20	1	1.525	1.411	1.122
		2	1.572	1.418	1.276
		3	1.565	1.454	1.285
L5	-24.0	1	1.636	1.461	1.165
		2	1.545	1.232	1.130
		3	1.575	1.485	1.294
L6	-28	1	1.745	1.519	1.248
		2	1.620	1.525	1.350
		3	1.643	1.532	1.364
L7	-35	1	1.851	1.752	1.616
		2	1.900	1.606	1.542
		3	1.902	1.622	1.454
L8	-40	1	1.909	1.867	1.703
		2	1.880	1.803	1.686
		2	1.898	1.816	1.543

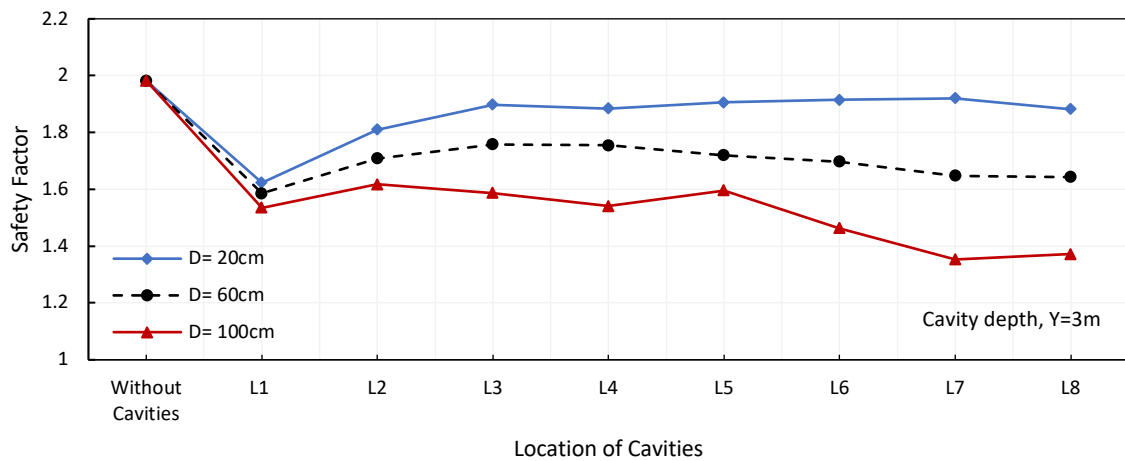
The results of the analysis for the downstream side are shown in Figure 4.36 and Table 4.13. The results prove that increasing the cavity diameter decreases the stability of the earth-dam model. For example, the SF values changed from 1.828 to 1.578, from 1.854 to 1.598 and from 1.898 to 1.587 when increasing the cavity diameter for models with cavity locations (17, -1), (17, -2) and (17, -3), respectively. However, the displacement value increases when increasing the cavity diameter, as expected, as it increased from 26.94 to 27.25, from 26.92mm to 27.06mm and from 26.71mm to 27.11mm, respectively, for the same models. This influence was observed for all models containing a cavity, wherever it was created in the subsoil (refer to Table 4.13 for details of the SF values).



(a)



(b)



(c)

Figure 4.36: Impact of cavity’s diameter on the FS of downstream using the HS and MC models for different positions and depths: (a) Y= 1m, (b) Y= 2m, (c) Y= 3m

Table 4.13: The locations and diameters of the cavity and the corresponding SF values for the downstream side

Cavity location	Coordinates of position (X), m	Cavity depth (Y), m	SF		
			Diameter of cavity, cm		
			20	60	100
Without cavities			1.982		
L1	0.0	1	1.611	1.571	1.486
		2	1.612	1.574	1.491
		3	1.623	1.586	1.535
L2	8.0	1	1.838	1.781	1.596
		2	1.803	1.748	1.513
		3	1.810	1.709	1.617
L3	17.0	1	1.828	1.790	1.578
		2	1.854	1.753	1.598
		3	1.898	1.758	1.587
L4	20.0	1	1.889	1.804	1.589
		2	1.877	1.749	1.512
		3	1.884	1.755	1.541
L5	24.0	1	1.892	1.816	1.605
		2	1.900	1.760	1.557
		3	1.906	1.720	1.596
L6	28.0	1	1.901	1.855	1.698
		2	1.912	1.691	1.418
		3	1.915	1.697	1.463
L7	35.0	1	1.910	1.847	1.707
		2	1.905	1.720	1.369
		3	1.920	1.648	1.353
L8	40.0	1	1.895	1.852	1.601
		2	1.867	1.678	1.371
		3	1.882	1.643	1.372

#### 4.7 Impact of the number of cavities

The fourth section details the investigation to evaluate the impact of the existence of more than one cavity on the slope stability of the earth dam. Different vertical and horizontal locations of cavities were considered in the analysis. The stability analyses were performed to consider the existence of circular cavities with a diameter of 60cm. Most of the cavities' horizontal positions were selected depending on the results of the location impact analysis detailed in the previous section.

### 4.7.1 Impact of the existence of dual cavities modelled using the MC model

The effect of the existence of two cavities in the subsoil of the earth dam on its stability is examined in this section. Different horizontal positions of cavities were considered in the analysis. Table 4.14 presents the coordinates of the location of cavities in the X-direction and Y-direction. The Mohr-Coulomb model was utilized to model an earth dam.

Table 4.14: Coordinates of cavities' locations for dual-cavity models at the same depth

Cavity location	Cavity depth, m	Coordinates of positions in X-axis, m	
		Cavity 1	Cavity 2
L1	1	-8	0
L2	1	0	+35
L3	1	-8	-24
L4	1	-24	0
L5	1	-8	+35
L6	1	-24	+35
L7	1	+35	+40
L8	1	-8	+40
L9	1	-24	+40
L10	1	0	+40

(-): Indicates that the cavity is under the upstream slope; (+): indicates that the cavity is under the downstream slope.

This simulation was performed to consider two cavities situated at a depth of 1m. Figure 4.37 displays an example of the cavity arrangement for models with two cavities situated at the same depth. The impact on the stability of the existence of two cavities for various locations of cavities is shown in Figure 4.38. It is clear that the existence of two cavities results in a significant drop in the stability of the earth dam. The SF value decreased from 2.036 to 0.384 for models without a cavity and with two cavities at location L3, respectively, compared from 2.036 to 0.715 for models without a cavity and with a cavity, respectively. The displacement value increased from 24.91mm to 32.51mm, compared to 24.91mm to 29.46mm for the same models, respectively. The percentage reduction in the SF value is 81.1% for a dual-cavity model, as opposed to 64.9% for a single-cavity model, while the percentage increase in the displacement is 30.5% for a dual-cavity model, compared to 18.1% for a single-cavity model. Furthermore, the analyses indicate that the SF values decrease considerably when one or two cavities are sited beneath the upstream slope. The SF values are less than the required limit

for the safety of earth dams (1.2–1.3) (NRCS, 2005; USBR, 2011; ULDC, 2012) for models with cavities at locations L1, L3, L4, L5, L8 and L9. Table 4.15 details the cavities' locations and corresponding SF values. This means that increasing the number of cavities makes the dam unsafe if one of the cavities is present beneath the upstream. This behaviour can indicate that the condition of rapid drawdown is one of the most critical conditions for the upstream slope.

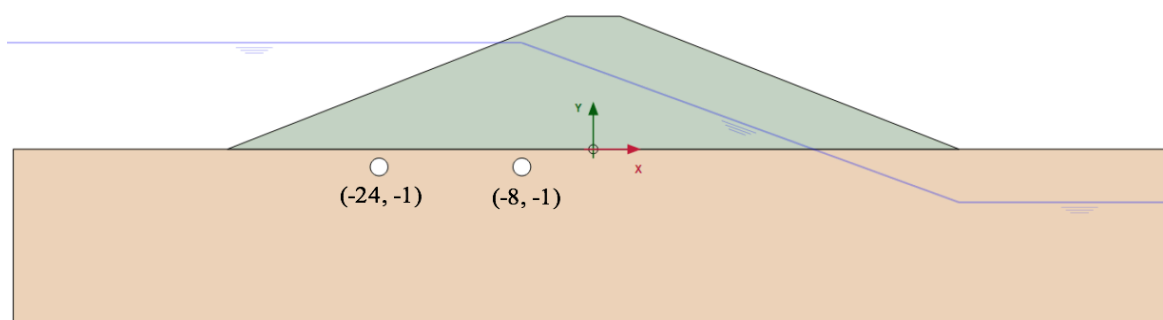


Figure 4.37: Example cavity arrangement for models with two cavities sited at the same depth (L3)

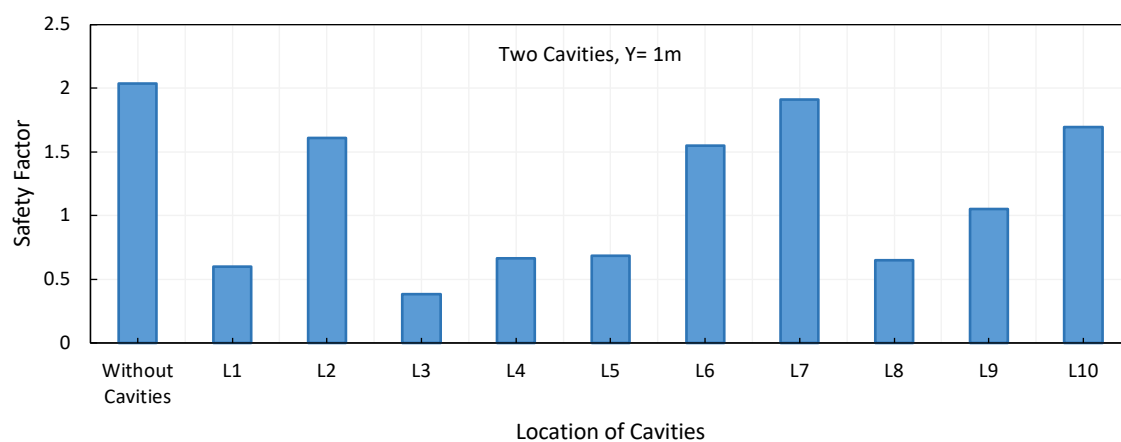


Figure 4.38: Impact on the SF for models with two cavities sited at a depth of 1m using the MC model

The impact of the depth of the two cavities on the stability was examined in these analyses. Three depths of cavities were considered;  $Y = 1\text{m}$ ,  $2\text{m}$  and  $3\text{m}$ . Table 4.15 shows the input data and the results of the stability analysis. The impact of the depth of the two cavities on a slope's stability as demonstrated in Figure 4.39. It appears that the SF values vacillate (increasing or decreasing) when the cavities' depth increase from 1m to 3m. For example, the

SF values increased from 0.597, 0.384 and 0.686 to 0.809, 1.043 and 0.989 for models containing two cavities at locations L1, L3 and L5, respectively; however, it reduced from 1.610, 1.910 and 1.697 to 1.654, 1.851 and 1.687 for dual-cavity models with cavities at locations L2, L7 and L10, respectively.

Table 4.15: Coordinates of cavities' locations and the corresponding SF values for the dual-cavity models for different depths

Cavity location	The coordinates of positions in X-axis, m		SF		
	Cavity 1	Cavity 2	Cavity depth, m		
			Y= 1m	Y= 2m	Y= 3m
	Without cavities		2.036		
L1	-8	0	0.597	0.676	0.809
L2	0	+35	1.610	1.627	1.654
L3	-8	-24	0.384	0.580	1.043
L4	-24	0	0.665	0.416	1.043
L5	-8	+35	0.686	0.970	0.989
L6	-24	+35	1.549	1.550	1.563
L7	+35	+40	1.910	1.802	1.851
L8	-8	+40	0.652	0.673	0.875
L9	-24	+40	1.050	1.398	1.529
L10	0	+40	1.697	1.685	1.687

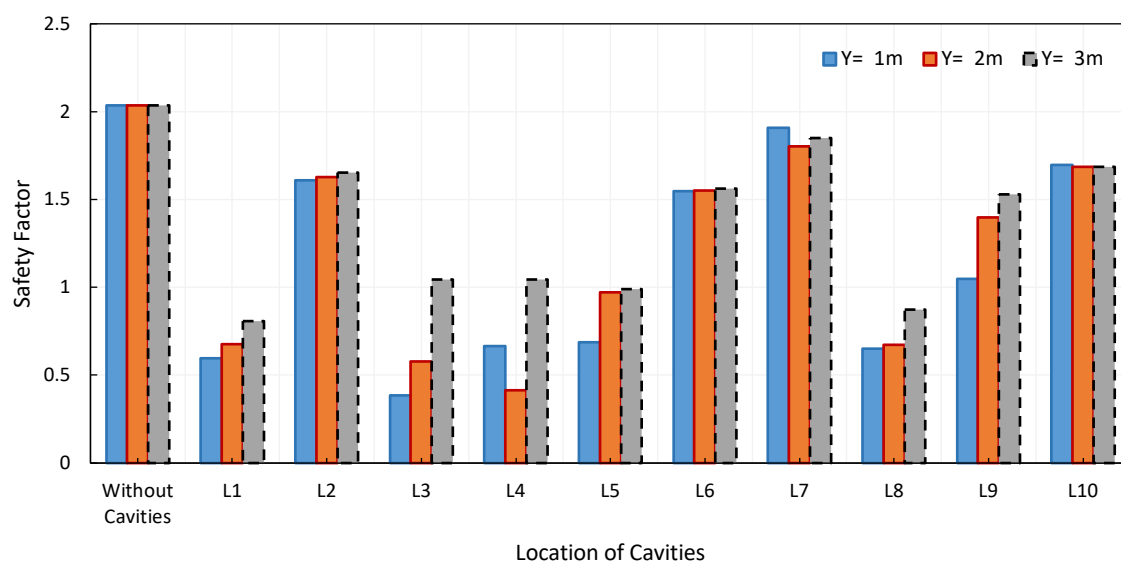


Figure 4.39: Impact on the SF of the existence of two cavities at different positions and depths using the MC model

Figure 4.40 shows a comparison between the impact on stability of two cavities situated at the same depth and mirrored X positions under the upstream and downstream sides. The coordinates of the cavities' locations in both directions are detailed in Table 4.16. The results demonstrate that the presence of two cavities under the upstream slope affects stability dramatically. For example, for the model at location L1, the SF value decreased from 2.036 to 0.597 for models without a cavity and with cavities sited under the upstream slope, respectively, while it decreased to 1.573 for a similar model sited under the downstream slope. There is an exception at location L4, where the SF values are 1.824 for the model under the upstream side, compared to 1.910 for the model under the downstream side. This behaviour may be because the cavities do not intersect with the failure surface at this location under the upstream side.

Table 4.16: Coordinates of cavities' locations for dual-cavity models sited under upstream and downstream at the same depth

Cavity location	Cavity depth, m	The coordinates of cavities locations in X direction, m	
		Cavity 1	Cavity 2
L1	1	±8.0	0.0
L2	1	±8.0	±24.0
L3	1	±24.0	0.0
L4	1	±35.0	±40.0
L5	1	±17.0	±28.0
L6	1	±15.0	±25.0
L7	1	±8.0	±35.0

(-): Indicates that the cavity is under upstream, (+): indicates that the cavity is under downstream



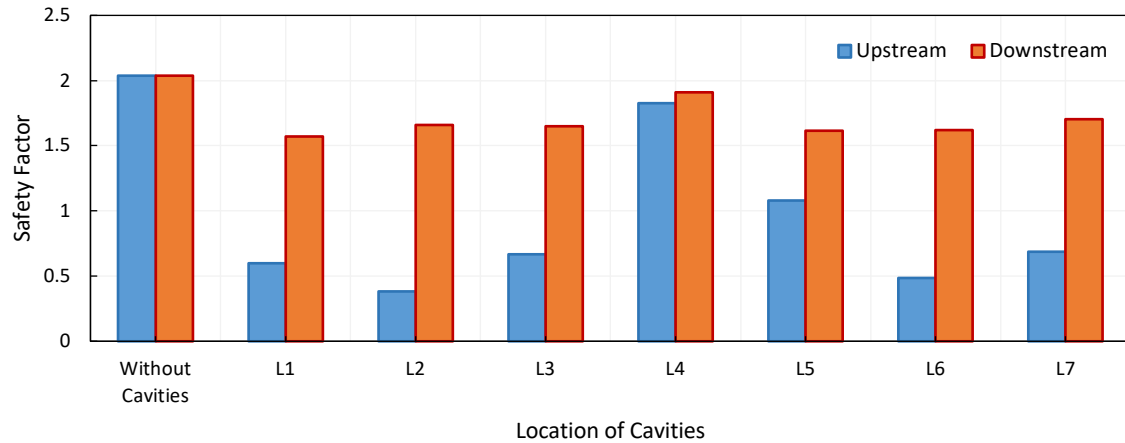


Figure 4.40: Comparison between the impact on the SF of two cavities situated under upstream and downstream using the MC model

A comparison was made to assess the influence of the existence of two cavities positioned at different depths and in mirrored horizontal positions under the upstream and downstream. The coordinates of the locations of the cavities, in the X and Y axes, are listed in Table 4.17. The results in Figure 4.41 indicate that the existence of two cavities under the upstream face affects the stability of the dam significantly, no matter where these cavities are found under the upstream face, although their depth varies. The SF values for the upstream side are smaller than the downstream side and less than the required limit for the safety of earth dams, except for location L4; the SF is 1.824 for a model under the upstream, compared to 1.665 for a model under the downstream. Figure 4.42 shows a typical cavity arrangement for models with two cavities sited at the different depths.

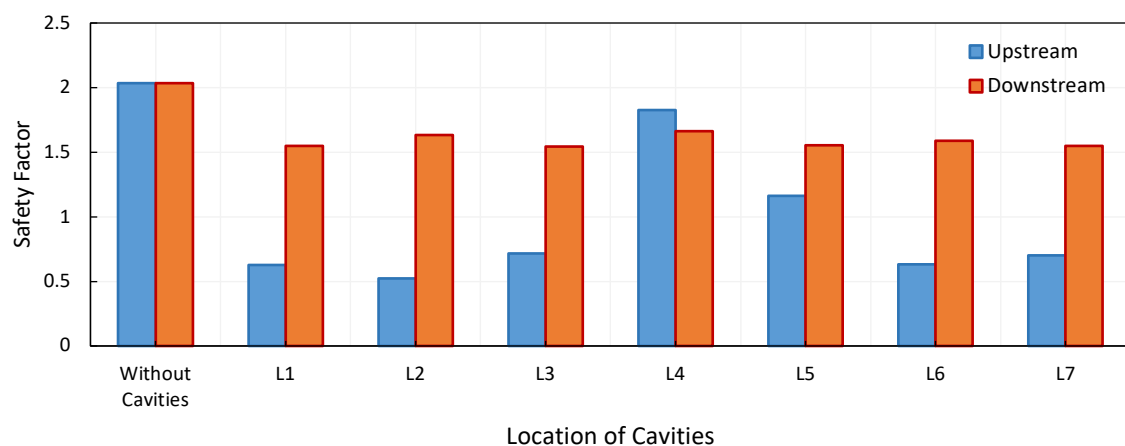


Figure 4.41: Comparison between the impact on the SF of two cavities sited under upstream and downstream at various depths using the MC model

Table 4.17: Coordinates of cavities' locations for dual-cavity models sited under upstream and downstream at the different depths

Cavity location	Cavity depth, m		The coordinates of cavities locations in X direction, m	
	Cavity 1	Cavity 2	Cavity 1	Cavity 2
L1	-1	-2	±8.0	0.0
L2	-3	-1	±8.0	±24.0
L3	-3	-1	±24.0	0.0
L4	-1	-2	±35.0	±40.0
L5	-2	-3	±17.0	±28.0
L6	-1	-2	±15.0	±25.0
L7	-2	-3	±8.0	±35.0

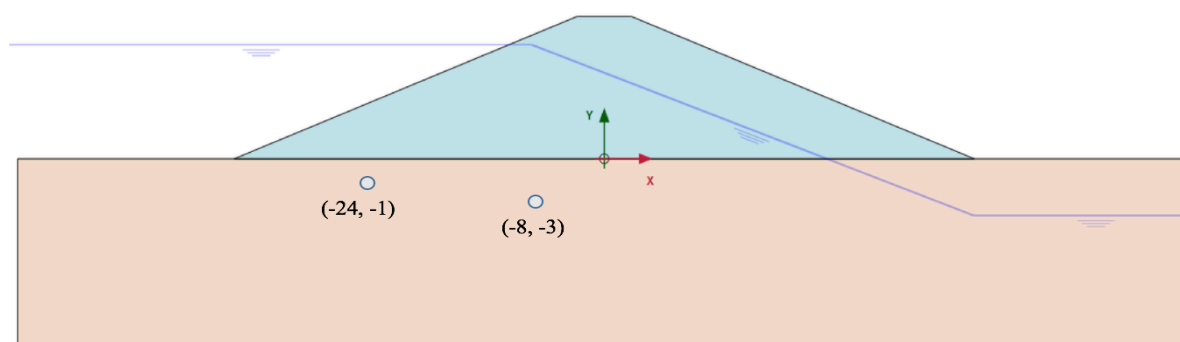


Figure 4.42: Typical cavity arrangement for models with two cavities sited at the different depths (L2)

Figure 4.43 reveals the impact on the SF values of variations in the depth of the two cavities located within the same model. All cavity models are created below the upstream side. The coordinates of the cavities' locations in the X and Y directions are detailed in Table 4.18. It is clear that two cavities existing at the same depth have more of an influence on the slope's stability compared to two cavities existing at different depths within the same model. For example location L5, the SF is 1.16 for a model with two cavities located at various depths, as opposed to 1.078 for one with two cavities located at the same depth. Overall, the SF values for models with cavities located at different depths are bigger for all assumed locations, with an exception at location L4, where the SF values were equal for both sides and amounted to 1.824.

Table 4.18: Coordinates of cavities locations in X and Y directions for the dual-cavity models sited under upstream

Cavity location	The coordinates of locations of cavities in X and Y directions, m			
	Cavities at the same depth		Cavities at the different depth	
	Cavity 1	Cavity 2	Cavity 1	Cavity 2
L1	(-8, -1)	(0, -1)	(-8, -1)	(0, -2)
L2	(-8, -1)	(-24, -1)	(-8, -3)	(-24, -1)
L3	(-24, -1)	(0, -1)	(-24, -3)	(0, -1)
L4	(-35, -1)	(-40, -1)	(-35, -1)	(-40, -2)
L5	(-17, -1)	(-28, -1)	(-17, -2)	(-28, -3)
L6	(-15, -1)	(-25, -1)	(-15, -1)	(-25, -2)
L7	(-8, -1)	(-35, -1)	(-8, -2)	(-35, -3)

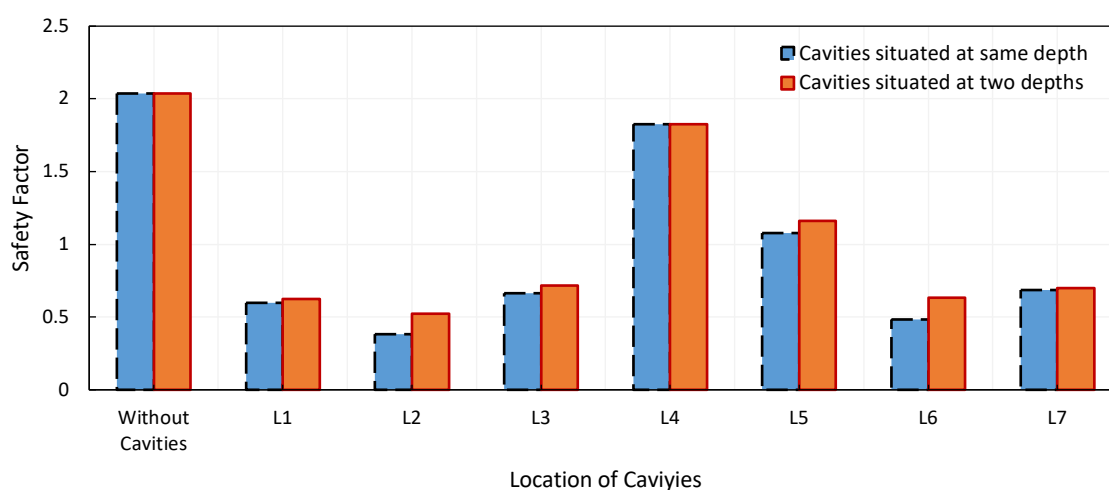


Figure 4.43: Comparison between the impact on the SF of the depth of two cavities within the same model using the MC model

#### 4.7.2 Impact of dual cavities modelled using the HS and MC models

The influence of the existence of dual cavities was studied considering a case where these cavities are situated at various horizontal positions and a depth of 1m. The coordinates of the cavities in the X-direction are as previously presented in Table 4.14. The HS and MC models were utilized to model the embankment and subsoil respectively.

The impact on the SF of the existence of two cavities situated at different horizontal positions and a depth of 1m are shown in in Figure 4.44. It is obvious that two cavities existing decreases the SF noticeably, which is equivalent to 81.5%. The lowest value is 0.366, which correpondes to a dual-cavity model with cavities situated at location L3, compared to 1.982 for a cavity-free model. Conversely, the existence of cavities results in an increase in the displacement that is equivalent to 84.3%, where it increased from 26.48mm to 48.89mm for the model with cavities located at L3. It seems that the SF reduces greatly in the case that one or both cavities exist under the upstream slope. It is clear that the impact of increasing the number of cavities is associated with the effect of their horizontal positions. For example, the percentage decreases in SF values are 12.6% and 19.4% for models with cavities at locations L7 and L2, respectively, compared to 79.5% and about 80%, for models with cavities at L1, L4 and L3, respectively (see Table 4.19 for the horizontal location details and the corresponding SF values).

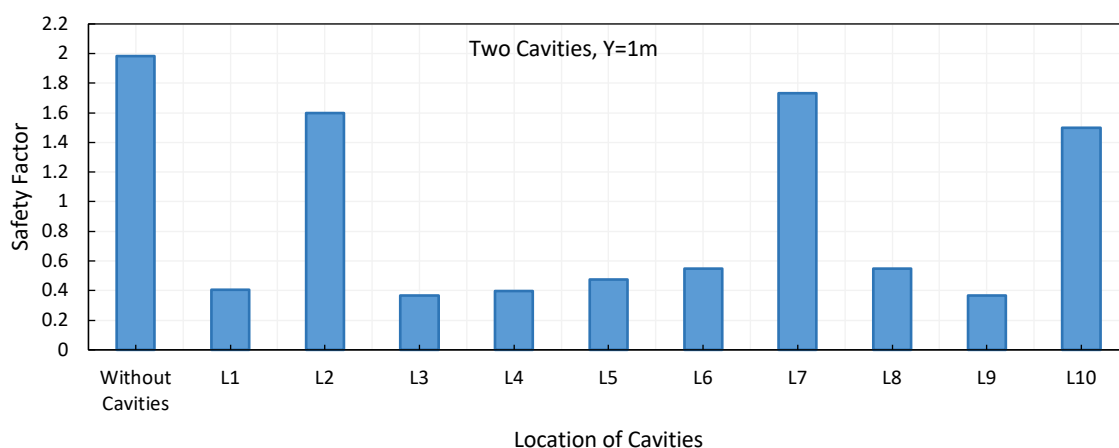


Figure 4.44: Impact on the SF of the existence of two cavities for models with cavities sited at a depth of 1m using the HS and MC models

The influence of the depth of the two cavities on slope stability is shown in Figure 4.45. The coordinates of the cavities' locations and the corresponding S.F values are outlined in Table 4.19. As revealed in Figure 4.45, increasing the cavity depth from 1m to 3m causes changes (increases or decreases) in the SF values for all models studied, wherever the cavities in these models exist horizontally. In general, the SF values have dropped below the minimum values stipulated by the codes of practice for the stability of dam slopes during rapid-drawdown conditions (1.2–1.3), except for locations L2, L7 and L10. For instance, the SF increased from 0.406 to 0.718 when the depth was increased to 3m for models with cavities at location

L1, while it decreased from 1.731 to 1.634 when the depth was increased for models with cavities at location L7. This may have occurred because the cavities at these locations may have intersected or got close enough to potential failure surfaces, resulting in the SF values dropping, but the impact was not sufficient to create a failure.

Table 4.19: Coordinates of cavities' locations and the corresponding SF values for the dual-cavity models sited for different depths

Cavity location	The coordinates of positions in X-axis, m		SF		
	Cavity 1	Cavity 2	Cavity depth, m		
			Y= 1m	Y= 2m	Y= 3m
Without cavities			1.982		
L1	-8	0	0.406	0.479	0.718
L2	0	+35	1.597	1.507	1.514
L3	-8	-24	0.366	0.319	0.404
L4	-24	0	0.397	0.325	0.356
L5	-8	+35	0.475	0.469	0.497
L6	-24	+35	0.548	0.480	0.491
L7	+35	+40	1.731	1.619	1.634
L8	-8	+40	0.549	0.489	0.625
L9	-24	+40	0.367	0.456	0.502
L10	0	+40	1.500	1.434	1.460

(-): Indicates that the cavity is under upstream, (+): indicates that the cavity is under downstream

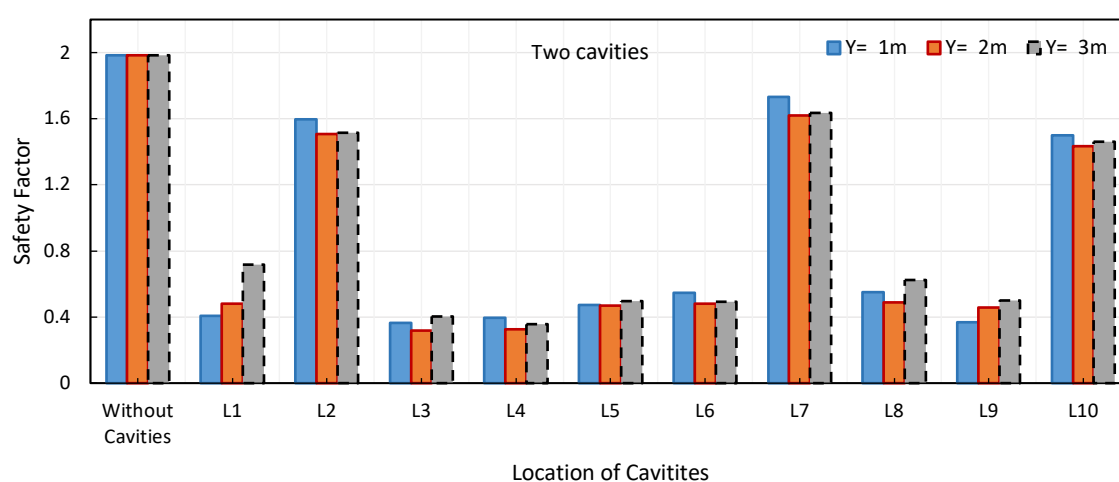


Figure 4.45: Impact on the SF of the existence of two cavities at different positions and depths using the HS and MC models

A comparison has been executed of the impact of the existence of dual cavities on the stability of the upstream and downstream sides of the model earth dam. The detail of the cavities' location is identified in Table 4.16. Figure 4.46 shows the results of the analysis. It appears that the existence of cavities beneath the upstream slope affects stability noticeably. There is a huge difference between the SF values for both the upstream and downstream slopes. For example, the SF decrease is equivalent to 81.5% for cavities modelled at location L2 below the upstream side, compared to 14.63% for the downstream side. The SF values ranged from 0.366 to 1.431 for dual-cavity models sited beneath the upstream slope, while the values ranged from 1.582 to 1.762 for similar models beneath the downstream slope. In contrast, the displacement values ranged from 29.25mm to 48.89mm for the upstream side; however, these values ranged from 28.74mm to 32.63mm for the downstream side.

Based on obtained results, the existence of a cavity has more influence on the SF values than the displacement values. Therefore, the next analyses will be depended on the impact of cavities on SF.

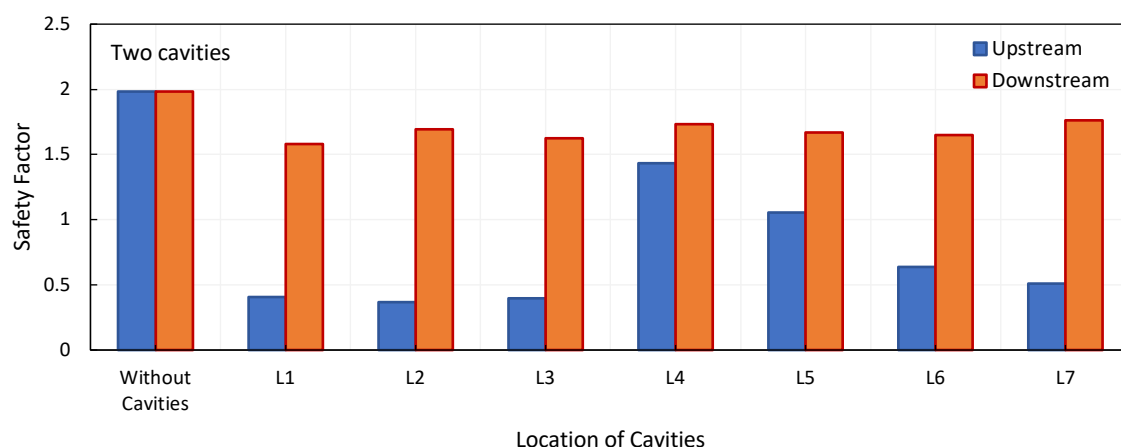


Figure 4.46: Comparison between the impact on the SF of two cavities situated at the same depth under upstream and downstream using the HS and MC models

The impact of the existence of two cavities situated at the various depths within the same model and mirrored horizontal positions under both slopes has been investigated. Figure 4.47 displays an example for some locations of cavities containing two cavities at different depths. Table 4.17 demonstrates the coordinates of the cavities' locations in both directions, X and Y. It is apparent from Figure 4.47 that the existence of two cavities under the upstream face has more of an effect on stability. The SF values obtained are larger for all models under the

downstream side than the values for the models under the upstream side, and these values are bigger than the minimum value specified for slope stability under rapid-drawdown conditions (1.2–1.3). However, the SF values are smaller than the allowable limit values for the upstream side, except for models with cavities at locations L4 and L5, where the SF values are 1.507 and 1.446, respectively.

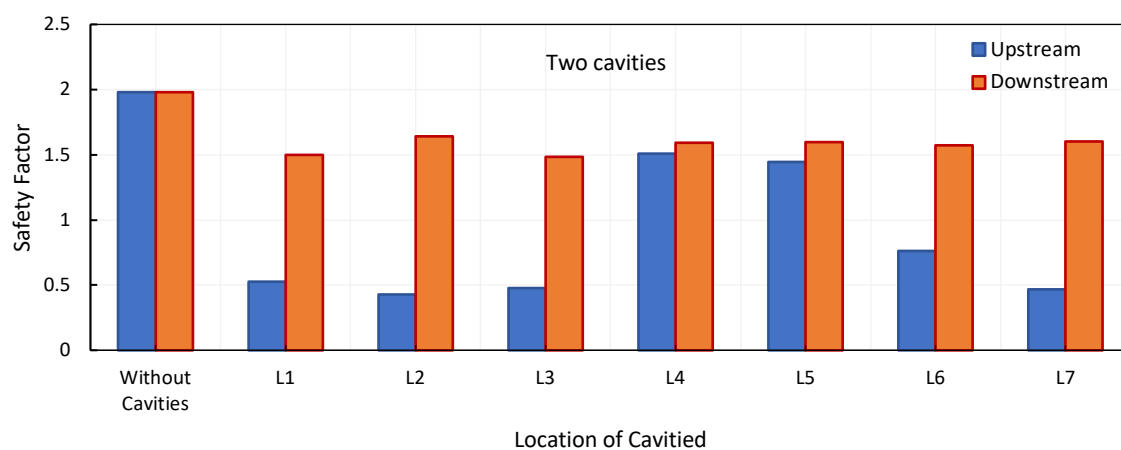


Figure 4.47: Comparison between the impact on the SF of two cavities situated under upstream and downstream at various depths using the HS and MC models

Figure 4.48 compares the effect on the stability of the existence of dual cavities positioned at the same depth with their effect when created at different depths. The positions and depths of the cavities are detailed in Table 4.18. Overall, the outcomes demonstrate that the SF values for models with two cavities situated at different depths are greater than for those with cavities positioned at the same depth, except for location L7. For example, for location L3, the SF value is 0.397 for the model with cavities positioned at the same depth under the upstream side, compared with a value of 0.479 for the model with cavities positioned at different depths. It can be concluded that the existence of two cavities at the same depth in the subsoil of the dam has a greater impact on its slope stability.

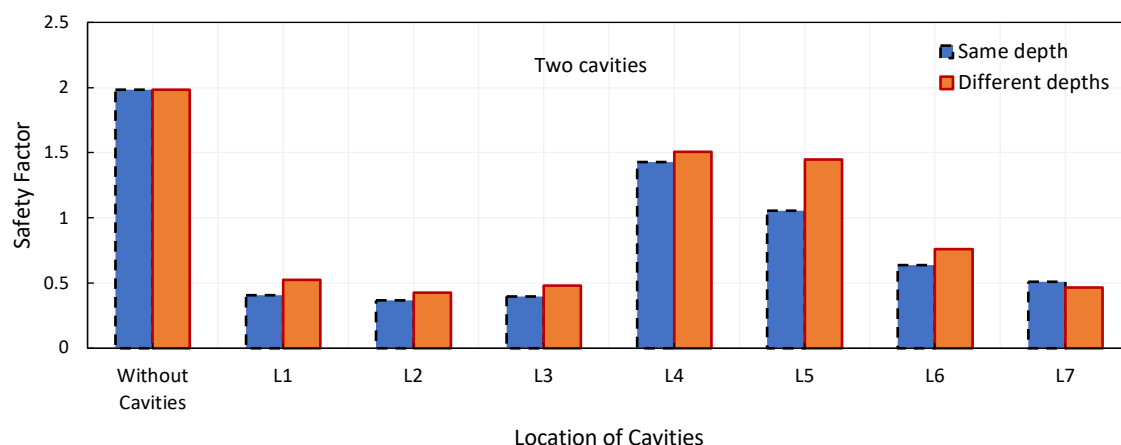


Figure 4.48: Comparison between the impact on the SF of the depth of two cavities within the same model using the HS and MC models

### 4.7.3 Impact of three cavities modelled using the MC model

This section discusses the effects of the existence of three cavities in the subsoil of the earth dam on the stability of its slopes.

To estimate the impact of the horizontal position of the three cavities on the dam's stability, ten different positions were chosen. In all numerical models, the three cavities were created at the one depth within the same model. Table 4.20 shows the coordinates of the cavities' locations the in X and Y directions. It is clear from Figure 4.49 that the existence of three cavities makes the modelled earth-dam model unstable for all models except L5. The SF values dropped to less than the required limit for the stability of earth dams (1.2–1.3) (NRCS, 2005; USBR, 2011; ULDC, 2012) during rapid-drawdown conditions. The SF value decreased from 2.036 to a minimum value of 0.252, which is equivalent to 87.6% reduction for models without a cavity and with cavities at location L2, respectively. The percentage increases in the displacement value equal to 33.8% for a triple-cavity model, as opposed to 18.1% for a single-cavity model. It is obvious that the SF value of 1.571, for the model with cavities at location L5, is bigger than the required limit; this is because the cavities were created in positions that were far from the failure slip surfaces, which are  $X=0, +35\text{m}$  and  $+40\text{m}$ . The maximum drop in the SF value for a dual-cavity model is 81.1%, compared to 87.6% for a triple-cavity model. This indicates that increasing the number of cavities causes a marked decrease in the SF value of a slope.



Table 4.20: Coordinates of cavities' locations for triple-cavity models at the same depth

Cavity location	Cavity depth, m	The coordinates of positions in		
		X-axis, m		
		Cavity 1	Cavity 2	Cavity 3
L1	1	-8	0	+35
L2	1	-8	-24	0
L3	1	-8	-24	+35
L4	1	-8	+35	+40
L5	1	0	+35	+40
L6	1	-8	-24	+40
L7	1	-8	0	+40
L8	1	-24	0	+35
L9	1	-24	0	+40
L10	1	-24	+35	+40

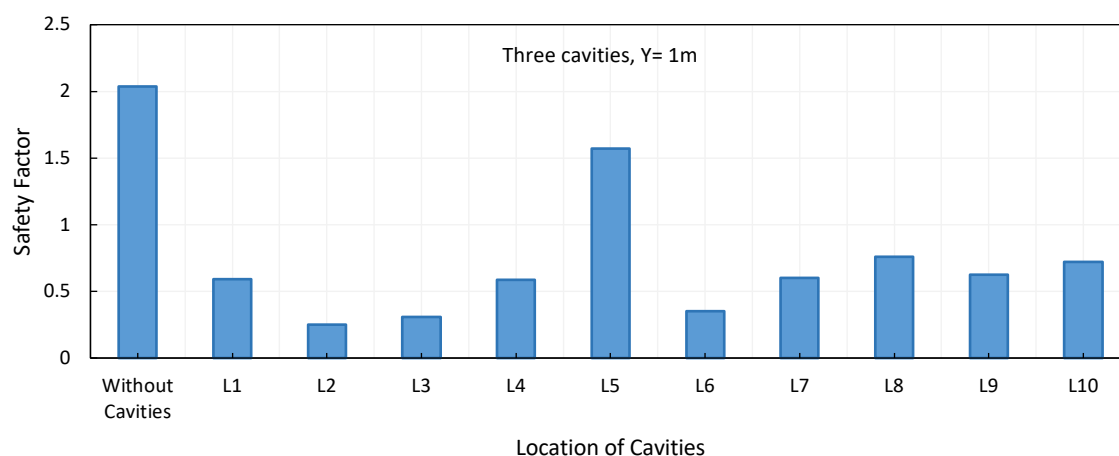


Figure 4.49: Impact on SF of the presence of three cavities at different positions and depth  $Y= 1m$  using the MC model

Figure 4.50 illustrates the combined effects of the depth of the three cavities and their horizontal positions on the SF. Table 4.21 identifies the positions and depths of the cavities and the corresponding SF values. The results show that the stability increases when the cavities' depth is increased from 1m to 3m for all models, with the exception of the models with cavities situated at location L5. The SF values increased from 0.589, 0.306 and 0.601 to 0.821, 0.429 and 0.83 for models with cavities at locations L1, L3 and L7, respectively. However, for the model with cavities at location L5, the SF value decreased from 1.631 to 1.607 at depth of 2m and then increased to 1.618 at a depth of 3m. This could be due to the

location of cavities being further away from the failure surfaces as the cavities' depth increases.

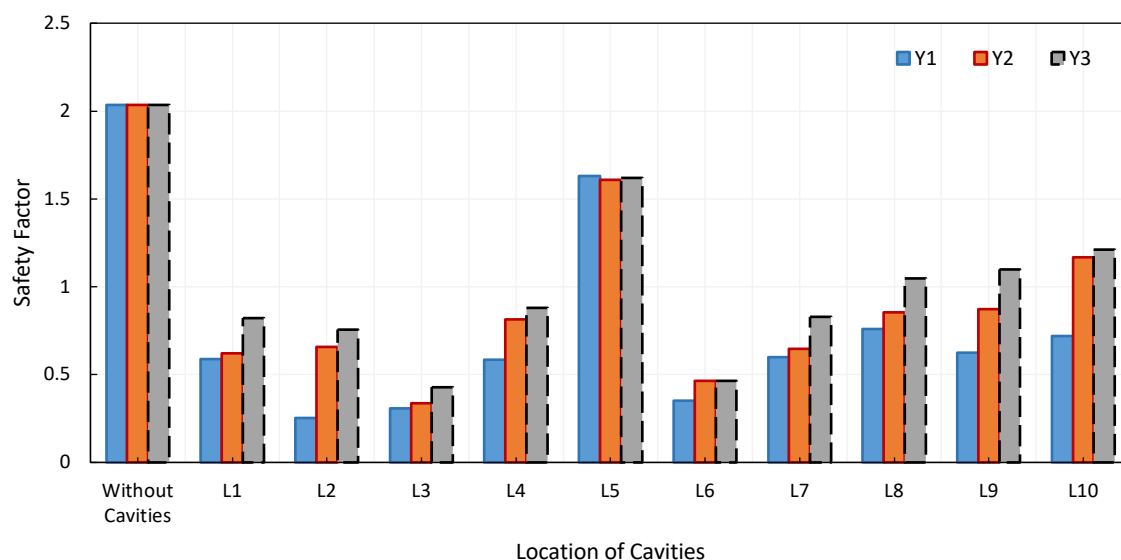


Figure 4.50: Impact on the SF of the existence of three cavities at different positions and depths using the MC model

Table 4.21: Coordinates of cavities' locations and the corresponding SF values for the triple-cavity models for different depths

Cavity location	The coordinates of positions in X-axis, m			SF		
	Cavity 1	Cavity 2	Cavity 3	Cavity depth, m		
				Y= 1m	Y= 2m	Y= 3m
	Without cavities			1.982		
L1	-8	0	+35	0.589	0.620	0.821
L2	-8	-24	0	0.252	0.656	0.756
L3	-8	-24	+35	0.306	0.338	0.429
L4	-8	+35	+40	0.585	0.815	0.881
L5	0	+35	+40	1.631	1.607	1.618
L6	-8	-24	+40	0.350	0.464	0.465
L7	-8	0	+40	0.601	0.645	0.830
L8	-24	0	+35	0.758	0.854	1.048
L9	-24	0	+40	0.624	0.871	1.100
L10	-24	+35	+40	0.721	1.166	1.210

The impact on stability of the existence of three cavities situated under the upstream and downstream slopes is revealed in Figure 4.51. The assumed cavities' locations are displayed in Table 4.22. Similar to the upstream-side findings detailed previously, it is clear that the dam's stability was significantly reduced when cavities were situated below the upstream slope, irrespective of their horizontal positions. For the upstream side, the minimum SF value amounted to 0.382 for a model with cavities situated at location L3, compared to 1.515 for a similar model with cavities situated under the downstream side. This could be due to the existence of cavities coinciding with the effect of the rapid reduction in the amount of water in the reservoir.

Table 4.22: Coordinates of cavities' locations for triple-cavity models sited under upstream and downstream at the same depth

Cavity location	Cavity depth, m	The coordinates of cavities locations in X direction, m		
		Cavity 1	Cavity 2	Cavity 3
L1	1	±8	±17	±40
L2	1	±8	±25	±30
L3	1	±15	±20	±35
L4	1	±5	±18	±27
L5	1	±10	±15	±24
L6	1	0	±8	±40
L7	1	0	±10	±35
L8	1	±17	±20	±40

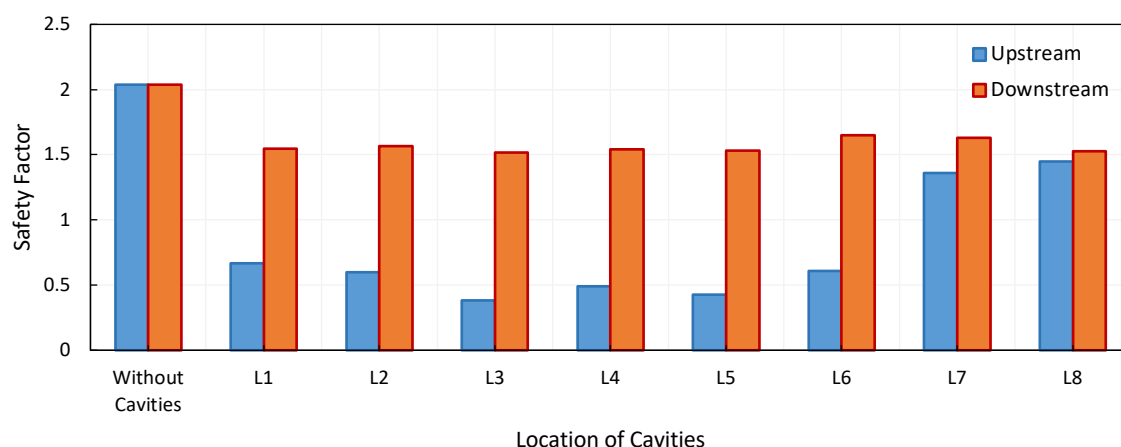


Figure 4.51: Comparison between the impact on the SF of three cavities at the same depth situated under upstream and downstream using the MC model

The effect of the existence of three cavities positioned at different positions and depths under upstream and downstream sides has been studied. The coordinates of the cavities' locations are listed in Table 4.23. Figure 4.52 reveals the SF values for the models with cavities positioned under both sides at various locations. As mentioned previously, it appears that the SF values for models with triple cavities under the upstream side are lower than the SF values for similar models with cavities under the downstream side. The SF values ranged from 0.213 to 1.169 for models with triple cavities under the upstream slope at locations L5 and L7, respectively, as opposed to 1.482 and 1.471, respectively, for similar models with cavities under the downstream slope.

Table 4.23: Coordinates of cavities' locations for triple-cavity models sited under upstream and downstream at the different depths

Cavity location	Cavity depth, m			The coordinates of cavities locations in X direction, m		
	Cavity 1	Cavity 2	Cavity 3	Cavity 1	Cavity 2	Cavity 3
L1	-1	-2	-3	±8	±17	±40
L2	-3	-1	-1	±8	±25	±30
L3	-2	-2	-1	±15	±20	±35
L4	-3	-2	-1	±5	±18	±27
L5	-2	-1	-3	±10	±15	±24
L6	-3	-2	-1	0	±8	±40
L7	-2	-1	-3	0	±10	±35
L8	-2	-1	-3	±10	±17	±20

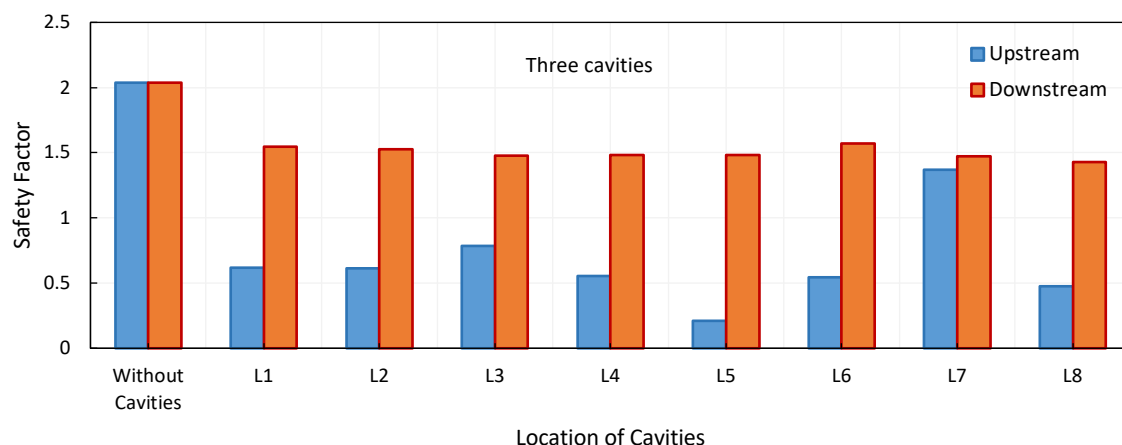


Figure 4.52: Comparison between the impact on the SF of three cavities at different depths situated under upstream and downstream using the MC model

Figure 4.53 compares the influence of the existence of three cavities sited at the same depth under the upstream side with their influence when created at different depths. The positions and depths of the cavities are specified in Table 4.24. As mentioned in the previous analyses, the existence of the three cavities at one depth has more influence on the stability than their existence at different depths within the same model. According to Figure 4.53, the SF values for the models with three cavities sited at the same depth are less than the values for models with cavities sited at different depths. This behaviour applies to all horizontal positions for models containing three cavities, except for location L5, in which the SF is smaller when the cavities are sited at different depths. For location L3, the SF is 0.382 for the model with cavities at the same depth, compared with 0.785 for the model with cavities at different depths.

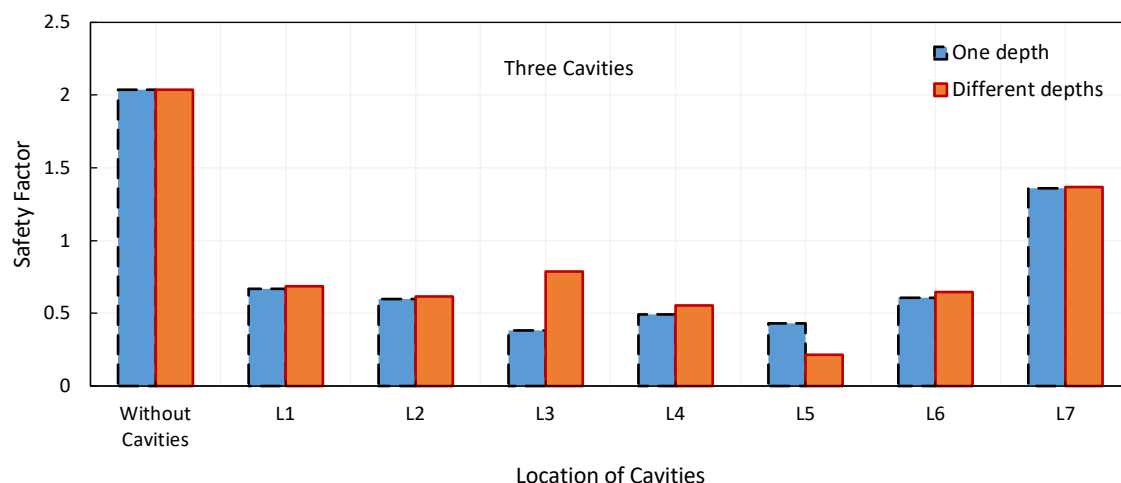


Figure 4.53: Comparison between the effect on the SF of a change in depth for triple-cavity models using the MC model

Table 4.24: Coordinates of cavities locations in X and Y directions for the triple-cavity models sited under upstream

Location of cavities	The coordinates of locations of cavities in X and Y directions, m					
	Cavities at the same depth			Cavities at the different depth		
	Cavity 1	Cavity 2	Cavity 3	Cavity 1	Cavity 2	Cavity 3
L1	(-8, -1)	(-17, -1)	(-40, -1)	(-8, -1)	(-17, -2)	(-40, -3)
L2	(-8, -1)	(-25, -1)	(-30, -1)	(-8, -3)	(-25, -1)	(-30, -1)
L3	(-15, -1)	(-20, -1)	(-35, -1)	(-15, -2)	(-20, -2)	(-35, -1)
L4	(-5, -1)	(-18, -1)	(-27, -1)	(-5, -3)	(-18, -2)	(-27, -1)
L5	(-10, -1)	(-15, -1)	(-24, -1)	(-10, -2)	(-15, -1)	(-24, -3)
L6	(0, -1)	(-8, -1)	(-40, -1)	(0, -3)	(-8, -2)	(-40, -1)
L7	(0, -1)	(-10, -1)	(-35, -1)	(0, -2)	(-10, -1)	(-35, -3)

#### 4.7.4 Impact of three cavities modelled using the HS and MC models

This section presents an investigation to evaluate the effects of the existence of three cavities on the slopes' stability, which is modelled by using the HS and MC models.

To study the effect of the cavities' position in the X direction, the cavities were created at different positions, as detailed in Table 4.20. All these cavities were situated at a depth of 1m. As Figure 4.54 shows, the existence of three cavities has more of an influence on the slope stability of an earth dam. The SF value dropped from 1.982 to 0.217, which is equivalent to

89.1% decrease, for models without a cavity and with three cavities; however, it decreased to 0.366, which is equivalent to 81.5%, for a dual-cavity model. The SF values decreased to values that are lower than the value specified by the codes of practice for the safety of earth dams (1.2–1.3) for all triple-cavity models. Generally, the SF values ranged from 0.3 to 0.4.

Similar to the MC model simulation, it is found that the model where cavities exist at location L5 is the only model for which the recorded SF value is greater than the required limit; it is equal to 1.496 (refer to Table 4.25 for the SF values that relate to the dual-cavity analysis).

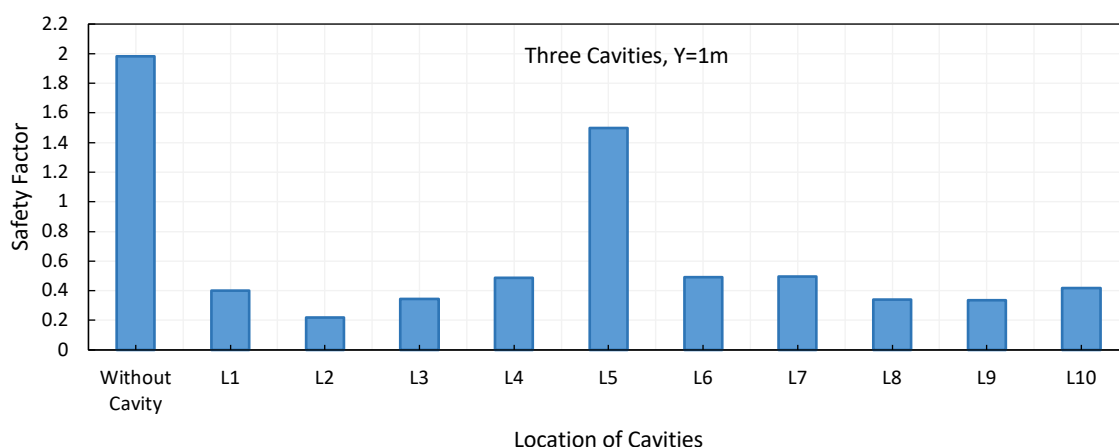


Figure 4.54: Impact on SF of the presence of three cavities at different positions and depth  $Y = 1\text{m}$  using the HS and MC models

Figure 4.55 illustrates the influence of the depth of the three cavities on the earth dam's stability. The coordinates of the location of the cavities and the corresponding S.F values are shown in Table 4.25. Like to the results obtained from the previous analyses, the results showed that the horizontal position of a cavity has a greater influence on slope stability than its depth. It is clear that, by increasing the cavity's depth, the dam's stability is increased slightly for the majority of locations chosen in the simulation. For example, the SF values for models with cavities at location L1 are 0.402, 0.418 and 0.422 at depths of 1m, 2m and 3m, respectively; however, the SF values are 1.496, 1.514 and 1.529 for models with cavities at location L5. It seems that there are exceptions at cavity locations L3, L6 and L7, where the SF values decreased at a depth of 2m, and thereafter increased at a depth of 3m (refer to Table 4.25 for the SF values that relate to the dual-cavity analysis).

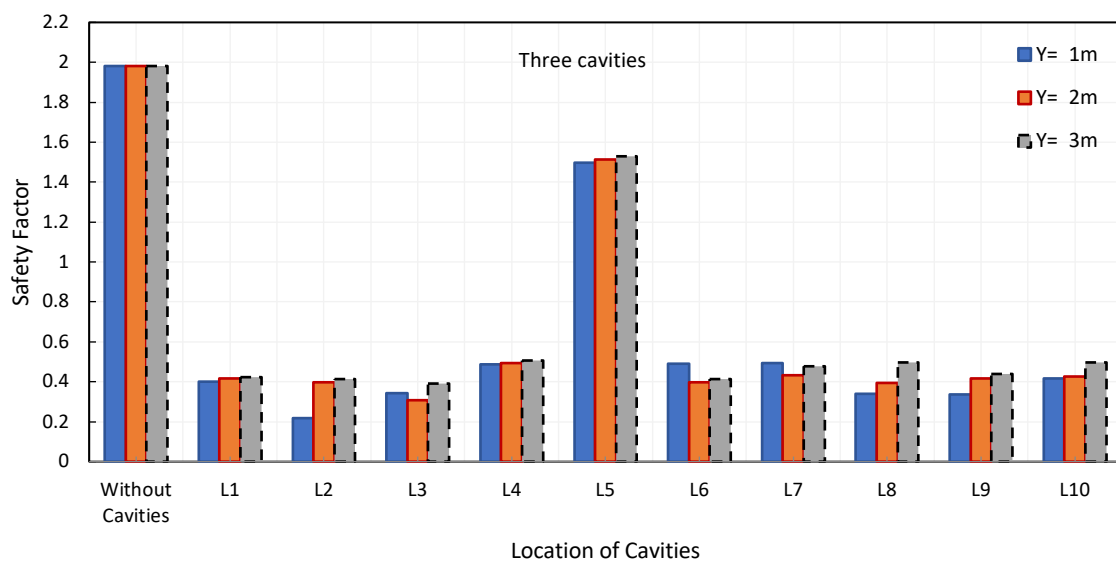


Figure 4.55: Impact on SF of the existence of three cavities at different positions and depths using the HS and MC models

Table 4.25: Coordinates of cavities' locations and the corresponding SF values for the triple-cavity models sited for different depths using the HS and MC models

Cavity location	The coordinates of positions in X-axis, m			SF		
	Cavity 1	Cavity 2	Cavity 3	Cavity depth, m		
				Y= 1m	Y= 2m	Y= 3m
	Without cavities			1.982		
L1	-8	0	+35	0.402	0.418	0.422
L2	-8	-24	0	0.217	0.399	0.412
L3	-8	-24	+35	0.343	0.308	0.392
L4	-8	+35	+40	0.487	0.494	0.508
L5	0	+35	+40	1.496	1.514	1.529
L6	-8	-24	+40	0.492	0.339	0.412
L7	-8	0	+40	0.495	0.434	0.478
L8	-24	0	+35	0.339	0.394	0.497
L9	-24	0	+40	0.335	0.418	0.440
L10	-24	+35	+40	0.416	0.425	0.498



Figure 4.56 shows a comparison between the impact on stability of three cavities positioned at the same depth and in mirrored X positions under the upstream and downstream sides. The coordinates of the cavities' locations in the X and Y directions are as described previously in Table 4.22. These are comparable to the results of the impact of dual cavities presented previously, so it can be seen that the stability of the earth dam decreases significantly when the three cavities are in the subsoil of the upstream slope. This observation is applicable irrespective of horizontal variations in the cavities' positions. For instance, for locations L3 and L7, the SF values are 0.370 and 0.405 for the models with cavities situated under the upstream side, compared to 1.567 and 1.606 for the models for the downstream side. This behaviour occurred because the stability of the upstream side is affected by rapid-drawdown conditions in addition to the effect of the presence of cavities.

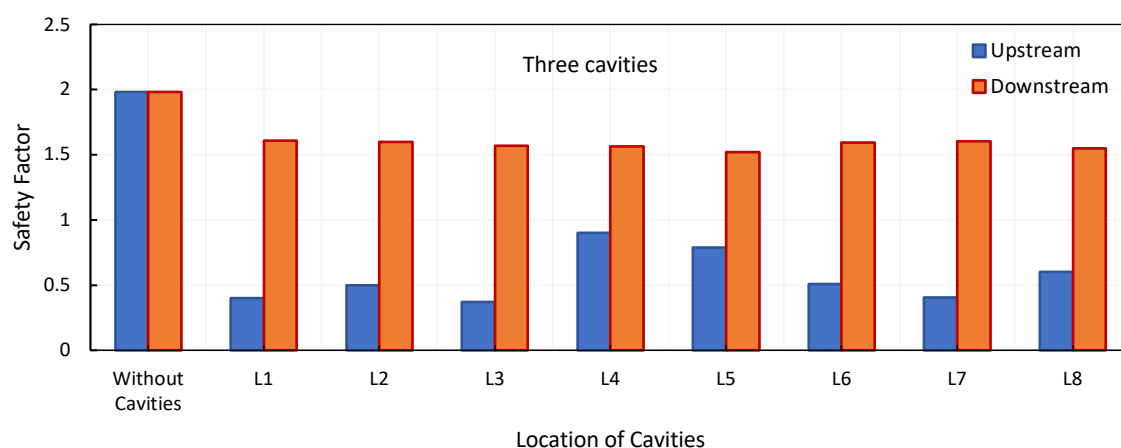


Figure 4.56: Comparison between the impact on the SF of three cavities being situated under upstream and downstream using the HS and MC models

The influence on stability of the existence of three cavities at different depths sited at reflected X positions under the upstream and downstream slopes is revealed in Figure 4.57. The coordinates of the cavities' locations in both the X and Y directions are as defined previously in Table 4.23. It should be noted that the existence of cavities under the upstream side at location L1 has the most effect on earth-dam stability: the SF value reached the lowest value obtained (0.29) in all the analyses carried out in this investigation. However, the smallest value of SF for a model with cavities sited under the downstream slope was 1.43 at location L6, which is greater than the minimum recommended value (1.2–1.3). This observation is applicable to all models with cavities situated under the downstream side, no matter where the cavities were sited horizontally. This indicates that an earth dam is more

stable under rapid-drawdown conditions when cavities are situated beneath the downstream side in contrast with the upstream, where the existence of cavities could lead to big losses in stability.

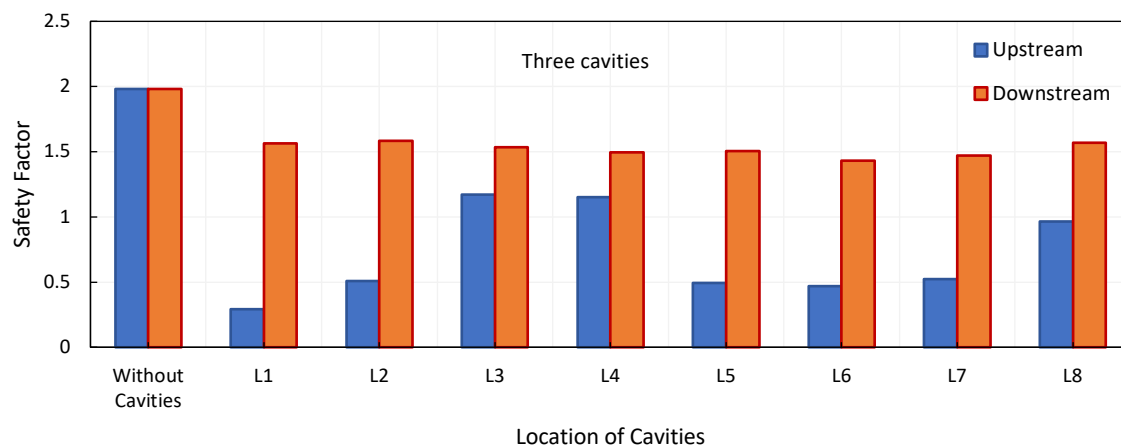


Figure 4.57: Comparison between the impact on the SF of three cavities at various depths being situated under upstream and downstream using the HS and MC models

Figure 4.58 presents a comparison between the effect of the presence of three cavities positioned under the upstream side at the same depth and those cavities positioned at the same X locations, but, at different depths. The coordinates of the cavities' locations in the X and Y directions are detailed in Table 4.24. The results show that the SF values for models with three cavities situated at the same depth are less than those with cavities situated at different depths. The lowest SF value was recorded for the model with three cavities positioned at the same depth in location L3, which equals 0.37; this is compared with a SF value of 1.17 for the similar model with the cavities positioned at different depths.

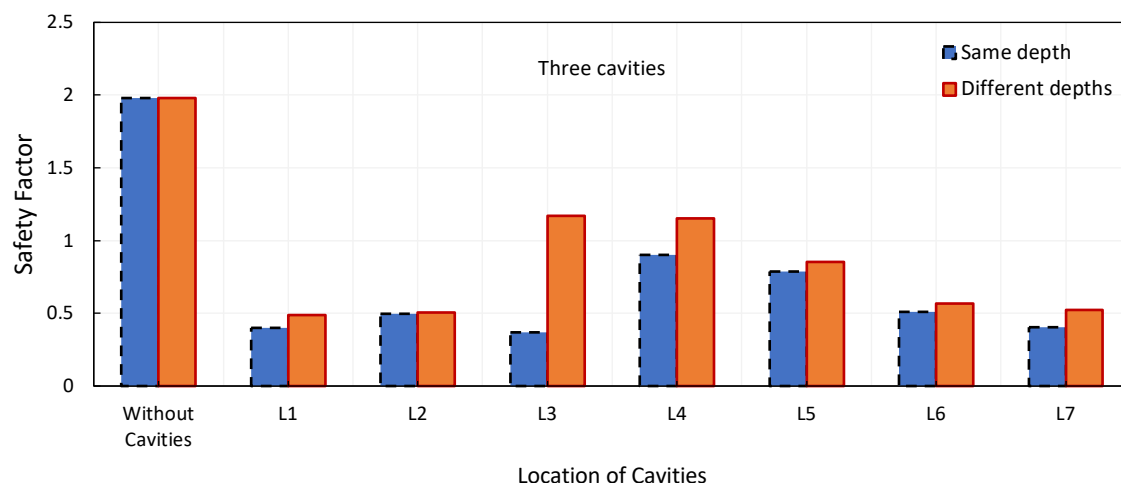


Figure 4.58: Comparison between the effect on the SF of a change in depth for triple-cavity models using the HS and MC models

#### 4.8 Joint impact of the existence of cavities and shear-strength parameters

This investigation includes a parametric study to estimate the joint impact of the existence of cavities and embankment shear-strength parameters ( $c$  and  $\phi$ ) on the stability of an earth dam in rapid-drawdown conditions. This section of the study is divided into two subsections. In the first subsection, the joint impact of shear-strength parameters, the existence of cavities and their locations analysed. In the second subsection, the investigation simulates the joint effects of shear-strength parameters, modelling material and the cavity diameter. The investigation was conducted considering the existence of a single circular cavity in the subsoil of the upstream slope. Based on the results obtained from the analysis and due to the fact that the rapid drawdown is one of the most crucial design states for the upstream side, the chosen positions for the cavity are under the upstream side. The coordinates of the selected cavity positions in the X direction are  $X_1 = -8\text{m}$ ,  $X_2 = -17\text{m}$  and  $X_3 = -24\text{m}$ . Three depths of cavity (1m, 2m and 3 m) were considered in conducting the analysis of the impact of cavity depth. In the analysis of the impact of the cavity location, cavities were created at depth of 1m and with a diameter of 60 cm, whereas the cavity diameter was set to 20cm, 60cm and 100cm for the analysis of the impact of cavity size.

### 4.8.1 Joint impact of the existence of a cavity and the soil's apparent cohesion

The soil cohesion values ( $c$ ) assumed in this simulation were 15kPa, 25kPa, 30kPa, 35kPa, 40kPa, 50kPa, 60 kPa and 80 kPa in all analyses.

#### 4.8.1.1 Joint impact of the soil's apparent cohesion and cavities modelled using the MC model

In the first part of this simulation, the soil of the earth dam was modelled using the MC model.

Figure 4.59 gives the SF values versus the soil cohesion values for models without a cavity and with cavities. It is clear that the SF values increased from 1.740 to 2.799, which is equivalent to 60.8%, due to increase in the cohesion value from 15kPa to 80kPa for the cavity-free models. This behaviour is attributed to increasing cohesion between the particles of soil, which leads to an increase in the resisting forces rather than the driving forces. It should be noted that the SF values for the models with a cavity at position X1= -8 kept more or less the same, with insignificant increases as the cohesion increased, and were less than the value specified for stability (1.2–1.3) (NRCS, 2005; USBR, 2011; ULDC, 2012). These values increased from 0.665 to 0.965 when the cohesion was increased from 15kPa to 80kPa. Obviously, increasing the embankment cohesion does not reduce the impact of cavities on stability when the cavities are situated at critical positions (positions where the recorded SF values are less than the stipulated values). For positions X2 and X3, the results show that, by increasing the cohesion value, the SF values increased gradually from 1.017 to 1.714 and from 1.221 to 1.767, respectively.

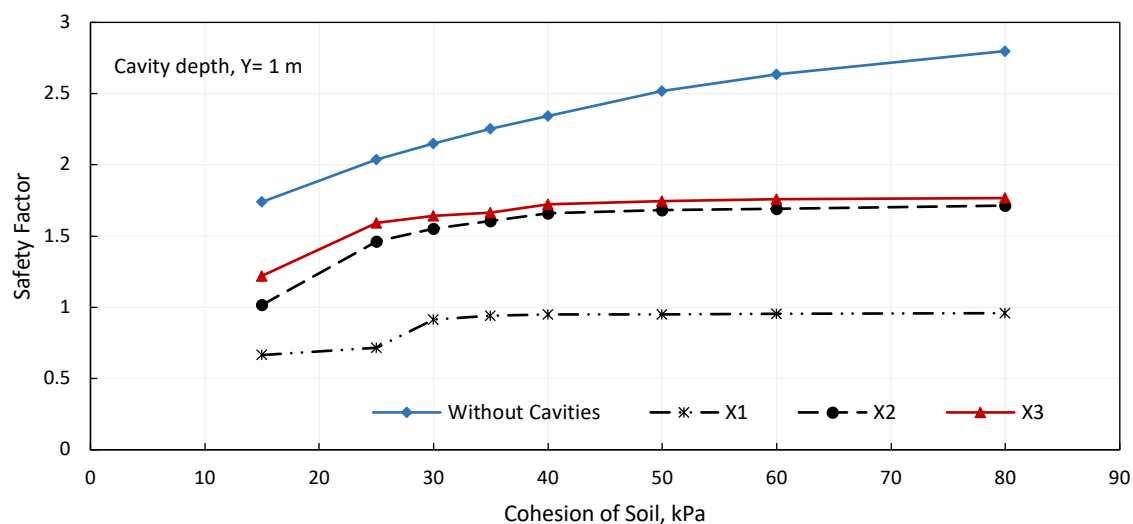
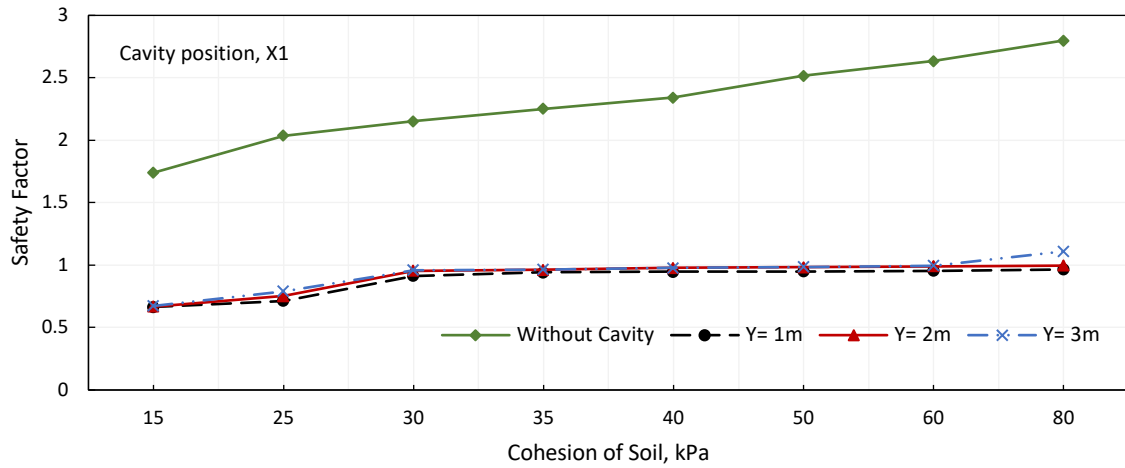


Figure 4.59: Joint impact on SF of the cavity position and soil cohesion using the MC model

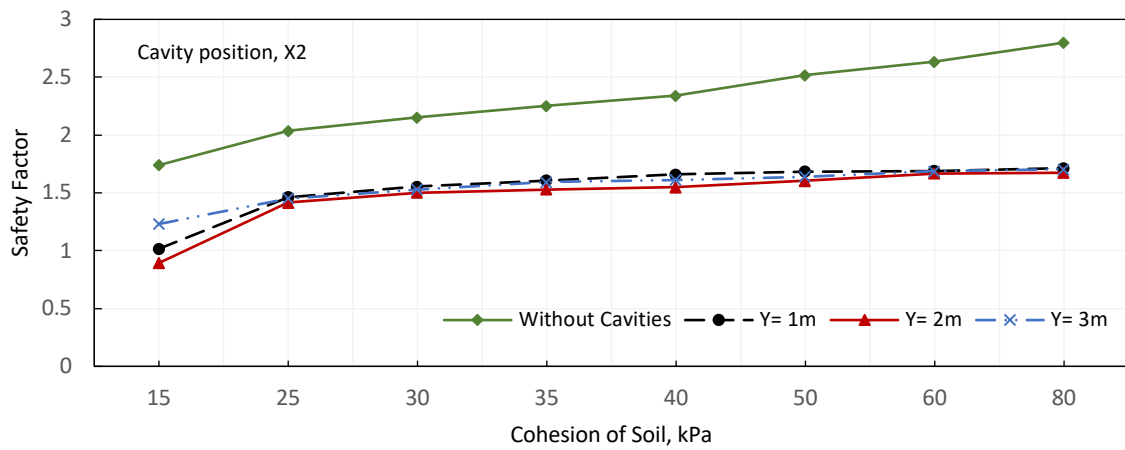
Figure 4.60 shows the joint impact on the SF of soil cohesion and cavity depth for models with and without cavities. The positions, diameters and depths of cavities are as defined previously. Table 4.26 presents the input and output parameters of the stability analysis. It is apparent that increasing the cavity depth leads to minor changes (increases or decreases) in the SF values, along with an increase in the cohesion value from 15kPa to 80kPa. The SF values for positions X1 and X3 increased when the cavity depth was increased. For example, the SF values increased from 0.665 to 0.673 as the cavity depth increased to 3m for a cohesion value of 15kPa for models with a cavity situated at position X1. Refer to Table 4.26 for the SF values that relate to the depth-effect analysis. It can be concluded that coincidentally increasing both the cavity depth and the cohesion value is not sufficient to reduce the impact of the cavity and make the dam stable when the cavity is located at a critical position.

Table 4.26: Input and output data showing the impact of soil cohesion and location of cavity on SF values

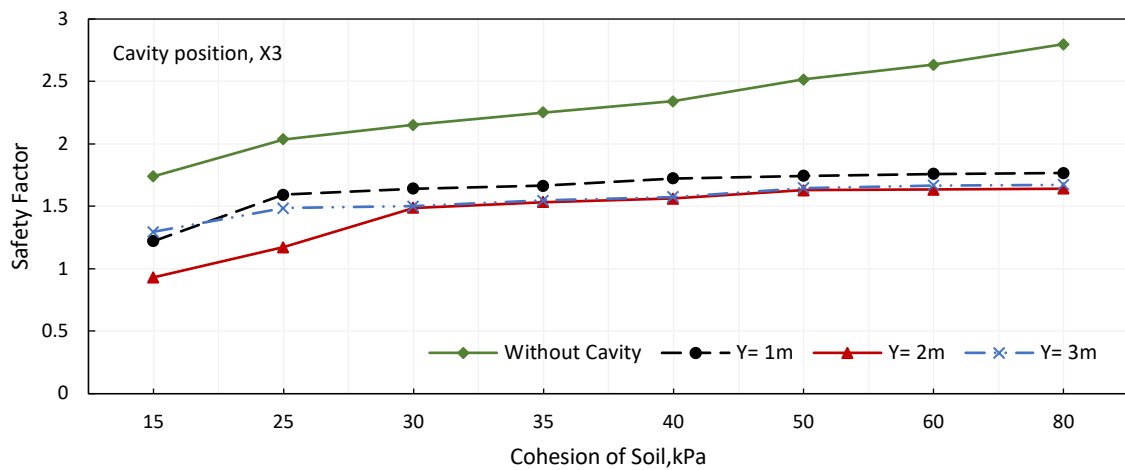
Cohesion of soil (kPa)	SF				
	Without cavities	Depth of cavity Y(m)	The coordinates of cavities X-axis (m)		
			X1 (-8)	X2 (-17)	X3 (-24)
15	1.740	1	0.665	1.017	1.221
		2	0.667	0.894	0.931
		3	0.673	1.231	1.296
25	2.036	1	0.715	1.463	1.594
		2	0.751	1.416	1.173
		3	0.791	1.452	1.485
30	2.151	1	0.915	1.554	1.641
		2	0.956	1.502	1.487
		3	0.960	1.530	1.500
35	2.253	1	0.943	1.608	1.665
		2	0.962	1.530	1.535
		3	0.964	1.592	1.546
40	2.341	1	0.948	1.660	1.725
		2	0.977	1.548	1.562
		3	0.979	1.613	1.575
50	2.517	1	0.950	1.683	1.745
		2	0.982	1.604	1.629
		3	0.985	1.639	1.648
60	2.635	1	0.954	1.691	1.759
		2	0.991	1.669	1.633
		3	0.995	1.687	1.657
80	2.799	1	0.965	1.714	1.767
		2	0.996	1.674	1.641
		3	1.110	1.704	1.672



(a)



(b)



(c)

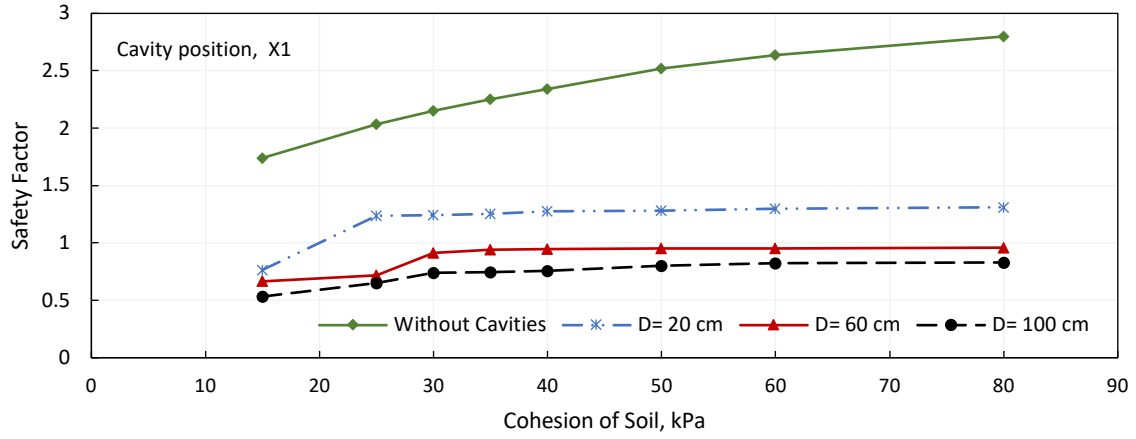
Figure 4.60: Joint impact of the cavity depth and soil cohesion on the SF using the MC model for the positions of cavity: (a) X1, (b) X2, (c) X3

The joint impact of the cavity diameter and the soil cohesion on stability has been studied. The input and output parameters of the stability analysis are presented in Table 4.27. Figure 4.61 reveals that increasing the cavity diameter from 20cm to 100cm results in significant reductions in the SF values. The decrease in SF values is from 1.244, 1.734 and 1.741 to 0.738, 1.374 and 1.481 for models with cavity positions X1, X2 and X3, respectively, and with a soil cohesion of 30 kPa. Refer to Table 4.27 for the SF values that relate to the diameter -effect analysis. Regardless of where the cavity is situated, any increase in the diameter of the cavity causes a significant reduction in the stability of the slope of the earth dam, although the soil cohesion increases.

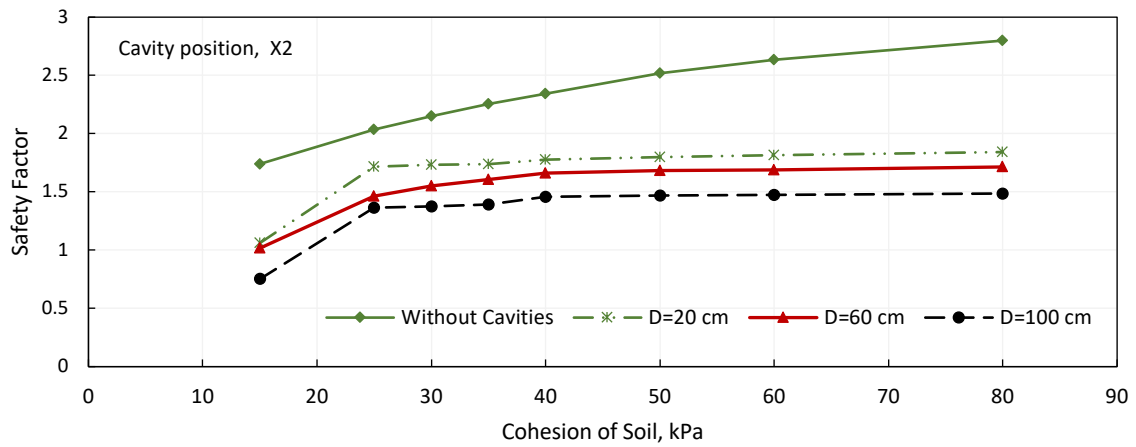
Table 4.27: Input and output data showing the impact of soil cohesion and cavity diameter on SF values

Cohesion of soil, kPa	SF				
	Without cavities	Diameter of Cavity, cm	The coordinates of cavities in X-axis, m		
			X1 (-8)	X2 (-17)	X3 (-24)
15	1.707	20	0.765	1.061	1.455
		60	0.665	1.017	1.221
		100	0.533	0.752	0.764
25	2.036	20	1.235	1.716	1.693
		60	0.715	1.463	1.594
		100	0.650	1.367	1.476
30	2.125	20	1.244	1.734	1.741
		60	0.915	1.554	1.641
		100	0.738	1.374	1.481
35	2.240	20	1.256	1.736	1.755
		60	0.943	1.608	1.665
		100	0.748	1.393	1.493
40	2.338	20	1.277	1.774	1.774
		60	0.948	1.660	1.725
		100	0.759	1.459	1.518
50	2.501	20	1.283	1.798	1.817
		60	0.950	1.683	1.745
		100	0.803	1.469	1.537
60	2.600	20	1.297	1.813	1.836
		60	0.954	1.691	1.759
		100	0.826	1.475	1.558
80	2.768	20	1.311	1.842	1.869
		60	0.965	1.714	1.767
		100	0.830	1.486	1.575

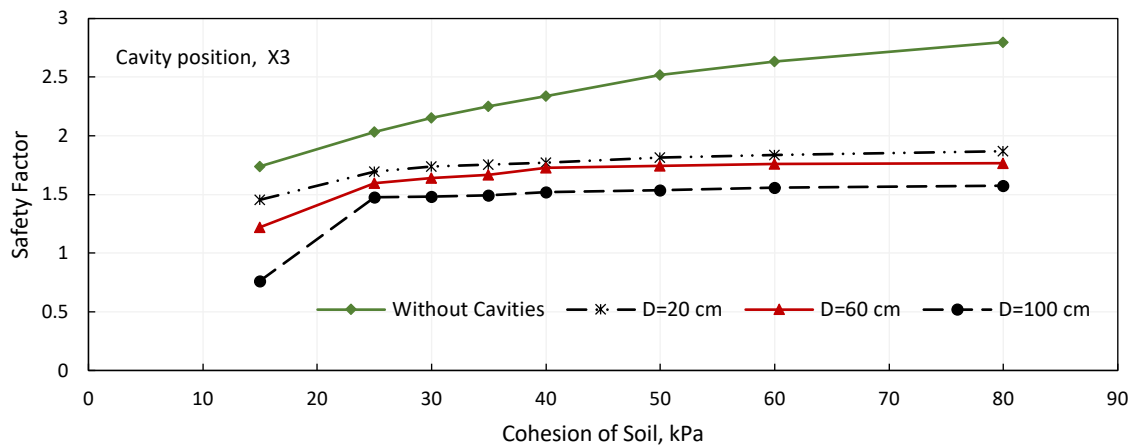




(a)



(b)



(c)

Figure 4.61: Joint impact of cavity diameter and soil cohesion on the SF using the MC model for the positions of cavity: (a) X1, (b) X2, (c) X3

#### 4.8.1.2 Joint impact of the soil's apparent cohesion and cavities modelled using the HS and MC models

This section, the HS and MC models were employed to model the embankment and subsoil, respectively. The joint impact of the cavity's location and soil cohesion on slope stability has been also analysed.

Figure 4.62 and Table 4.28 depict the effect of cavities' positions and soil cohesion on the SF values. The positions, diameters and depths of cavities are as described previously. It is clear that, by increasing the soil cohesion from 15kPa to 80kPa, the SF increased from 1.662 to 2.785 for cavity-free models; however, the SF increased from 0.61 to 0.968 for models containing cavities at position X1= -8m. In the case of the existence of cavities in critical positions, such as X1, it appears that the earth-dam model remains unstable even when the cohesion of the embankment is increased. The SF values for models with a cavity at X1 are close to each other and smaller than the value specified for stability (1.2–1.3). In other words, increasing the cohesion does not reduce the impact of cavities when they exist at critical positions. Overall, the SF values for models containing cavities situated at X2 and X3 increased from 1.041 to 1.638 and from 1.329 to 1.723, as cohesion increased from 15kPa to 80kPa, respectively.

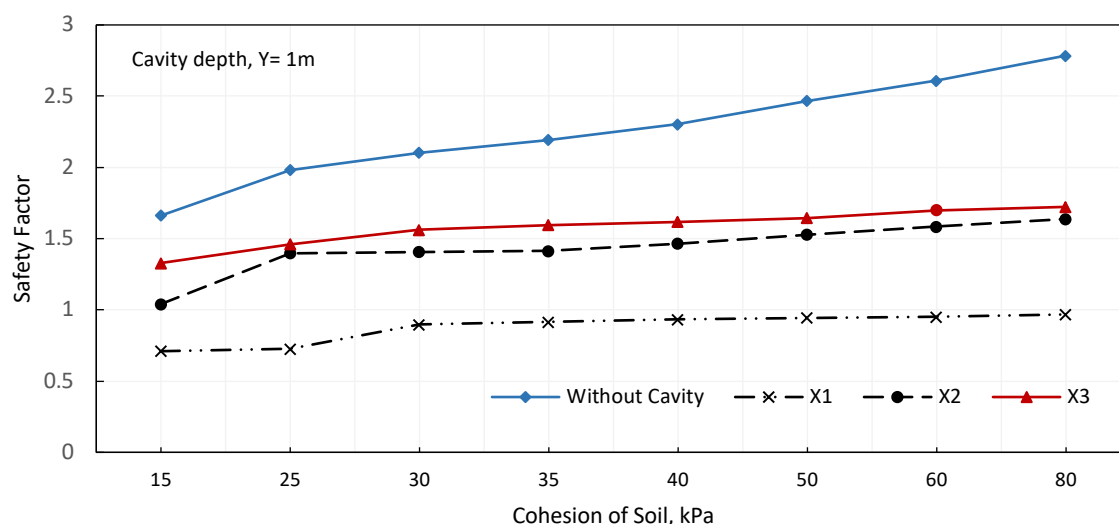
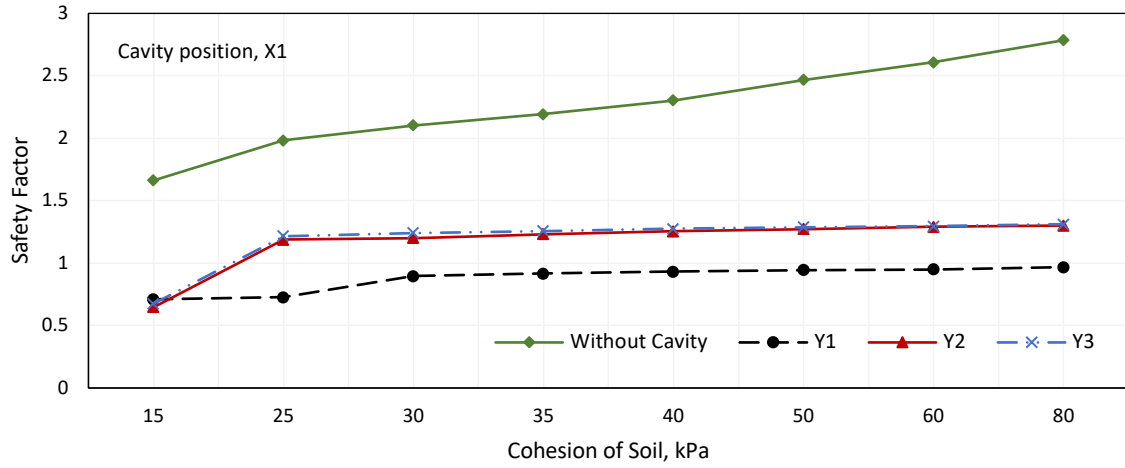


Figure 4.62: Joint impact on SF of the cavity position and soil cohesion using the HS and MC models

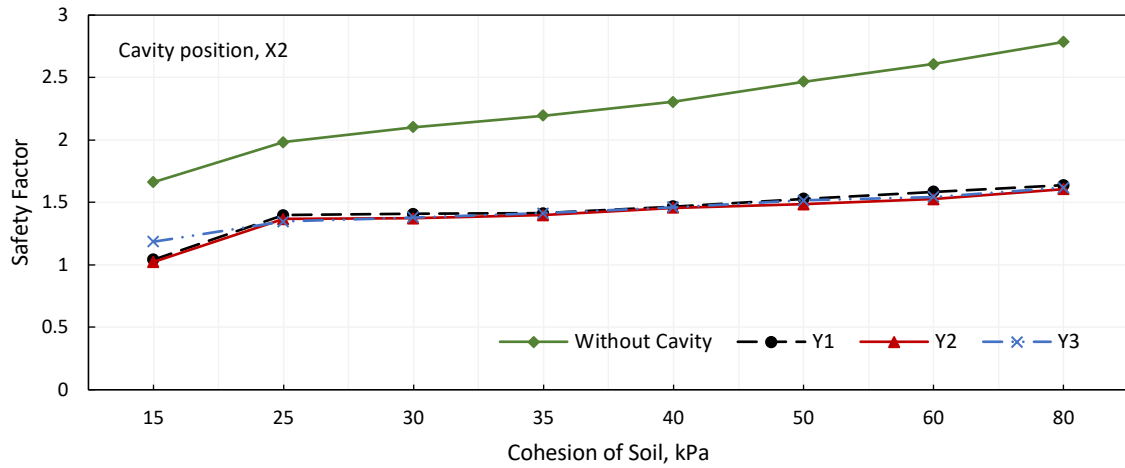
The joint impact of depth and soil cohesion on the SF is shown in Figure 4.63 and Table 4.28. The positions, diameters and depths of cavities as described previously. It should be mentioned that the new findings are consistent with the results obtained from previous analyses. It is apparent that increasing the cavity depth along with increasing the cohesion value from 15kPa to 80kPa led to a slight change in the SF values. In general, by increasing both the cohesion and the cavity depth, the SF increases for models with a cavity at position X1, where the SF increased from 0.61 to 0.675 with an increasing cavity depth and a cohesion of 15kPa. For models with cavity positions X2 and X3, the SF drops at the depth of 2m and then it goes up when the depth is increased to 3m. For example, it decreased from 1.041 to 1.023 and then increased to 1.185 as the cavity depth increased for models with a cavity at position X2. For more details, see Table 4.28. For more details, see Table 4.28

Table 4.28: Input and output data showing the impact of soil cohesion and location of cavity on SF values

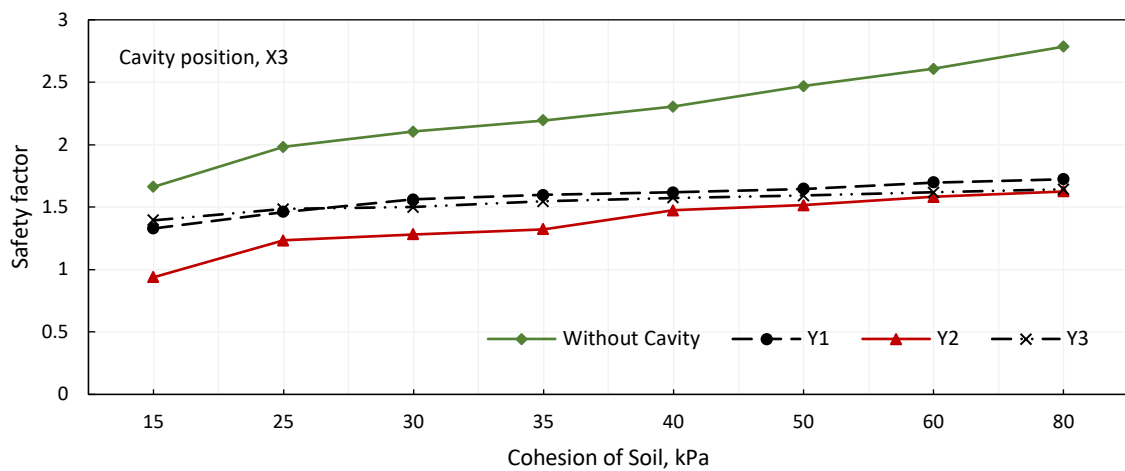
Cohesion of soil (kPa)	SF				
	Without cavities	Cavity depth Y, m	Coordinates of cavities X-axis (m)		
			X1 (-8)	X2 (-17)	X3 (-24)
15	1.662	1	0.610	1.041	1.329
		2	0.646	1.023	0.938
		3	0.675	1.185	1.394
25	1.982	1	0.727	1.398	1.461
		2	1.189	1.366	1.232
		3	1.215	1.347	1.485
30	2.104	1	0.896	1.408	1.562
		2	1.201	1.373	1.282
		3	1.243	1.381	1.500
35	2.194	1	0.916	1.414	1.596
		2	1.231	1.398	1.322
		3	1.257	1.412	1.546
40	2.304	1	0.932	1.466	1.618
		2	1.255	1.457	1.474
		3	1.275	1.463	1.575
50	2.468	1	0.945	1.529	1.645
		2	1.273	1.484	1.516
		3	1.289	1.515	1.591
60	2.608	1	0.950	1.584	1.698
		2	1.291	1.525	1.581
		3	1.295	1.545	1.618
80	2.785	1	0.968	1.638	1.723
		2	1.301	1.606	1.625
		3	1.312	1.619	1.643



(a)



(b)



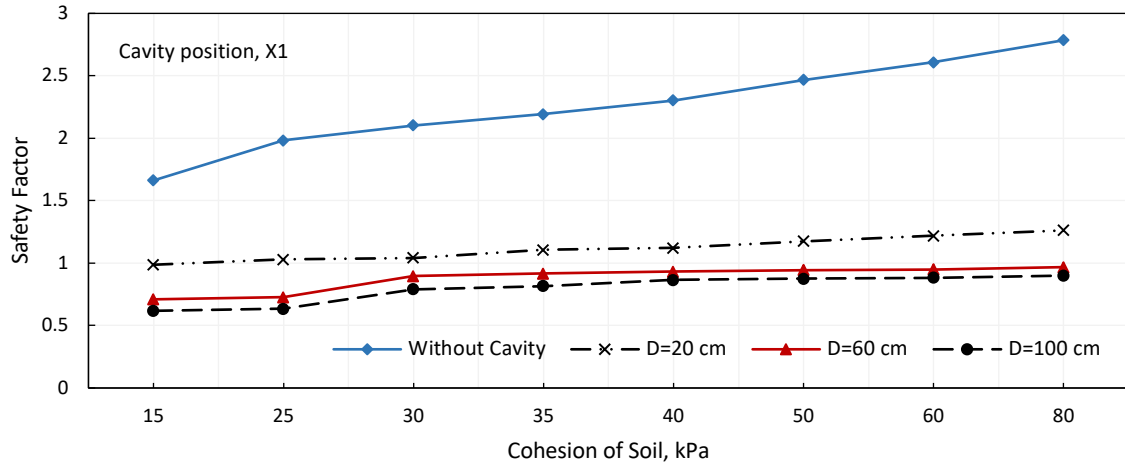
(c)

Figure 4.63: Joint impact of the cavity depth and soil cohesion on the SF using the HS and MC models for the positions of cavity: (a) X1, (b) X2, (c) X3

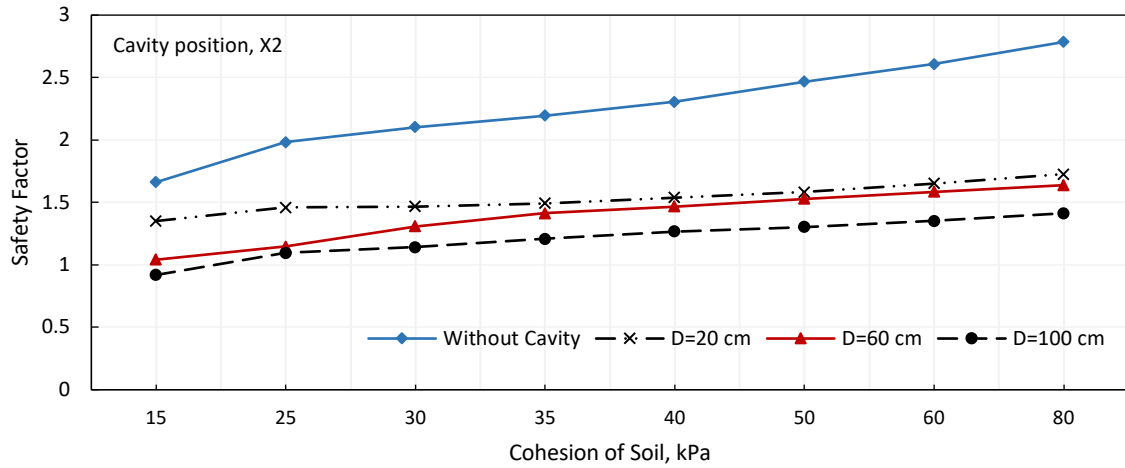
This study also included an investigation to estimate the combined effect of the cavity diameter and soil cohesion on slopes stability. The positions, diameters and depths of cavities are as designated previously. The results of the analysis are shown in Table 4.29 and Figure 4.64. It is obvious that increasing the cavity's diameter from 20cm to 100cm results in a considerable reduction in the SF values for all models wherever the cavities exist and regardless of the increase in the soil cohesion. For instance, it is clear from the results that belong to the model with a cavity located at position X1, the S.F decreased from 0.987 to 0.618 and from 1.262 to 0.9 with an increase the cavity diameter upon cohesion corresponding to 15 and 80kPa, respectively. It is essential to mention that increasing the cavity diameter made the dam model unsafe for all models with a cavity at position X1, despite the increase in the soil cohesion. It can be observed that the SF values are below the limit (1.2-1.3) for most models with cavity at position X2 and X3.

Table 4.29: Input and output data showing the impact of cohesion and cavity diameter on SF values

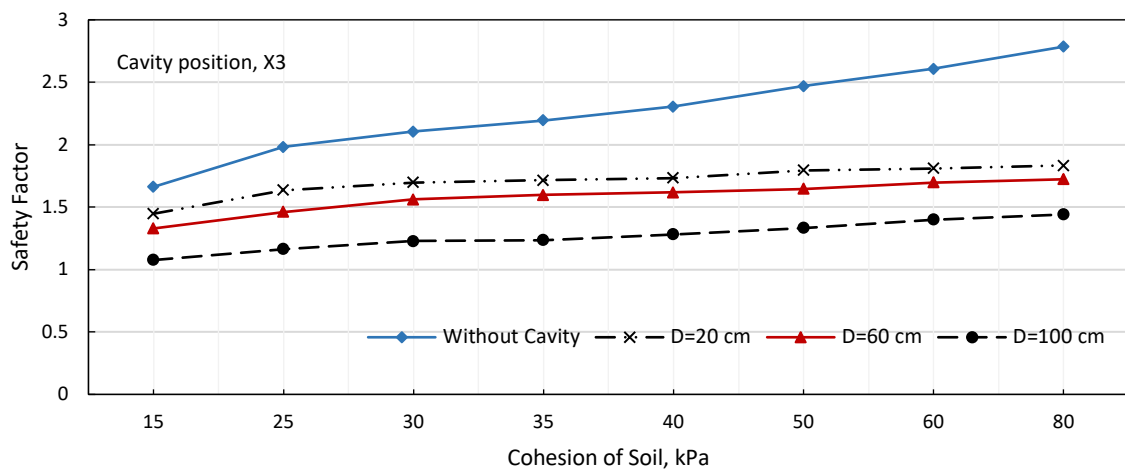
Cohesion of soil, kPa	SF				
	Without cavities	Diameter of Cavity (cm)	Coordinates of cavities in X-axis (m)		
			X1 (-8)	X2 (-17)	X3 (-24)
15	1.662	20	0.987	1.351	1.447
		60	0.610	1.041	1.329
		100	0.618	0.919	1.076
25	1.982	20	1.030	1.460	1.636
		60	0.727	1.146	1.461
		100	0.634	1.096	1.165
30	2.104	20	1.043	1.466	1.697
		60	0.896	1.308	1.562
		100	0.790	1.141	1.219
35	2.194	20	1.106	1.492	1.715
		60	0.916	1.414	1.596
		100	0.816	1.208	1.216
40	2.304	20	1.121	1.539	1.734
		60	0.932	1.466	1.618
		100	0.865	1.266	1.281
50	2.468	20	1.176	1.583	1.794
		60	0.945	1.529	1.645
		100	0.876	1.304	1.333
60	2.608	20	1.219	1.651	1.810
		60	0.950	1.584	1.698
		100	0.883	1.352	1.401
80	2.785	20	1.262	1.727	1.834
		60	0.968	1.638	1.723
		100	0.900	1.413	1.441



(a)



(b)



(c)

Figure 4.64: Joint impact of cavity diameter and soil cohesion on the SF using the HS and MC models for the positions of cavity: (a) X1, (b) X2, (c) X3

## 4.8.2 Joint impact of the existence of a cavity and the angle of internal friction ( $\phi$ )

This investigation focuses on the joint impact on stability of the angle of internal friction ( $\phi$ ) and the cavity presence in terms of the change in its location and size on stability. This simulation was executed assuming the values of ( $\phi$ ) were  $10^\circ$ ,  $15^\circ$ ,  $22.5^\circ$ ,  $27^\circ$ ,  $30^\circ$ ,  $33^\circ$  and  $35^\circ$ .

### 4.8.2.1 Joint impact of the angle of internal friction ( $\phi$ ) modelled using the MC model

Figure 4.65 shows the SF values versus values of ( $\phi$ ) for models without a cavity and with a cavity at positions X1, X2 and X3. The positions, diameters and depths of cavities are as defined previously. It can be observed that, by increasing ( $\phi$ ) from  $10^\circ$  to  $35^\circ$ , the SF increases from 1.485 to 2.449 for cavity-free models. Similar to the soil-cohesion analysis, although the ( $\phi$ ) value increased, the SF increased slightly from 0.667 to 1.103 for models with a cavity at the position X1, which remains less than the specified limit for the safety of an earth dam. However, the SF values rose gradually with the increase in the ( $\phi$ ) value for positions X2 and X3, in which the SF increased from 0.710 to 1.614 and 0.853 to 1.669, respectively. The slope stability of earth dams under rapid-drawdown conditions increases with an increase in the soil cohesion and ( $\phi$ ); however, these increases are minimal compared to the considerable effects of the cavities on stability, and while they introduce improvements, they are unable to compensate for the significant disturbing effects of the cavities. This effect is even greater when the cavities are situated in positions with a maximum impact on stability.

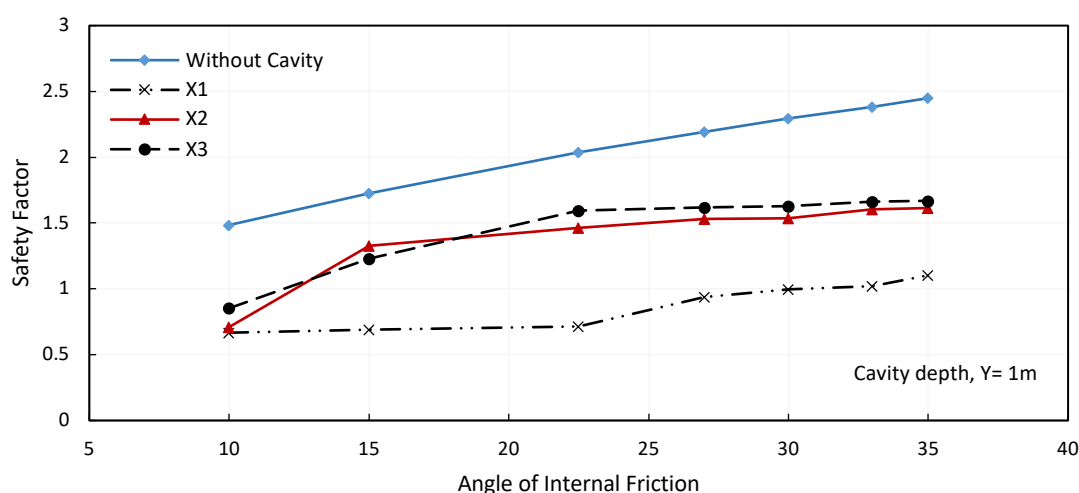


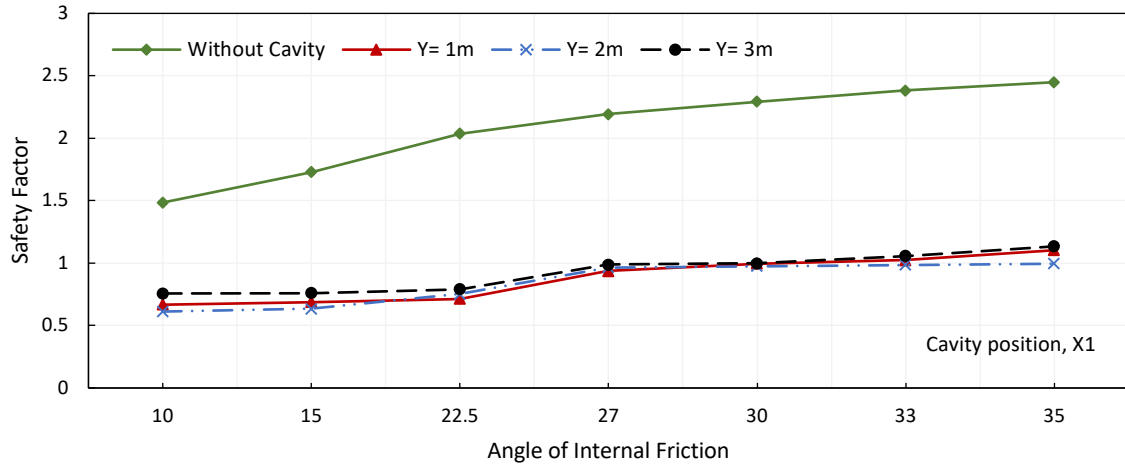
Figure 4.65: Joint impact of the cavity position and the ( $\phi$ ) on SF using the MC model

Figure 4.66 and Table 4.30 illustrate the joint impact of cavity depth and ( $\phi$ ) on slope stability. The depths and positions of cavities are as described previously. It appears that increasing the cavity depth from 1m to 3m resulted in a small fluctuation (increasing or decreasing) in the SF, with an increase of ( $\phi$ ) from  $10^\circ$  to  $35^\circ$ . Generally, by increasing the values of ( $\phi$ ), the SF values were reduced at depth of 2m and then increased when the cavity depth was increased to 3m for most models with a cavity situated at the chosen location. For example, the SF decreased from 0.667 to 0.667 and then increased to 0.757 when the cavity depth was increased from 1m to 2m then to 3m for models with a cavity situated at position X1, with ( $\phi$ ) corresponding to  $10^\circ$ ; however, the SF was equal to 1.103, 0.995 and 1.134 with ( $\phi$ ) corresponding to  $35^\circ$  at depths of 1m, 2m and 3m, respectively (refer to Table 4.30 for details of the SF values). As revealed in the previous section, increasing the ( $\phi$ ) value along with increasing the cavity depth does not decrease the influence of a cavity on stability in the case where the cavity exists at a critical position.

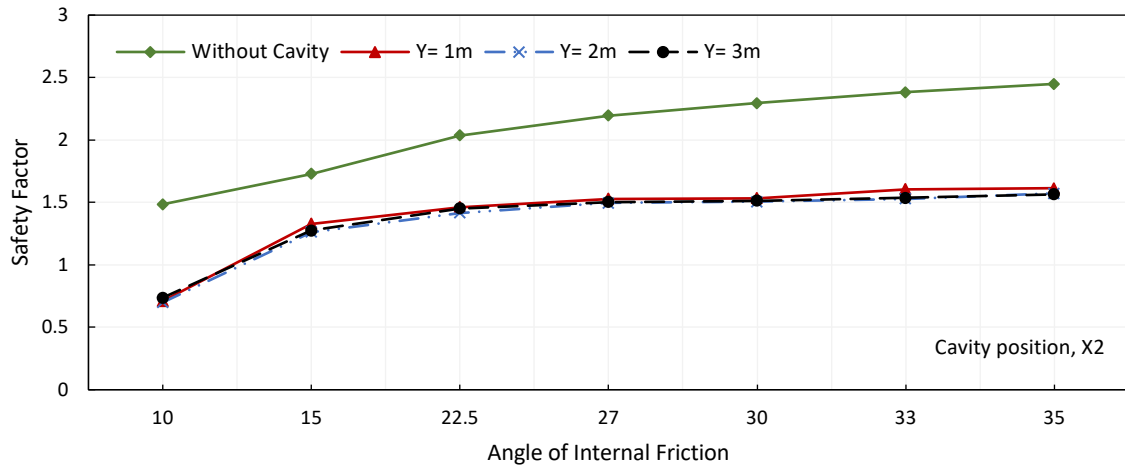
Table 4.30: Input and output data showing the impact of the ( $\phi$ ) and location of cavity on SF values

Values of ( $\phi$ ), degree	SF				
	Without cavity	Depth of cavity Y, m)	Coordinates of cavities in X-axis, m		
			X1 (-8)	X2 (-17)	X3 (-24)
10	1.485	1	0.667	0.710	0.851
		2	0.612	0.699	0.564
		3	0.757	0.737	0.851
15	1.728	1	0.689	1.328	1.231
		2	0.635	1.263	0.905
		3	0.761	1.276	1.230
22.5	2.036	1	0.715	1.463	1.595
		2	0.751	1.416	1.173
		3	0.791	1.452	1.489
27	2.194	1	0.938	1.529	1.617
		2	0.966	1.494	1.317
		3	0.988	1.504	1.535
30	2.294	1	0.996	1.534	1.627
		2	0.976	1.506	1.331
		3	0.998	1.512	1.567
33	2.383	1	1.023	1.606	1.664
		2	0.985	1.529	1.353
		3	1.057	1.535	1.579
35	2.449	1	1.103	1.614	1.669
		2	0.995	1.573	1.368
		3	1.134	1.564	1.607

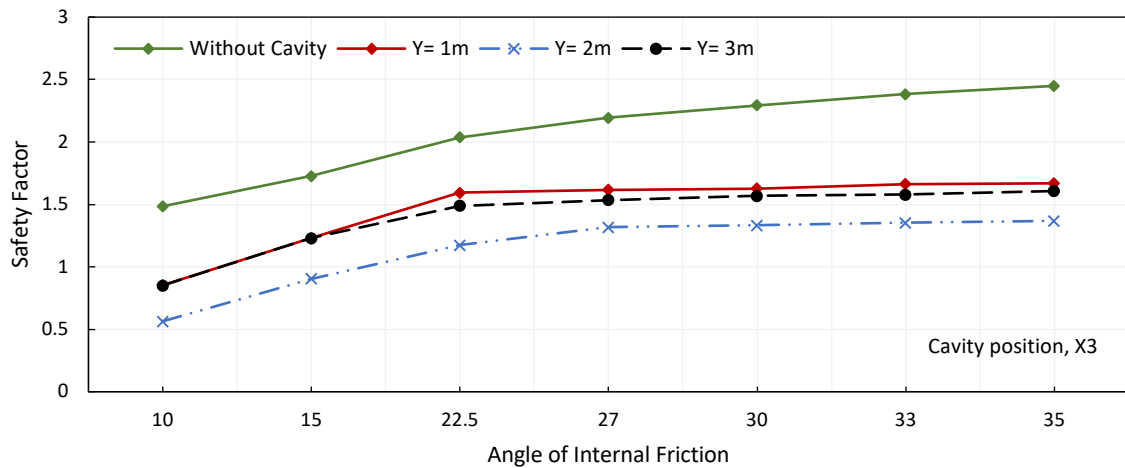




(a)



(b)



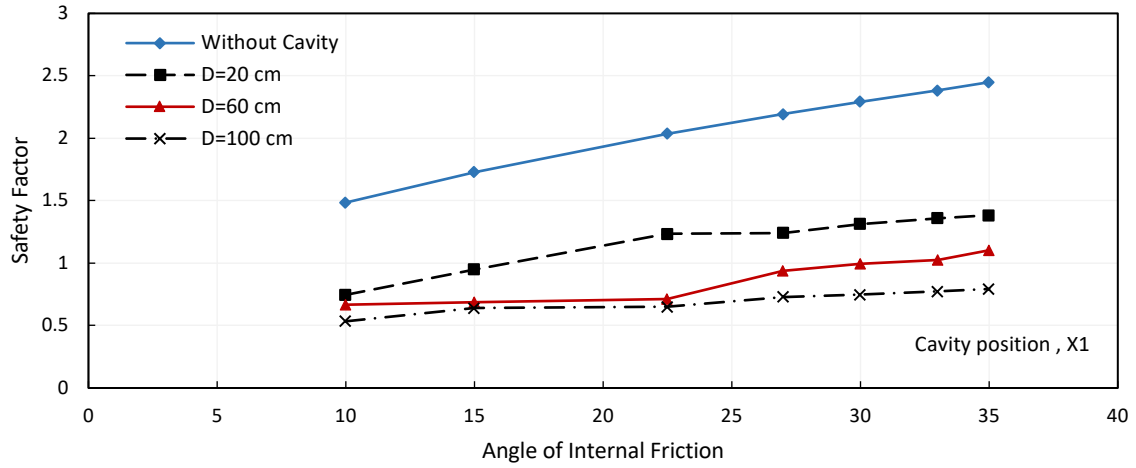
(c)

Figure 4.66: Joint impact of the cavity depth and the  $(\phi)$  on the SF using the MC model for the positions of cavity: (a) X1, (b) X2, (c) X3

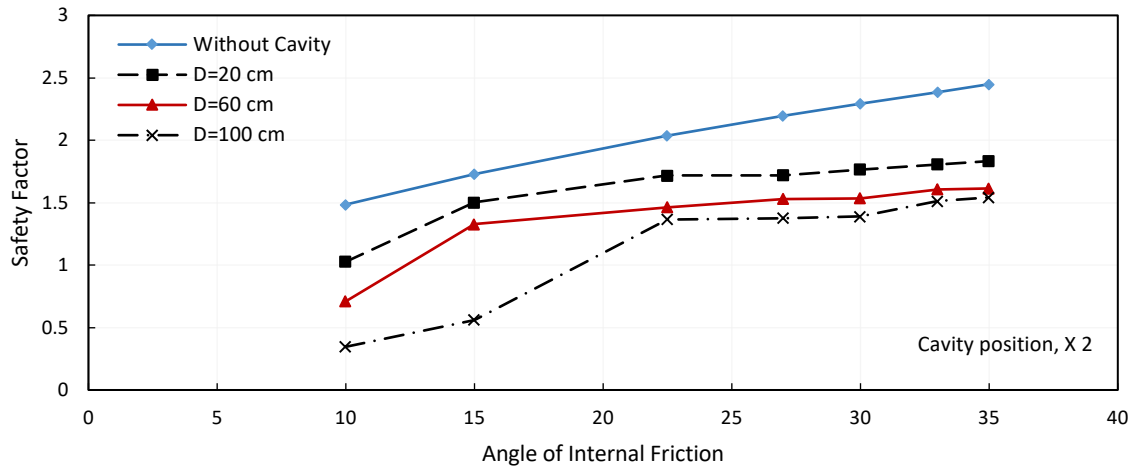
The joint impact of the cavity diameter and ( $\phi$ ) on stability has been simulated in these analyses. The diameters, depths and positions of cavities are as detailed previously. Figure 4.67 and Table 4.31 reveal the results of the stability simulations. It is clear that increasing the cavity diameter from 20cm to 100cm causes a reduction in the SF values for all models considered, wherever the cavity exists below the upstream, despite increasing the value of ( $\phi$ ) from  $10^\circ$  to  $35^\circ$ . For example, for models with cavity positions X1 and X3, the SF dropped from 0.949 to 0.639 and from 1.402 to 0.967, when the cavity diameter was increased from 20cm to 100cm, respectively, with the value of ( $\phi$ ) equal to  $15^\circ$ . It conveys the fact that the cavity diameter can have a much more significant disturbing effect on slope stability in earth dams under rapid-drawdown conditions; this may be compared to the milder improving effects that result from increasing the ( $\phi$ ) of the dam's material. This could be due to there being a more significant drop in the shear strength of the soil resulting from the presence of a bigger cavity, which cannot be compensated for by using a more frictional material.

Table 4.31: Input and output data showing the impact of the ( $\phi$ ) and cavity diameter on SF values

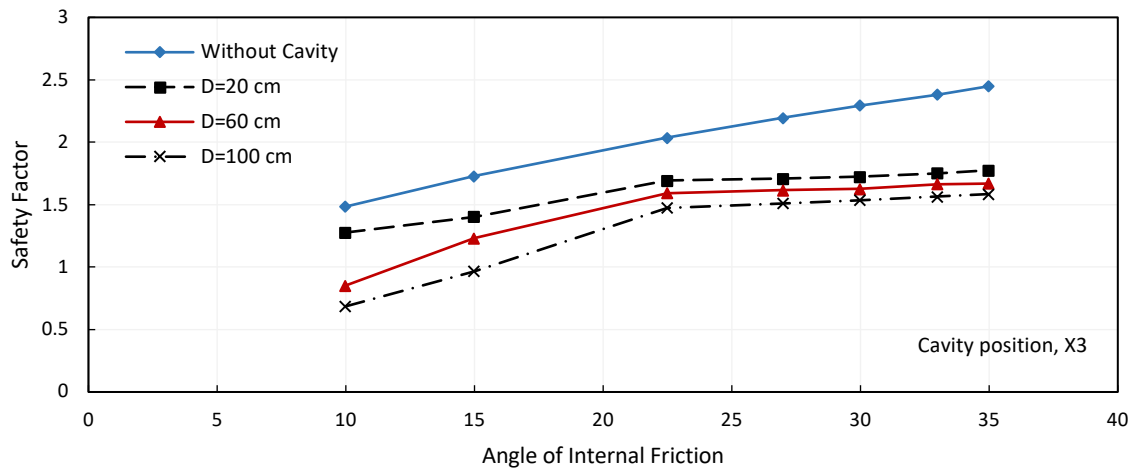
Values of ( $\phi$ )	SF				
	Without cavities	Location of cavities	Diameter of Cavity (cm)		
			D=20	D=60	D=100
10	1.503	X1	0.746	0.667	0.534
		X2	1.027	0.710	0.346
		X3	1.277	0.853	0.686
15	1.716	X1	0.949	0.689	0.639
		X2	1.502	1.328	0.560
		X3	1.402	1.231	0.967
22.5	2.036	X1	1.235	0.715	0.650
		X2	1.716	1.463	1.367
		X3	1.693	1.594	1.476
27	2.156	X1	1.242	0.938	0.730
		X2	1.721	1.529	1.377
		X3	1.707	1.617	1.510
30	2.246	X1	1.313	0.996	0.747
		X2	1.766	1.534	1.388
		X3	1.724	1.627	1.537
33	2.335	X1	1.361	1.023	0.772
		X2	1.807	1.606	1.513
		X3	1.751	1.664	1.564
35	2.399	X1	1.384	1.103	0.793
		X2	1.833	1.614	1.542
		X3	1.776	1.669	1.585



(a)



(b)



(c)

Figure 4.67: Joint impact of cavity diameter and the ( $\phi$ ) on the SF for the positions of cavity:

(a) X1, (b) X2, (c) X3

#### 4.8.2.1 Joint impact of the angle of internal friction ( $\phi$ ) modelled using the HS and MC models

The joint impact of ( $\phi$ ) and the existence of a cavity, in terms of its location and diameter, is discussed in this subsection. The ( $\phi$ ) values used in the analysis are  $10^\circ$ ,  $15^\circ$ ,  $22.5^\circ$ ,  $27^\circ$ ,  $30^\circ$ ,  $33^\circ$  and  $35^\circ$ . The positions, diameters and depths of cavities are as described previously. Figure 4.68 shows the SF values versus the values of ( $\phi$ ) for models without a cavity and with cavity positions X1, X2 and X3. It is obvious from the figure that the SF increased from 1.453 to 2.441 when ( $\phi$ ) increased from  $10^\circ$  to  $35^\circ$  for the cavity-free models. In general, it seems that the SF increased gradually when ( $\phi$ ) was increased from  $10^\circ$  to  $35^\circ$  for all cavity models under consideration. Accordingly, it has been found that the SF increased from 0.635 to 1.061, from 0.864 to 1.585 and from 1.112 to 1.635 for models with cavity positions X1 (-8m), X2 (-17m) and X3 (-24m), respectively. For position X1, it should be mentioned that the SF increased slightly as ( $\phi$ ) was increased and stayed below the minimum recommended values for dam stability during rapid-drawdown conditions, where the SF values were less than (1.2–1.3) and ranged from 0.635 to 1.061. This means that, even although the ( $\phi$ ) value increased, the earth-dam model remained unstable when a cavity was created at position X1. This is similar to the results obtained from using the MC model. For more details, see Table 4.32.

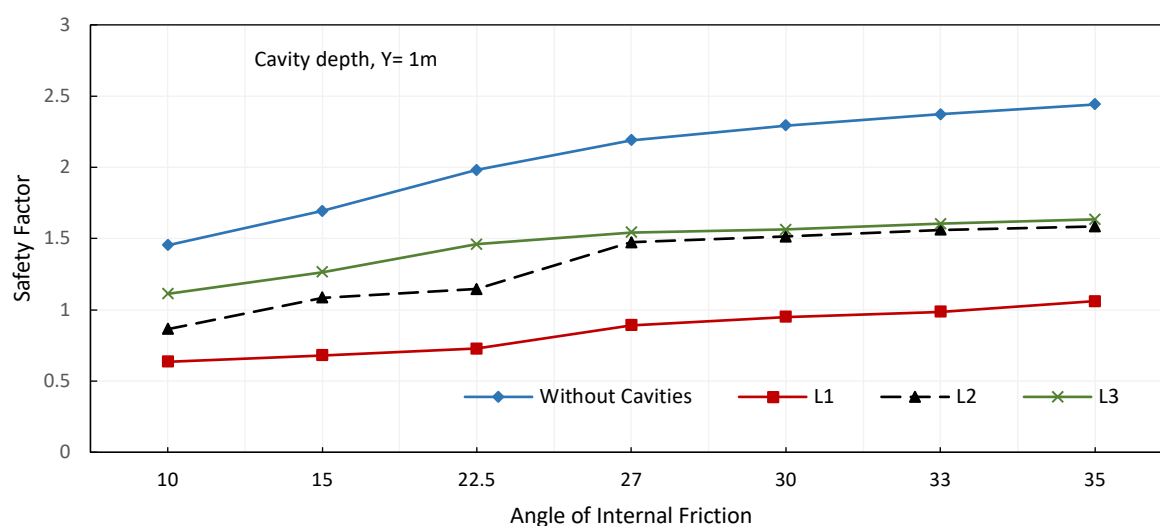
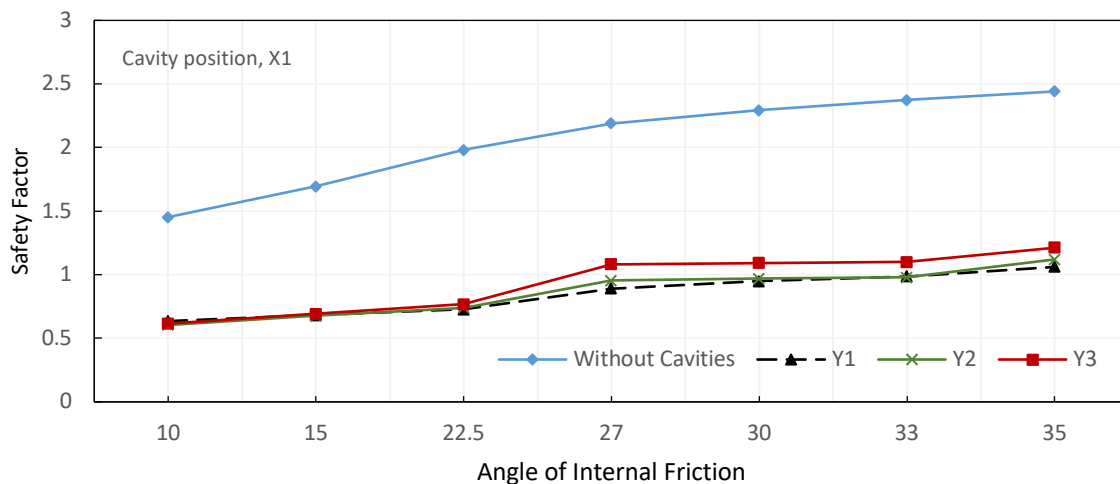


Figure 4.68: Joint impact of the cavity position and the ( $\phi$ ) on SF using the HS and MC models

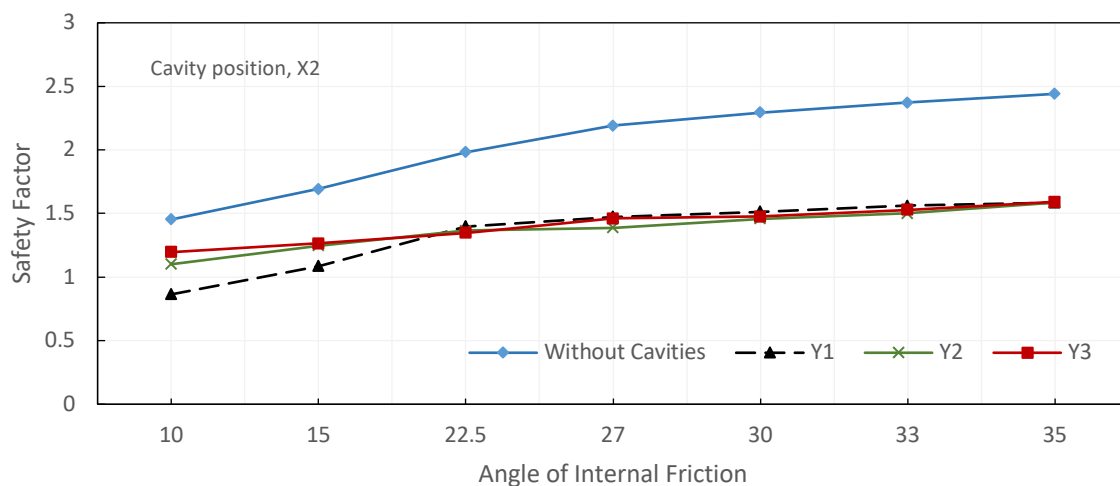
Figure 4.69 demonstrates the influence of  $(\phi)$  and cavity depth on slopes stability. The positions, diameters and depths of cavities are as defined previously. The details of the input data and the PLAXIS 2D output are listed in Table 4.32. Overall, the results show that, by increasing the cavity depth and the  $(\phi)$  value, the SF decreased when the depth was increased to 2m and then increased again when the depth was increased to 3m. For example, the SF values altered from 0.681 to 0.677 and then to 0.693 for position X1 with  $(\phi)$  corresponding to  $15^\circ$ . Similar to the results obtained from the depth-impact analysis using the MC model, it is observed that, despite the increase in the cavity depth and the  $(\phi)$  value, it did not make the dam stable when a cavity was present at position X1; thus, all SF values were less than the specified value (1.2–1.3), regardless of the cavity's depth and the value of  $(\phi)$ . The maximum value of SF is equal to 1.212 with the  $(\phi)$  value corresponding to  $35^\circ$  for a model with a cavity situated at depth of 3m. This denotes that the cavity depth has less influence on stability than its horizontal position.

Table 4.32: Input and output data showing the impact of the  $(\phi)$  and location of cavity on SF values

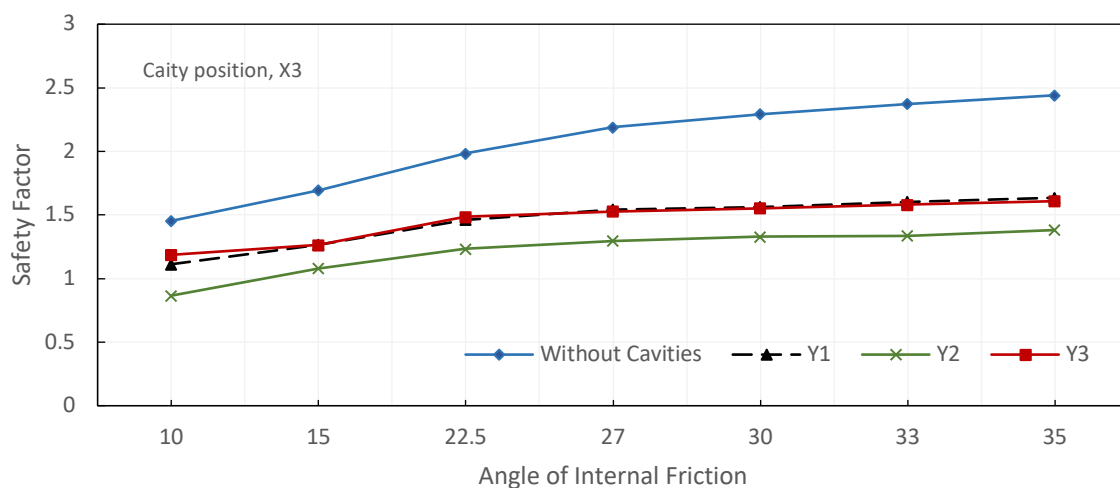
Values of $(\phi)$ , degree	SF				
	Without cavity	Depth of cavity Y, m	Coordinates of cavities in X-axis, m		
			X1 (-8)	X2 (-17)	X3 (-24)
10	1.453	1	0.635	0.864	1.112
		2	0.604	1.101	0.865
		3	0.615	1.196	1.186
15	1.693	1	0.681	1.085	1.265
		2	0.677	1.248	1.080
		3	0.693	1.264	1.262
22.5	1.982	1	0.727	1.398	1.461
		2	0.739	1.366	1.232
		3	0.767	1.347	1.485
27	2.190	1	0.892	1.474	1.543
		2	0.953	1.389	1.296
		3	1.081	1.460	1.528
30	2.294	1	0.949	1.513	1.563
		2	0.969	1.459	1.328
		3	1.092	1.475	1.553
33	2.373	1	0.987	1.562	1.604
		2	0.978	1.500	1.335
		3	1.100	1.530	1.581
35	2.441	1	1.061	1.585	1.635
		2	1.120	1.586	1.381
		3	1.212	1.592	1.608



(a)



(b)



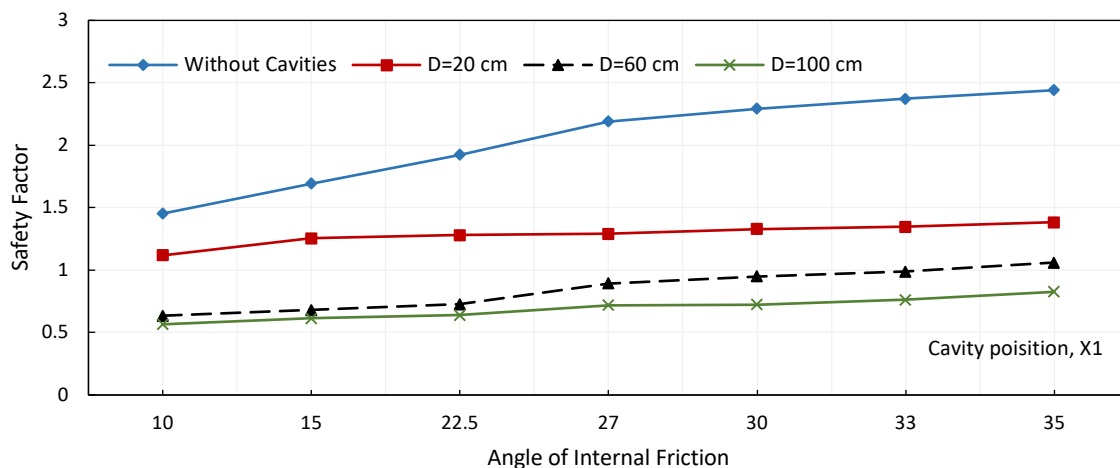
(c)

Figure 4.69: Joint impact of the cavity depth and the ( $\phi$ ) on the SF using the HS and MC models for the positions of cavity: (a) X1, (b) X2, (c) X3

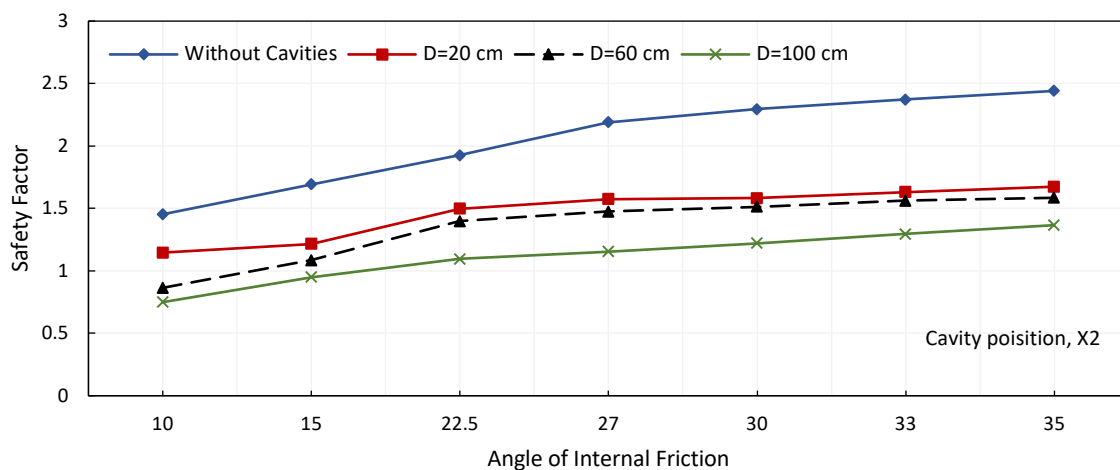
The analysis of the joint influence of cavity diameter and ( $\phi$ ) is presented in this subsection. A cavity was created at positions X1, X2 and X3 and depth of 1m. Figure 4.70 and Table 4.33 show the results of the analysis. According to the results, it appears that increasing the ( $\phi$ ) value from  $10^\circ$  to  $35^\circ$  is not sufficient to reduce the impact on stability of increasing of the cavity diameter. Overall, by increasing the cavity diameter coupled with increasing the ( $\phi$ ) value, the SF values had dropped below minimum stipulated value for slopes safety under rapid-drawdown conditions (1.2-1.3). Consequently, in most models, the earth dam became unstable when the cavity diameter was increased from 20cm to 100cm; refer to Table 4.33 for details of the SF values. This may be due to a more important reduction in the shear strength of the soil because of the existence of a larger cavity, which cannot be recompensed by increasing the value of the soil's internal friction.

Table 4.33: Input and output data showing the impact of the ( $\phi$ ) and cavity diameter on SF values

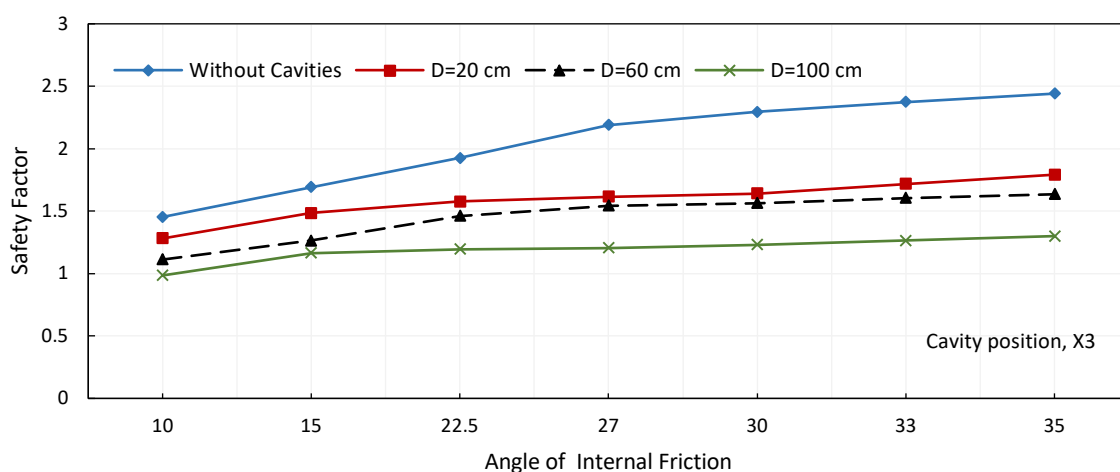
Values of ( $\phi$ ), degree	SF				
	Without cavity	Cavity diameter, cm	Coordinates of cavities in X-axis, m		
			X1 (-8)	X2 (-17)	X3 (-24)
10	1.453	20	1.118	1.146	1.281
		60	0.635	0.864	1.112
		100	0.566	0.749	0.985
15	1.693	20	1.254	1.215	1.484
		60	0.681	1.085	1.265
		100	0.613	0.950	1.163
22.5	1.982	20	1.280	1.498	1.526
		60	0.727	1.398	1.461
		100	0.639	1.096	1.195
27	2.190	20	1.291	1.574	1.614
		60	0.892	1.474	1.543
		100	0.719	1.155	1.205
30	2.294	20	1.328	1.583	1.641
		60	0.949	1.513	1.563
		100	0.725	1.221	1.231
33	2.373	20	1.347	1.631	1.718
		60	0.987	1.562	1.604
		100	0.763	1.296	1.265
35	2.441	20	1.384	1.674	1.792
		60	1.061	1.585	1.635
		100	0.826	1.366	1.300



(a)



(b)



(c)

Figure 4.70: Joint impact of cavity diameter and the ( $\phi$ ) on the SF using the HS and MC models for the positions of cavity: (a) X1, (b) X2, (c) X3

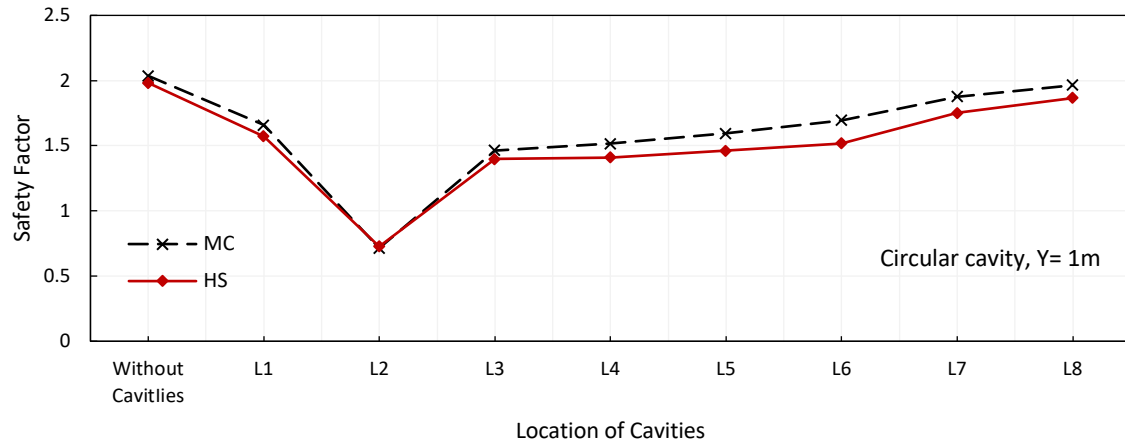


## 4.9 Comparative study

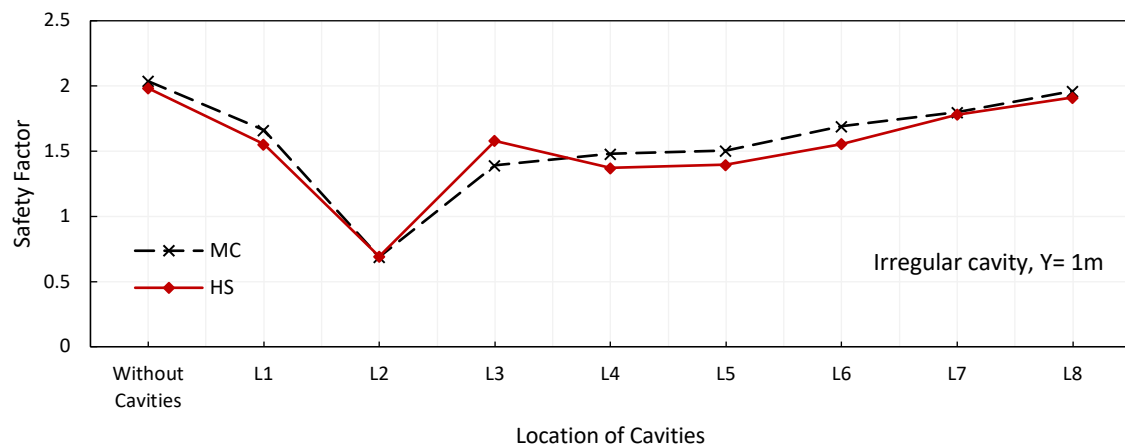
This section gives a summary that illustrates the joint impact of the existence of cavities and using different constituted materials on the stability of slopes. To assess the impact of modelling of the embankment using the MC and HS models on slope stability, a series of comparisons have been drawn from the analyses discussed in this chapter. The subsoil of earth dam model was modelled employing the MC model in all analyses.

### 4.9.1 Joint impact of a cavity's horizontal position and the type of model

Figure 4.71(a) illustrates the effect of the type of model used for modelling on the SF, when considering the existence of circular cavities in the subsoil of the upstream slope, while Figure 4.71 (b) shows their impact on the SF when considering the existence of irregular cavities. In these analyses, the cavities with a diameter of 60cm were created under the upstream side at depth of 1m and in the horizontal positions as detailed in Table 4.3. As revealed in Figure 4.71 (a), the SF values obtained using the MC model were larger than those obtained from the HS model, except when the cavity exists at location L2 (-8, -1), where the value is 0.715 for the MC model compared to 0.727 for the HS model. The same behaviour has been observed on the SF values obtained using models with irregular cavities, as shown in Figure 4.71 (b), except for models with cavity locations L2 and L3 (-17, -1). In the locations L2 and L3, the SF values are 0.688 and 1.391 for the MC model, compared to 0.692 and 1.58 for the HS model, respectively. It is clear that the impact resulting from the existence of circular or irregular cavities is similar, whether the MC model or HS model is used for the modelling. It appears that the type of model used for modelling does not reduce the cavity's influence when it exists in an effective position, such as location L2. The SF values obtained using the MC and HS models were 0.715 and 0.727, respectively, which are below the recommended value (1.2–1.3).



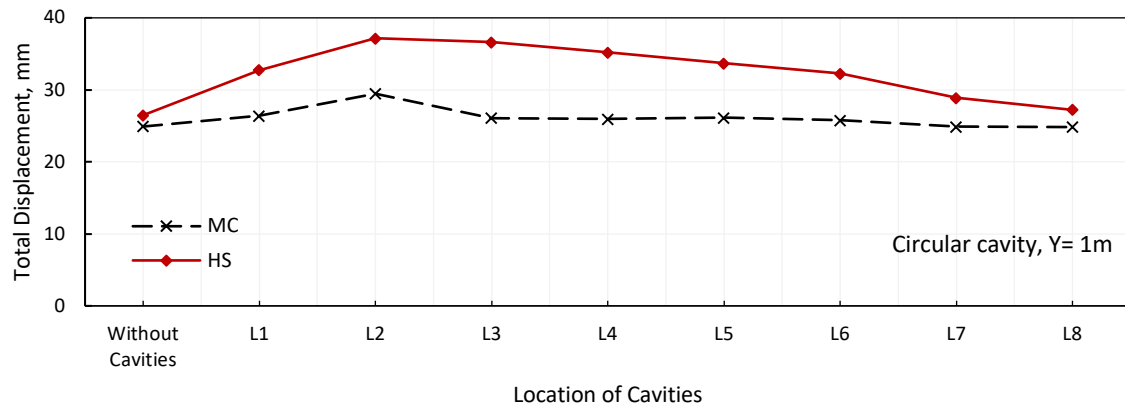
(a)



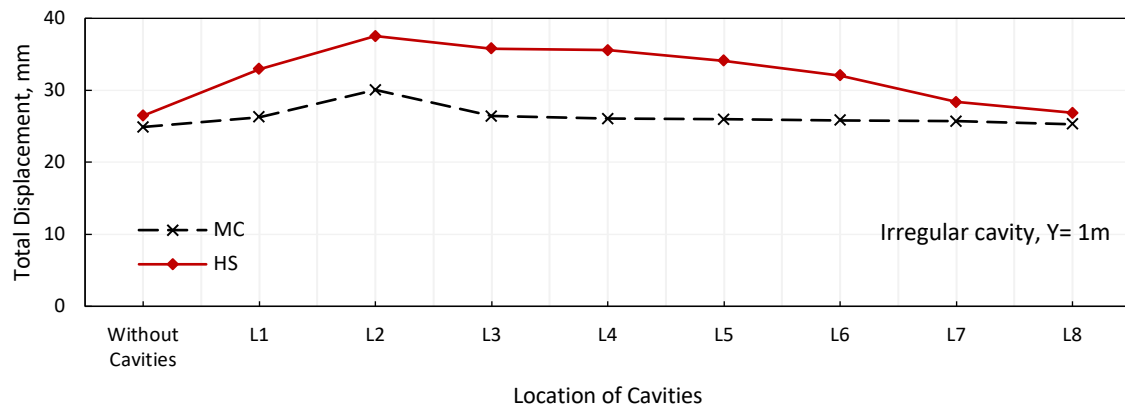
(b)

Figure 4.71: Joint impact of the cavity position and the type of model on the SF of upstream for the presence of a cavity: (a) circular, (b) irregular

Figure 4.72 shows the effect on the displacement values of the type of model used for modelling, considering the existence of circular and irregular cavities below the upstream slope. It should be noted that the displacement values obtained using the HS model are bigger than those obtained using the MC model for all cavity models, whether circular or irregular. The biggest displacement value was 29.46mm for the MC model when a circular cavity exists at the location L2, compared to 37.17mm for the HS model. However, for the impact of irregular cavities, the maximum value of displacement is 30.06mm for the MC model, compared to 37.54mm for the HS model.



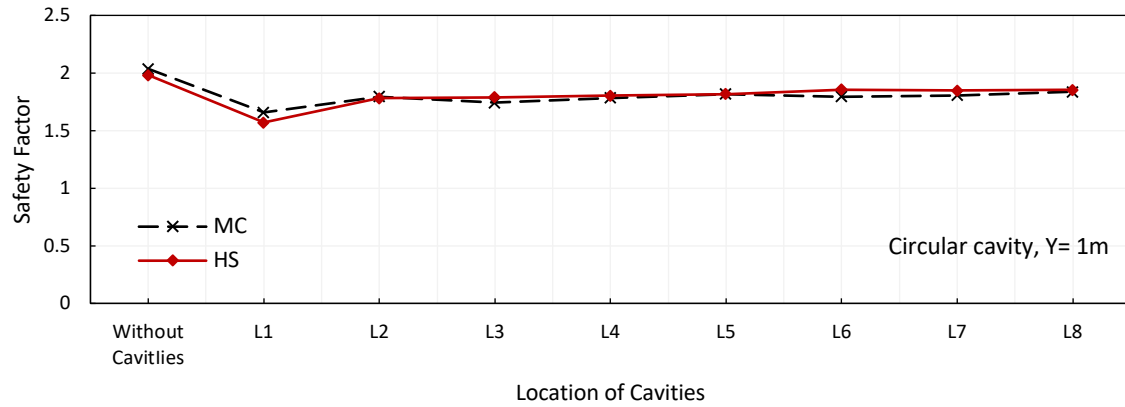
(a)



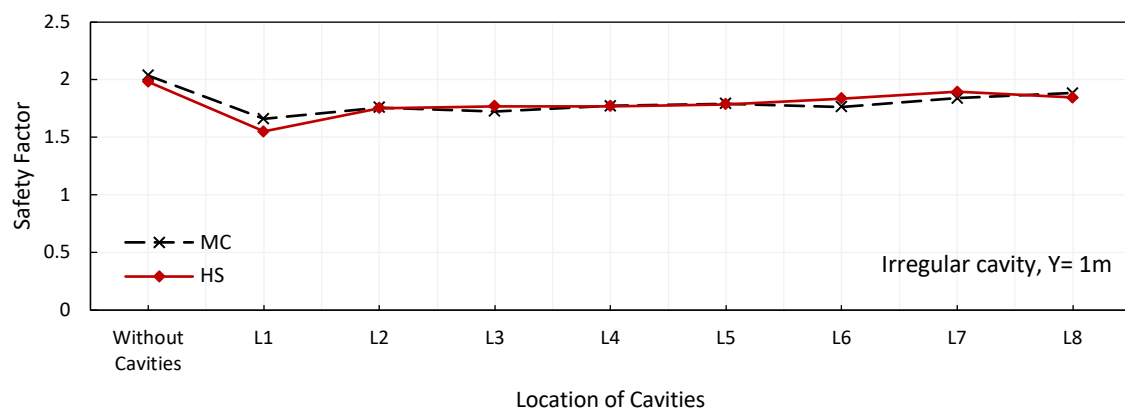
(b)

Figure 4.72: Impact of the cavity position and the type of model on the maximum of the total displacement of upstream for the cavity's presence: (a) a circular cavity, (b) an irregular cavity

With respect to the downstream, Figure 4.73 reveals the joint impact on an earth dam's stability of the type of model and the existence of cavities, in terms of their shape and position. It is clear that the SF values obtained using the MC model are close to those obtained using the HS model for all cavity models. The SF is 1.658 for the MC model for a circular cavity, compared to 1.571 for the HS model for a circular cavity; however, it is equal to 1.661 for the MC model for an irregular cavity, compared to 1.552 for the HS model for an irregular cavity. All SF values obtained are greater than the minimum stipulated values. Similar to the downstream side analyses in previous sections, it is clear that the modelled earth dam stays safe during rapid-drawdown conditions, regardless of the type of model used for modelling.



(a)

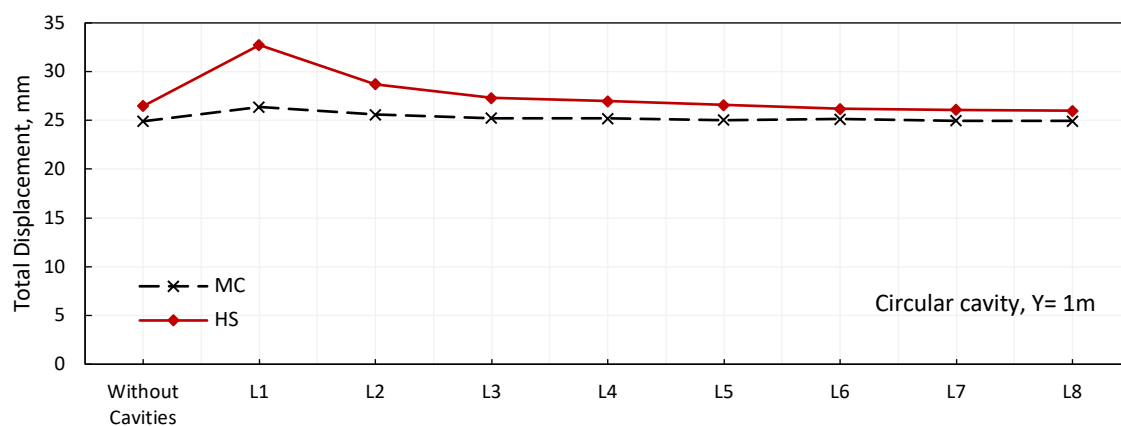


(b)

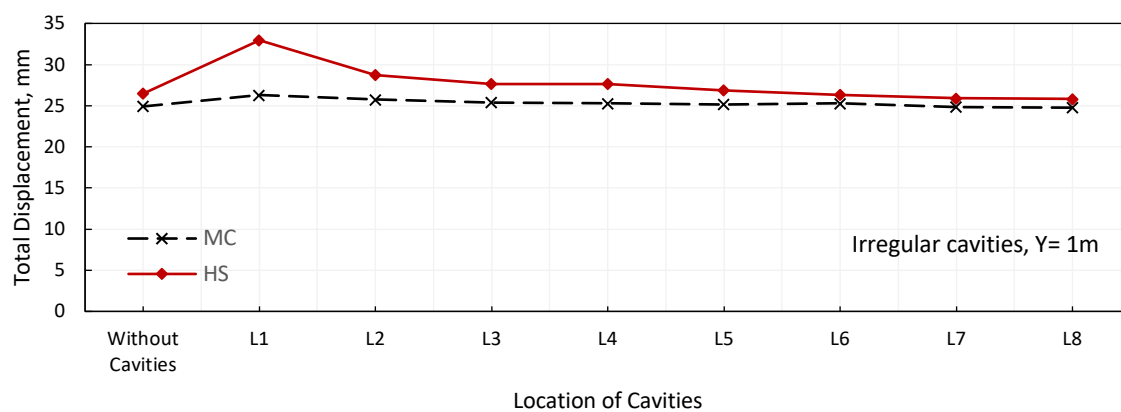
Figure 4.73: Joint impact of the cavity position and the type of model on the SF of downstream for the presence of a cavity: (a) circular cavity, (b) irregular cavity

Figure 4.74 shows the Joint impact of the type of model and the presence the existence of circular and irregular cavities under downstream on the displacement values. In general, it is observed that the displacement values recorded for the HS model are greater than those for the MC model if both a circular cavity or an irregular cavity are used. It should be noted that this behaviour applies to all locations chosen in this analysis without exception. It has been remarked that the displacement value increased by about 23.6% for the HS model when a circular cavity exists under the centerline of the dam (L1), compared to 5.9 % for the MC, but the values of the displacement increased by about 24.4% for the HS model when an irregular cavity exists at the same location (L1), compared to 5.9% for the MC. The difference between the values obtained using the MC and the HS models may be attributed to the fact that modelling using the HS model is more flexible than the MC model; in addition, the HS

model includes more parameters for soil modelling (Keyvanipour et al., 2012). However, the results obtained from modelling using both models are close to each other in general.



(a)



(b)

Figure 4.74: Impact of the cavity position and the type of model on the maximum of the total displacement of downstream for the cavity's presence: (a) a circular cavity, (b) an irregular cavity

### 4.9.2 Joint impact of cavity depth and the modelling material

Figure 4.75 and Figure 4.76 reveal the joint impact on an earth dam's stability of the type of model and the existence of a circular cavity, in terms of their position and depth. Based on the results obtained from the simulation of the effect of depth when using both the MC and HS models, it can be concluded that the cavity depth has an insignificant impact on the stability of the slopes of an earth dam, except for models with a cavity at position  $X_2=-8\text{m}$ , where the SF increased by about 43.7% for MC model with a circular cavity as the cavity depth increased from 1m to 4m, compared to 72.3% for HS model. However, for example, for models at position  $X_4=20\text{m}$ , the SF decreased by about 1.7% for MC model with a circular cavity as the cavity depth increased, compared to 0.3% for HS model. In general, the SF values for both the MC and HS models are smaller or bigger than each other but remain close to each other with increasing the cavity depth.

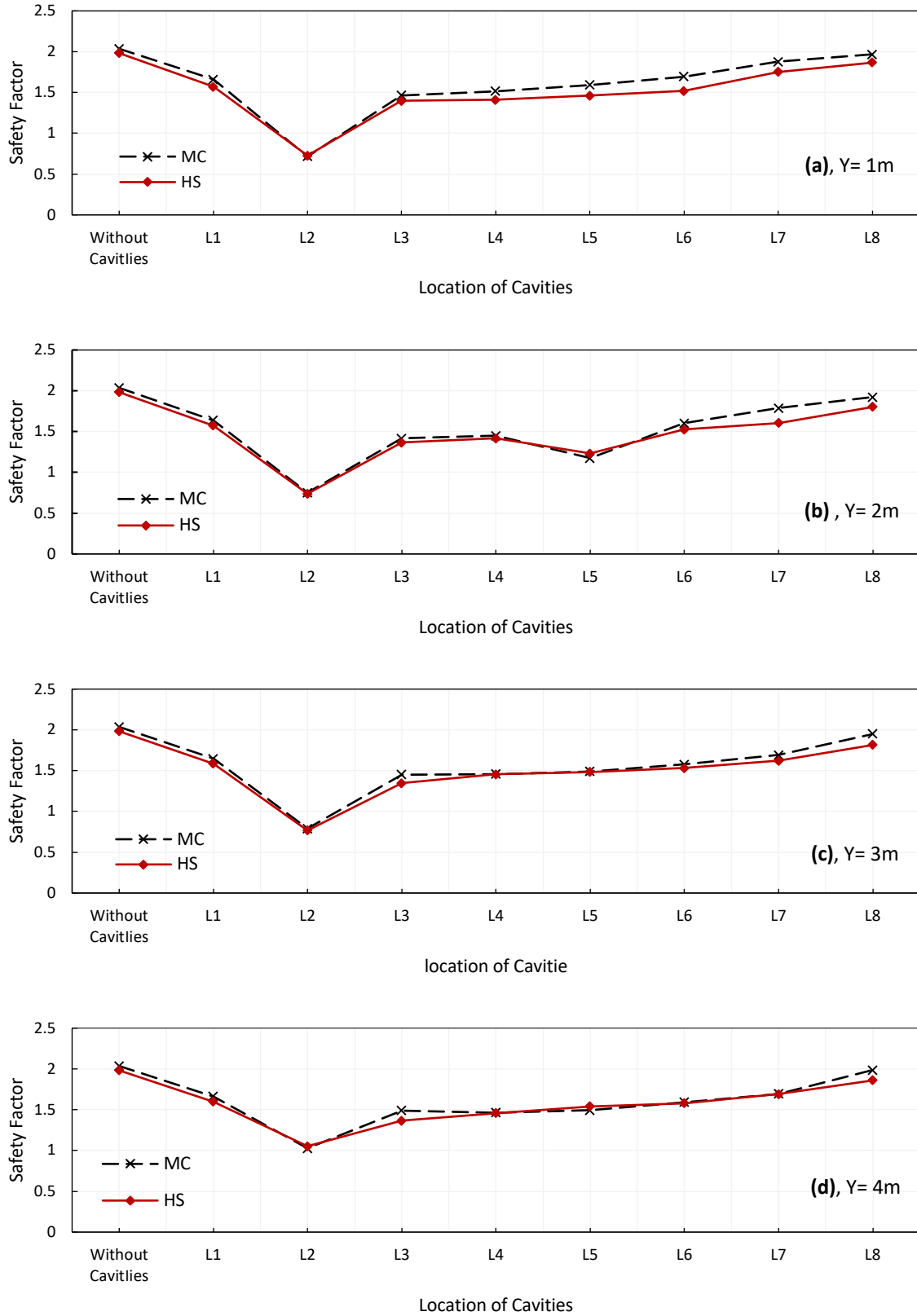


Figure 4.75: Joint impact on stability of the type of model and the cavity's horizontal position under upstream: (a) Y= 1m, (b) Y= 2m, (c) Y= 3m, (d) Y= 4m

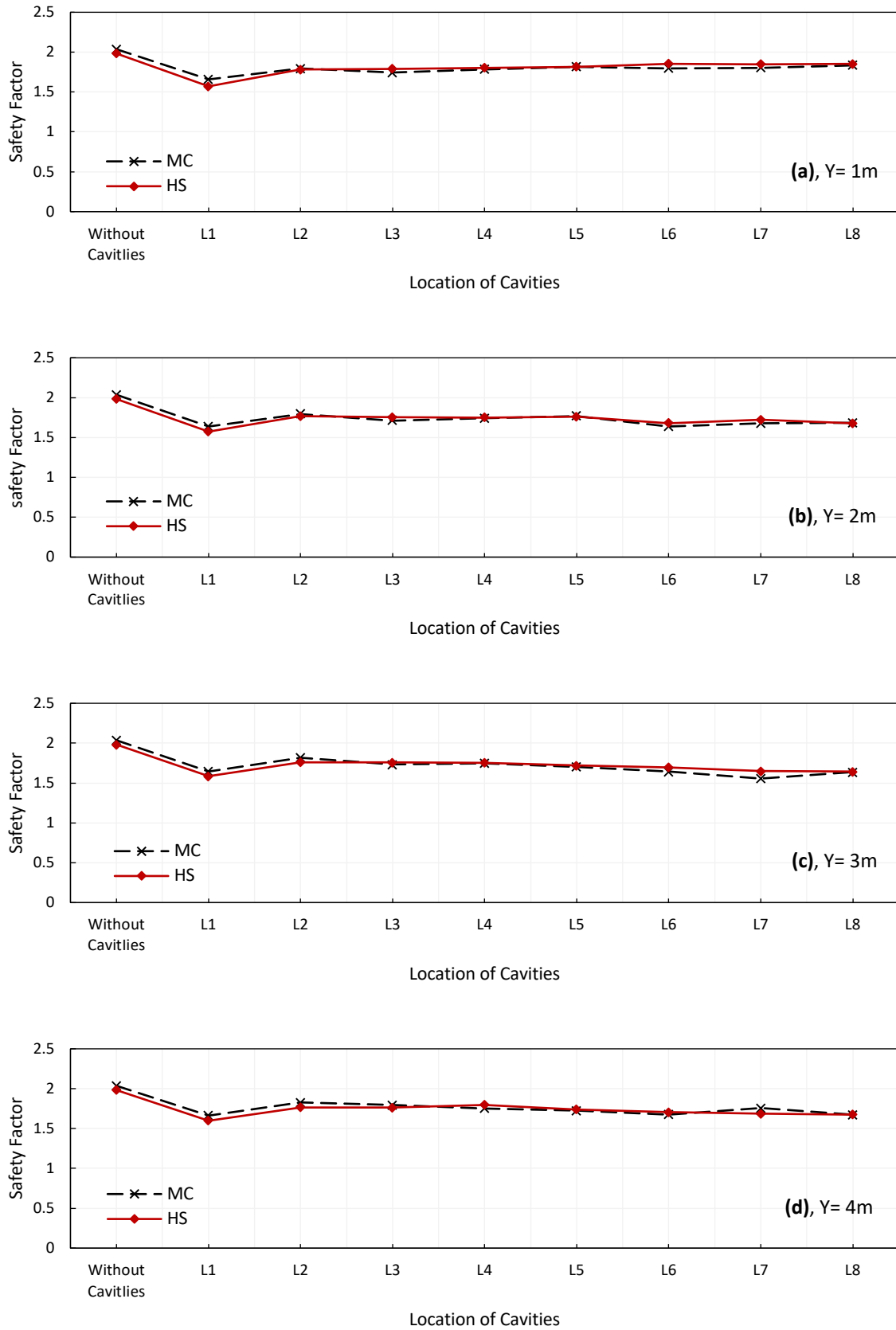


Figure 4.76: Joint impact on stability of the type of model and the cavity's horizontal position under downstream: (a) Y= 1m, (b) Y= 2m, (c) Y= 3m, (d) Y= 4m



## 4.10 Conclusions

To investigate the influence of the existence of cavities on earth-dam slope stability under conditions of rapid drawdown, a series of 2D finite-element analyses was carried out using PLAXIS 2D, and factors such as the cavity's horizontal position, depth, diameter and shape, and the number of cavities were considered. The combined effects on the stability of slopes of both cavities and the strength parameters (soil cohesion and friction angle) were also investigated and parametrically analysed. The stability results generally indicate that in conditions of rapid drawdown, the presence of a cavity in the subsoil of the upstream side decreases slope stability noticeably, compared to its presence in the subsoil of the downstream side. Furthermore, variations in the horizontal positions of the cavity have more influence on stability than the variations in the vertical positions (depth) of cavity: the SF values increase or decrease slightly as a result of changing the depth of cavity. The results also reveal that increasing the number of cavities decreases the SF value noticeably, and the considered earth dam is safe during conditions of rapid drawdown when cavities are positioned under the downstream side, regardless of the number of them. Moreover, any increase in the size of existing cavities decreases the SF significantly. The stability of the dam's slopes increases with an increase in the value of cohesion and angle of internal friction, as expected; however, the stability-analysis results reveal that increasing the material properties of embankment (soil cohesion and friction angle) does not reduce the effect of cavities on stability when those cavities are in critical positions. According to the results, the shape of the cavity impacts slightly the stability of earth dam. The type of model used does not reduce the cavity's influence when it exists in a crucial position, and the impact resulting from the existence of circular or irregular cavities is similar, whether the MC model or HS model is used for the modelling of the embankment. The existence of a cavity has more influence on the SF values than the displacement values.

Finally, according to the results of the analyses carried out in this study, it is concluded that the location of the cavity in the X direction (horizontal position) is the most important parameter among all the studied parameters of cavity (depth, shape, diameter, and number) and type of model and it is necessary to give it particular attention when analysing and assessing the effects of cavities on the stability of slopes and earth dams based on cavitied soil.

## CHAPTER FIVE: SEEPAGE ANALYSIS

### 5.1 Introduction

This chapter details the results obtained from the numerical analysis of seepage. Finite element PLAXIS 2D software was utilized to study seepage through earth dams. All seepage analyses were executed to simulate seepage during rapid-drawdown conditions. A parametric study was conducted to assess the impact of the existence of cavities on the flow rate in terms of i) cavity position, which is the coordinates of the cavity in the X direction; ii) cavity depth, which is the coordinates of the cavity in the Y direction; iii) cavity shape; and iv) the number of cavities, as identified in chapter four.

This study involves two main stages of analysis. The first was carried out using the Mohr-Coulomb (MC) model to model the body of the dam (embankment) and the subsoil. However, in the second stage, the Hardening Soil (HS) and MC models were utilized to model the embankment and subsoil, respectively. The material parameter values implemented in the models is detailed in Table 4.1 and Table 4.2. The seepage analysis was accomplished using a numerical model, as characterized previously in section 3.6.1. Cavities with a diameter of 60cm were considered in the simulation.

### 5.2 Impact of a varying cavity position in the horizontal direction (X)

In order to verify this impact, fifteen horizontal positions were assumed for a cavity beneath the upstream and downstream slopes. The coordinates of the cavity locations are detailed in Table 5.1.

Table 5.1: Coordinates of the locations of cavities in X and Y directions

Cavity location (L)	Cavity depth (Y), m	The coordinates of position in X-axis (X), m	
		Upstream	Downstream
L1	1	0	0
L2	1	-8	+8
L3	1	-17	+17
L4	1	-20	+20
L5	1	-24	+24
L6	1	-28	+28
L7	1	-35	+35
L8	1	-40	+40

### 5.2.1 Modelling of an earth dam using the MC model

In this simulation, the constitutive MC model was utilized to model the embankment and subsoil.

Figure 5.1 shows the flow rates for models without a cavity and with a circular cavity situated at various horizontal positions under the upstream side. The results indicate that the presence of a cavity impacts the flow rates significantly; the flow rates increased from  $2.571 \times 10^{-3}$  m/day for a cavity-free model to  $459.8 \times 10^{-3}$  m/day for the model with a cavity at location L2 (-8, -1). It is clear that flow rates decrease when the distance between the position of cavity and the centreline of the dam is increased, where the flow rate reduced from  $459.8 \times 10^{-3}$  m/day to  $2.81 \times 10^{-3}$  m/day for models with cavity locations L2 (-8, -1) and L8 (-40, -1), respectively. It also shows a large jump in the flow-rate value as the cavity location moves from L1 (under the centreline) to the first location on the upstream side. This could be due to the faster downward stream under the upstream side, as the gravity and the pressure head act to affect the flow rate. During the rapid drawdown, the soil within the body of the dam stays saturated, which generates shear stresses, while the shear resistance is reduced greatly as a result of the development of the water pressures (Ranjan and Rao, 2007). In addition, seepage starts from inside the dam body to the upstream slope; seepage and hydrodynamic pressures produce forces towards the upstream slope, which reduce the shear resistance of the upstream slope (Tran, 2004). Consequently, the flow rate increases in these positions as a result of removing the supporting water forces from the upstream side .

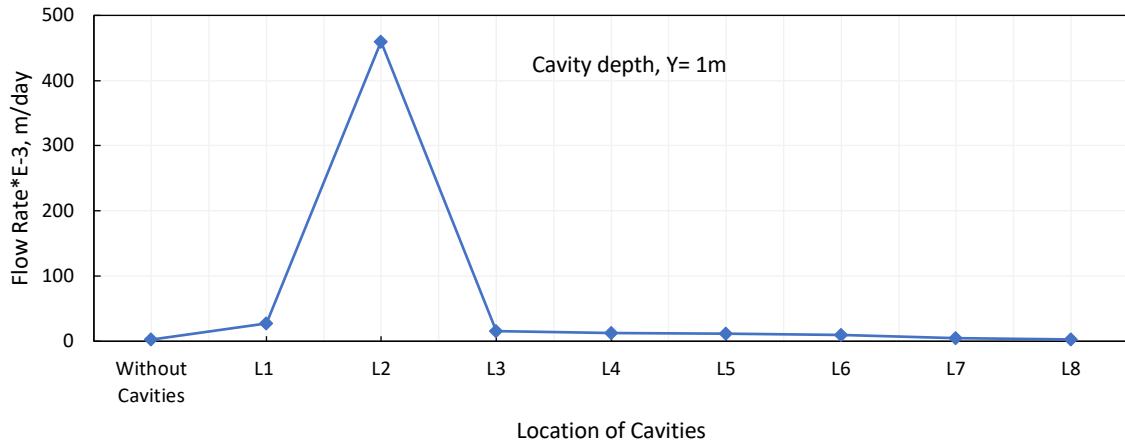


Figure 5.1: Flow rate vs location of a circular cavity beneath upstream using the MC model

Figure 5.2 reveals the impact on the flow rate of the position of a circular cavity situated under the downstream side. It can be seen that a cavity being present causes an increase in the flow rate. The flow rate increased from  $2.571 \times 10^{-3} \text{m/day}$  to  $16.5 \times 10^{-3} \text{m/day}$  for models without a cavity and with a cavity at location L2 (8, -1), respectively. In general, it has been found that the flow rate drops significantly as the horizontal distance between the cavity and the dam's centreline increases. For example, the flow rate decreased from  $27.72 \times 10^{-3} \text{m/day}$  to  $2.65 \times 10^{-3} \text{m/day}$  for models with cavity locations L1 (0, -1) and L8 (40, -1), respectively.

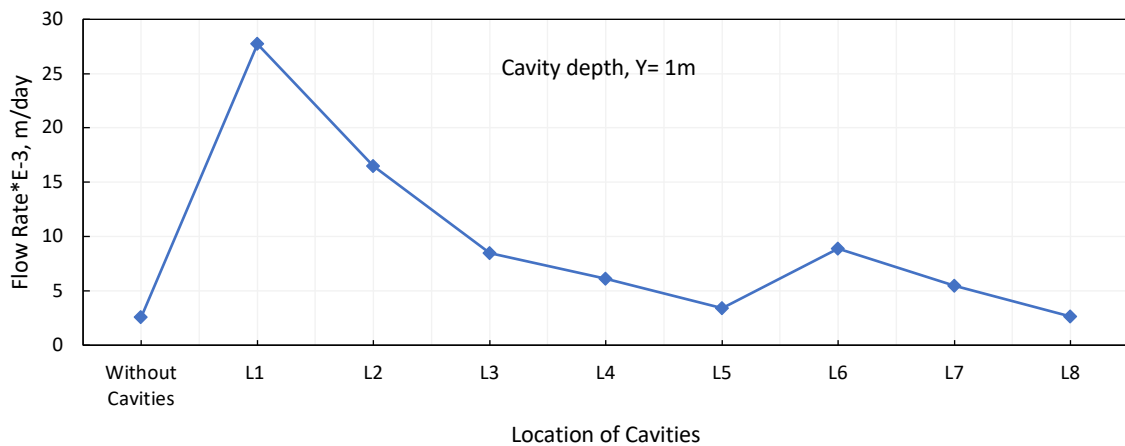


Figure 5.2: Flow rate vs location of a circular cavity beneath downstream using the MC model

## 5.2.2 Modelling of an earth dam using the HS and MC models

The soil of the embankment and the subsoil were modelled using the HS and MC models, which is presented in this section. The coordinates of each cavity location are as previously listed in Table 5.1

Figure 5.3 illustrates the influence on the flow rate of the horizontal position of a cavity situated under the upstream slope. It is observed that the presence of a cavity at location L2 led to a large increase in the flow rate, in which this value amounted to  $459.2 \times 10^{-3} \text{m/day}$ , compared to  $2.58 \times 10^{-3} \text{m/day}$  for a cavity-free model. It should be that the flow-rate values ranged from  $3.05 \times 10^{-3} \text{m/day}$  to  $26.4 \times 10^{-3} \text{m/day}$  for cavity locations L8 (-40, -1) and L1 (0, -1), respectively. This implies that, as the cavity position approaches the end of the dam base towards location L8, the effect of a cavity begins to fade, leading to a significant decrease in flow rate, where the flow rate amounted to  $3.05 \times 10^{-3} \text{m/day}$  as opposed to  $2.58 \times 10^{-3} \text{m/day}$  for a cavity-free model.

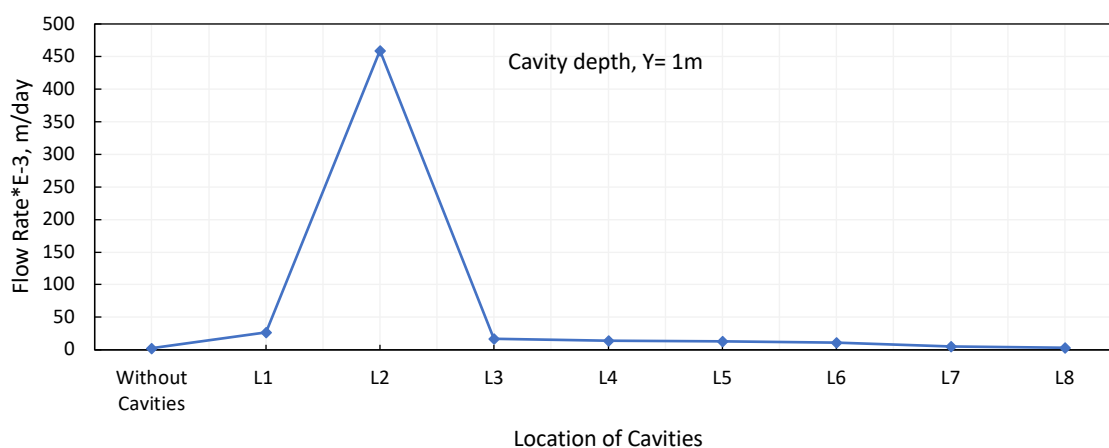


Figure 5.3: Flow rate vs location of a circular cavity beneath upstream using the HS and MC models

Figure 5.4 exhibits the effect on the flow rate of the position of a cavity situated under the downstream slope. It should be noted that the flow rate decreased considerably from  $2.58 \times 10^{-3} \text{m/day}$  to the maximum value  $26.4 \times 10^{-3} \text{m/day}$  for models without a cavity and with a cavity at location L1(0, -1). This means that the critical cavity position for the downstream side is under the centreline of the dam. As mentioned previously, the influence of the cavity almost disappears as the cavity's position moves towards the dam end at location L8 (40, -1), where the flow-rate value was equal to  $2.66 \times 10^{-3} \text{m/day}$ , compared to  $2.58 \times 10^{-3} \text{m/day}$  for a cavity-free model.

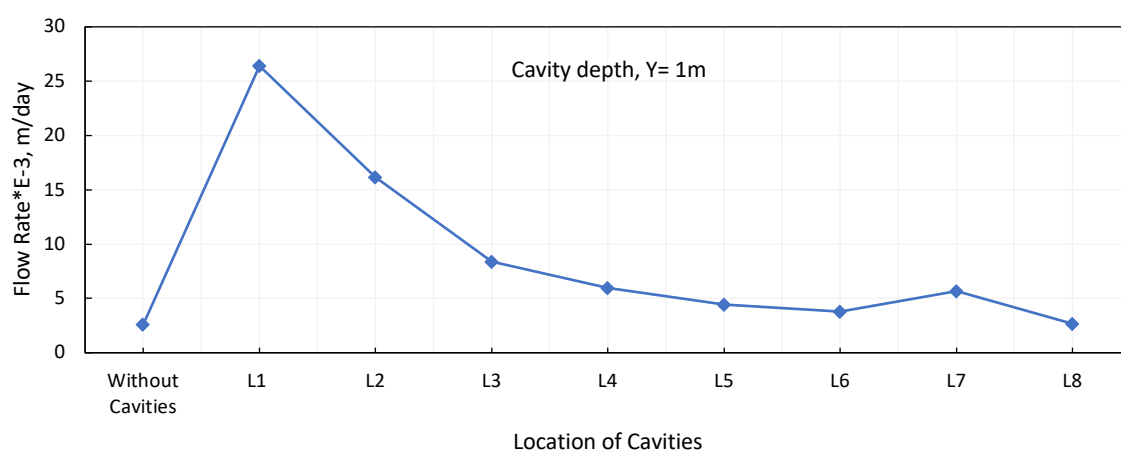


Figure 5.4: Flow rate vs location of a circular cavity under downstream using the HS and MC models

### 5.3 Impact of cavity depth

A series of seepage analyses were carried out to assess the impact of cavity depth on flow rate through earth dams. Four depths for cavities in the subsoil of the upstream and downstream slopes were selected, which are  $Y=1\text{m}$ ,  $2\text{m}$ ,  $3\text{m}$  and  $4\text{m}$ . A cavity was created at one of fifteen positions that varied horizontally, as described in Table 5.1.

#### 5.3.1 Modelling of an earth dam using the MC model

Figure 5.5 and Table 5.2 present the effect on the flow rate of the depth of a circular cavity situated beneath the upstream side. As shown in Figure 5.5, the flow-rate value increases slightly when the cavity depth is increased from  $1\text{m}$  to  $4\text{m}$ , except for cavities at locations L1 or L2. For example, by increasing the depth from  $1\text{m}$  to  $4\text{m}$ , the flow rate increased from  $15.47 \times 10^{-3}\text{m/day}$  to  $19.13 \times 10^{-3}\text{m/day}$  and from  $2.81 \times 10^{-3}\text{m/day}$  to  $4.16 \times 10^{-3}\text{m/day}$  for models with cavity locations L3 and L8, respectively. This increase is more significant when the model contains a cavity situated at location L2, where the flow rate increase from  $459.8 \times 10^{-3}\text{m/day}$  at the depth of  $1\text{m}$  to  $721.2 \times 10^{-3}\text{m/day}$  at the depth of  $2\text{m}$  and then reduces to  $527.5 \times 10^{-3}\text{m/day}$  at a depth  $4\text{m}$ .

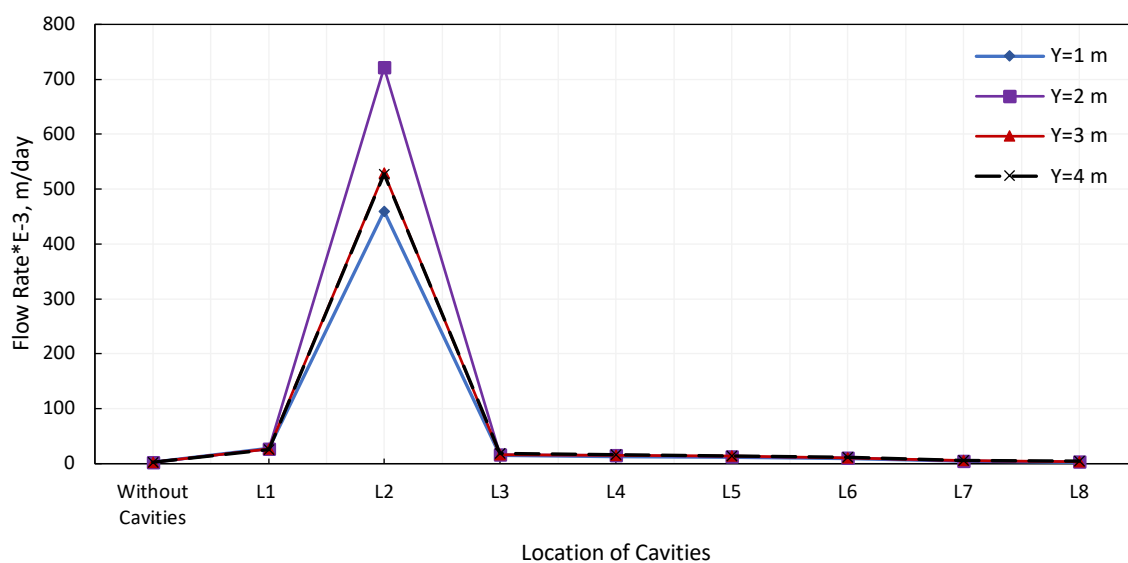


Figure 5.5: Flow rate vs location of a circular cavity beneath the upstream at various depths using the MC model

Table 5.2: Impact of the depth of a circular cavity beneath the upstream and downstream slopes on the flow rate

Cavity location	Cavity position (X), m	Flow rate $\times E-3$ , m/day							
		Upstream slope				Downstream slope			
		Cavity depth (Y), m				Cavity depth (Y), m			
		1m	2m	3m	4m	1m	2m	3m	4m
Without cavities		2.571				2.571			
L1	0	27.72	26.36	26.27	25.20	27.72	26.36	26.27	25.20
L2	$\pm 8$	459.8	721.2	529.2	527.5	16.50	15.35	15.27	15.20
L3	$\pm 17$	15.47	14.74	16.49	19.13	8.482	8.829	8.798	8.622
L4	$\pm 20$	13.11	14.60	15.15	16.22	6.120	6.241	6.510	6.282
L5	$\pm 24$	11.90	11.28	14.19	14.31	3.432	3.515	3.629	3.605
L6	$\pm 28$	9.240	10.14	10.32	11.17	8.913	5.550	5.290	5.056
L7	$\pm 35$	4.830	5.140	6.130	6.170	5.478	11.77	13.76	15.58
L8	$\pm 40$	2.810	3.060	3.710	4.160	2.650	7.435	12.18	18.88

Figure 5.6 shows the influence of cavity depth on the flow rate for models with a cavity situated beneath the downstream slope. The detail of the cavity's location and corresponding flow-rate values are outlined in Table 5.2. The results show that increasing the cavity's depth from 1m to 4m causes fluctuations in flow rates (increasing or decreasing) generally. For models with cavity locations L1 and L6, by increasing the cavity depth to 4m, the flow rates dropped from  $27.72 \times 10^{-3} \text{m/day}$  to  $25.2 \times 10^{-3} \text{m/day}$  and from  $8.913 \times 10^{-3} \text{m/day}$  to  $5.056 \times 10^{-3} \text{m/day}$ , respectively. There is an insignificant increase in flow rates for models with a cavity at locations L3, L4 and L5, when the cavity depth is increased, for example, the flow rate increased from  $8.482 \times 10^{-3} \text{m/day}$  to  $8.622 \times 10^{-3} \text{m/day}$  for models with a cavity at location L3. However, the increase in flow rate was more significant when the cavity was situated at location L7 and L8. It can be deduced from the results that the horizontal variation in the location of the cavity has more influence on flow-rate values compared to the vertical variation in the location, whether the cavity is located under upstream or downstream.

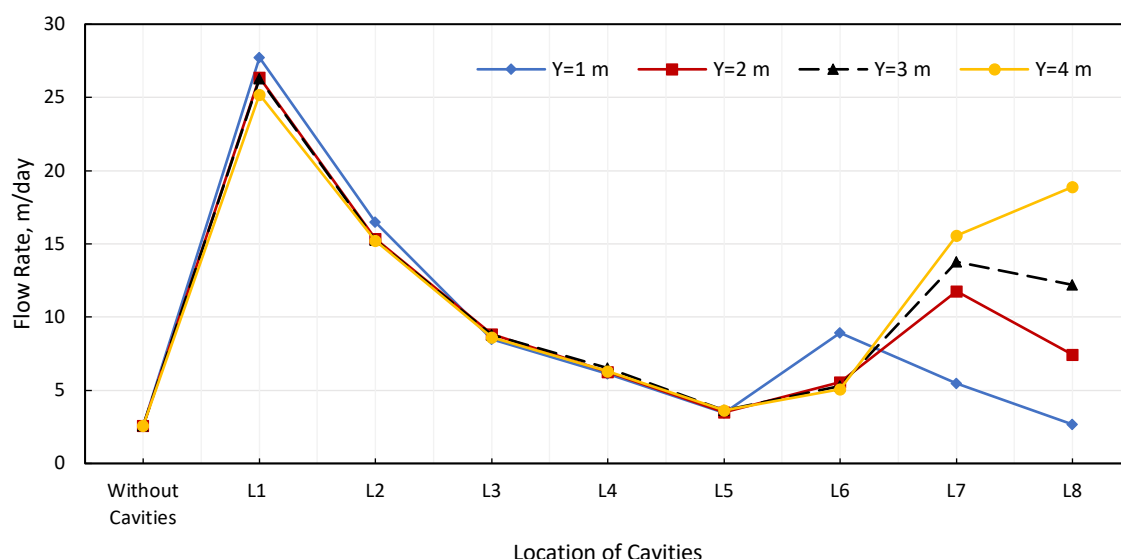


Figure 5.6: Flow rate vs location of circular cavities beneath downstream at various depths using the MC model

### 5.3.2 Modelling of an earth dam using the HS and MC models

The influence of the cavity depth on flow rate for HS and MC models with a cavity under the upstream side is shown in Figure 5.7. The detail of the cavity's location and the corresponding flow-rate values, as outlined in Table 5.3 Similar to the results obtained from the modelling using the MC model, it is found that increasing the cavity's depth has a slight impact on flow rates compared to its horizontal position. The flow-rate values fluctuate



somewhat (increase or decrease) when the cavity depth is increased. Generally, the flow rates went up as the cavity depth increased from 1m to 4m for all models, except for locations L1 and L2. The flow rate decreased a little from  $26.4 \times 10^{-3} \text{m/day}$  to  $25.32 \times 10^{-3} \text{m/day}$  for models with a cavity at location L1 when the cavity depth was increased, while it increased from  $459.2 \times 10^{-3} \text{m/day}$  to  $720.5 \times 10^{-3} \text{m/day}$  at a depth of 2m and then decreased to  $514 \times 10^{-3} \text{m/day}$  at a depth of 4m for models with a cavity at location L2.

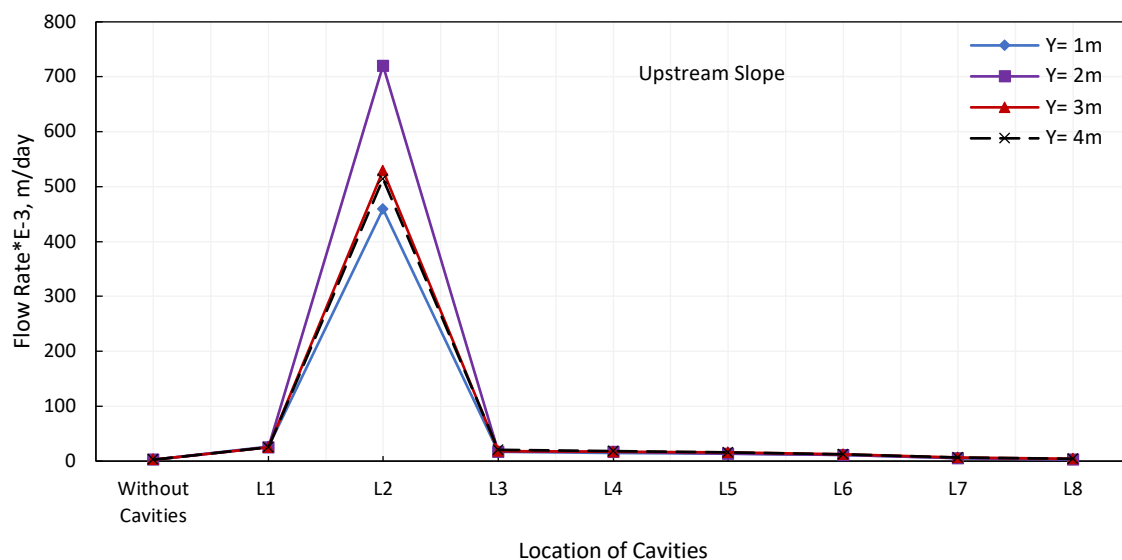


Figure 5.7: Flow rate vs location of a circular cavity at various depths beneath upstream using the HS and MC models

Table 5.3: Impact of the depth of a circular cavity beneath the upstream and downstream slopes on the flow rate

Cavity location	Cavity position (X), m	Flow rate $\times E-3$ , m/day							
		Upstream slope				Downstream slope			
		Cavity depth (Y), m				Cavity depth (Y), m			
		1m	2m	3m	4m	1m	2m	3m	4m
Without cavities		2.580				2.580			
L1	0	26.40	25.78	25.58	25.32	26.40	25.78	25.58	25.32
L2	$\pm 8$	459.2	720.5	529.0	514.0	16.19	15.76	15.59	14.75
L3	$\pm 17$	16.91	17.05	17.87	20.51	8.410	8.386	8.251	8.104
L4	$\pm 20$	14.37	16.55	16.84	18.35	5.980	5.810	5.770	5.390
L5	$\pm 24$	13.28	13.62	15.84	15.87	4.440	3.930	3.550	3.290
L6	$\pm 28$	11.09	11.48	12.19	12.57	5.760	5.320	5.215	5.120
L7	$\pm 35$	5.540	5.740	6.570	6.348	5.645	13.15	13.73	15.70
L8	$\pm 40$	3.050	3.570	3.970	4.606	2.660	7.520	12.26	18.95

Figure 5.8 reveals the flow-rate values versus the cavity location for models containing a cavity positioned beneath the downstream side at different depths. The detail of the cavity's location and corresponding flow-rate values are shown in Table 5.3. As mentioned previously, the results indicate that the cavity depth somewhat impacts the flow rate; this observation applies to cavity locations L1 to L6. In these locations, there was a slight decrease in the flow rate when the cavity depth increased from 1m to 4m. For example, the flow rate reduced from  $8.41 \times 10^{-3}$  m/day to  $8.104 \times 10^{-3}$  m/day and from  $5.76 \times 10^{-3}$  m/day to  $5.12 \times 10^{-3}$  m/day for cavity models at locations L3 and L6, respectively. An exception was observed for models with a cavity locations L7 and L8, where the flow rates increased considerably from  $5.645 \times 10^{-3}$  m/day to  $15.7 \times 10^{-3}$  m/day and from  $2.66 \times 10^{-3}$  m/day to  $18.95 \times 10^{-3}$  m/day when the depth was increased respectively.

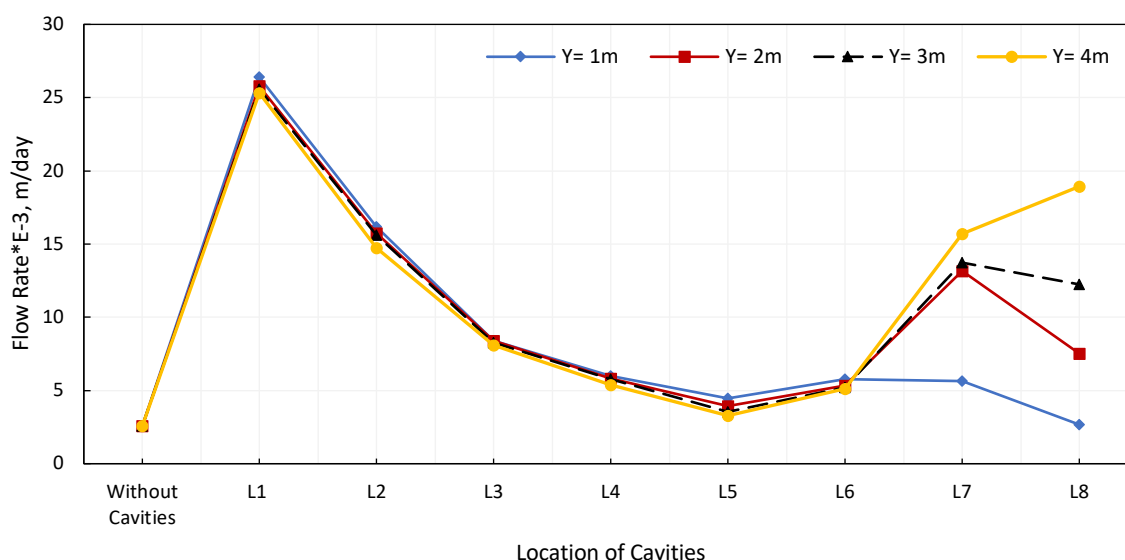


Figure 5.8: Flow rate vs location of a circular cavity at various depths beneath downstream using the HS and MC models

## 5.4 Impact of cavity shape

Most research works carried out in various geotechnical engineering fields has paid great attention to studying the effect of circular cavities. The present study involves an attempt to assess the influence of the existence of irregular cavities as well as circular cavities on the flow rate through earth dams while considering the impact of the cavity's position and depth. Similar to the previous analyses, models with an irregular cavity of 60cm diameter were adopted. The horizontal position of each cavity is as detailed previously in Table 5.1. The depth values of the cavities considered were  $Y=1\text{m}$ ,  $2\text{m}$ ,  $3\text{m}$  and  $4\text{m}$ .

### 5.4.1 Modelling of an earth dam using the MC model

Figure 5.9 and Table 5.4 show a comparison between the effect on flow rate of an irregular cavity and a circular cavity, each situated under the upstream slope. It is clear that the existence of an irregular cavity in the upstream subsoil increases the flow rate greatly, as the flow rate rose from  $2.571 \times 10^{-3}\text{m/day}$  to  $482 \times 10^{-3}\text{m/day}$  for models without a cavity and with a cavity situated at location L2 (-8, -1). It was found that this impact reduces gradually as the cavity's position approaches from the end of the embankment towards location L8 (-40, 0), where the flow rate reaches the lowest value of  $3.286 \times 10^{-3}\text{m/day}$ . Conversely, it is obvious that the flow rates obtained for irregular-cavity models were close to those obtained for circular-cavity models, regardless of where the cavity exists, vertically and horizontally,

below the upstream side. Overall, the flow rates for the irregular-cavity models were greater than those for the circular-cavity models. However, the opposite behaviour was found for models with a cavity locations L7 and L8. For example, the flow rates were  $459.8 \times 10^{-3}$  m/day and  $527.5 \times 10^{-3}$  m/day for circular-cavity models with cavity locations (-8, -1) and (-8, -4), respectively, compared to  $482 \times 10^{-3}$  m/day and  $554 \times 10^{-3}$  m/day, respectively, for irregular-cavity models with the same cavity locations. The flow rates were equal to  $2.81 \times 10^{-3}$  m/day and  $4.16 \times 10^{-3}$  m/day for circular-cavity models, as opposed to  $3.286 \times 10^{-3}$  m/day and  $4.594 \times 10^{-3}$  m/day for irregular-cavity models with a cavity location (-40, -1) and (-40, -4) respectively.

Table 5.4: Comparison between the impact of the presence of a circular cavity and an irregular cavity on flow rate

Cavity location	Cavity Position (X), m	Flow rate $\times$ E-3, m/day, Upstream slope							
		Cavity depth, m							
		Y= 1m		Y= 2m		Y= 3m		Y= 4m	
		Circular	Irregular	Circular	Irregular	Circular	Irregular	Circular	Irregular
Without cavities		2.571							
L1	0	27.72	29.63	26.36	27.88	26.27	27.69	25.20	27.2
L2	-8	459.8	482.0	721.2	764.0	529.2	658.0	527.5	554.0
L3	-17	15.47	16.98	14.74	17.72	16.49	18.76	19.13	19.43
L4	-20	13.11	15.89	14.60	16.86	15.15	16.89	16.22	18.39
L5	-24	11.90	13.26	11.28	14.23	14.19	15.14	14.31	14.85
L6	-28	9.240	10.60	10.14	10.83	10.32	13.90	11.17	13.54
L7	-35	4.830	6.404	5.140	6.630	6.130	6.800	6.170	7.383
L8	-40	2.810	3.286	3.060	3.732	3.710	4.089	4.160	4.594
Flow rate $\times$ E-3, m/day, Downstream slope									
L1	0	27.72	29.63	26.36	27.88	26.27	27.69	25.20	26.20
L2	+8	16.50	19.56	15.35	16.93	15.27	16.79	15.20	16.28
L3	+17	8.482	9.851	8.829	9.954	8.798	9.647	8.622	8.250
L4	+20	6.120	6.679	6.241	6.850	6.510	6.343	6.282	6.234
L5	+24	3.432	3.94	3.515	4.195	3.629	4.356	3.605	4.363
L6	+28	8.913	8.88	5.550	6.018	5.290	5.563	5.056	5.465
L7	+35	5.478	7.124	11.77	13.81	13.76	17.15	15.58	16.36
L8	+40	2.650	2.665	7.435	8.815	12.18	14.93	18.88	20.16

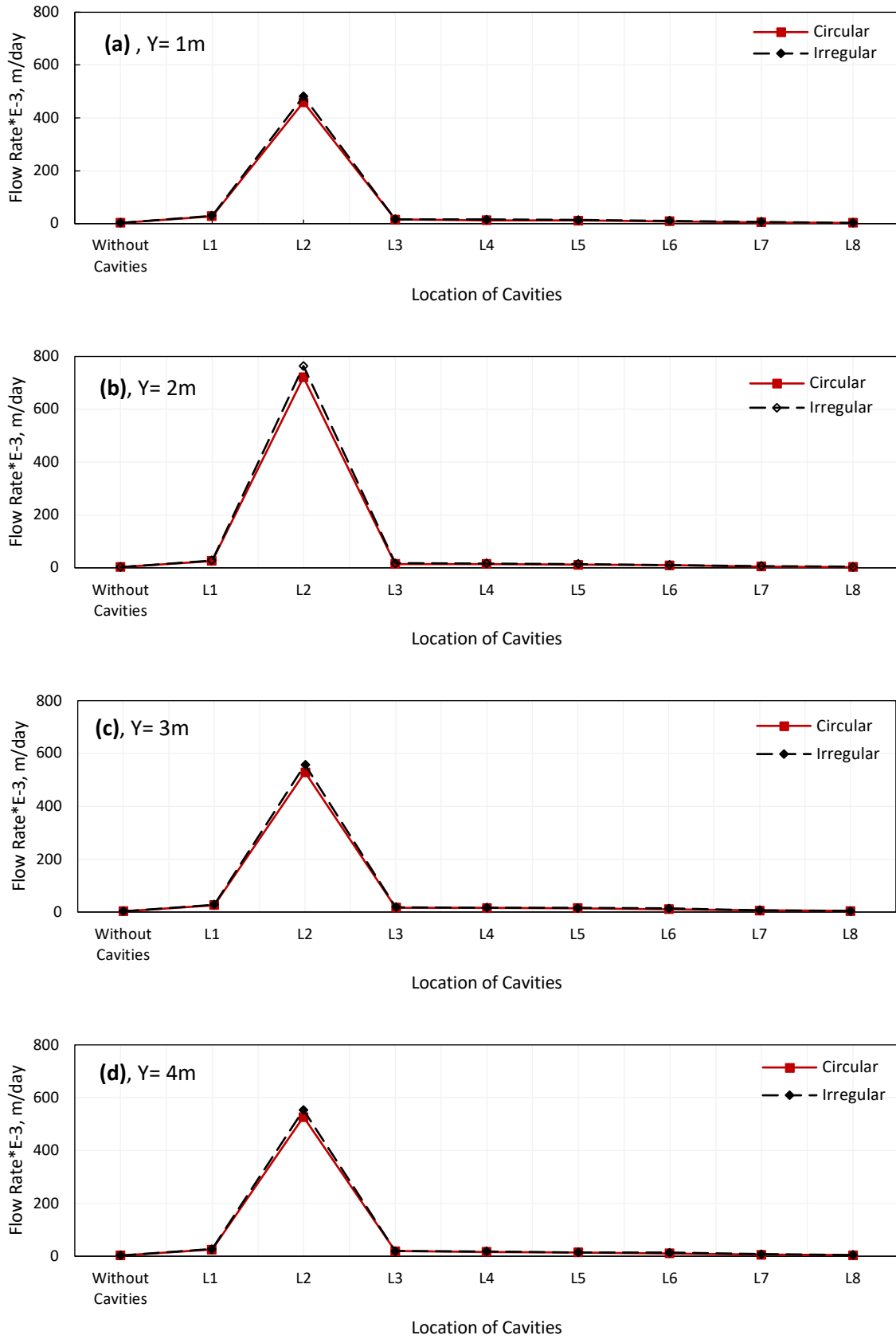


Figure 5.9: Comparison between the impact of a circular cavity and an irregular cavity under upstream on the flow rate using the MC model for depths (Y=1m to Y=4m)

Figure 5.10 and Table 5.4 show a comparison between the effect on flow rate of an irregular cavity and a circular cavity, each situated under the downstream slope. It is clear that the existence of an irregular cavity led to an increase in the flow rate. The flow rates decreased gradually as the distance between the dam centreline and the cavity centreline increased. This increase ranged from  $2.571 \times 10^{-3} \text{m/day}$  to  $29.63 \times 10^{-3} \text{m/day}$  and  $2.665 \times 10^{-3} \text{m/day}$  for models without a cavity and with cavity locations L1 (0, -1) and L8 (40, -1), respectively. Like the upstream side, the flow rates obtained from irregular-and circular-cavity models were close to each other generally. The flow rates for irregular cavity models were somewhat greater than those for circular cavity models when the cavity depth was increased to 4m and, wherever a cavity was created horizontally. For example, the flow rate was  $16.5 \times 10^{-3} \text{m/day}$  for a circular-cavity model with cavity location (8, -1), compared to  $19.56 \times 10^{-3} \text{m/day}$  for an irregular-cavity model with the same cavity location; however, it was  $15.2 \times 10^{-3} \text{m/day}$  for a circular-cavity model with cavity location (8, -4), compared to  $16.28 \times 10^{-3} \text{m/day}$  for an irregular-cavity model with the same cavity location.

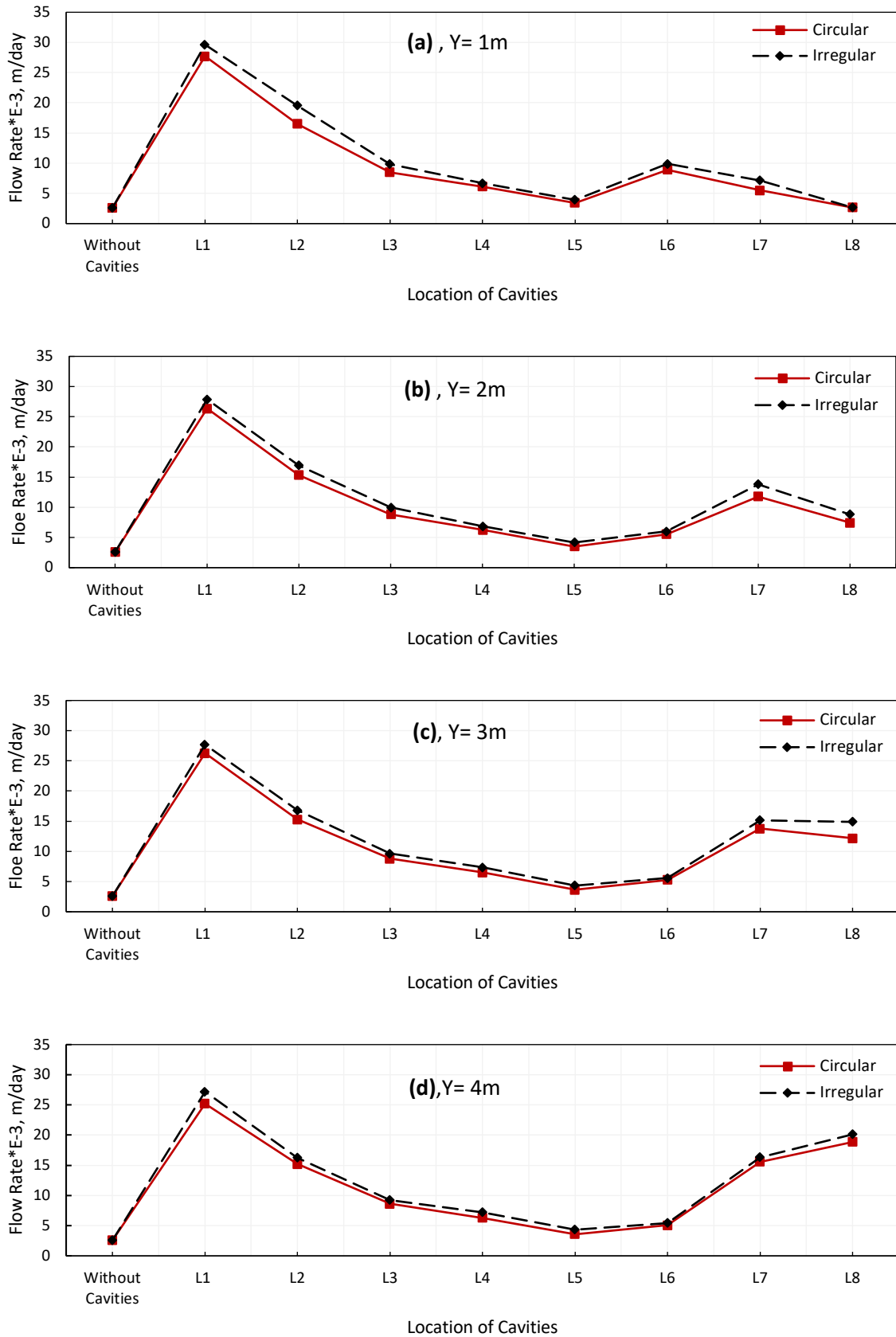


Figure 5.10: Comparison between the impact of a circular cavity and an irregular cavity under downstream on the flow rate using the MC model for depths ( $Y=1\text{m}$  to  $Y=4\text{m}$ )

### 5.4.2 Modelling of an earth dam using the HS and MC models

Figure 5.11 and Table 5.5 illustrate a comparison between the effect on the flux rate through an earth dam of the existence of an irregular cavity and the existence of a circular cavity, each situated under the upstream side. Similar to the results of the simulation in subsection 5.4.1, the flow rate increases considerably owing to the existence of an irregular cavity at location L2 (-8, -1), as it rose from  $2.58 \times 10^{-3} \text{m/day}$  to  $492.4 \times 10^{-3} \text{m/day}$  for models without a cavity and with a cavity, respectively. The results also show that the flow rates reduced when the cavity moved away from the centreline of the dam towards its end (to position  $X = -40\text{m}$ ). The flow rates were equal to  $17.95 \times 10^{-3} \text{m/day}$  and  $3.532 \times 10^{-3} \text{m/day}$  for models with cavity locations L3 (-17, -1) and L8 (-40, -1). According to the results, it can be concluded that the existence of a cavity beneath the upstream side, whether circular or irregular, has a similar effect on the flow rate of water passing through dams. It is clear that the flow-rate values for irregular-cavity models were somewhat bigger than those values for circular-cavity models. This behaviour has been observed wherever the cavities exist below the upstream, regardless of their horizontal or vertical position. For example, for locations (-8, -1) and (-8, -2), the flow rates amounted to  $459.2 \times 10^{-3} \text{m/day}$  and  $720.5 \times 10^{-3} \text{m/day}$  for circular-cavity models, compared to values of  $492.4 \times 10^{-3} \text{m/day}$  and  $779.9 \times 10^{-3} \text{m/day}$  for irregular-cavity models, respectively. However, for locations (-40, -2) and (-40, -4), the flow rates were equal to  $3.57 \times 10^{-3} \text{m/day}$  and  $4.606 \times 10^{-3} \text{m/day}$  for circular-cavity models, as opposed to  $3.7 \times 10^{-3} \text{m/day}$  and  $4.713 \times 10^{-3} \text{m/day}$  for irregular-cavity models respectively. Refer to Table 5.5 for the details of cavity locations and the corresponding flow-rate values.



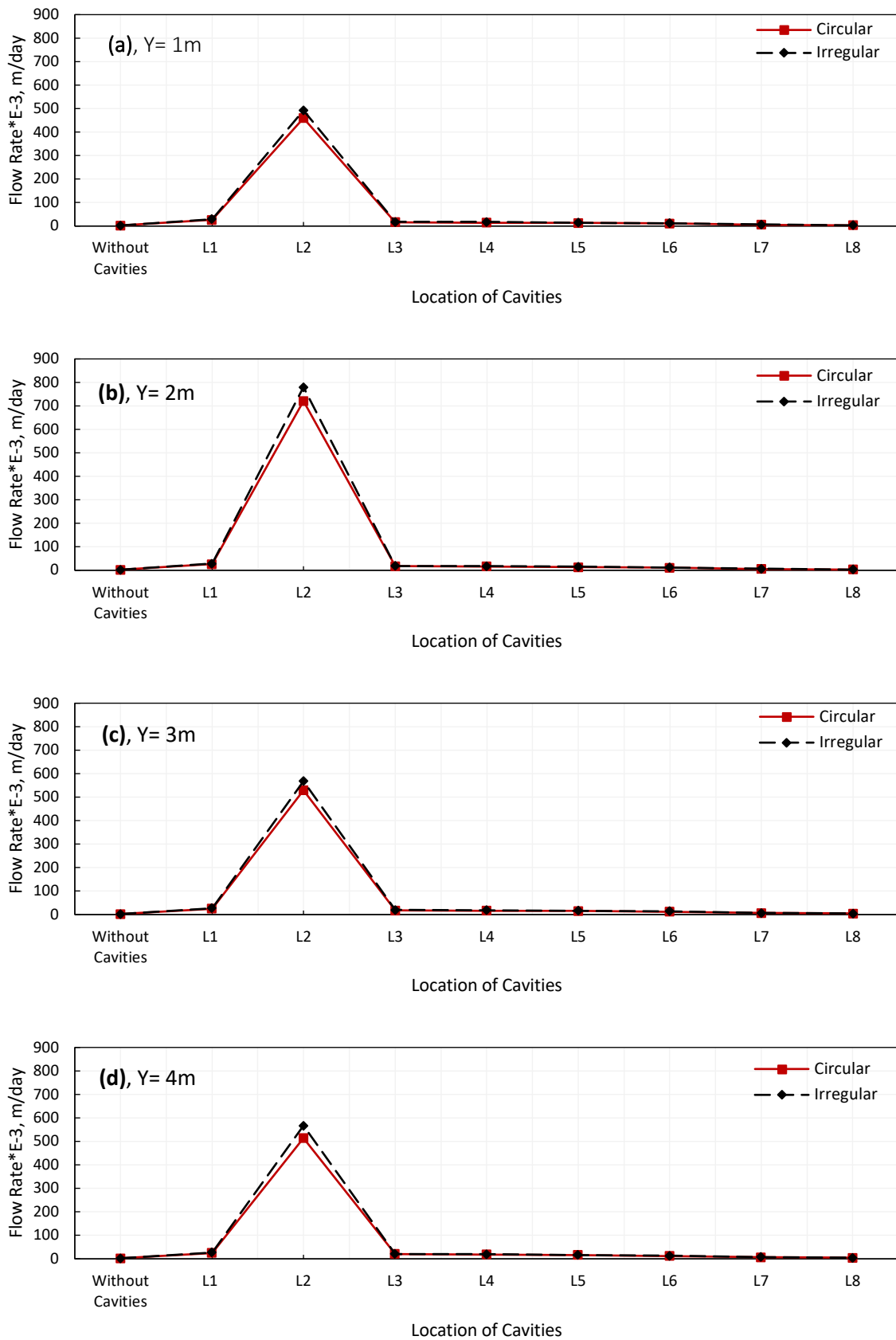


Figure 5.11: Comparison between the impact of a circular cavity and an irregular cavity under upstream on the flow rate using the HS and MC models for depths (Y=1m to Y=4m)

Table 5.5: Comparison between the impact of the presence of a circular cavity and an irregular cavity on flow rate

Cavity location	Cavity Position (X), m	Flow rate $\times$ E-3, m/day, Upstream slope							
		Cavity depth, m							
		Y= 1m		Y= 2m		Y= 3m		Y= 4m	
		Circular	Irregular	Circular	Irregular	Circular	Irregular	Circular	Irregular
Without cavities		2.58							
L1	0	26.40	28.92	25.78	28.25	25.58	27.47	25.32	27.30
L2	-8	459.2	492.4	720.5	779.9	529.0	567.8	514.0	567.0
L3	-17	16.91	17.95	17.05	19.04	17.87	20.00	20.51	20.50
L4	-20	14.37	17.40	16.55	17.92	16.84	18.31	18.35	19.85
L5	-24	13.28	14.55	13.62	15.61	15.84	16.31	15.87	15.96
L6	-28	11.09	11.96	11.48	12.52	12.19	13.90	12.57	13.54
L7	-35	5.540	6.404	5.740	6.503	6.570	6.900	6.348	7.939
L8	-40	3.050	3.532	3.570	3.700	3.970	4.412	4.606	4.713
Flow rate $\times$ E-3, m/day, Downstream slope									
L1	0	26.40	29.92	25.78	28.25	25.58	28.17	25.32	27.30
L2	+8	16.19	19.84	15.76	17.39	15.59	17.16	14.75	16.18
L3	+17	8.410	9.951	8.386	9.526	8.251	9.191	8.104	8.670
L4	+20	5.980	6.870	5.810	7.340	5.770	7.250	5.390	6.893
L5	+24	4.440	3.855	3.930	4.523	3.550	4.324	3.290	4.190
L6	+28	3.760	9.01	5.320	6.265	5.215	5.514	5.120	5.493
L7	+35	5.645	7.197	13.15	13.89	13.73	18.13	15.70	16.98
L8	+40	2.660	2.65	7.520	8.896	12.26	14.98	18.95	20.19

Figure 5.12 and Table 5.5 indicate the combined effects on seepage through the earth dam of the presence of an irregular cavity and a circular cavity, each positioned beneath the downstream side. It can be observed that the existence of a circular cavity notably increases the flow rate. The flow rate increased from  $2.58 \times 10^{-3}$  m/day for a cavity-free model to the highest value  $29.92 \times 10^{-3}$  m/day for a model with a cavity at L1(0, -2). Furthermore, the flow rates reduced gradually to  $2.65 \times 10^{-3}$  m/day when the position of the cavity was moved away from the centre of the dam towards location L8. Similar to the results presented previously, it can be noticed that the presence of a circular cavity and an irregular cavity impact the flow rate in the same way. Overall, the flow-rate values obtained using circular- and irregular-cavity models for all assumed locations are close to each other. For example, for location L3 (17, -1), the flow rate was  $8.410 \times 10^{-3}$  m/day for a circular-cavity model, compared to

$9.951 \times 10^{-3}$  m/day for an irregular-cavity model, while, for location L5 (24, -3), it was of  $3.550 \times 10^{-3}$  m/day for a circular-cavity model, compared to  $4.324 \times 10^{-3}$  m/day for an irregular-cavity model.

The results obtained indicate that the presence of a circular cavity and an irregular cavity have an approximately similar impact on the flow rate through the earth dams. However, modelling an irregular cavity with PLAXIS 2D takes longer than modelling a circular cavity; thus, a circular cavity is easier to use in applications. Consequently, all analyses in the following sections were conducted using a circular-cavity model.

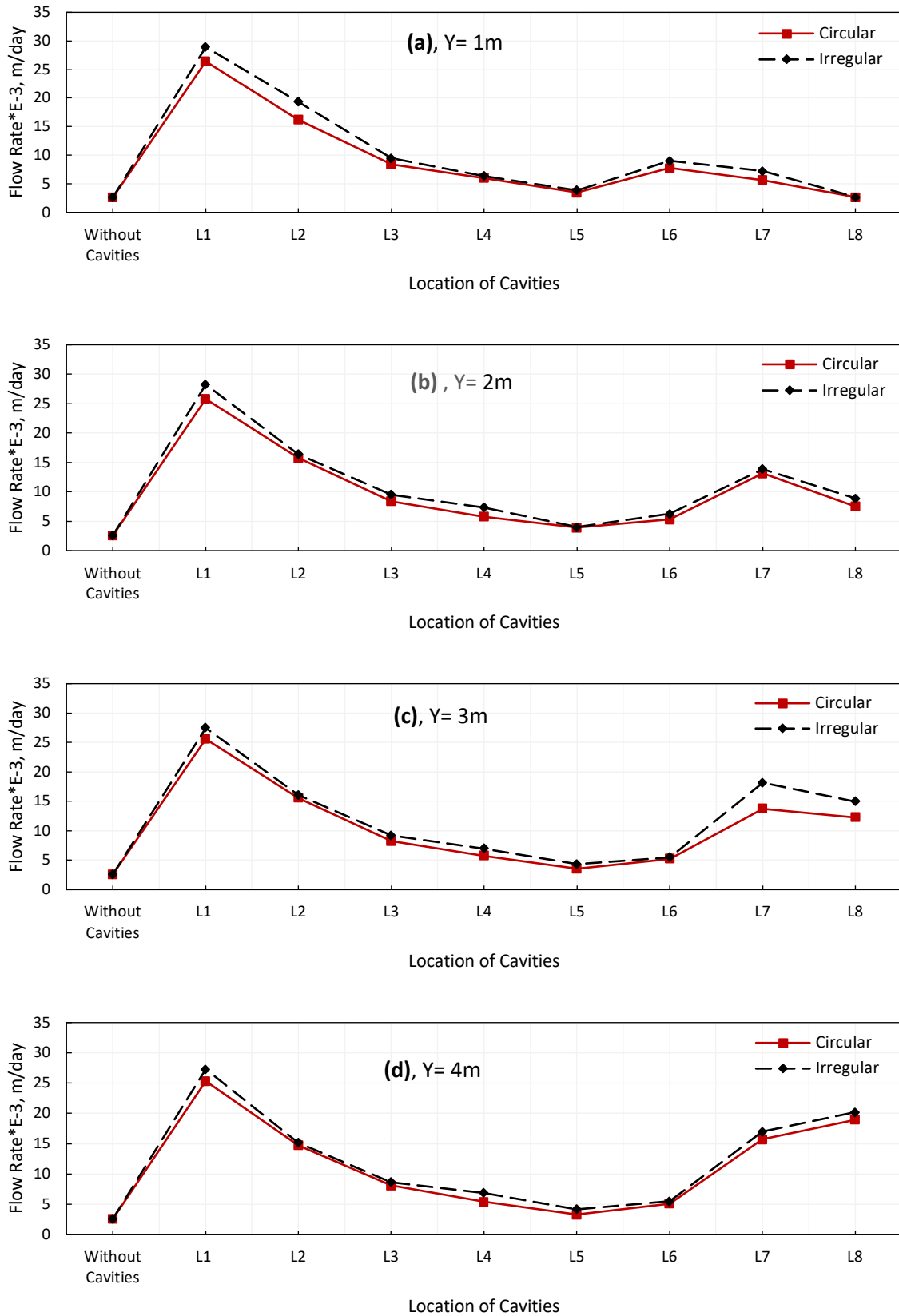


Figure 5.12: Comparison between the impact of a circular cavity and an irregular cavity under downstream on the flow rate using the HS and MC models for depths (Y=1m to Y=4m)

## 5.5 Impact of the number of cavities

This section discusses the effect of the number of cavities on the flow rate. All analyses were performed using PLAXIS 2D models with circular cavities of 60cm diameter and that were created at different locations varying vertically and horizontally. The positions of most cavities were selected based on the findings of the location-effect analysis mentioned in section 4.4.

### 5.5.1 Impact of the existence of dual cavities

The influence of the presence of dual cavities was examined, using cavities that were situated at different horizontal positions and depths. An example of the arrangement of the cavities for models with two cavities situated at the same depth are displayed in Figure 4.34.

#### 5.5.1.1 Modelling of an earth dam using the MC model

The effects on seepage of the existence of two cavities, with respect to the horizontal and vertical variation in cavity location, were evaluated. Cavities were created at various locations, as listed in Table 5.6.

Figure 5.13 demonstrates the flow-rate values versus the location of cavities for models containing two cavities situated at a depth of 1m. It is apparent that increasing the number of cavities led to a big increase of about 54.1% in the flow rate. The maximum value of the flow rate amounted to  $459.8 \times 10^{-3} \text{m/day}$  for a single-cavity model, compared to  $708.7 \times 10^{-3} \text{m/day}$  for a dual-cavity model. It should be mentioned that the flow rate increases considerably when one of the two cavities exists at a critical position (for which the recorded SF values are less than the required limit) under the upstream slope, such as in locations L1, L3, L5 and L8. For example, the flow rates were  $502.7 \times 10^{-3} \text{m/day}$  and  $708.7 \times 10^{-3} \text{m/day}$  for cavity models with cavity locations L1 and L3, However, the flow rates amounted to  $5.81 \times 10^{-3} \text{m/day}$  and  $29.63 \times 10^{-3} \text{m/day}$  for models with cavity locations L2 and L7.

Table 5.6: The coordinates of cavities' locations in X and Y directions for dual-cavity models

Cavity location	Cavity depth, m	The coordinates of positions in X-axis, m	
		Cavity 1	Cavity 2
L1	1	-8	0
L2	1	0	+35
L3	1	-8	-24
L4	1	-24	0
L5	1	-8	+35
L6	1	-24	+35
L7	1	+35	+40
L8	1	-8	+40
L9	1	-24	+40
L10	1	0	+40

(-): Indicates that the cavity is under upstream, (+): indicates that the cavity is under downstream

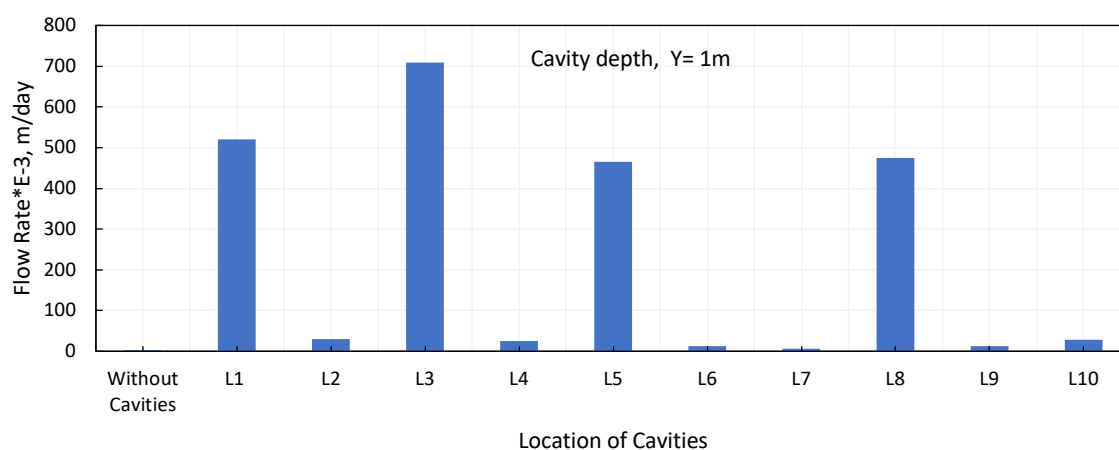


Figure 5.13: Flow rate vs location of cavities for models with dual cavities situated at a depth of 1m using the MC model

Figure 5.14 shows the influence of the depth of the two cavities on the seepage through the earth dams. The coordinates of the cavities' locations and corresponding flow-rate values are illustrated in Table 5.7. It should be noted that, by increasing the depth of the cavities from 1m to 3m, the flow-rate values were increased for models with cavities situated at locations L2, L6, L7, L9 and L10. For example, the flow rate increased from  $29.63 \times 10^{-3} \text{m/day}$  to  $30.63 \times 10^{-3} \text{m/day}$  for models with cavities at location L2. However, the flow rate increased as the depth increased to 2m, and then decreased at a depth of 3m for locations L1, L3, L5 and L8. For example, the flow rate increased from  $520.7 \times 10^{-3} \text{m/day}$  to  $750.2 \times 10^{-3} \text{m/day}$  and then

reduced to  $600.6 \times 10^{-3}$  m/day for models with cavities at location L1. It can be concluded that the varying the position of the cavity in the vertical direction has little influence, even when the number of cavities is increased.

Table 5.7: The input and output data showing the effect of presence of two cavities on flow rate

Location of cavity	The coordinates of locations in X-axis (m)		Flow rate $\times E-3$ , m/day		
	Cavity 1	Cavity 2	Depth of cavity		
			Y= 1m	Y= 2m	Y= 3m
Without cavities			2.571		
L1	-8	0	520.7	750.2	600.6
L2	0	+35	29.63	29.89	30.63
L3	-8	-24	708.7	728.3	567.0
L4	-24	0	25.64	24.41	24.35
L5	-8	+35	464.8	728.0	533.7
L6	-24	+35	12.51	15.62	22.46
L7	+35	+40	5.801	10.93	12.99
L8	-8	+40	474.2	724.5	538.0
L9	-24	+40	12.90	13.51	16.94
L10	0	+40	27.90	28.18	28.61

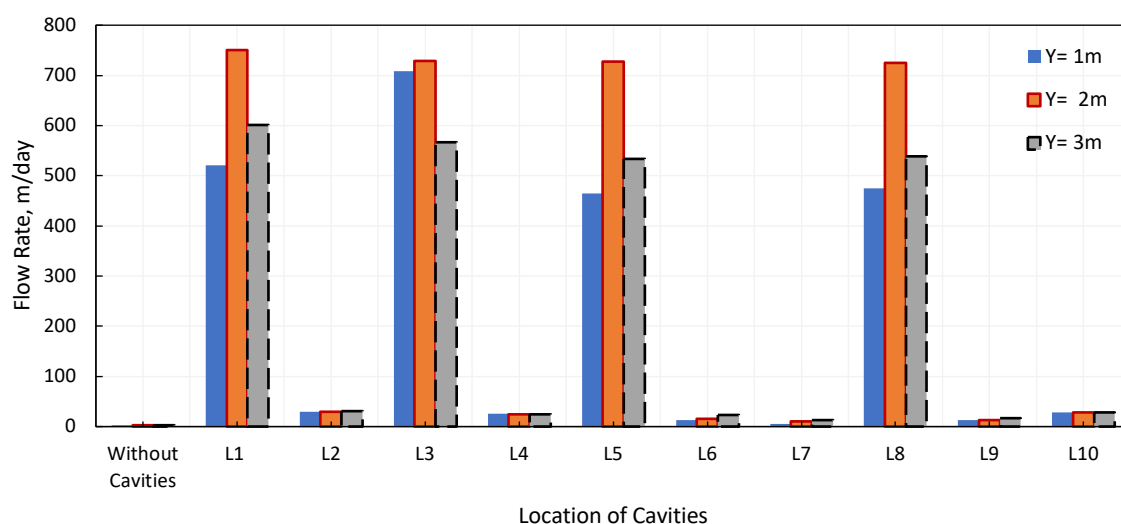


Figure 5.14: Flow rate vs location of cavities for models with dual cavities at various depths using the MC model

### 5.5.1.2 Modelling of an earth dam using the HS and MC models

Analyses were executed to consider the impact of the existence of two cavities on flow rate, as depicted previously in section 5.5. The coordinates of the locations of the cavities are as described previously in Table 5.6.

The impact on the flow rate of the existence of two cavities positioned at a depth of 1m is explained in Figure 5.15. The findings indicate that the existence of two cavities caused an increase in flow rate of about 49%, compared to flow rate for the existence of a single cavity. The maximum flow-rate value was equal to  $684.1 \times 10^{-3} \text{m/day}$  for a model with two cavities at location L3, while it was equal to  $459.2 \times 10^{-3} \text{m/day}$  for a model with a single cavity at L2 (-8, -1). The seepage analysis reveals that the flow rates increase considerably in the case of where one or two cavities exist beneath the upstream side. This is clear at locations L1, L3, L5 and L8, where the flow rates of these locations were  $520.9 \times 10^{-3} \text{m/day}$ ,  $684.1 \times 10^{-3} \text{m/day}$ ,  $564 \times 10^{-3} \text{m/day}$  and  $564.6 \times 10^{-3} \text{m/day}$ , respectively, compared to other locations. For example, the flow rate was  $10.5 \times 10^{-3} \text{m/day}$  for a model with cavity location L7. Refer to Table 5.6 for details of the horizontal positions. The huge variation in the flow-rate values of the models studied confirms that seepage through earth dams is affected greatly by the cavities' horizontal position in the subsoil.

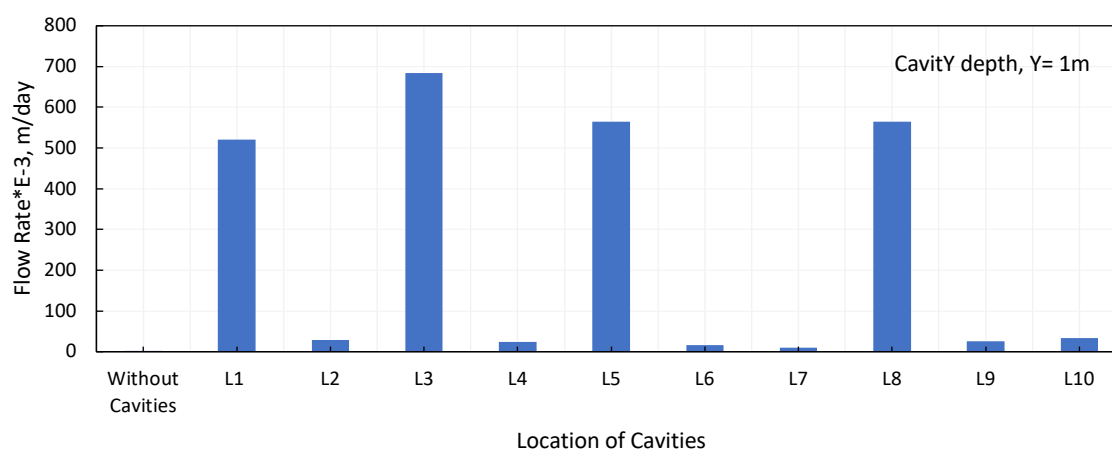


Figure 5.15: Flow rate vs location of cavities for models with dual cavities at a depth of 1m using the HS and MC models

The flow rate values versus the location of cavities for models with dual cavities for various depths are as revealed in Figure 5.16. The locations of cavities and corresponding flow-rate values are presented in Table 5.8 It should be noted that increasing the depth of the two cavities led to an increase or decrease in flow rates depending on the horizontal position of



the cavities in the subsoil. For example, the flow rate increased by 2.7 % and 26.4 % when the cavities' depth was increased from 1m to 3m for models with cavity locations L2 and L7, respectively; however, it decreased by 1.8% for models with cavity location L4. It is also observed that, by increasing the depth to 2m, the flow rates increased and thereafter dropped as the depth increased to 3m for models with cavity locations L1, L3, L4, L5 and L8. For example, the flow rates increased from  $520.9 \times 10^{-3} \text{m/day}$  to  $796.4 \times 10^{-3} \text{m/day}$ , which is equivalent to 52.8 % at a depth of 2m and then reduced to  $599.6 \times 10^{-3} \text{m/day}$ , which is equivalent to 24.7 % at a depth of 3m for a model with cavity location L1.

Table 5.8: The input and output data showing the effect of presence of two cavities on flow rate

Location of cavity	The coordinates of locations in X-axis, (m)		Flow rate $\times E-3$ , m/day		
	Cavity 1	Cavity 2	Depth of cavity		
			Y1= 1m	Y= 2m	Y= 3m
	Without cavities		2.58		
L1	-8	0	520.9	796.4	599.6
L2	0	-35	28.76	29.01	29.55
L3	-8	-24	684.1	726.8	563.2
L4	-24	0	24.13	23.73	23.69
L5	-8	+35	564.0	722.4	537.1
L6	-24	+35	15.35	15.82	22.63
L7	+35	+40	10.50	11.08	13.28
L8	-8	+40	564.6	723.9	538.3
L9	-24	+40	25.76	12.61	11.51
L10	0	+40	33.42	28.55	27.96

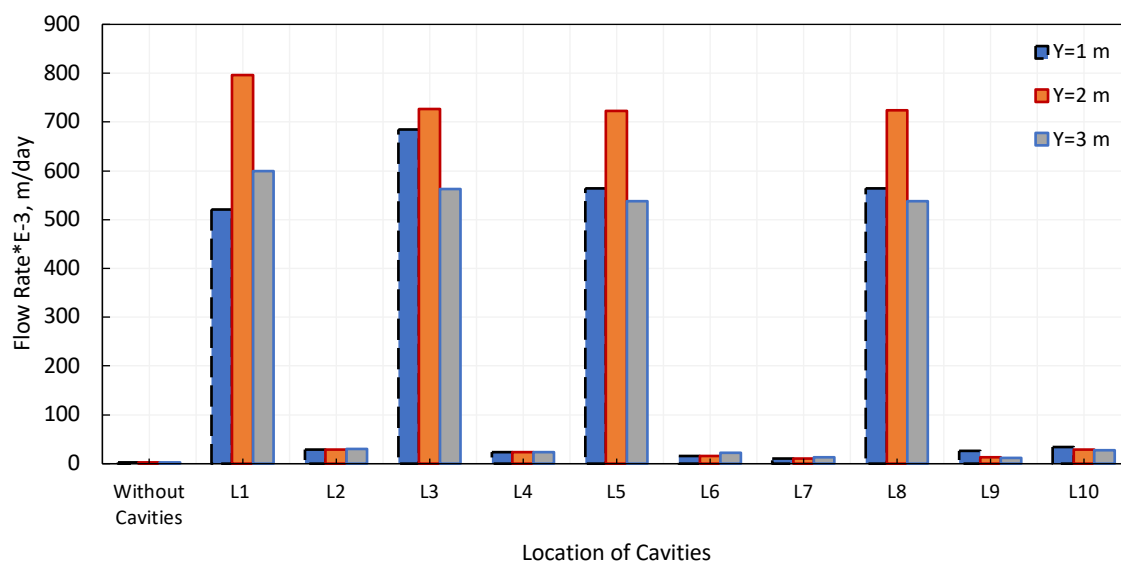


Figure 5.16: Flow rate vs location of cavities for models with dual cavities at various depths using the HS and MC models

## 5.5.2 Impact of the existence of three cavities

The effect of the existence of three cavities on the flow rate is evaluated in this section. Various locations of cavities, in both directions, were considered. Models with circular cavities of 60cm diameter were used.

### 5.5.2.1 Modelling of an earth dam using the MC model

All studied earth-dam models in this analysis were modelled using MC models. Figure 5.17 shows the effect of three cavities on the seepage for models with cavities situated at a depth of 1m. Table 5.9 displays the horizontal and vertical coordinates of the cavities' locations. It seems that by increasing the number of cavities to three cavities, the flow rate was increased. The flow rate increased to  $734.2 \times 10^{-3} \text{m/day}$ , which is equivalent to 59.6% for a model with three cavities at location L2, compared to  $459.8 \times 10^{-3} \text{m/day}$  for a model with a single cavity. It appears that the increasing in the flow rate for a model that contains three cavities is relatively small compared to a model which contains two cavities; the flow rate increased from  $708.7 \times 10^{-3} \text{m/day}$  to  $734.2 \times 10^{-3} \text{m/day}$ , which is equivalent to 3.6%, for models with two and three cavities, respectively. It should be noticed that the highest flow rates were obtained from the models with cavities located at the influential positions, such as ( $X = -8$ ). This implies that the horizontal position of the cavity is the most influential parameter among all the parameters examined with respect to the flow rate. In general, for other locations, the

flow rates ranged from  $11.40 \times 10^{-3} \text{m/day}$  to  $647.2 \times 10^{-3} \text{m/day}$  for models with cavities situated at locations L10 and L1, respectively (see Table 5.9 for details of the horizontal positions).

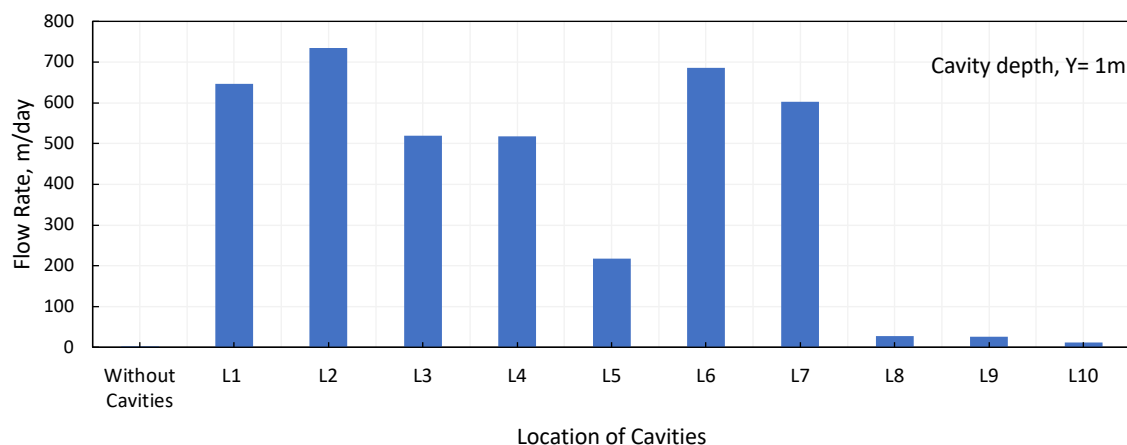


Figure 5.17: Flow rate vs location of cavities for models with three cavities at a depth of 1m using the MC model

Table 5.9: The coordinates of cavities locations in X and Y directions for triple-cavity model

Cavity location	Cavity depth, m	The coordinates of positions in X-axis, m		
		Cavity 1	Cavity 2	Cavity 3
L1	1	-8	0	+35
L2	1	-8	-24	0
L3	1	-8	-24	+35
L4	1	-8	35	+40
L5	1	0	35	+40
L6	1	-8	-24	+40
L7	1	-8	0	+40
L8	1	-24	0	+35
L9	1	-24	0	+40
L10	1	-24	+35	+40

The impact of the depth of the three cavities on the flow rate through earth dam is demonstrated in Figure 5.18. The assumed depths of the cavities are 1m, 2m and 3m. The three cavities were created at the same depth within the same model. Table 5.10 presents the detail of the cavities' locations and the corresponding flow-rate values. It should be noted

that, by increasing the depth of the three cavities from 1m to 3m, the flow rates were increased for models with cavities sited at locations L5, L7 and L10. For example, the flow rate increased from  $217.14 \times 10^{-3} \text{m/day}$  to  $307.1 \times 10^{-3} \text{m/day}$  as the depth increased from 1m to 3m for a model with cavities at L5. However, the flow decreased from  $27.57 \times 10^{-3} \text{m/day}$  to  $27.24 \times 10^{-3} \text{m/day}$  when the depth of the cavities was increased for models with cavities at location L8. Conversely, it appears that, in some instances, the flow rates increase when the depth is increased to 2m, and, afterwards, the flow rates decrease as the depth is increased to 3m. This behaviour was noticed for models with cavities at locations L1, L2, L3, L4, L6 and L8. As mentioned previously, this simulation proves that the depth of cavities somewhat impacts the flow rate, which increases or decreases slightly when the depth of the cavities is increased, in general.

Table 5.10: The input and output data showing the effect of presence of three cavities on flow rate

Cavity location	The coordinates of positions in X-axis, m			Flow rate $\times E-3$ , m/day		
				Cavity depth, m		
	Cavity 1	Cavity 2	Cavity 3	Y= 1m	Y= 2m	Y= 3m
	Without cavities				2.571	
L1	-8	0	+35	647.2	787.4	673.7
L2	-8	-24	0	734.2	765.4	604.7
L3	-8	-24	+35	518.7	747.4	664.7
L4	-8	35	+40	517.5	735.4	636.7
L5	0	35	+40	217.1	279.2	307.1
L6	-8	-24	+40	685.6	760.0	564.2
L7	-8	0	+40	603.0	767.1	794.6
L8	-24	0	+35	27.57	27.68	27.24
L9	-24	0	+40	26.43	25.99	24.53
L10	-24	+35	+40	11.40	13.96	15.92

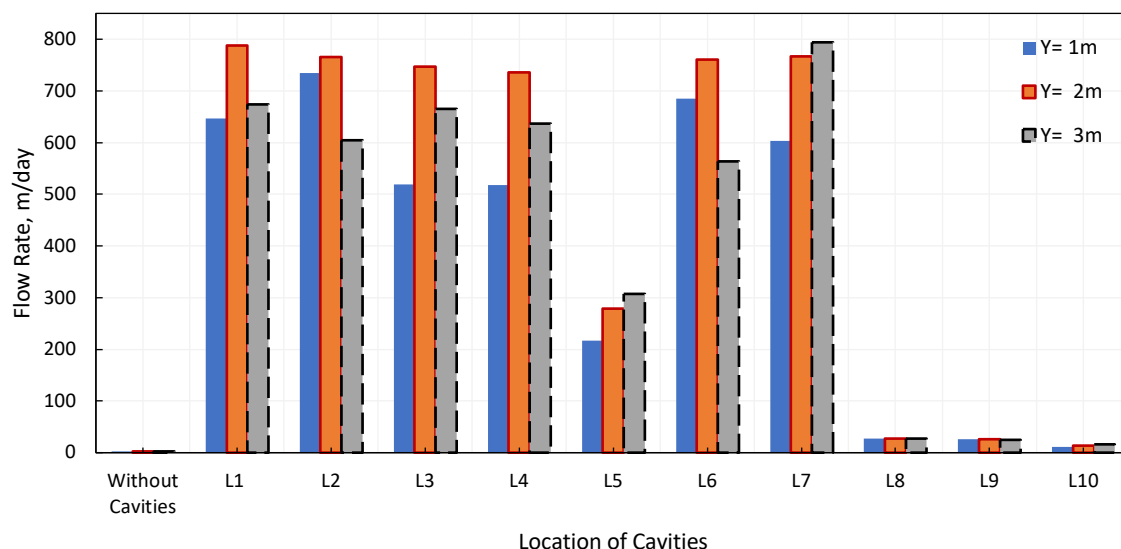


Figure 5.18: Flow rate vs location of cavities for models with three cavities at various depths using the MC model

### 5.5.2.2 Modelling of an earth dam using the HS and MC models

Figure 5.19 reveals the effect on seepage of the presence of three cavities situated below the dam base at a depth of 1m. The coordinates of cavities' locations are listed in Table 5.9. As mentioned in the previous section, the results indicate that increasing the flow rate does not depend only on increasing the number of cavities, but it depends significantly on their location in the X direction beneath the upstream slope. For instance, the flow rate was  $647.1 \times 10^{-3} \text{m/day}$  for a model with cavities at location L1, compared to  $14.73 \times 10^{-3} \text{m/day}$  for a model with cavities at location L10. Refer to Table 5.9 for details of the horizontal positions. In addition, the maximum value of the flow rate was  $735.1 \times 10^{-3} \text{m/day}$  for a triple-cavity model compared to  $459.2 \times 10^{-3} \text{m/day}$  for a single-cavity model. The percentage of increase in flow rate due to the existence of three cavities amounted to about 60%.

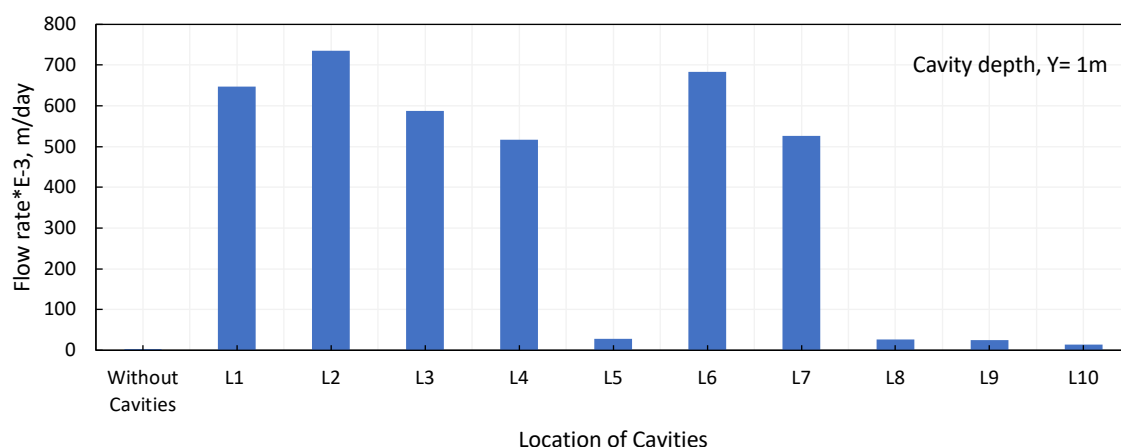


Figure 5.19: Flow rate vs location of cavities for models with three cavities at a depth of 1m using the HS and MC models

Figure 5.20 and Table 5.11 show the effect of the depth of the three cavities on the flow rate. It is obvious that increasing the depth of the cavities resulted in fluctuating (increasing or decreasing) flow-rate values for the models studied. The flow rate rose as the depth of cavities was increased from 1m to 2m, then it reduced when the depth was increased to 3m; this is for all models except those with cavities at locations L5, L8 and L10. The flow rates increased when the cavities' depth was increased for models at the aforementioned locations. For example, for location L1, the flow rate went up from  $647.1 \times 10^{-3} \text{m/day}$  to  $786.8 \times 10^{-3} \text{m/day}$  and then dropped to  $572.5 \times 10^{-3} \text{m/day}$  when the depth was increased. However, the flow rate went up from  $28.21 \times 10^{-3} \text{m/day}$  to  $29.78 \times 10^{-3} \text{m/day}$ , which is equivalent to 5.6% when the depth was increased for models with cavities at locations L5. The new results also prove that the cavities' depth has an insignificant effect compared to their horizontal position.

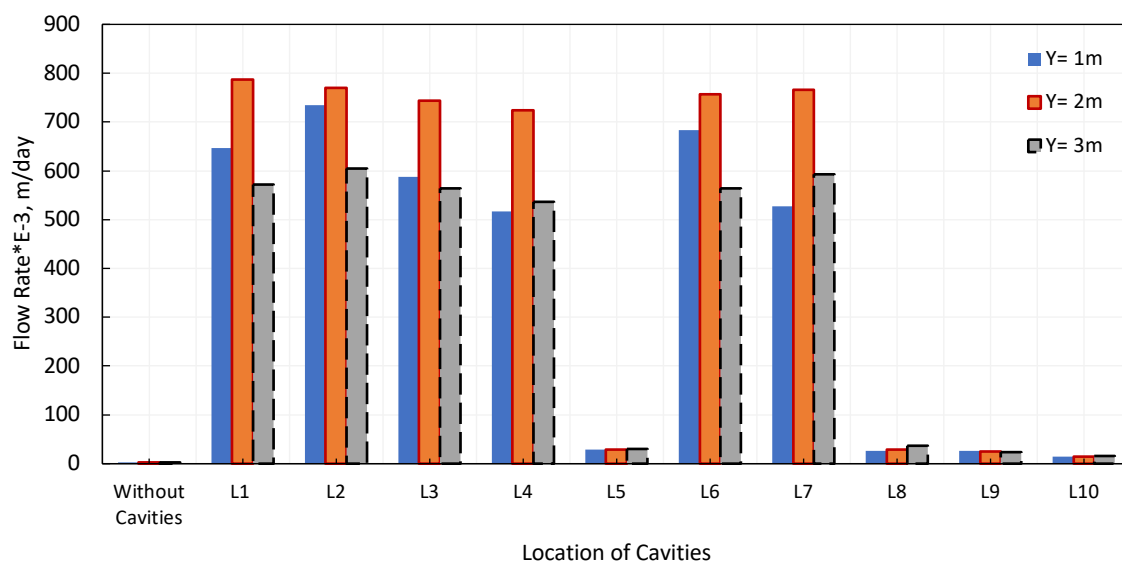


Figure 5.20: Flow rate vs location of cavities for models with three cavities at various depths using the HS and MC models

Table 5.11: The input and output data showing the effect of presence of three cavities on flow rate

Cavity location	The coordinates of positions in X-axis, m			Safety Factor		
	Cavity 1	Cavity 2	Cavity 3	Cavity depth, m		
				Y= 1m	Y= 2m	Y= 3m
Without cavities					2.58	
L1	-8	0	+35	647.1	786.8	572.5
L2	-8	-24	0	735.1	770.2	604.0
L3	-8	-24	+35	587.4	744.0	564.3
L4	-8	35	+40	516.2	724.6	537.0
L5	0	35	+40	28.21	28.32	29.78
L6	-8	-24	+40	683.0	756.7	563.8
L7	-8	0	+40	526.9	766.2	593.4
L8	-24	0	+35	26.54	28.51	36.21
L9	-24	0	+40	25.63	24.30	23.88
L10	-24	+35	+40	14.73	14.16	16.14

## 5.6 Comparative study

A series of finite element simulations were accomplished to assess the impact of the existence of cavities in the subsoil of the upstream and downstream sides.

### 5.6.1 Impact of cavities that are situated at the same depth level

This section discusses a set of comparisons that were done to assess the impact on the flow rate of the cavities existing in the subsoil of the upstream and downstream slopes. All cavities were created at the same depth within the same model, regardless of the number of them and their horizontal positions.

#### 5.6.1.1 Modelling of an earth dam using the MC model

A comparison between the influence on seepage of a single cavity beneath the upstream and downstream slopes was achieved by using the MC model. The cavities' horizontal positions detailed in Table 5.1 were adopted in these analyses. Cavities were generated at four different depths:  $Y = 1\text{m}$ ,  $2\text{m}$ ,  $3\text{m}$  and  $4\text{m}$ .

Figure 5.21 indicates that the presence of cavities under the upstream side has more of an effect on flow rate than their presence under the downstream side. The flow rate increased from  $2.571 \times 10^{-3}\text{m/day}$  to  $721.2 \times 10^{-3}\text{m/day}$  for a cavity-free model and ones with a cavity under the upstream slope at location L2 (-8, -2), respectively; however, it increased to  $15.35 \times 10^{-3}\text{m/day}$  for a model with a cavity situated under the downstream slope at L2 (8, -2). This behaviour was seen in all models, regardless of where the cavities were situated vertically, except for models with cavities at locations L7 and L8, where the flow rates were greater for models containing cavities under the downstream slope at depths  $2\text{m}$ ,  $3\text{m}$  and  $4\text{m}$ . For models with cavities situated at locations L7 (35, -2) and L8 (40, -2), the flow rates were  $5.14 \times 10^{-3}\text{m/day}$  and  $3.06 \times 10^{-3}\text{m/day}$  for the upstream side, respectively, as opposed to  $11.77 \times 10^{-3}\text{m/day}$  and  $7.435 \times 10^{-3}\text{m/day}$  for the downstream side, respectively. Refer to Table 5.2 for details of the locations of cavities and corresponding flow-rate values.



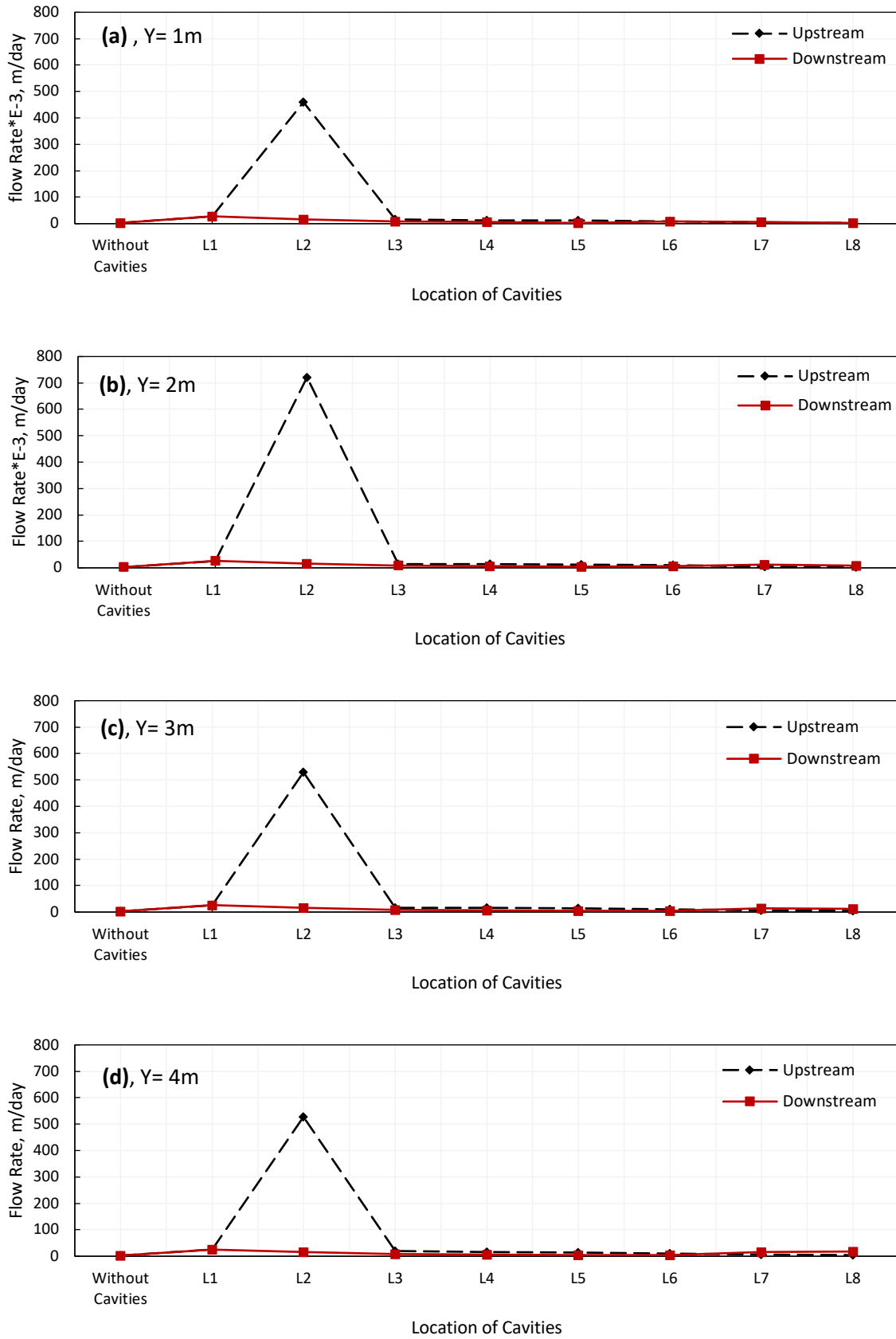


Figure 5.21: Comparison between the effect of the cavity’s presence under upstream and downstream for depths (Y=1m to Y=4m) using the MC model

Figure 5.22 presents a comparison between the influence on the flow rate of two cavities beneath the upstream and downstream slopes. Cavities were created in the horizontal positions and depths listed previously in Table 4.16. The results demonstrate that the existence of one of the cavities in a critical position under the upstream slope greatly affects seepage. For example, the flow rate increased from  $2.571 \times 10^{-3} \text{m/day}$  to ( $708.7 \times 10^{-3} \text{m/day}$  and  $5.801 \times 10^{-3} \text{m/day}$ ) for models without a cavity and with a cavity at locations L2 and L4 under the upstream slope, respectively; however, the flow rates increased to  $23.16 \times 10^{-3} \text{m/day}$  and  $3.756 \times 10^{-3} \text{m/day}$  for the models with a cavity at the aforementioned locations but under the downstream slope, respectively. For locations L3 and L5, it appears that the flow rates are slightly larger for the downstream side than the upstream side. The flow rate is equal to  $31.83 \times 10^{-3} \text{m/day}$  for a model with a cavity sited at location L3 under the downstream slope, compared to  $25.64 \times 10^{-3} \text{m/day}$  for a model with a cavity sited at location L3 under the upstream slope.

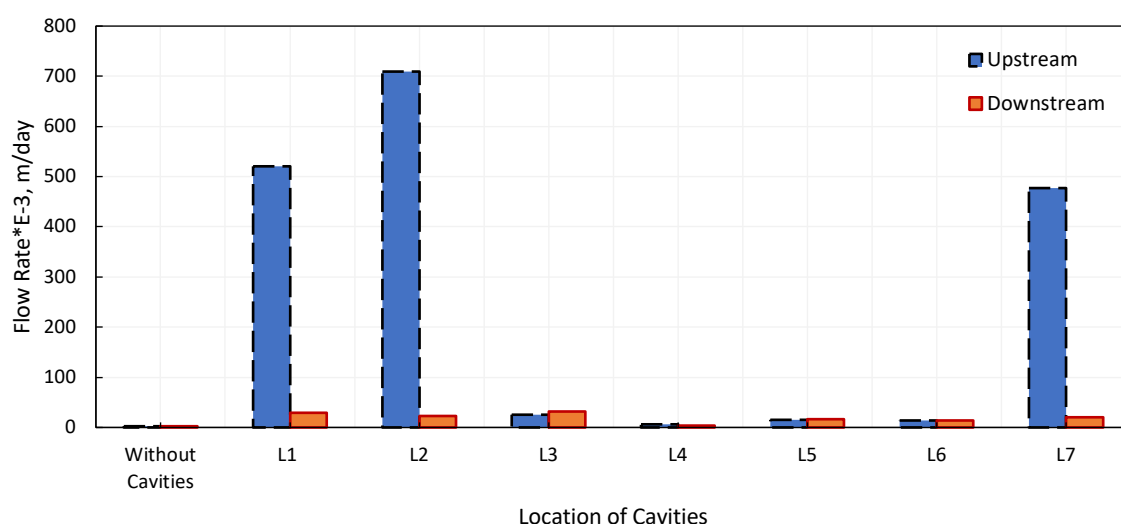


Figure 5.22: Comparison between the effect on flow rate of the presence of two cavities located under upstream and downstream, for different positions and at a depth of 1m using the MC model

A comparison between the effect on flow rate of the existence of three cavities situated beneath upstream and downstream is shown in Figure 5.23. All analyses were carried out considering three cavities situated at a depth of 1m. The cavities' locations in the X direction are presented in Table 4.22. Overall, the results imply the presence of cavities in the subsoil of the upstream slope has more influence on the flow rate than for cavities existing under the downstream slope. It is clear that the flow rates increased enormously for models with three

cavities at locations L1, L2 and L6 under the upstream side compared to similar models under the downstream side. The flow rate amounted to  $578.1 \times 10^{-3} \text{m/day}$  for a model with cavities situated at location L1 under the upstream side, compared to  $18.94 \times 10^{-3} \text{m/day}$  for model with cavities located at the corresponding positions under the downstream side. It is also clear that the effect of increasing the number of cavities is associated with the impact of their horizontal position. For example, for locations L3 and L4, the flow-rate values were  $13.13 \times 10^{-3} \text{m/day}$  and  $31.41 \times 10^{-3} \text{m/day}$  for the upstream side; however, these values amounted to  $12.58 \times 10^{-3} \text{m/day}$  and  $23.46 \times 10^{-3} \text{m/day}$  for the models with cavities at the corresponding locations on the downstream side.

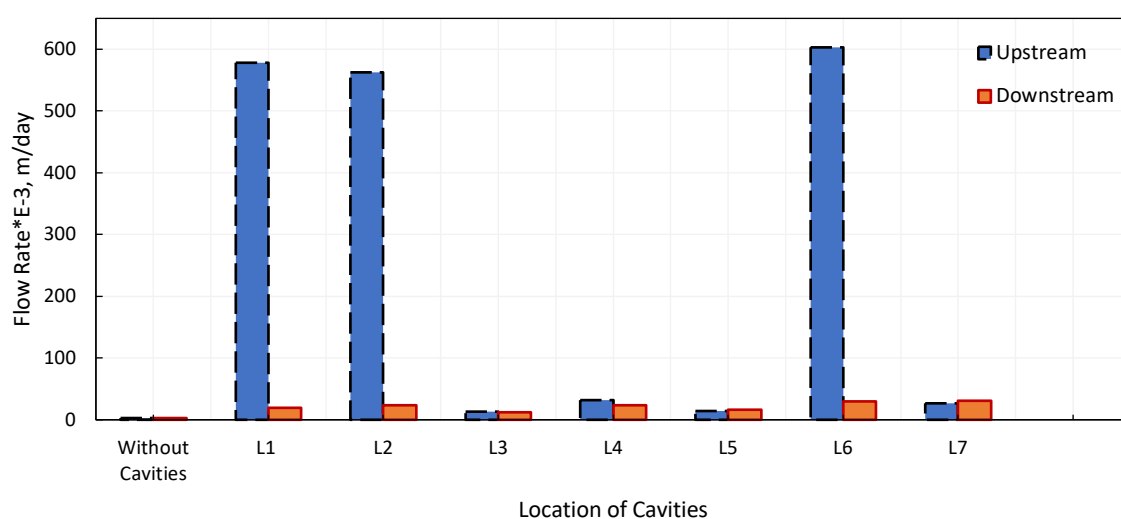


Figure 5.23: Comparison between the effect on flow rate of the presence of three cavities located under upstream and downstream, for different positions and at a depth of 1m using the MC model

### 5.6.1.2 Modelling of an earth dam using the HS and MC models

In these comparisons, HS and MC models were used to model the behaviour of the embankment and subsoil, respectively.

Figure 5.24 illustrates a comparison between the effect of the existence of a single cavity beneath upstream and downstream. The horizontal cavity positions detailed in Table 5.1 were adopted in these analyses. The cavity is positioned at depths of 1m, 2m, 3m and 4m. Similar to the results that were obtained using the MC model, the existence of a single cavity beneath the upstream slope has a significant impact on the flow rate compared to its existence beneath downstream slope. This behaviour applies to all models, regardless of the depth of the cavity,

with the exception of cavity locations L7 and L8. For example, the flow rates were equal to  $459.2 \times 10^{-3} \text{m/day}$  and  $17.87 \times 10^{-3} \text{m/day}$  for models with cavity locations L2 (-8, -1) and L3 (-17, -3) under the upstream slope, respectively, compared to values  $16.19 \times 10^{-3} \text{m/day}$  and  $8.251 \times 10^{-3} \text{m/day}$  for the models with corresponding cavity locations beneath the downstream slope, respectively. However, for a single-cavity model at location L7 (35, -2), the flow rate amounted to  $13.15 \times 10^{-3} \text{m/day}$  for the downstream side compared to  $5.74 \times 10^{-3} \text{m/day}$  for the upstream side. Refer to Table 5.3 for details of the locations of cavities and corresponding flow-rate values.

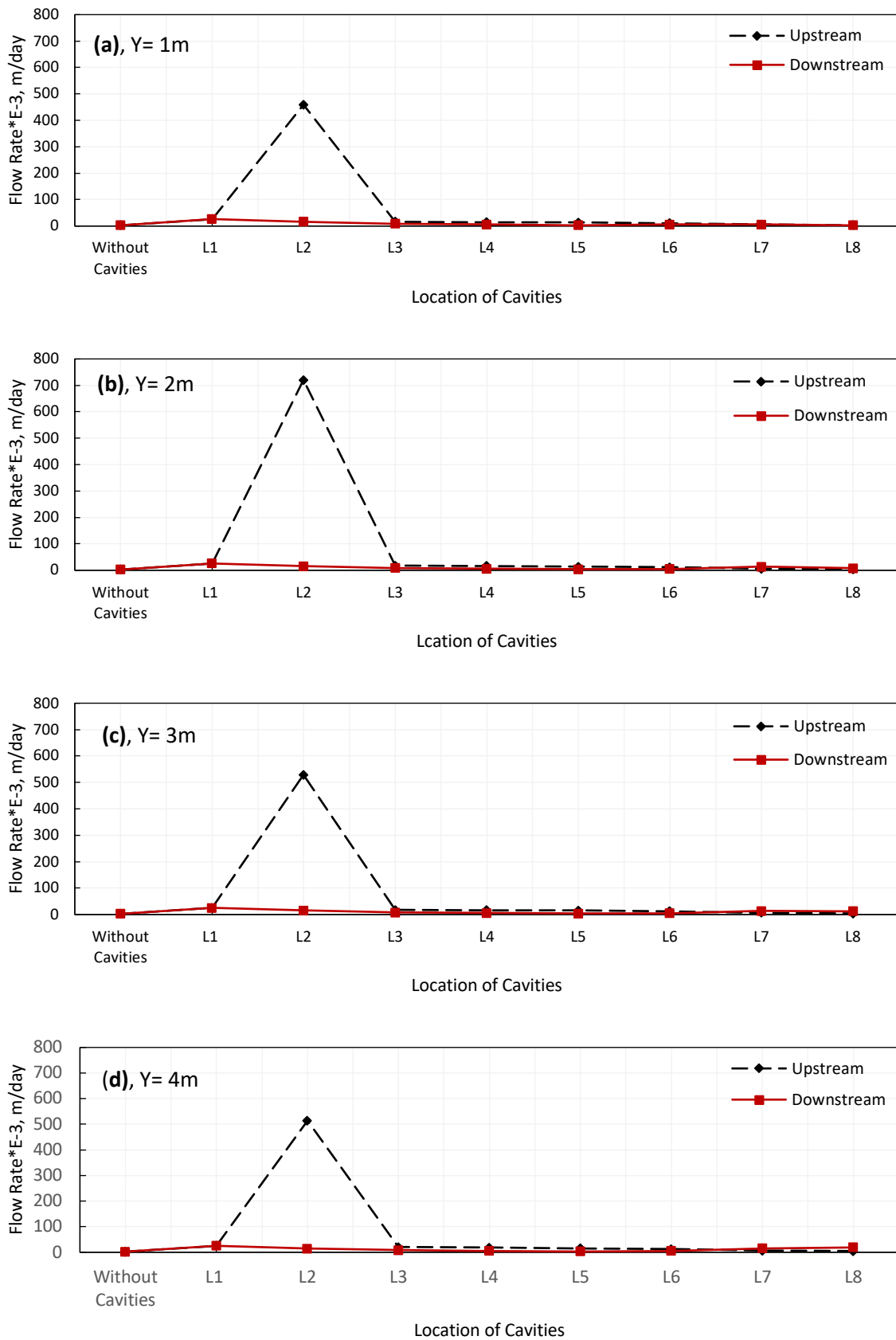


Figure 5.24: Comparison between the effect of the cavity's presence under upstream and downstream on flow rate for depths ( $Y=1\text{m}$  to  $Y=4\text{m}$ ) using the HS and MC models

A comparison between the impact on seepage of two cavities existing in the subsoil of the upstream and downstream slopes is shown in Figure 5.25. The horizontal and vertical coordinates of the cavities are as specified previously in Table 4.16. Generally, it is found that the flow-rate values for the upstream side are greater than those for the downstream side. The cavities existing under the upstream slope result in an increase in flow rates in varying proportions, depending on their horizontal positions. The flow rates increased from  $2.58 \times 10^{-3} \text{m/day}$  to  $520.9 \times 10^{-3} \text{m/day}$  for models without a cavity and with two cavities under the upstream slope at location L1, compared to  $25.5 \times 10^{-3} \text{m/day}$  for the similar model with cavities at location L1 under the downstream slope. However, the opposite behaviour was observed for models with cavities situated at locations L3 and L5, where the flow rates were somewhat higher for the downstream side. For location L3, the flow rate is  $31.1 \times 10^{-3} \text{m/day}$  for the downstream side as opposed to  $24.13 \times 10^{-3} \text{m/day}$  for the upstream side.

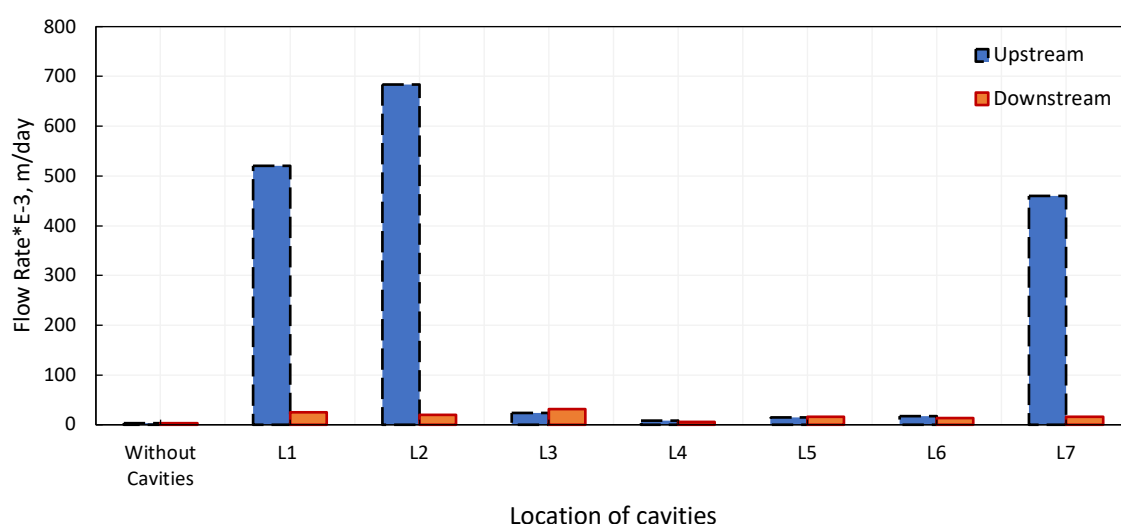


Figure 5.25: Comparison between the effect on flow rate of the presence of two cavities located under upstream and downstream for different positions and at a depth of 1m using the HS and MC models

Figure 5.26 demonstrates a comparison between the impact on the flux rate of the existence of three cavities situated under the upstream and downstream slopes. The coordinates of the cavities' locations are as listed previously in Table 4.22. Similar to the previous simulations, the results prove that the existence of three cavities influences the flow rate considerably when one of the cavities is situated at a critical position under the upstream slope (the critical positions are defined in subsection 5.5.1.1), such as locations L1, L2 and L7. The flow rates for these locations are  $480.3 \times 10^{-3} \text{m/day}$ ,  $504.1 \times 10^{-3} \text{m/day}$  and  $714.1 \times 10^{-3} \text{m/day}$  for the

upstream side, respectively, compared to  $19.84 \times 10^{-3} \text{m/day}$ ,  $21.27 \times 10^{-3} \text{m/day}$  and  $26.09 \times 10^{-3} \text{m/day}$  for the downstream side, respectively. There is an exception at location L5, where the flow rate is  $16.2 \times 10^{-3} \text{m/day}$  for the upstream side, compared to  $17.01 \times 10^{-3} \text{m/day}$  for the downstream side.

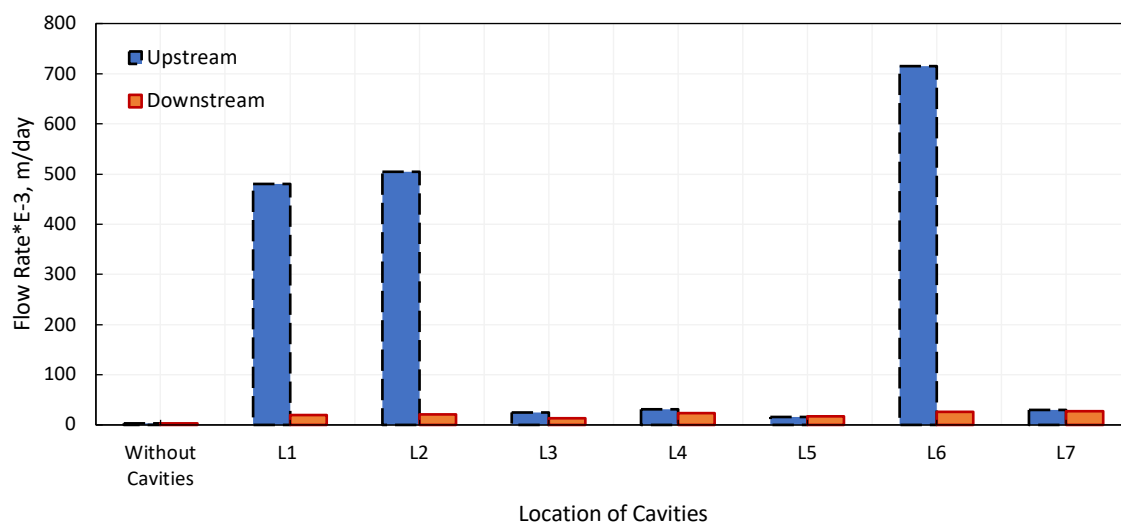


Figure 5.26: Comparison between the effect on flow rate of the presence of three cavities located under upstream and downstream, for different positions and at a depth of 1m using the HS and MC models

## 5.6.2 Impact of cavities that are situated at different depths

This section details an investigation to evaluate the influence of the variation in the depth of cavities within the same model on the flow through earth dams.

### 5.6.2.1 Modelling of an earth dam using the MC model

The earth dam in this simulation was modelled using the MC model. Figure 5.27 demonstrates a comparison between the impact on flow rate for the presence of two cavities situated under upstream and downstream at different depths within the same model. The positions and depths of the cavities that are assumed in this simulation are shown in Table 4.17. It can be seen that the flow rates are greater for models with cavities under the upstream slope than the flow rates for the models with cavities under the downstream slope, except for locations L3 and L4. The flow rate was equal to  $532.10 \times 10^{-3} \text{m/day}$  and  $28.29 \times 10^{-3} \text{m/day}$  for models with cavities located at L1 under the upstream and downstream slopes, respectively. However, the flow rate is  $28.48 \times 10^{-3} \text{m/day}$  and  $32.39 \times 10^{-3} \text{m/day}$  for models with cavities

located at L3 under the upstream and downstream sides, respectively. Refer to Table 4.17 for details of the cavities' locations.

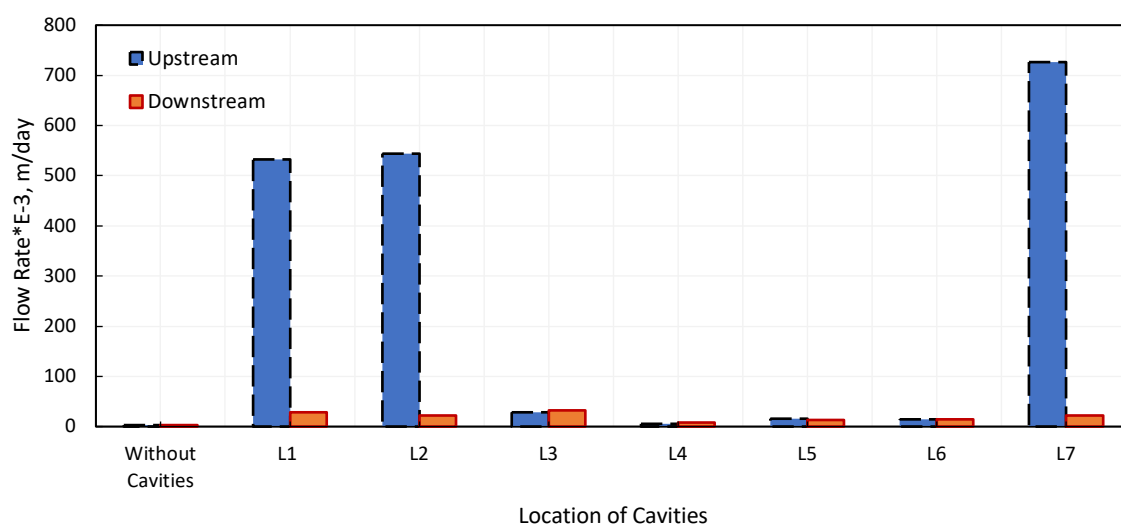


Figure 5.27: Comparison between the effect on flow rate of the presence of two cavities located under upstream and downstream, for different positions and depths using the MC model

A comparison between the effect on flow rate of the existence of three cavities situated beneath the upstream and downstream sides at various depths is illustrated in Figure 5.28. The coordinates of the cavities' locations in both directions (X and Y) are as defined previously in Table 4.23. As mentioned in the previous sections, the presence of cavities under the upstream slope has a greater impact on flow rate compared to their presence under the downstream slope when one cavity is created at an influential position in the X direction, such as locations L1, L2 and L7. The value of the flow rate is equal to  $436.5 \times 10^{-3} \text{m/day}$  for a triple-cavity model with cavities at location L1 beneath the upstream slope, compared to  $20.49 \times 10^{-3} \text{m/day}$  for the model with cavities situated at corresponding locations beneath the downstream slope. Conversely, the flow rates for models containing cavities situated at locations L3, L4, L5 and L6 are somewhat close to each other for both sides of the dam. For example, for models with cavities at location L3, the flow rate is  $28.48 \times 10^{-3} \text{m/day}$  for the upstream side, compared to  $32.39 \times 10^{-3} \text{m/day}$  for the downstream side.



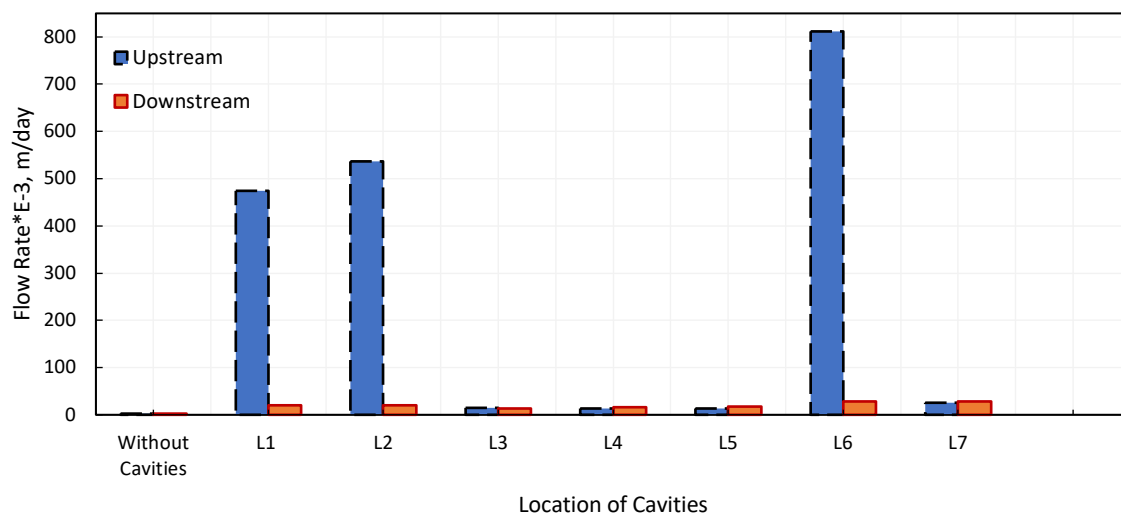


Figure 5.28: Comparison between the effect on flow rate of the presence of three cavities located under upstream and downstream, for different positions and depths using the MC model

### 5.6.2.2 Modelling of an earth dam using the HS and MC models

This simulation was conducted using the HS model to model the embankment of the earth dam. Figure 5.29 shows a comparison between the impact on flow rate of the existence of two cavities located under the upstream and downstream slopes at different depths within the same model. The coordinates of the cavities' locations are as explained previously in Table 4.17. Regarding the upstream side, it appears that the flow rates are high, as opposed to those below the downstream side, especially when cavities are in influential positions (as defined previously). For instance, the flow rate was equal to  $609.6 \times 10^{-3} \text{m/day}$  for a model containing cavities at location L2 beneath the upstream side; however, it is  $19.05 \times 10^{-3} \text{m/day}$  for the model with cavities sited at the corresponding location beneath the downstream side. With respect to location L4, the flow rate is 17.5% bigger for the downstream side than for the upstream side, and the flow rates are  $6.451 \times 10^{-3} \text{m/day}$  and  $5.49 \times 10^{-3} \text{m/day}$  for models with cavities under the downstream and upstream slopes, respectively.

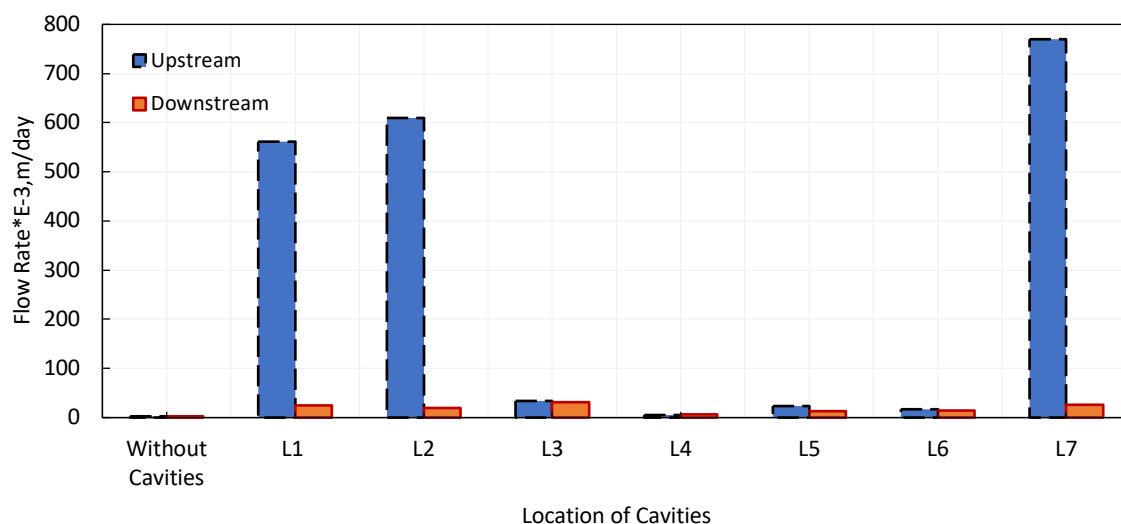


Figure 5.29: Comparison between the effect on flow rate of the presence of two cavities located under upstream and downstream, for different positions and depths using the HS and MC models

The influence on seepage of the existence of three cavities located under upstream and downstream at various depths within one model is revealed in Figure 5.30. The horizontal positions and depths of cavities are as specified previously in Table 4.23. The results show that the existence of three cavities below the upstream has more influence on the flow rate in the case where there is at least one cavity in an influential position in the X direction. Generally, this behaviour applies to all locations except locations L5 and L7, where the flow rates were somewhat greater for the downstream side than the upstream side. For example, the flow amounted to  $700.7 \times 10^{-3} \text{m/day}$  for a model with cavities at location L6 under the upstream slope, compared to  $25.49 \times 10^{-3} \text{m/day}$  for the model with cavities at the corresponding location under the downstream slope; however, it amounted to  $16.44 \times 10^{-3} \text{m/day}$  for a model with cavities located at location L5 on the upstream side, compared to  $18.22 \times 10^{-3} \text{m/day}$  for the model with cavities at the corresponding location under the downstream slope.

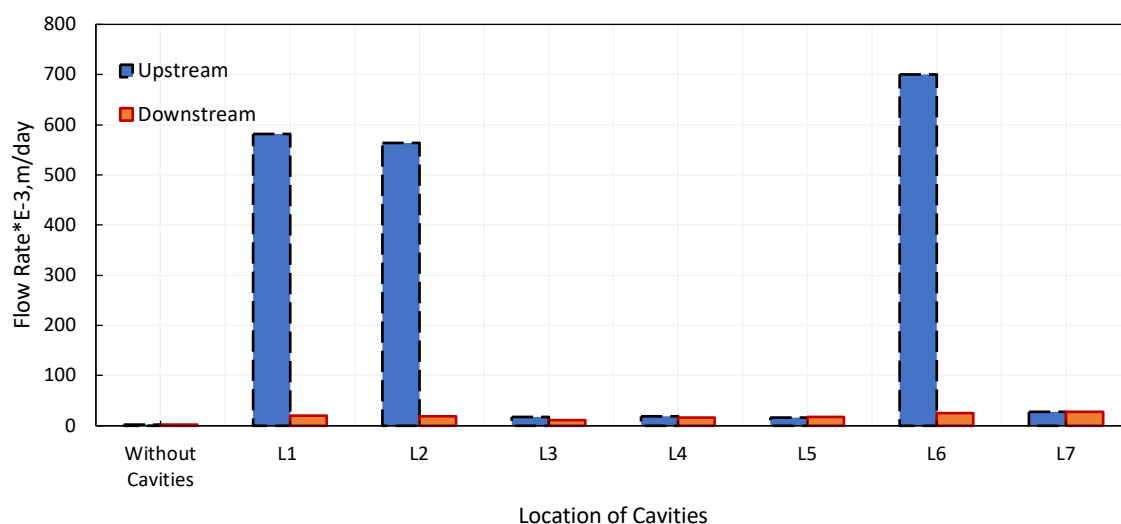


Figure 5.30: Comparison between the effect on flow rate of the presence of three cavities located under upstream and downstream, for different positions and depths using the HS and MC models

### 5.6.3 Impact of the type of model using for modelling

A comparison was made to evaluate the effect of the type of model used (MC and HS) for modelling the embankment of earth dam on the flow rate. This comparison was done considering the existence of a circular cavity below the upstream and downstream slopes at positions, varying horizontally and vertically. Similar horizontal positions of cavities to those used in part one of the analyses were adopted (refer to Table 5.1 for the horizontal positions of cavities).

Figure 5.31 illustrates the joint impact on seepage of cavities existing beneath the upstream slope and the type of model used for modelling. The results indicate that the flow-rate values obtained using the HS model are close to those obtained using MC model, regardless of the variation in a cavity's position and depth. For instance, the flow rates amounted to  $459.2 \times 10^{-3} \text{m/day}$  and  $529 \times 10^{-3} \text{m/day}$  for HS models with cavities situated at locations L2 (-8, -1) and L2 (-8, -3) compared to  $459.8 \times 10^{-3} \text{m/day}$  and  $529.2 \times 10^{-3} \text{m/day}$  for MC models with cavities situated at the same locations. However, the flow rates amounted to  $5.74 \times 10^{-3} \text{m/day}$  and  $6.348 \times 10^{-3} \text{m/day}$  for HS models with cavities situated at L7 (-35, -2) and L2 (-35, -4) as opposed to  $5.14 \times 10^{-3} \text{m/day}$  and  $6.17 \times 10^{-3} \text{m/day}$  for MC models with cavities at the same locations.

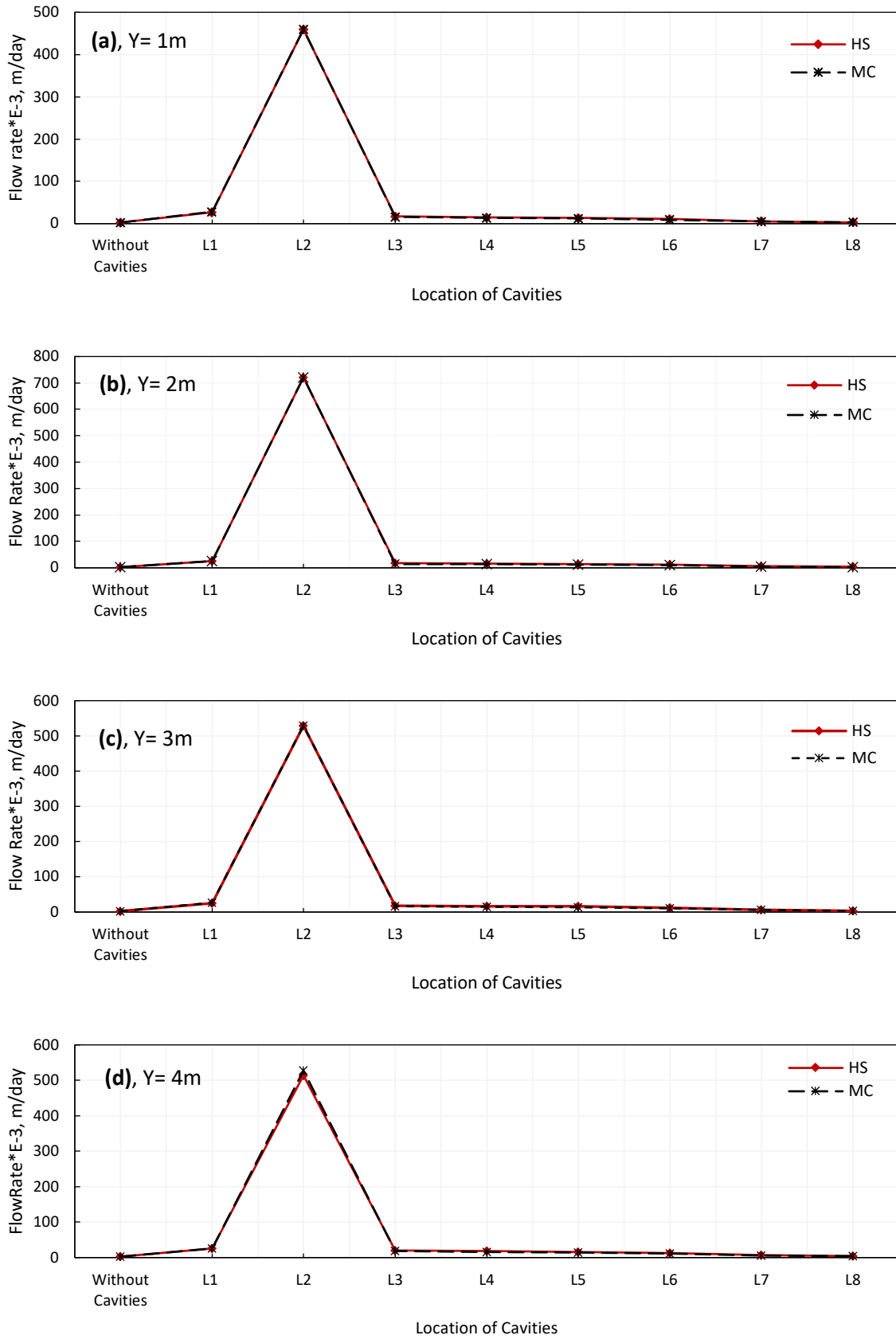


Figure 5.31: Impact of the type of mode on flow rate for cavities present under upstream using the HS and MC models for depths: (a)  $Y=1\text{m}$ , (b)  $Y=2\text{m}$ , (c)  $Y=3\text{m}$ , (d)  $Y=4\text{m}$

Figure 5.32 and Table 5.5 demonstrate the combined influence on flow rate of the cavities existing beneath the downstream slope and the modelling materials used. Similar to the upstream-side results presented previously, it is clear that the impact of a cavity's presence determined using the MC model is somewhat similar to the impact found by using the HS model, regardless of where the cavity exists below the downstream slope. For instance, the flow-rate values ranged from  $16.19 \times 10^{-3} \text{m/day}$  to  $14.75 \times 10^{-3} \text{m/day}$  when the depth was increased from 1m to 4m for HS models with cavity locations (8, -1) and (8, -4), compared to  $16.5 \times 10^{-3} \text{m/day}$  and  $15.2 \times 10^{-3} \text{m/day}$  for MC models with the same cavity locations. Moreover, flow rates decreased by about 1.9% and 2.9% when using the HS model for models with cavities at locations (8, -1) and (8, -4), respectively. It implies that the impact of the presence of a cavity in the subsoil of the earth dam is not associated with the behaviour of the modelling materials, whether they are linear or nonlinear, and the most influential parameter is the horizontal position of the cavity.

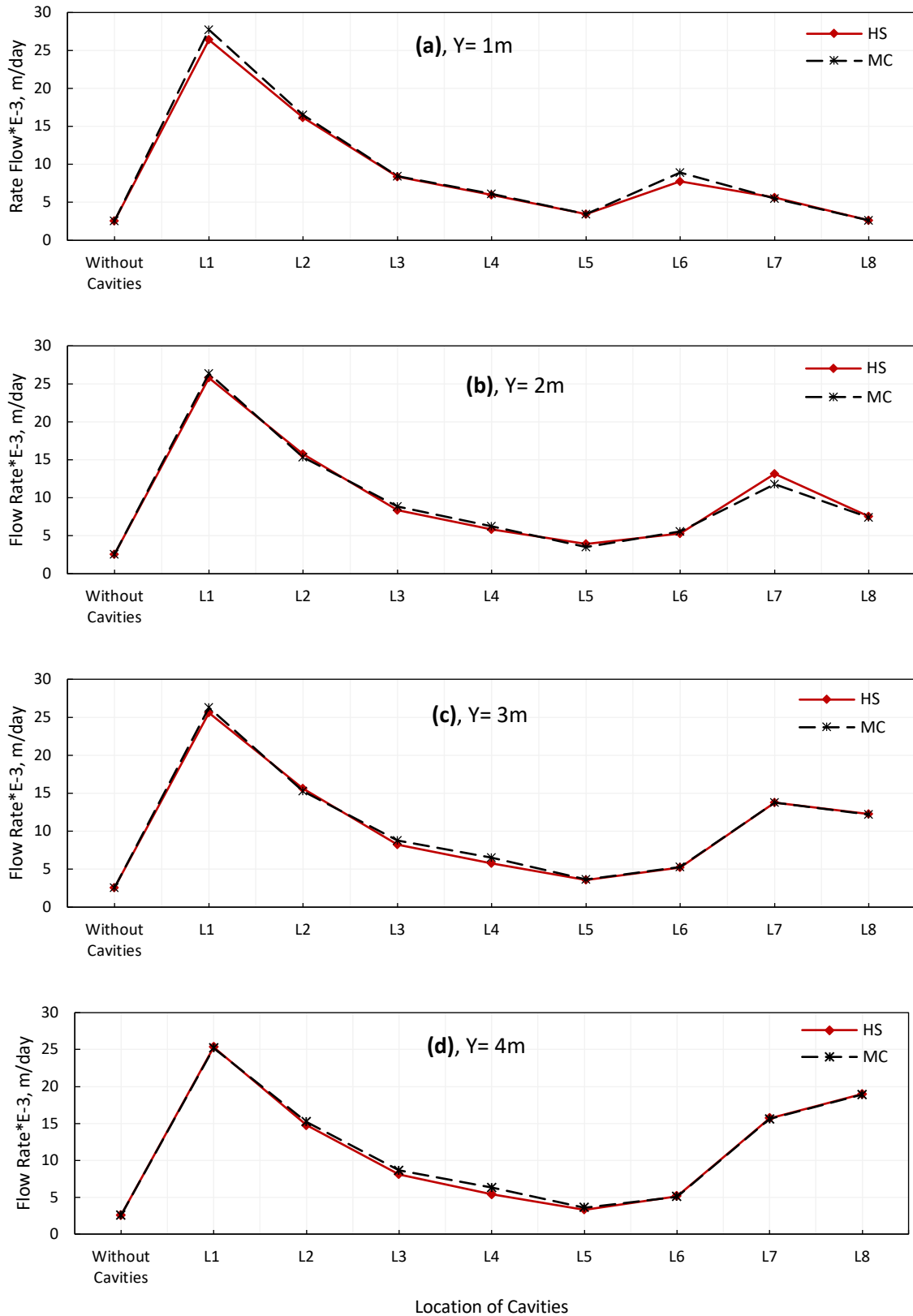


Figure 5.32: Impact of the type of mode on flow rate for cavities present under downstream for depths: (a)  $Y=1\text{m}$ , (b)  $Y=2\text{m}$ , (c)  $Y=3\text{m}$ , (d)  $Y=4\text{m}$

## 5.7 Conclusions

The current study includes a numerical analysis, which was accomplished by means of PLAXIS 2D software, to investigate the influence on seepage through an earth dam of the presence of cavities in terms of their horizontal position, depth and shape, and the number of cavities under conditions of rapid drawdown. The results prove that the existence of cavities in the subsoil of the upstream side increases the flow rates considerably more than when they exist in the subsoil of the downstream side. Studying the impact of variations in the depth of the cavity shows that the horizontal position of the cavity is the factor that has the most influence on seepage, in which the cavity depth has an insignificant influence on flow rates. Furthermore, the flow-rate values go up noticeably with an increase in the number of cavities. However, the outcomes indicate that the presence of a circular cavity or an irregular cavity has the same impact on the flow-rate value. Finally, the type of model used for modelling the embankment with the presence of the cavities has an unimportant influence on the flow rates, irrespective of the presence circular or irregular cavity, and if cavity exists under the base of the dam vertically and horizontally. The most influential parameter on flow rate through the simulated slope is the horizontal position of the cavity.

## CHAPTER SIX: CONCLUSIONS AND RECOMMENDATIONS

### 6.1 General overview

Assessing the stability of slopes is an important, interesting and challenging aspect of the geotechnical engineering field. However, the existence of cavities in soils is a significant area of interest within the field of geotechnical engineering. The current study addresses the impact of the existence of cavities situated beneath the slopes of earth dams on their stability and the flow rates of water passing through them. The seepage and slope stability of earth dam was assessed under conditions of rapid drawdown by means of PLAXIS 2D software. The parametric and comparative studies were fulfilled using Mohr-Coulomb (MC) and Hardening Soil (HS) constitutive models with respect to soil behaviour, considering the parameters of the cavity's horizontal position, depth, diameter and shape, and the number of cavities. In addition, a further analysis was conducted to investigate the combined effects on slope stability of the location and diameter of cavities, with the variations in the shear-strength parameters of the embankment. The following details the key conclusions that can be drawn from the findings presented in this study:

### 6.2 Impact of a cavity on slope stability of earth dam

The main conclusions related to the influence of the existence of a cavity on the slope stability of an earth dam under conditions of rapid drawdown are as follows:

#### 6.2.1 Impact of the horizontal position of the cavity

1. The existence of a cavity beneath the upstream side under conditions of rapid drawdown impacts slope stability significantly, resulting in considerably more damage to the stability, compared to the same cavity being present on the downstream side. The earth dam model considers unstable when a cavity is situated at the position X2 under the upstream side, where the SF value does not satisfy the minimum limit for the stability of dam slopes in rapid-drawdown conditions.



2. The impact of the existence of a cavity decreases as the horizontal distance from the dam's centreline to the cavity's centreline increases, for which the SF values for increase, while the displacement values decrease.
3. The existence of a cavity has more influence on the SF values than the displacement values.
4. The cavity's position in the horizontal direction is the factor that has the most influence on slope stability of all the factors considered in this investigation.

### **6.2.2 Impact of the cavity depth**

1. Variations in the horizontal position of the cavity are more influential on the stability than the variation in the vertical position (depth) of cavity: the SF and displacement values fluctuate (increasing or decreasing) slightly by changing cavity depths, whether the cavity is situated either under the upstream slope or the downstream slope.
2. Increasing the number of cavities (two or three) along with the increasing the depth of cavities within the same model has a little impact on the earth dam's stability, where caused a vacillating (increasing or decreasing) in the SF and displacement values, regardless of where the cavities exist horizontally in the subsoil of the upstream or downstream slopes.

### **6.2.3 Impact of the cavity shape**

1. A circular cavity has a similar effect to the existence of an irregular cavity on dam stability, irrespective of vertical and horizontal changes in the location of the cavity. In general, the SF values for irregular-cavity models are smaller than the SF values for circular cavity models.
2. Regarding the impact of cavity shape on the displacement, a same behaviour also observed, wherever the cavity exists horizontally and vertically in the subsoil of both sides of the dam model.

### **6.2.4 Impact of the cavity diameter**

Regardless of the location of the cavity and under which slope the cavity is situated, either upstream or downstream, any increase in the diameters of extant cavities decreases the SF significantly and drives the structure towards imminent failure. In some of the selected

locations beneath the upstream slope, increasing the cavity diameter caused the earth-dam model to be unsafe; where the SF values were smaller than the minimum stipulated values for slope stability under conditions of rapid drawdown.

### **6.2.5 Impact of the number of cavities**

1. Increasing the number of cavities results in a significant drop in the stability of the earth dam, for which the SF values decrease while the displacement values increase.
2. The SF value drops notably when one of the cavities in the model (with two or three cavities in total) is below the upstream slope; the SF value becomes less than the required minimum limit for the safety of earth dams when the cavity is situated at the critical horizontal position.
3. The dam's stability drops tremendously when two or three cavities are situated under the upstream side, irrespective of their horizontal positions, although their depth varies.
4. The existence of two or three cavities at the same depth has more of an influence on the slope's stability compared to them existing at different depths within the same model.
5. The effect of increasing the number of cavities on stability is related to the effect of their horizontal position in the subsoil of the dam.

### **6.2.6 Combined effect of the existence of cavities and shear-strength parameters**

1. Slope stability in an earth dam under rapid-drawdown conditions increases with an increase in the soil cohesion and angle of internal friction; however, these increases are minimal compared to the considerable effects of cavities on the stability and, while introducing improvements, are unable to compensate for the significant disturbing effects of cavities. This effect is even greater when the cavity or cavities are situated in one of those horizontal positions that has the maximum impact on stability.
2. Overall, the SF values for models with a cavity at position X1 are more or less the same, with small increases as the soil cohesion and shear friction angle ( $\phi$ ) increase and were under the minimum recommended SF value.

### 6.2.7 Impact of the type of model

1. Using either the MC model or the HS model for modelling the embankment gives a similar result for the impact on the dam's stability in the case of the existence of a circular or an irregular cavity, no matter where these cavities are found under the upstream or downstream slope.
2. The SF values recorded for the MC model are somewhat greater than those obtained from the HS for models with a circular cavity or an irregular cavity.
3. The displacement values obtained from the MC model are slightly higher than those from the HS model for all cavity models regardless of whether a circular cavity or an irregular cavity are used.
4. The type of model used does not reduce the cavity's influence when it exists in a critical position, such as location L2.

### 6.3 Impact of the existence of a cavity on flow rate through earth dam

The following key conclusions are drawn based on the results obtained from the numerical seepage analysis.

#### 6.3.1 Impact of the cavity location (horizontal position and depth)

1. The existence of a cavity in the subsoil of an earth dam under conditions of rapid drawdown affects the flow rates of water passing through it; the flow-rate value increases dramatically when the cavity is situated at the critical horizontal position (positions where the recorded SF values are less than the minimum value required).
2. The presence of a cavity below the upstream slope of the earth dam has a significant effect on the flow rate compared to the case where a cavity exists below the downstream slope.
3. The presence of cavity and its influence on flow rates (compared to the case with no cavity) becomes less significant with an increase in the horizontal distance between the centreline of the earth dam and the centreline of the cavity (the distance between positions X1 and X8).
4. Varying in the location of the cavity in the horizontal direction affects flow rates considerably, while this effect is smaller when the cavity moves in the vertical direction.

5. Increasing the vertical distance between the base of the earth dam and the centreline of the cavity has a lower influence on the change in flow rate; however, generally, the flow rate fluctuates (increasing or decreasing) with an increase in the cavity depth.

### 6.3.2 Impact of the cavity shape

1. The effect of the existence of a circular cavity on flow rates is similar to the effect of an irregular cavity, irrespective of the vertical and horizontal position of the cavity beneath the upstream slope.
2. Overall, the flow rates recorded for the irregular-cavity models under the upstream side are greater than those for the circular-cavity models.
3. With respect to the downstream side, the flow rates recorded for irregular- and circular-cavity models are close to each other generally.
4. The flow rates for irregular-cavity are somewhat higher than those for circular-cavity models when the cavity depth is increased from 1m to 4m, wherever a cavity was created horizontally.

### 6.3.3 Impact of the number of cavities

1. Increasing the number of cavities under the base of the earth dam increases the flow rates through the earth-dam model dramatically.
2. Present of a cavity existing in a critical position (for which the recorded SF values are less than the minimum stipulated values) under the upstream side significantly influences the flow rate through the earth-dam model. This demonstrates that the influence of increasing the number of cavities is coupled with the influence of their horizontal position in the subsoil of the dam.
3. Varying the position of the cavity in the vertical direction has little influence, even when the number of cavities is increased.
4. The presence of cavities below the upstream slope has more influence on the flow rate than their presence below the downstream slope, no matter where the cavities are situated, either horizontally or vertically.

### 6.3.4 Impact of the type of model

1. The effect of the existence of cavity in the earth dam's foundation on seepage is not associated with the type of the model using for modelling, regardless of the cavity shape and where the cavity is situated horizontally or vertically.
2. The flow-rate values obtained using the HS model are close to those obtained using the MC model, regardless of the variation in a cavity's position and depth.

The most influential parameter on seepage is the horizontal position of the cavity.

### 6.4 Recommendations for future work

1. This study can be extended to involve further analyses of the downstream slope in the steady state.
2. It is recommended that numerical analyses utilizing PLAXIS 3D software are conducted.
3. It is suggested that the influence of the existence of a cavity under the base of a zoned earth dam is estimated.
4. It is recommended that numerical analyses are carried out using other shapes of cavity.
5. It would be useful to conduct a parametric study with the anisotropic condition.

## REFERENCES

- Abbas, A.L., 2015. Influence of head elevation on the stability of earth fill dam, Fada dam as a case study. *Diyala Journal of Engineering Sciences*, 8(4), pp.110-120.
- Abdulsattar, A.A., Faris, M.R. and Zedan, A.J., 2017. Seepage Analysis through an Earth Dam (KHASA-CHAI Dam) as a Case Study. *Engineering and Technology Journal*, 35(2 Part (A) Engineering), pp.172-181.
- PS, M.A. and Balan, T.A., 2014. Numerical analysis of seepage in Embankment dams. *IOSR Journal of Mechanical and Civil Engineering (IOSR-JMCE), ICICE*, vol. 4, pp.13-23.
- Abhyankar, S.P. and Bhole, S.D., 2011. Application of FEM in Civil Engineering applications. *International Journal of Earth Sciences and Engineering*, 4(6), pp.748-751.
- Aboelela, M.M., 2016. Control of seepage through earth dams based on pervious foundation using toe drainage systems. *Journal of Water Resource and Protection*, 8(12), pp.1158-1174.
- Abramson, L. W., Lee, T. S., Sharma, S., and Boyce, G. M., 2002. Slope Stability Concepts. Slope Stabilisation and Stabilisation Methods, Second edition, published by John Willey & Sons, Inc., pp. 329-461.
- Albataineh, N., 2006. *Slope stability analysis using 2D and 3D methods* (Doctoral dissertation, University of Akron).
- Al-Jazaairry, A. and Toma-Sabbagh, T.M., 2017, April. Effect of cavities on the behaviour of model pile under axial loading in sand. In *Proceedings of the 2nd World Congress on Civil, Structural, and Environmental Engineering (CSEE'17)* (Vol. 2, No. 4, pp. 1-10). International ASET Inc.
- Al-Jazaairry, A.A. and Toma-Sabbagh, T.M., 2017. Performance of axially loaded single pile embedded in cohesive soil with cavities. *International Journal of Environmental, Chemical, Ecological, Geological and Geophysical Engineering*, 11(7), pp.602-606.
- Al-Jorany, A.N.,1996. *Slope Stability Analysis* (Doctoral dissertation, Department of Civil Engineering, University of Baghdad).
- Al-Taie, S.M., Al-Shakarchi, Y.J. and Al-Mosawe, M.J., 2007. Embedded in sandy soils with cavities. *Journal of Engineering*, 13(1), pp.1168-1185.
- Anagnosti, P., 1969. Three-dimensional stability of fill dams. In *Proceeding of 7th International Conference on Soil Mechanics and Foundation Engineering, Mexico* (pp. 275-280).

- Arellano, D. and Stark, T.D., 2000. Importance of three-dimensional slope stability analyses in practice. In *Slope Stability 2000* (pp. 18-32).
- Arora, K.R., 2002. *Irrigation, water power and water resources engineering*. Standard Publisher Distributors.
- Arslan, C.A. and Mohammad, S.A., 2011. Experimental and Theoretical Study for Pizometric Head Distribution under Hydraulic Structures. *Department of Civil engineering*.
- Aryal, K. P., 2006. *Slope stability evaluations by limit equilibrium and finite element methods*. (Doctoral dissertation, Department of Civil and Transport, Faculty of Engineering Science and Technology, Norwegian University of Science and Technology).
- Athani, S.S., Solanki, C.H. and Dodagoudar, G.R., 2015. Seepage and stability analyses of earth dam using finite element method. *Aquatic Procedia*, 4(2015), pp.876-883.
- Atkinson, J.H. and Potts, D.M., 1977. Stability of a shallow circular tunnel in cohesionless soil. *Geotechnique*, 27(2), pp.203-215.
- Azam, G., Hsieh, C.W. and Wang, M., 1991. Performance of strip footing on stratified soil deposit with void. *Journal of geotechnical engineering*, 117(5), pp.753-772.
- Aziz, L. J., 2008. *Lateral Resistance of Single Pile Embedded in Sand with Cavities* (Doctoral dissertation, University of Technology, Iraq).
- Aziz, L.J., Mahmoud, M.R. and Shlash, K.T., 2012. Lateral Resistance of a Single Pile Embedded in Sand with Cavities. *Engineering and Technology Journal*, 30(15), pp.2641-2663.
- Badie, A. and Wang, M.C., 1984. Stability of spread footing above void in clay. *Journal of Geotechnical Engineering*, 110(11), pp.1591-1605.
- Basile, F., 2014. Effects of tunnelling on pile foundations. *Soils and Foundations*, 54(3), pp.280-295.
- Bathe, K.J. and Khoshgoftaar, M.R., 1979. Finite element free surface seepage analysis without mesh iteration. *International Journal for Numerical and Analytical Methods in Geomechanics*, 3(1), pp.13-22.
- Baus, R.L. and Wang, M.C., 1983. Bearing capacity of strip footing above void. *Journal of Geotechnical Engineering*, 109(1), pp.1-14.
- BDS (1994). *The British Dam Society at the Institution of Civil engineers*, Great George Street, London, SW1P 3AA. <http://britishdams.org/conferences>
- Bear, J. and Verruijt, A., 2012. *Modeling groundwater flow and pollution* (Vol. 2). Springer Science & Business Media.

- Berilgen, M.M., 2007. Investigation of stability of slopes under drawdown conditions. *Computers and Geotechnics*, 34(2), pp.81-91.
- Berisavljević, Z., Berisavljević, D., Čebašek, V. and Rakić, D., 2015. Slope stability analyses using limit equilibrium and strength reduction methods. *Građevinar*, 67(10.), pp.975-983.
- Billstein, M., Svensson, U. and Johansson, N., 1999. Development and Validation of a Numerical Model of Flow Through Embankment Dams—Comparisons with Experimental Data and Analytical Solutions. *Transport in Porous Media*, 35(3), pp.395-406.
- Bishop, A.W., 1955. The use of the slip circle in the stability analysis of slopes. *Geotechnique*, 5(1), pp.7-17.
- Boleve, A., Janod, F., Revil, A., Lafon, A. and Fry, J.J., 2011. Localization and quantification of leakages in dams using time-lapse self-potential measurements associated with salt tracer injection. *Journal of Hydrology*, 403(3-4), pp.242-252.
- Brinkgreve, R.B.J., Kumarswamy, S.M, Swolfs, W.M. and Foria, F., 2018. PLAXIS finite element code for soil and rock analysis. Delft University of Technology & Plaxis bv, The Netherland. <https://www.plaxis.com>
- Calcano, C.E. and Alzura, P.R., 1967. Problems of dissolution of gypsum in some dam sites. *Bulletin of Venezuelan Society of Soil Mechanics and Foundation Engineering*, pp.75-80.
- Calvino, F., Costantino, F. and Mirri, F., 1981. Design criteria for a dam, reservoir and irrigation system on a Middle East evaporite formation. *Bulletin of the International Association of Engineering Geology-Bulletin de l'Association Internationale de Géologie de l'Ingénieur*, 24(1), pp.53-55.
- Carthy, D.F., 1982. *Essentials of Soil Mechanics and Foundations*. New Jersey-Prentice Hall.
- Casagerande, A., 1937. Seepage Through Earth Dams, in *Contribution to Soil Mechanics 1925- 1940*, Boston Society of Civil Engineers, Boston, 295.
- Cavounidis, S., 1987. On the ratio of factors of safety in slope stability analyses. *Geotechnique*, 37(2), pp.207-210.
- Cedergren, H.R., 1997. *Seepage, drainage, and flow nets*(Vol. 16). John Wiley & Sons.
- Chandrakant S. D., and Johan T.C., 1977. *Numerical Methods in Geotechnical Engineering*. McGraw-Hill series.
- Chaudhary, K.B., Domingos, V.H., Gitirana Jr, G., Fredlund, M. and Lu, H., 2016. Three-Dimensional Slope Stability: Geometry Effects. In *Tailings and Mine Waste Conference*(Vol. 16).



- Cheng, C.Y., Dasari, G.R., Leung, C.F., Chow, Y.K. and Rosser, H.B., 2004. 3D numerical study of tunnel-soil-pile interaction. *Tunnelling and Underground Space Technology*, 19(4), pp.381-382.
- Cheng, Y.M., Lansivaara, T. and Wei, W.B., 2007. Two-dimensional slope stability analysis by limit equilibrium and strength reduction methods. *Computers and geotechnics*, 34(3), pp.137-150.
- Cheng, Y.M., Liu, H.T., Wei, W.B. and Au, S.K., 2005. Location of critical three-dimensional non-spherical failure surface by NURBS functions and ellipsoid with applications to highway slopes. *Computers and Geotechnics*, 32(6), pp.387-399.
- Cooper, A. H., and Calow, R. C., 1998. *Avoiding gypsum geohazards: guidance for planning and construction*, British Geological Survey. Technical report WC/98/5 overseas geological series.
- Costa, J.E., 1985. *Floods from dam failures* (Vol. 85, No. 560). US Geological Survey.
- Craig, R.F., 2004. *Craig's soil mechanics*. CRC press.
- Crapps, D.K., 2010. The Effects of Cavities upon Foundation Design & Construction. In *Art of Foundation Engineering Practice* (pp. 206-223).
- Culshaw, M.G. and Waltham, A.C., 1987. Natural and artificial cavities as ground engineering hazards. *Quarterly Journal of Engineering Geology and Hydrogeology*, 20(2), pp.139-150.
- Davey, P. G., and Eccles, P. G., 1983. The Carsington Scheme- Reservoir and Aqueduct. *Journal of the Institution of Water Engineers and Scientists*, 37(3).
- Dawson, E.M., Roth, W.H., and Drescher, A., 1999. Slope stability analysis by strength reduction. *Geotechnique*, 49(6), pp.835-840.
- Dreybrodt, W., Romanov, D., and Gabrovsek, F., 2002. Karstification below dam sites: a model of increasing leakage from reservoirs. *Environmental Geology*, 42(5), pp.518-524.
- Dreybrodt, W., Romanov, D. and Gabrovsek, F., 2002. Karstification below dam sites: a model of increasing leakage from reservoirs. *Environmental Geology*, 42(5), pp.518-524.
- Duncan, J. M. ,1992. State-of-the-art: Static stability and deformation analysis. In *Proc. of Specialty Conf. Stability and Performance of Slopes and Embankments-II* (Vol. 1, pp. 222-266). ASCE.
- Duncan, J. M., 1996. State of the art: limit equilibrium and finite-element analysis of slopes. *Journal of Geotechnical engineering*, 122(7), pp.577-596.

- Duncan, J.M. and Chang, C.Y., 1970. Nonlinear analysis of stress and strain in soils. *Journal of Soil Mechanics & Foundations Div*, 96, pp.1629-1653.
- Dupuit, J.É.J., 1863. *Études théoriques et pratiques sur le mouvement des eaux dans les canaux découverts et à travers les terrains perméables: avec des considérations relatives au régime des grandes eaux, au débouché à leur donner, et à la marche des alluvions dans les rivières à fond mobile*. Dunod.
- Eid, H.T., Elleboudy, A.M., Elmarsafawi, H.G. and Salama, A.G., 2006. Stability analysis and charts for slopes susceptible to translational failure. *Canadian geotechnical journal*, 43(12), pp.1374-1388.
- Elshemy, M., Nasr, R.I., Bahloul, M.M. and Rashwan, I.M., 2002. The effect of blockages through earth dams on the seepage characteristics. *Faculty of Engineering, Tanta University, Egypt*.
- Er-Xiang, S., 1997. Finite element analysis of safety factor for soil structures. *Chinese Journal of Geotechnical Engineering*, 19(2), pp.1-7.
- Fakhari, A. and Ghanbari, A., 2013. Note: A SIMPLE METHOD FOR CALCULATING THE SEEPAGE FROM EARTH DAMS WITH CLAY CORE. *Journal of GeoEngineering*, 8(1), pp.27-32.
- Farhadian, H., Aalianvari, A. and Katibeh, H., 2012. Optimization of analytical equations of groundwater seepage into tunnels: A case study of Amirkabir tunnel. *Journal of the Geological Society of India*, 80(1), pp.96-100.
- Farshidfar, N. and Nayeri, A., 2015. Slope stability analysis by shear strength reduction method. *Civil Engineering and Urbanism Journal*, 5, pp.35-37.
- Fathani, T.F. and Legono, D., 2010. Pengaruh Fluktuasi Muka Air Reservoir terhadap Stabilitas Bendungan Tanah Uji model di Laboratorium. *Penelitian DPP/SPP Fakultas Teknik UGM, Yogyakarta*.
- Fattah, M.Y., Omran, H.A. and Hassan, M.A., 2015. Behavior of an Earth Dam during Rapid Drawdown of Water in Reservoir—Case Study. *International Journal of Advanced Research (2015)*, 3(10), pp.110-122.
- Fattah, M.Y., Omran, H.A. and Hassan, M.A., 2017. Flow and stability of Al-Wand earth dam during rapid drawdown of water in reservoir. *Acta Montanistica Slovaca*, 22(1), pp.43-57.
- Fell, R., MacGregor, P. and Stapledon, D., 1992. *Geotechnical engineering of embankment dams*. Balkema.
- Fell, R., Wan, C.F., Cyganiewicz, J. and Foster, M., 2003. Time for development of internal erosion and piping in embankment dams. *Journal of geotechnical and geoenvironmental engineering*, 129(4), pp.307-314.

- Fellenius, W., 1936. Calculation of the Stability of Earth Dams. Trans, 2nd Cong, Large Dams, vol. (4).
- Feng, H., & Po, C., 2011. Affect the overall stability of the excavation of soil constitutive model of strength reduction. *Rock and Soil Mechanics*, 32 (Appendix 2): pp.592–597.
- Fipps, G.A., Skaggs, R.W. and Nieber, J.L., 1986. Drains as a boundary condition in finite elements. *Water resources research*, 22(11), pp.1613-1621.
- Foster, M.A. and Fell, R., 1999. *A framework for estimating the probability of failure of embankment dams by piping using event tree methods*. University of New South Wales, School of Civil and Environmental Engineering.
- Fredlund, D.G. and Krahn, J., 1977. Comparison of slope stability methods of analysis. *Canadian geotechnical journal*, 14(3), pp.429-439.
- Fredlund, D.G., Xing, A. and Huang, S., 1994. Predicting the permeability function for unsaturated soils using the soil-water characteristic curve. *Canadian Geotechnical Journal*, 31(4), pp.533-546.
- Fredlund, M., Lu, H. and Feng, T., 2011. Combined seepage and slope stability analysis of rapid drawdown scenarios for levee design. In *Geo-Frontiers 2011: Advances in Geotechnical Engineering* (pp. 1595-1604).
- Fu, J.F. and Sheng, J.I.N., 2009. A study on unsteady seepage flow through dam. *Journal of Hydrodynamics, Ser. B*, 21(4), pp.499-504.
- Garg K. S., 1984. *Irrigation Engineering and Hydraulic Structures*. 5th Ed. Khanna Publishers, New Delhi, India.
- Goodman, R., D. Moye, A. Schalkwyk, and Javendel, I., 1965. Groundwater inflow during tunnel driving. *Engineering Geology*, (1), pp.150-162.
- Ranjan, G. and Rao, A.S.R., 2007. *Basic and applied soil mechanics*. New Age International.
- Griffiths, D.V. and Lane, P.A., 1999. Slope stability analysis by finite elements. *Geotechnique*, 49(3), pp.387-403.
- Griffiths, D.V. and Marquez, R.M., 2007. Three-dimensional slope stability analysis by elasto-plastic finite elements. *Geotechnique*, 57(6), pp.537-546.
- Gutierrez, F., Desir, G. and Gutierrez, M., 2002. Causes of the catastrophic failure of an earth dam built on gypsiferous alluvium and dispersive clays (Altorricn, Huesca Province, NE Spain). *Environmental Geology*, 43(7), pp.824-851.
- Hammouri, N.A., Malkawi, A.I.H. and Yamin, M.M., 2008. Stability analysis of slopes using the finite element method and limiting equilibrium approach. *Bulletin of Engineering Geology and the Environment*, 67(4), p.471.

- Harr, M.E., 2012. *Groundwater and seepage*. Courier Corporation.
- Hasani, H., Mamizadeh, J. and Karimi, H., 2013. Stability of slope and seepage analysis in earth fills dams using numerical models (Case Study: Ilam Dam-Iran). *World Applied Sciences Journal*, 21(9), pp.1398-1402.
- He, B. and Zhang, H., 2012. Stability analysis of slope based on finite element method. *International Journal of Engineering and Manufacturing*, 3, pp.70-74.
- Hill, R., 1998. *The mathematical theory of plasticity* (Vol. 11). Oxford university press.
- Hnang, T.K., 1996. Stability analysis of an earth dam under steady state seepage. *Computers & structures*, 58(6), pp.1075-1082.
- Hsu, Y.C., Tung, Y.K. and Kuo, J.T., 2011. Evaluation of dam overtopping probability induced by flood and wind. *Stochastic environmental research and risk assessment*, 25(1), pp.35-49.
- Hu, X.W., Tang, H.M. and Liu, Y.R., 2005. Physical model studies on stability of Zhaoshuling landslide in area of Three Gorges Reservoir. *Yanshilixue Yu Gongcheng Xuebao/Chin. J. Rock Mech. Eng.*, 24(12), pp.2089-2095.
- Huang, S.Q., Liu, J. and Kong, X.J., 2008. DDA with strength reduction technique and its application to stability analysis of rock slope. *Chinese Journal of Rock Mechanics and Engineering*, 27(S1), pp.2799-2805.
- Hungr, O., 1987. An extension of Bishop's simplified method of slope stability analysis to three dimensions. *Geotechnique*, 37(1), pp.113-117.
- ICOLD., 1973. International Commission on Large Dams. Lessons from Dam Incidents, reduced edition, Paris.
- Irzooki, R.H., 2016. Computation of seepage through homogenous earth dams with horizontal toe drain. *Engineering and Technology Journal*, 34(3 Part (A) Engineering), pp.430-440.
- S Ismaeel, K. and Noori, B.M., 2011. Evaluation of seepage and stability of duhok dam. *AL-Rafdain Engineering Journal (AREJ)*, 19(1), pp.42-58.
- Ismail, M.A.M., Ng, S.M. and Gey, E.K., 2012. Stability Analysis of Kelau Earth-Fill Dam Design under Main Critical Conditions. *The Electronic Journal of Geotechnical Engineering*, 17, pp.3209-3219
- Jairry, H.H.A., 2010. 2D-flow analysis through zoned earth dam using finite element approach. *Engineering and Technology Journal*, 28(21), pp.6315-6324.
- Jalil, A., 2011. The analysis slope stability Reservoir Keuliling with finite element methods. *Journal of Civil Engineering*, 18(3), pp.239-250.

- James, A.N. and Lupton, A.R.R., 1978. Gypsum and anhydrite in foundations of hydraulic structures. *Geotechnique*, 28(3), pp.249-272.
- Janbu, N., 1973. Slope stability computations. *Publication of: Wiley (John) and Sons, Incorporated*.
- Jansen, R.B., Lowe, J., Kramer, R.W. and Poulos, S.J., 1988. Advanced dam engineering for design, construction, and rehabilitation. In Jansen, R.B. (ed). *Earthfill dam, Design and Analysis: Kluwer Academic Publishers*, pp.256-258.
- Jao, M. and Wang, M.C., 1998. Stability of strip footings above concrete-lined soft ground tunnels. *Tunnelling and underground space technology*, 13(4), pp.427-434.
- Jayamohan, J., Aarya, V. and Rajeev, K.P., 2015. Effect of underground void on footings resting on reinforced foundation bed. *International Advanced Research Journal in Science, Engineering and Technology*, 5(Special Issue 1), pp.190-194.
- Jia, G.W., Zhan, T.L., Chen, Y.M. and Fredlund, D.G., 2009. Performance of a large-scale slope model subjected to rising and lowering water levels. *Engineering Geology*, 106(1-2), pp.92-103.
- Jiang, Q.H., Deng, S.S., Zhou, C.B. and Lu, W.B., 2010. Modeling unconfined seepage flow using three-dimensional numerical manifold method. *Journal of hydrodynamics*, 22(4), pp.554-561.
- Shuhai, J., 1999. The design standard for flood prevention and safety of dam [J]. *Journal of Hydraulic Engineering*, 30 (5), pp.19-25.
- Jie, Y., Jie, G., Mao, Z. and Li, G., 2004. Seepage analysis based on boundary-fitted coordinate transformation method. *Computers and Geotechnics*, 31(4), pp.279-283.
- Johansson, S. and Dahlin, T., 1996. Seepage monitoring in an earth embankment dam by repeated resistivity measurements. *European Journal of Engineering and Environmental Geophysics*, 1(3), pp.229-247.
- Kahlström, M., 2013. Plaxis 2D comparison of Mohr-Coulomb and soft soil material models. M.Sc., Department of Civil, Environmental and Natural Resources Engineering, Division of Mining and Geotechnical Engineering, Luleå University of Technology.
- Kamanbedast, A., and Shahosseini, M., 2011. Determination of seepage and analysis of earth dams (case study: Karkheh dam). *Iranica Journal of Energy and Environment*, 2(3), pp.201-207.
- Kelley, J.R., Wakeley, L.D., Broadfoot, S.W., Pearson, M.L., McGrath, C.A., McGill, T.E., Jorgeson, J.D. and Talbot, C.A., 2007. *Geologic setting of Mosul Dam and its engineering implications* (No. ERDC-TR-07-10). ENGINEER RESEARCH AND DEVELOPMENT CENTER VICKSBURG MS.

- Kerkes, D.J. and Fassett, J.B., 2006, April. Rapid drawdown in drainage channels with earthen side slopes. In *Proceedings of the ASCE Texas Section Spring Meeting, Beaumont, TX* (pp. 19-22).
- Keyvanipour, M., Moharrampour, M. and Faghieh, S., 2012. An Evaluation and Comparison of Bar Embankment Behavior with Instrumentation Data and Software PLAXIS. In *International Conference on Environment Science and Engineering, Singapore, IPCBEE 32(2012)*, pp.197-200.
- Khabbaz, H., Fatahi, B. and Nucifora, C., 2012. Finite element methods against limit equilibrium approaches for slope stability analysis. In *Australia New Zealand Conference on Geomechanics*. Geomechanical Society and New Zealand Geotechnical Society, pp.1293-1298.
- Khalil, A. A., 2012. Numerical Modeling of Pore Water Pressure Development within a Thin Clay Core in an Earth Dam. *AL Rafdain Engineering Journal*, 20(1), pp.93-109.
- Khassaf, S. I., Abdoul- Hameed, M. R. and Shams Al-deen, N. N., 2013. Slope Stability Analysis under Rapid drawdown Condition and Seismic Loads of Earth. *IJRSET*, 2(12), pp.7114- 7118.
- Khattab, S. A., 2010. Stability Analysis of Mosul Dam under Saturated and Unsaturated Soil Conditions. *AL Rafdain Engineering Journal*, 18(1), pp.13-27.
- Khattab, S. A. and Khalil, A. A., 2009. Effect of Cavity on Stress Distribution and Settlement under Foundation. *Journal of Al-Rafidain Engineering*, 17(6), pp.14-29.
- Khattab, S.A. and Khalil, A.A., 2013. Numerical Modeling of Pore Water Pressure Development in MOSUL Dam. *Engineering and Technology Journal*, 31(4) Part (A) Engineering, pp.618-631.
- Kirra, M. S., Zeidan, B. A., Shahien, M. and Elshemy, M., 2015. Seepage Analysis of Walter F. George Dam, USA: A case Study. In *International Conference on Advances in Structural and Geotechnical Engineering*, pp.1-13.
- Kondner, R. L., 1963. A hyperbolic stress-strain formulation for sands. In *Proc. 2 nd Pan Am. Conf. on Soil Mech. and Found. Eng., Brazil, 1963* (Vol. 1, pp. 289-324).
- Kwon, H.H. and Moon, Y.I., 2006. Improvement of overtopping risk evaluations using probabilistic concepts for existing dams. *Stochastic Environmental Research and Risk Assessment* 20 (4), pp.223–237.
- Lam, L. and Fredlund, D., 1993. A General Limit Equilibrium Model for Three Dimensional Slope Stability Analysis. *Canadian Geotechnical Journal*, 30, pp.905-919.

- Lam, L. and Fredlund, D. G., 1984. Saturated-unsaturated transient finite element seepage model for geotechnical engineering. In *Finite Elements in Water Resources* (pp. 113-122). Springer, Berlin, Heidelberg.
- Lam, L., Fredlund, D.G. and Barbour, S.L., 1987. Transient seepage model for saturated–unsaturated soil systems: a geotechnical engineering approach. *Canadian Geotechnical Journal*, 24(4), pp.565-580.
- Lambe, T.W., & Whitman, R.V. (1969). *Soil Mechanics*. John Wiley & Sons, New York.
- Lane, P. A. and Griffiths, D. V., 2000. Assessment of stability of slopes under drawdown conditions. *Journal of geotechnical and geoenvironmental engineering*, 126(5), pp.443-450.
- Lavasan, A. A., Talsaz, A., Ghazavi, M. and Schanz, T., 2016. Behavior of shallow strip footing on twin voids. *Geotechnical and Geological Engineering*, 34(6), 1791-1805.
- Lee, J. K., Jeong, S., & Ko, J. (2014). Undrained stability of surface strip footings above voids. *Computers and Geotechnics*, 62, pp.128-135.
- Lee, J. K., Jeong, S. and Ko, J., 2014. Undrained stability of surface strip footings above voids. *Computers and Geotechnics*, 62, pp.128-135.
- Lefebvre, G. and Duncan, J.M., 1971. *Three-Dimensional Finite Element Analyses of Dams* (No. TE-71-5). CALIFORNIA UNIV BERKELEY OFFICE OF RESEARCH SERVICES.
- Lei, S. (1999). An analytical solution for steady flow into a Tunnel. *Groundwater*, 37(1), pp.23-26.
- Leong, E. C. and Rahardjo, H., 2012. Two and three-dimensional slope stability reanalyses of Bukit Batok slope. *Computers and geotechnics*, 42, pp.81-88.
- Levasseur, S., Mattsson, H. and Knutsson, S., 2014. Inverse Hardening Soil Parameter Identification of an Earth and Rockfill Dam by Genetic Algorithm Optimization. *The Electronic journal of geotechnical engineering*, 19(N), pp.3327-3349.
- Li, E., Zhuang, X., Zheng, W. and Cai, Y., 2014. Effect of graph generation on slope stability analysis based on graph theory. *Journal of Rock Mechanics and Geotechnical Engineering*, 6(4), pp.380-386.
- Li, G. C. and Desai, C. S., 1983. Stress and seepage analysis of earth dams. *Journal of Geotechnical Engineering*, 109(7), pp.946-960.
- Li, G., Ge, J. and Jie, Y., 2003. Free surface seepage analysis based on the element-free method. *Mechanics Research Communications*, 30(1), pp.9-19.

- López-Acosta, N. P., De La Fuente, H. A. and Auvinet, G., 2013. Safety of a protection levee under rapid drawdown conditions. Coupled analysis of transient seepage and stability. In *Proceedings 18th International Conference on Soil Mechanics and Geotechnical Engineering, Paris, France (enpreparación)*.
- Lukman, S., Otun, J. A., Adie, D. B., Ismail, A., & Oke, I. A. (2011). A brief assessment of a dam and its failure prevention. *Journal of Failure Analysis and Prevention*, 11(2), pp.97-109.
- Luo, X. Q., Liu, D. F., Wu, J., Cheng, S. G., Shen, H., Xu, K. X. and Huang, X. B., 2005. Model test study on landslide under rainfall and reservoir water fluctuation. *Yanshilixue Yu Gongcheng Xuebao/Chin. J. Rock Mech. Eng.*, 24(14), pp.2476-2483.
- Maatooq, J.S., Aziz, L.J. and Musa, T.A.A., 2014. Development of Empirical Formula for Influence of Cavities on Seepage under Sheet Pile Wall for Hydraulic Structures. *Kufa Journal of Engineering*, 5(2), pp.93-106.
- Majeed, Q.G., 2015. Flow and deformation analysis of zoned earth dam by the finite element method. *Diyala Journal of Engineering Sciences*, 8(3), pp.38-62.
- Maula, B. H. and Zhang, L., 2011. Assessment of embankment factor safety using two commercially available programs in slope stability analysis. *Procedia engineering*, 14, pp.559-566.
- Maximovich, N. G., and Meshcheryakova, O. Y., 2009. The influence of gypsum karst on hydrotechnical constructions in Perm region. In *Geological Engineering Problems in Major Construction Projects: Proceedings of the International Symposium and the 7th Asian Regional Conference of IAEG* (pp. 604-607).
- Middlebrooks, T. A., 1953. Earth-dam practice in the United States. *Transactions of the American Society of Civil Engineers*, (2), pp.697-722.
- Mollaei, R., Mollaei, M., Noori Gheidari, M. H. and Ali Elahi, H., 2015. Evaluation of Gelabar earth dam behavior during construction and first watering by the method of limited components and comparison with real amount resulted by precise instruments data. *European Online Journal of Natural and Social Sciences: Proceedings*, 3(4 (s)), pp-657.
- Mroueh, H. and Shahrour, I., 2002. Three-dimensional finite element analysis of the interaction between tunneling and pile foundations. *International Journal for Numerical and Analytical Methods in Geomechanics*, 26(3), pp.217-230.



- Nagtegaal, J. C., Parks, D. M. and Rice, J. R., 1974. On numerically accurate finite element solutions in the fully plastic range. *Computer methods in applied mechanics and engineering*, 4(2), pp.153-177.
- Narita, K., 2000. Design and construction of embankment dams. *Dept. of Civil Eng., Aichi Institute of Technology*.
- Navas, P. and López-Querol, S., 2013. Generalized unconfined seepage flow model using displacement based formulation. *Engineering geology*, 166, pp.140-151.
- Naylor, D. J., 1982. Finite elements and slope stability. In *Numerical methods in geomechanics* (pp. 229-244). Springer, Dordrecht.
- Nedriga, V.P. and Dem'yanova, E.A., 1986. Construction of Dams on Soils Containing Soluble Salts. *Gidrotekhnicheskoe Stroitel'stvo*, (2), pp.44-47.
- Newmark, N. M., 1965. Effects of earthquakes on dams and embankments. *Geotechnique*, 15(2), pp.139-160.
- Ng, C. W. W. and Lu, H., 2013. Effects of the construction sequence of twin tunnels at different depths on an existing pile. *Canadian Geotechnical Journal*, 51(2), pp.173-183.
- Nian, T. K., Huang, R. Q., Wan, S. S. and Chen, G. Q., 2012. Three-dimensional strength-reduction finite element analysis of slopes: geometric effects. *Canadian Geotechnical Journal*, 49(5), pp.574-588.
- Noori, B. M. A. and Ismaeel, K. S., 2011. Evaluation of seepage and stability of Duhok Dam. *Journal of Al-Rafidain Engineering*, 19(1), pp.42-58.
- NRCS, 2005. *Technical Release No. 60, Earth Dams and Reservoirs*, Natural Resources Conservation Service. available at [www.info.usda.gov/CED/ftp/CED/TR\\_210\\_60\\_Second\\_Edition.pdf](http://www.info.usda.gov/CED/ftp/CED/TR_210_60_Second_Edition.pdf)
- Obrzud, R. F., 2010. On the use of the Hardening Soil Small Strain model in geotechnical practice. *Numerics in Geotechnics and Structures*, pp.15-32.
- Panthulu, T. V., Krishnaiah, C. and Shirke, J. M., 2001. Detection of seepage paths in earth dams using self-potential and electrical resistivity methods. *Engineering Geology*, 59(3-4), pp.281-295.
- Papagianakis, A.T. and Fredlund, D.G., 1984. A steady state model for flow in saturated–unsaturated soils. *Canadian Geotechnical Journal*, 21(3), pp.419-430.

- Pham, H. T., Oo, H. Z. and Jing, C., 2013. Stability of slope and seepage analysis in earth dam using numerical finite element model. *Study Civ. Eng. Arch*, 2, pp.104-108.
- Potts, D.M. and Zdravkovic, L., 1999. Finite Element analysis in geotechnical engineering: Theory. Thomas Telford, Great Britain.
- PS, M. A. and Balan, T. A., 2014. Numerical Analysis of Seepage in Embankment Dams. *IOSR Journal of Mechanical and Civil Engineering (IOSR-JMCE)* e-ISSN: 2278-1684, p-ISSN: 2320-334X, pp.13-23.
- Punima, B.C., 1981. *Introductory irrigation engineering*. Standard Publishers Distributors, Nai Sarak, Delhi.
- Punmia B. C. and Lal P. B. B., 1992. *Irrigation and Water Power Engineering*. 12th Ed. J. udpur India. Laxmi Publications (P) Ltd.
- Qizhi, H., Zhou, L., Guihong, S. and Xinshan, Z., 2017. The Stability Analysis of Foundation Pit Under Seepage State Based on Plaxis Software. In *Proceedings of the 2nd Czech-China Scientific Conference 2016*, pp.346-356. IntechOpen.
- Reddi, L. N., 2003. *Seepage in soils: principles and applications*. John Wiley & Sons.
- Rezk, M. A. E. R. M., & Senoon, A. E. A. A. A. (2011). Analytical solution of seepage through earth dam with an internal core. *Alexandria Engineering Journal*, 50(1), pp.111-115.
- Rice, J.D., 2007. *Summaries of Case Histories"*, Chapter (3). scholar.lib.vt.edu/theses/available/etd.12102007.../ Chapter 3.pdf
- Rinaldi, M., Casagli, N., Dapporto, S. and Gargini, A., 2004. Monitoring and modelling of pore water pressure changes and riverbank stability during flow events. *Earth Surface Processes and Landforms*, 29(2), pp.237-254.
- Romanov, D., Gabrovšek, F. and Dreybrodt, W., 2003. Dam sites in soluble rocks: a model of increasing leakage by dissolutional widening of fractures beneath a dam. *Engineering Geology*, 70(1-2), pp.17-35.
- Rushton, K.R. and Redshaw, S. C., 1979. *Seepage and Groundwater Flow-Numerical analysis by analog and digital methods*. John Wiley and Sons.
- Sachpazis, C. I., 2014. Experimental Conceptualisation of the Flow Net system construction inside the body of homogeneous Earth Embankment Dams. *The Electronic Journal of Geotechnical Engineering*, 19, Bund. J, pp.2113-2136.
- Salih, N.B., 2013. *Stability of dams constructed on problematic substrates* (Doctoral dissertation, Brunel University School of Engineering and Design).

- Sazzed, M., Roy, M. and Rahman, S., 2015. FEM Based Seepage Analysis through Earth Dam. *International Journal of Advanced Structures and Geotechnical Engineering*, ISSN 2319-5347, 4(3), pp.158-164.
- Schafferank, F., 1917. Über die Standicherheit durchlaessiger geschuetteter Dämme, Allge, Eauzeitung.
- Schanz, T., 1998. Zur modellierung des mechanischen verhaltens von reibungsmaterialen, habilitation. *Stuttgart Universität, Stuttgart, Germany*.
- Schanz, T. and Vermeer, P. A., 1998. On the stiffness of sands. *Géotechnique*, 48, pp.383-387.
- Schanz, T., Vermeer, P. A. and Bonnier, P. G., 1999. The hardening soil model: formulation and verification. *Beyond 2000 in computational geotechnics*, pp.281-296.
- Selim, M.A., 1947. Dams on Porous Media. *Transaction ASCE*, (1).
- Shafiei, A., Dusseault, M.B. and Baghdardokht, Z., 2008, January. Geotechnical properties of soluble rocks from a dam site in Iran. In *The 42nd US Rock Mechanics Symposium (USRMS)*. American Rock Mechanics Association.
- Shen, J., & Karakus, M., 2013. Three-dimensional numerical analysis for rock slope stability using shear strength reduction method. *Canadian geotechnical journal*, 51(2), pp.164-172.
- Sherard, J. L., Woodward, R. J., Gizienski, S. F. and Clevenger, W. A., 1963. Earth and Earth-Rock Dams. *John Wiley. Hoboken. N. J.*
- Shivamanth, A., Athani, S. S., Desai, M. K. and Dodagoudar, G. R., 2015. Stability Analysis of Dyke Using Limit Equilibrium and Finite Element Methods. *Aquatic Procedia*, 4, pp.884-891.
- Siddappa, G., Hariprasad, K. S., & Ojha, C. S. P. (2007). Transient seepage analysis of an earth dam: sensitivity to anisotropy and soil properties. *Water and Energy Abstracts*, 16(3), pp.28-28.
- SIGIR, 2007. Relief and Reconstruction Funded Work at Mosul Dam, Mosul-Iraq. Special Inspector General for Iraq Reconstruction. [Online]. Available at: <http://www.sigir.mil/files/assessments/PA-07-105>.
- Singh, A.K., 2008. Analysis of flow in a horizontal toe filter. *International Association for Computer Methods and Advances in Geomechanics (IACMAG)*, pp.2449-2455.
- Singh, B. and Varshney, R. S., 1995. Engineering for embankment dams. *A. A. Balkema*. 745, p.745.

- Sloan, S. W., 1981. *Numerical analysis of incompressible and plastic solids using finite elements* (Doctoral dissertation, University of Cambridge).
- Sloan, S. W. and Randolph, M. F., 1982. Numerical prediction of collapse loads using finite element methods. *International Journal for Numerical and Analytical Methods in Geomechanics*, 6(1), pp.47-76.
- Spencer, E., 1967. A method of analysis of the stability of embankments assuming parallel inter-slice forces. *Geotechnique*, 17(1), pp.11-26.
- Stark, T. D. and Eid, H. T., 1998. Performance of three-dimensional slope stability methods in practice. *Journal of Geotechnical and Geoenvironmental engineering*, 124(11), pp.1049-1060.
- Stello, M. W., 1987. Seepage charts for homogeneous and zoned embankments. *Journal of geotechnical engineering*, 113(9), pp.996-1012.
- Styles, P., McGrath, R., Thomas, E. and Cassidy, N. J., 2005. The use of microgravity for cavity characterization in karstic terrains. *Quarterly Journal of Engineering Geology and Hydrogeology*, 38(2), pp.155-169.
- Subuh, M. A. A., 2002. *Finite Element Solution for Unconfined Seepage Problem with Reference to Al-Qadisiya Dam* (M. Sc. Thesis, College of Engineering, Babylon University).
- Sun, S. W., Wang, W. and Zhao, F., 2014. Three-dimensional stability analysis of a homogeneous slope reinforced with micropiles. *Mathematical Problems in Engineering*, 2014, Article ID 864017, pp.1-11.
- Tahmasebipoor, A., Noorzad, R., Shooshpasha, E. and Barari, A., 2012. A parametric study of stability of geotextile-reinforced soil above an underground cavity. *Arabian Journal of Geosciences*, 5(3), pp.449-456.
- Terzaghi, K. and Peck, R. B., 1967. *Soil Mechanics in Engineering Practice*, Second Edition, John Wiley & Sons. Inc., New York.
- Terzaghi, K., Peck, R. B. and Mesri, G., 1996. *Soil mechanics in engineering practice*. John Wiley & Sons.
- Toromanovic, J., Mattsson, H., Knutsson, S. and Sipola, J., 2016. Effects on an earth and rockfill dam undergoing dam safety measures. In *Nordic Geotechnical Meeting: Challenges in Nordic Geotechnics*, pp.747-756.

- Tran, T. X., 2002. Numerical analysis of an earthfill dam in staged construction on soft subsoil. In *Proc. Of the XXVIII International Scientific Conference Bratislava, Slovak Republic* (pp. 280-285).
- Tran, X. T., 2004. *Stability Problems of an Earthfill Dam in Rapid Drawdown Condition*. (Doctoral dissertation, Slovak University of Technology).
- U.S. Army Corps of Engineers., 2003. Slope Stability. Manual, EM 1110- 2-1902, Chapter 2.; Design Considerations.
- Ugai, K. and Leshchinsky, D. O. V., 1995. Three-dimensional limit equilibrium and finite element analyses: a comparison of results. *Soils and foundations*, 35(4), pp.1-7.
- ULDC, 2012. Urban Levee Design Criteria, *Engineering criteria and guidance for the design*, California Department of Water Resources.
- Uromeihy, A. and Barzegari, G., 2007. Evaluation and treatment of seepage problems at Chapar-Abad Dam, Iran. *Engineering Geology*, 91(2-4), pp.219-228.
- USACE, 2003. *Slope Stability*. Engineering Manual 1110-2-1902, Department of the Army, Corps of Engineers, Washington DC, United States of America, available at [www.usace.army.mil/inet/usacoe-docs/eng-manuals/em1110-2-1902/entire](http://www.usace.army.mil/inet/usacoe-docs/eng-manuals/em1110-2-1902/entire).
- USBR, 2011. United State Department of interior Bureau of Reclamation. *Design Standard DS-13(4), Embankment Dams, Static Stability Analysis*, Chapter (4).
- Vandenberge, D. R., 2014. Total stress rapid drawdown analysis of the Pilarcitos Dam failure using the finite element method. *Frontiers of Structural and Civil Engineering*, 8(2), pp.115-123.
- Varshney, R. S., 1973. Theory and Design of Irrigation Structures: Volume II Hydro-Power Structures. NEM Chand & Bros.
- Vick, S. G., 1983. *Planning, design, and analysis of tailings dams*. New York: Wiley.
- Vogelaar, B. B., 2001. *Cavity Detection* (M.Sc. Thesis, Earth Sciences Department, Utrecht University, Netherlands).
- Wang, M. C. and Badie, A., 1985. Effect of underground void on foundation stability. *Journal of Geotechnical Engineering*, 111(8), pp.1008-1019.
- Wang, M.C. and Baus, R.L., 1980, April. Settlement behavior of footing above a void. In *Proceedings of the 2nd conference on ground movement and structures*. Cardiff, UK (pp. 68-184).

- Wei, S., Hang, L. and Wei, R., 2011. FLAC3D in geotechnical engineering. Beijing: China Water Power Press.
- Wei, W., 2008. *Three-dimensional slope stability analysis and failure mechanism* (Doctoral dissertation, The Hong Kong Polytechnic University).
- Wei, W. B., Cheng, Y. M. and Li, L., 2009. Three-dimensional slope failure analysis by the strength reduction and limit equilibrium methods. *Computers and geotechnics*, 36(1-2), pp.70-80.
- Whitman, R.V. and Bailey, W.A., 1967. Use of computers for slope stability analysis. *Journal of Soil Mechanics & Foundations Div*, 93(SM4), pp.475-498.
- Wines, D., 2016. A comparison of slope stability analyses in two and three dimensions. *Journal of the Southern African Institute of Mining and Metallurgy*, 116(5), pp.399-406.
- Xu, S. J., Dang, F. N., Han, Q. and Cheng, S. Z., 2009. Analysis of stability of dam slope during rapid drawdown of reservoir water level. In *2009 International Conference on Engineering Computation* (pp. 221-224). IEEE.
- Yang, Q., Zhang, J., Xiong, Z. and Yang, H., 2010. Seepage field control system for Shuibuya concrete faced rock-fill dam. *Shuili Fadian Xuebao(Journal of Hydroelectric Engineering)*, 29(3), pp.164-169.
- Yanmaz, A.M. and Gunindi, M.E., 2008. Assessment of overtopping reliability and benefits of a flood detention dam. *Canadian Journal of Civil Engineering*, 35(10), pp.1177-1182.
- Yilmaz, I., 2001. Gypsum/anhydrite: some engineering problems. *Bulletin of Engineering Geology and the Environment*, 60(3), pp.227-230.
- Zaynal, M. S., 2004. DETECTION OF SUBSURFACE CAVITIES BY THE ELECTROMAGNETIC METHOD (Case Study at Haditha Area). *Bulletin of the Iraq Natural History Museum (P-ISSN: 1017-8678, E-ISSN: 2311-9799)*, 10(2), pp.79-89.
- Zebarjadi Dana, H., Khaloo Kakaie, R., Rafiee, R. and Yarahmadi Bafghi, A. R., 2018. Effects of geometrical and geomechanical properties on slope stability of open-pit mines using 2D and 3D finite difference methods. *Journal of Mining and Environment*, 9(4), pp.941-957.
- Zeidan, B. A., 1993. *A Numerical (FEM) Study of the Effect of Anisotropy on Phreatic Seepage Flows* (Doctoral dissertation, Civil Engineering Department, Indian Institute of Technology IIT, Powai, Bombay, India).

- Zeidana, B., Shahiena, M., Elshemya, M. and Kirraa, M.S., 2017. Combined Seepage and Slope Stability Analysis of Failed Earthen Dams. *Annual Meeting Prague, Czech Republic of International Commission on Large Dams*.
- Zhan, T. L., Zhang, W. J. and Chen, Y. M., 2006. Influence of reservoir level change on slope stability of a silty soil bank. In *Unsaturated Soils 2006* (pp. 463-472).
- Zhang G. C. (2005). The researches on the influence of the fluctuation of water level on landslide stability. China University of Geosciences, Wuhan.
- Zhang, J. F., Meng, X. Y. and Zhu, E. Q., 2004. Testing study on landslide of layered slope induced by fluctuation of water level. *Chinese Journal of Rock Mechanics and Engineering*, 23(16), pp.2676-2680.
- Zhang, J., Li, Z. and Qi, T., 2005. Q mechanism analysis of landslide of a layered slope induced by drawdown of water level. *Science in China Series E Engineering & Materials Science*, 48(1), pp.136-145.
- Zheng, H., Liu, D.F., Lee, C.F. and Tham, L.G.2005. A new formulation of Signorini's type for seepage problems with free surfaces. *International Journal for Numerical Methods in Engineering*, 64(1), pp.1-16.
- Zheng, K., Ping, C. A. O., Liu, Z. Y., Hu, H. H. and Gong, D. P., 2011. Simulation analysis on three-dimensional slope failure under different conditions. *Transactions of Nonferrous Metals Society of China*, 21(11), pp.2490-2502.
- Zheng, Y. R., Zhao, S. Y., Kong, W. X. and Deng, C. J., 2005. Geotechnical engineering limit analysis using finite element method. *Yantu Lixue(Rock Soil Mech.)*, 26(1), pp.163-168.
- Zheng, Y. R., Zhao, S. Y., & Song, Y. K. (2005). Advance of study on the strength reduction finite element method [J]. *Journal of Logistical Engineering University*, 3, 1-6
- Zhonghua, X. and Weidong, W., 2010. Deformation Control Criteria of Deep Excavations [J]. *Chinese Journal of Underground Space and Engineering*, 3.
- Zhu, D.Y., Lee, C.F. and Jiang, H.D., 2003. Generalised framework of limit equilibrium methods for slope stability analysis. *Geotechnique*, 53(4), pp.377-395.
- Zienkiewicz, O.C., Humpheson, C. and Lewis, R.W., 1975. Associated and non-associated visco-plasticity and plasticity in soil mechanics. *Geotechnique*, 25(4), pp.671-689.
- Zienkiewicz, O.C., Taylor, R.L., Nithiarasu, P. and Zhu, J.Z., 1977. *The finite element method* (Vol. 3). London: McGraw-hill.

## Appendix A: Model Setup with PLAXIS 2D

This appendix depicts the exemplary steps followed in setting up and analysing the stability of a reservoir dam during rapid drawdown condition with PLAXIS 2D software.

The height of dam to be considered is 15 m with slope 1V: 2.5H for both the upstream and downstream sides, the width of dam is 130 m at the base with crest width of 6 m. The earth dam placed on subsoil was about 20 m depth. The normal water level at the reservoir dam is 12 m high, and in sub-soil of the dam is 6 m beneath the ground surface. The geometry of the dam is described in Figure 1.

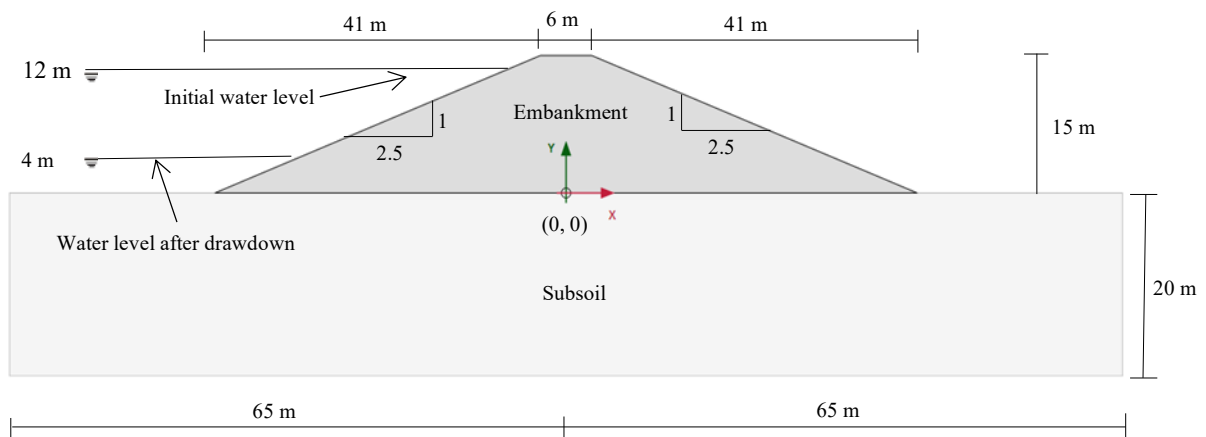


Figure 1: Geometry of the earth dam model

### 1. Input Geometry

**2D** Double click *Input Program* and select *Start a new project* from the quick select window. See Figure 2.

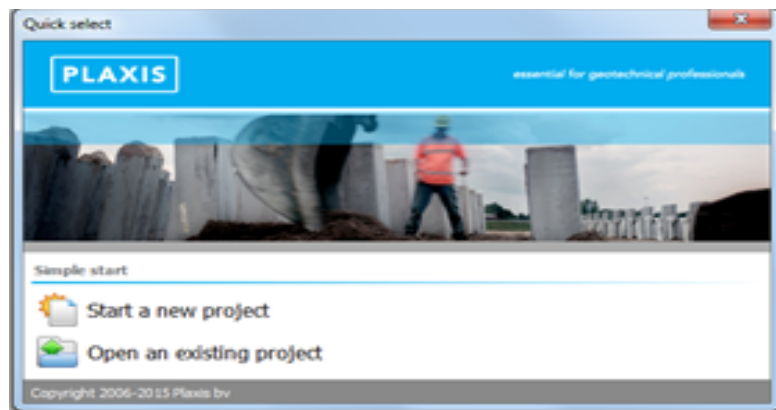


Figure 2: The input program 2D PLAXIS window



- In *Project properties* window click *Model* tabsheet.
- Select the units of parameters and enter the model dimensions, x min = -65 m, x max = 65 m, y min = -20 m and y max = 20 m.
- Click OK to close the Project properties window, as shown in Figure 3.

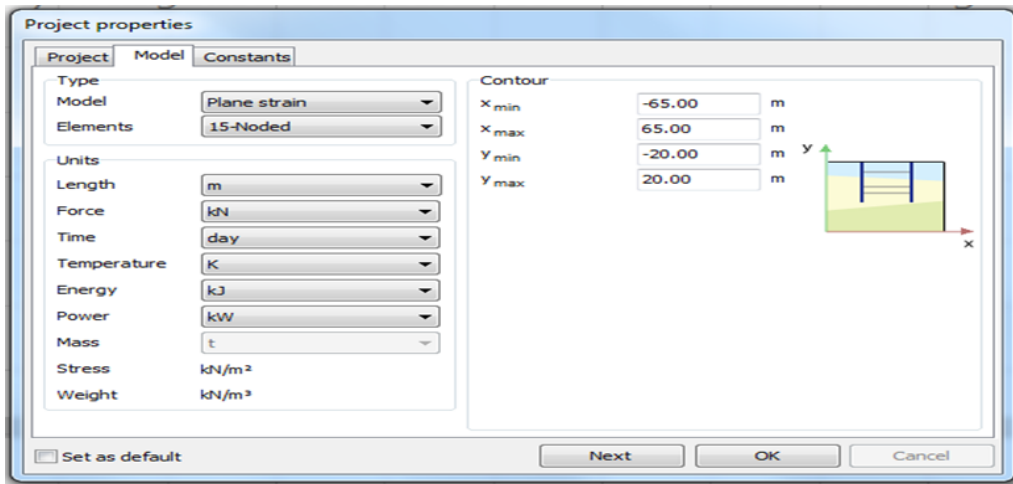



Figure 3: The project properties window

## 2. Definition of Soil

- To define the sub-soil of model:  
 Click *Create a borehole* button in side of toolbar at x = 0, The Modify soil layers window appears.
- Click *Add* button to add a soil layer beginning from ground surface to the depth of (y= -20.0). See Figure 4.

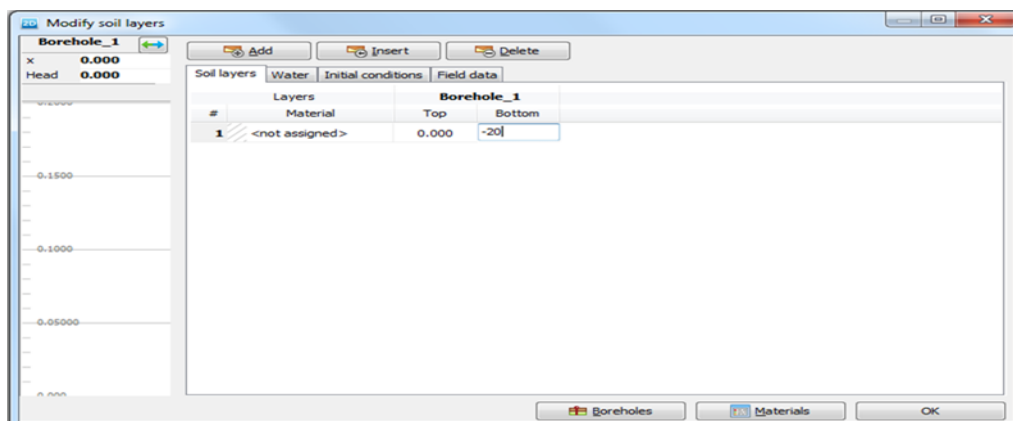


Figure 4: The modify soil layers window

- Click *Materials* button in the bottom of Modify soil layers window to set the properties of soil. The *Materials sets* window appears.
- Click *New* button to set material properties of sub-soil, as shown in Figure 5.

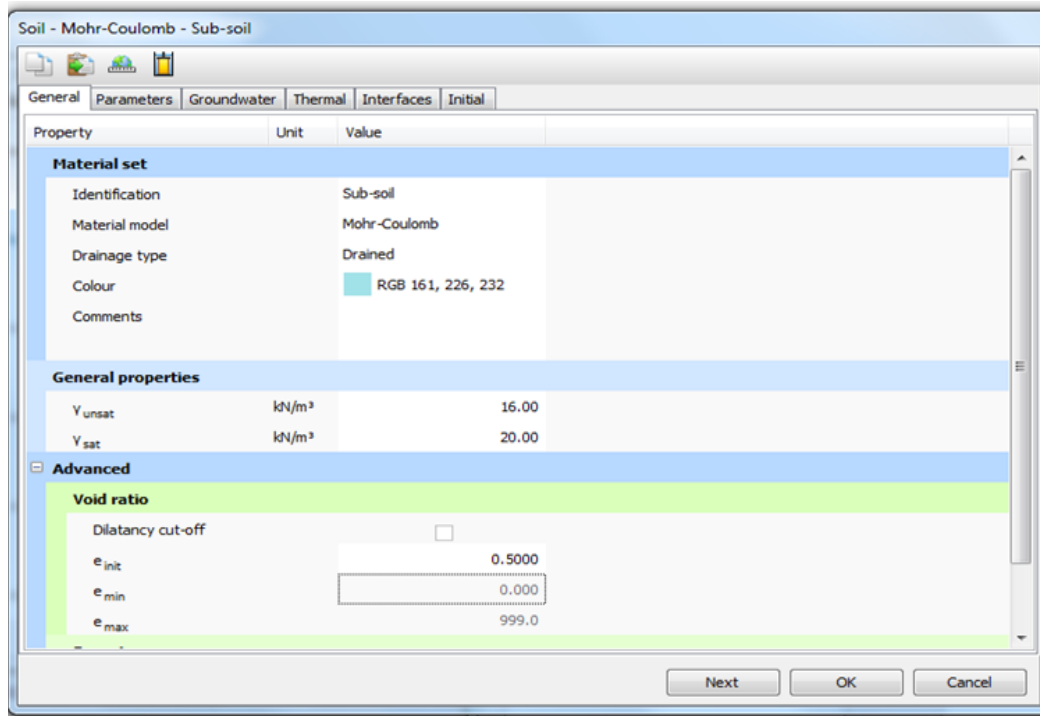


Figure 5: The material sets window

- Proceed to the *Structure* mode.
- Select *Create soil polygon* to define the embankment by assigning points located at (-41.0, 0.0), (41.0, 0.0), (3.0, 15.0) and (-3.0, 15.0). See Figure 6.
- Click *Materials* button in the side of Structure mode to set the properties of embankment.

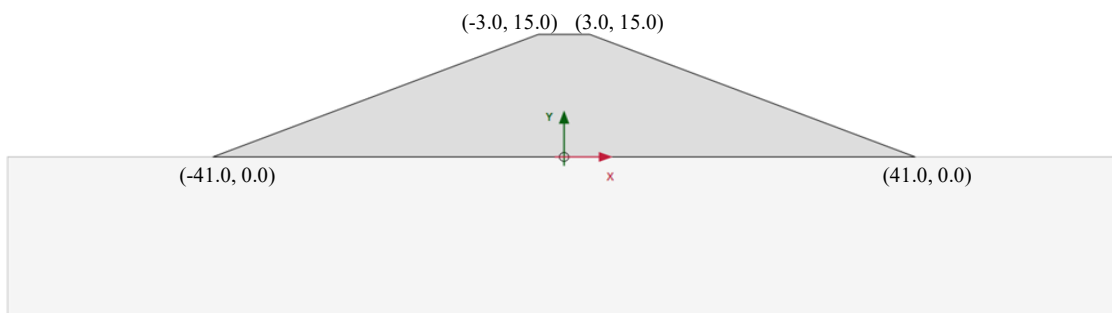


Figure 6: Embankment of earth dam model

### 3. Mesh Creation

- Select the *Mesh* mode.
- 🔍 Create the mesh, the *Mesh options* window pops up and choose Fine option for Element distribution. Click OK.
- 🔍 Click *View mesh* to display the mesh. See Figure 7.
- Close the Output program by clicking on the *Close* tabsheet.

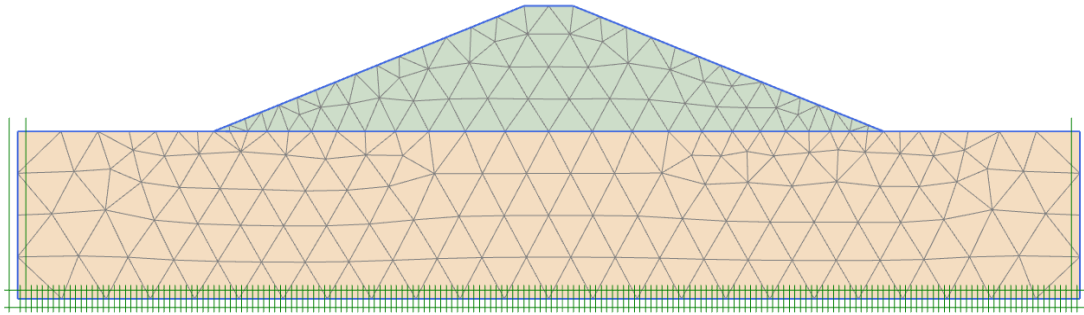


Figure 7: Finite element mesh



### 4. Calculation

In addition to the initial phase, the calculations involve seven phases. In the initial phase, the water pressure distribution is computed utilizing a steady-state groundwater flow calculation. The first and second phases begin from the initial phase (i.e. reservoir water level at 15 m) and the water level is brought down to 4 m. A distinction is made in the time interval at which it is made (i.e. various velocities of water level lowering; rapid drawdown and slow drawdown). In these phases, a coupled flow – deformation calculation is used for calculating the distribution of water pressure. The third phase considers long term behaviour of dam at low water level (i.e. of upstream water level of 4 m), as well this phase starts from the initial phase. In this phase, a steady-state groundwater flow calculation is deemed to compute the distribution of water pressure.

Lastly, the factor of safety is calculated for all water pressure conditions by shear strength reduction method. PLAXIS 2D code is considered the following cases to conduct the safety calculations.

1. Long term situation with high water level at 12 m (steady state).
  2. Water level drops quickly during 5 days.
  3. Water level drops slowly during 50 days.
  4. Long term situation with low water level at 5 m (steady state).
- Moved to Flow condition mode.

**Initial Phase:**

- In the *Phases explorer* double click *Initial phase*. The Phases windows appears.
-  Choose the *Gravity loading* for Calculation type.
-  Choose the *Steady state groundwater flow* option as Pore pressure calculation type. Click OK to close the Phases windows. See Figures 8.

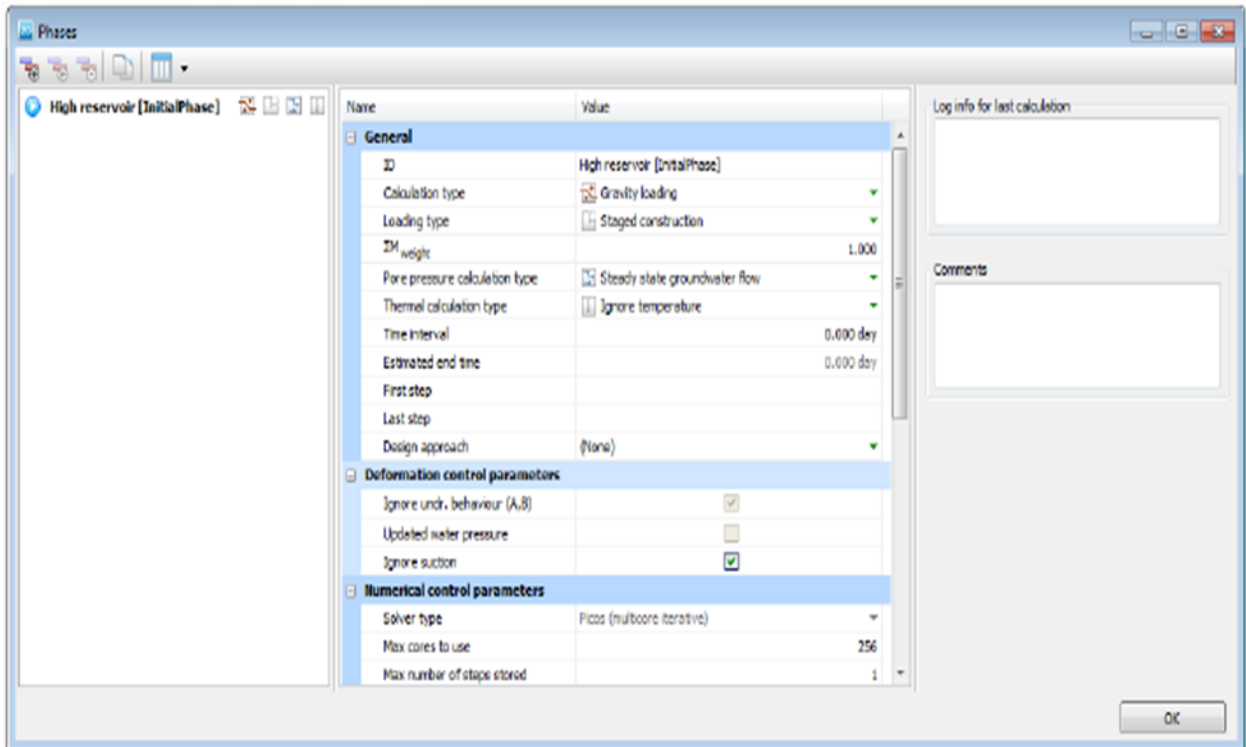



Figure 8: The phases window

-  Click *Create water level* to define the water level identical to the water level in the reservoir before to the drawdown. The water level starts at the left side at a level of 12 m above the ground surface (-68.0, 12.0) m; the second point is in the embankment at a level of 2 m, (-8.0, 12.0) m; the third point is in sub-soil at a level of 6 m below the ground surface (41.0, -6.0) m and the fourth point outside the right boundary (68.0, -6.0) m, as displayed in Figure 9.
- Right-click the generated water level and choose the ***Make global option*** in the appearing list.

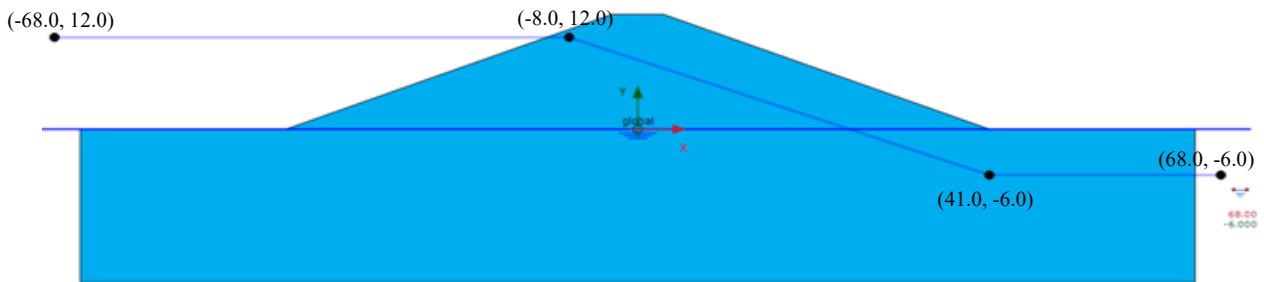


Figure 9: High water level

- In the *Model explorer* extend the **Attributes library**.
- Extend the *Water levels* subtree. The water levels formed in the *Flow conditions mode* are gathered under *User water levels*.
- Extend the *User water levels subtree*. The created water level will appear as '*UserWaterLevel\_1*'. Figure 10 shows the site of the water levels in Model explorer.

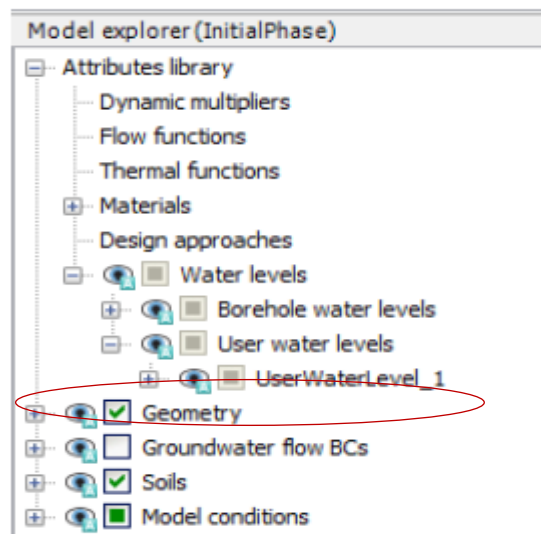


Figure 10: The site of the water levels in Model explorer

- Rename the generated water level as '*FullReservoir\_Steady*' by double clicking on it. Right click on '*UserWaterLevel\_1*' rename as '*FullReservoir\_Steady*'.
- Extend the *Model conditions* subtree.
- Extend the *Ground WaterFlow* subtree. Notice that the boundary at the down of the model must be closed, as showing in the Figure 11.

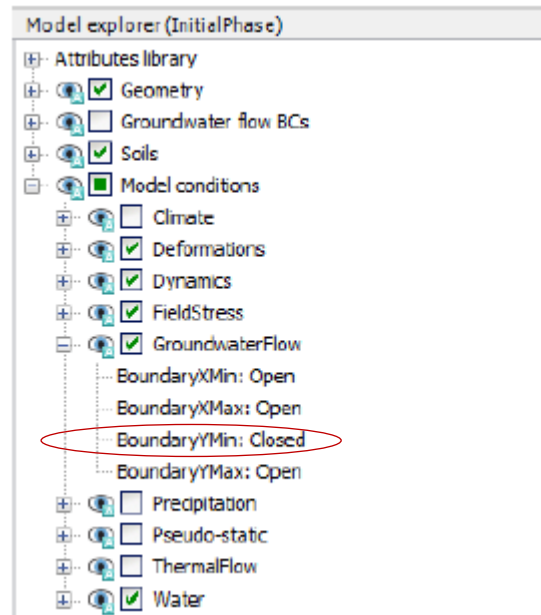




Figure 11: Ground WaterFlow boundary condition.

### Rapid Drawdown Phase:

- In the *Phases explorer* click  button to add a new phase.
- Double-click on the new phase 'Phase\_1'. The Phases window is exhibited.
- Expand the *General subtree*, rename the new phase as (e.g. Rapid drawdown). Notice that the Rapid drawdown phase starts from *High reservoir* phase which is automatically chosen from phase drop-down list.
-  Specify the *Fully coupled flow-deformation* option as calculation type.
- Appoint the value of *Time interval* parameter of 5 days.
- Make certain that the *Reset displacements to zero* and *Reset small strain* options are specified in the *Deformation control parameters* subtree. Then close the Phases window by clicking OK.
- In order to create a copy of water level.
- Right-click on *FullReservoir Steady* in Model explorer and specify the *Duplicate* option in the appearing list. See Figure 12.
- Double-click on the new water level to rename it as '*FullReservoir\_Rapid*'.

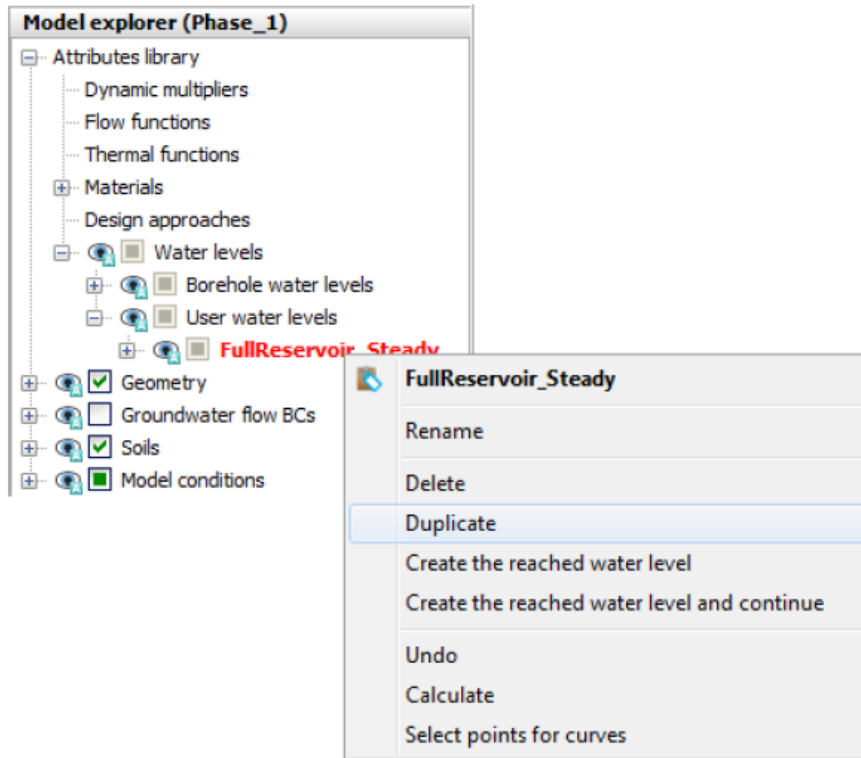


Figure 12: Duplication water levels in model explorer

The behaviour of the water levels is described by defining *Flow functions* as following: Notice that *Flow functions* are global entities and are obtainable from the *Attributes library* in Model explorer.

- Right-click on the *Flow functions* option and choose the *Edit option* in the appearing list. The Flow functions window is shown.
- Click **+** in the *Head functions* tabsheet to add a new function. The options of defining the new function are exhibited. The Flow functions appears.
- Assign an appropriate name to the function (e.g. Rapid).
- Specify the *Linear option* from the Signal drop-down list.
- Select a time interval of 5 days. Select a time of 5 days.
- Specify the value of head decrease ( **$\Delta$  Head**) of -8 m. See Figure 13.

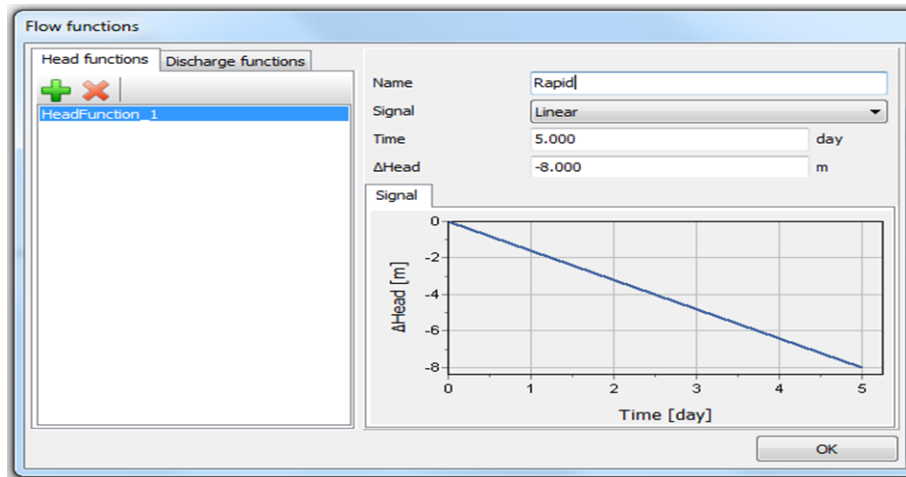


Figure 13: The flow function of rapid drawdown condition

- Shut the *Flow functions* window by clicking OK.
- In the Model explorer right-click on FullReservoir Rapid then specify the *Use as global phreatic level* option in the appearing list.
- Extend the *FullReservoir Rapid subtree* then choose the *WaterSegment* in the upstream shoulder.
- Extend the subtree of the specified segment and choose the *Time dependent* option for the *Time dependency* parameter.
- Assign the *Rapid option* for the *Head function* parameter. Figure 14 presents the chosen water segment in Model explorer.

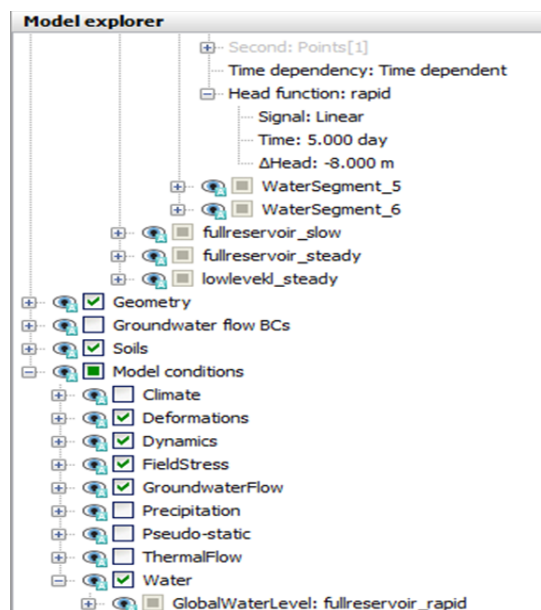


Figure 14: Properties of the water segment



- Make sure that the new water level (*FullReservoir\_Rapid*) is appointed to *Global WaterLevel* in the Water subtree beneath the Model conditions in the Model explorer. Figure 15 shows the arranging of the rapid drawdown phase.

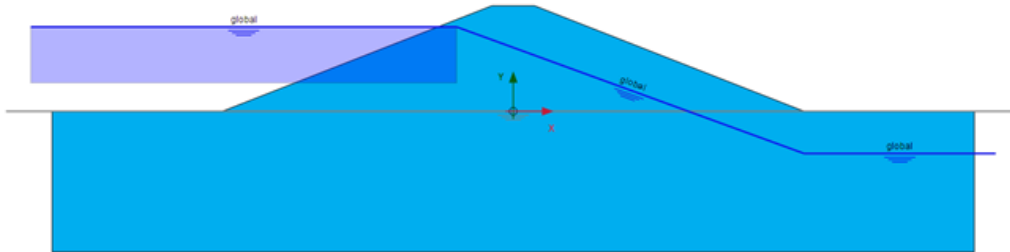



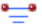


Figure 15: Arranging of the rapid drawdown phase.

### Slow Drawdown Phase:

To create the slow drawdown phase, reapply the previous steps which are followed at above for creating the Rapid drawdown phase. Note that the Time Interval must be changed from 5 days to 50 days.

### Low Level

- Specify the *High reservoir phase* in the Phases explorer.
- Click  to add a new calculation phase.
- Double click on the new phase. The Phases window is shown.
- In the *General subtree*, rename the phase as (*Low level*). Note that the Low-level phase starts from high reservoir phase which is automatically chosen from phase parameter.
-  Select the *Plastic* option as calculation type.
-  Select the *Steady state groundwater flow* option as Pore pressure calculation type.
- In the *Deformation control subtree*, specify *Ignore und. Behaviour (A, B)* and make certain that the *Reset displacements to zero* and *Reset small strain* options are chosen. Then close the Phases window by clicking OK.
-  Define the level of water identical to the water level in the reservoir after to the drawdown. The water level starts at the left side at a level of 12 m above the ground surface (-68.0, 4.0); the second point is in the embankment at a level of 12 m (-28.0, 4.0); the third point is in sub-soil at a level of 6 m below the ground surface (41.0, -6.0) and the fourth point outside the right boundary (68.0, -6.0), as displayed in Figure 16.
- Change the name of new created water level to '*LowLevel\_Steady*'.

- Right click on (*LowLevelL\_ Steady*) in order to assign as *Global WaterLevel*.

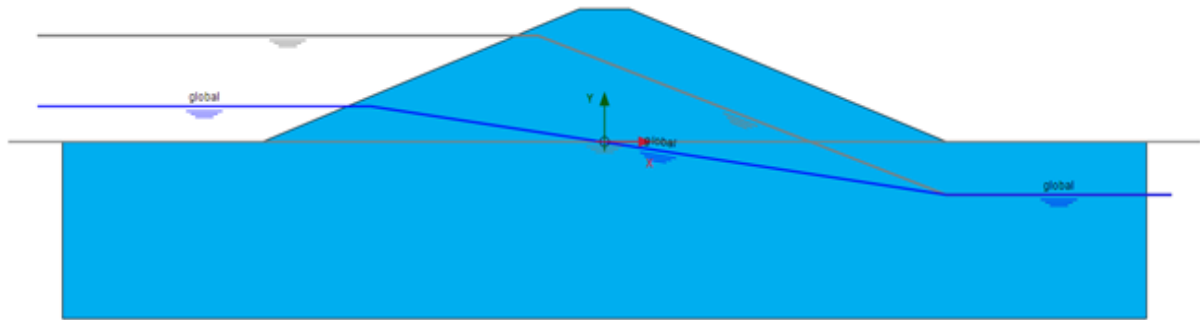




Figure 16: Low level phase

### Stability Calculations

- Specify the one of the phases in the *Phases explorer*.
- Click  to add a new phase.
- Double click on the new phase.
-  Assign *Safety* as *Calculation type*.
- In the *Deformation control* subtree, set Reset displacements to zero.
- In the *Numerical control* parameters subtree select the Max steps parameter to 30 or Phase 4 and to 50 for phases 5 to 7. Figure 17 displays the ultimate view of Phases explorer.

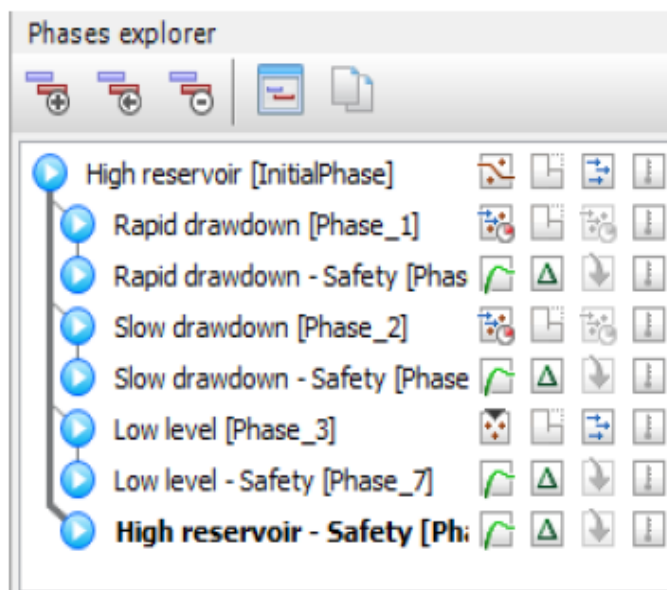






Figure 17: The ultimate view of Phases explorer





- Move to the *Staged construction* mode.
-  Set nodes located at the crest (-3.0, 15.0) and at the toe of the dam (-41.0 0.0).
- Click *Update* tabsheet to close output program.
-  Click *Calculate* button in the side toolbar to start the calculations.
-  Save the project.

## Results

-  Click in the side toolbar to view the results after the calculation process has completed.

## 5. Set up the cavity

The steps followed in setting up a cavity with PLAXIS 2D software are as following:

-  Click the Create tunnel button in the *Structures* mode and click in the area of drawing to assign the tunnel's location. The window of *Tunnel designer* appears.
  - Keep the default option in the **General** tabsheet.
  - Click on the Segments tab.
-  In the side toolbar, click the Add button.
-  Set the type of Segment in the box of segment info. Specify the radius and angle of the segment.
-  Chose the option of Extend to symmetry axis to complete the other half of the tunnel.
  - To complete the tunnel, click the Symmetric close button.
  - To update the tunnel, click on Generate and click Close.

## Appendix B: Training Courses

Date	Title of training course/module/conference	Key learning point
12-Oct-2016	Completing a Learning Agreement & the PhD	This session outlines the progression points that occur during your studies outlines the importance of the Learning Agreement and where it fits within the broader PhD lifecycle.
25-Oct-2016	Intro to Endnote X7	Endnote X7 is a useful bibliographic tool which can be used to manage all your references.
16-Nov-2016	PowerPoint-Creating Academic Posters	Learn how to create high impact academic poster presentation using PowerPoint
13-Dec-2016	PowerPoint: Enhancing your Presentations	This workshop examines PowerPoint features that can be used to further develop PowerPoint presentations.
9-Feb-2017	Doing a Literature Review	This session is designed to help you get started with your Literature Review, it explains what it is and what it is not, where and how to start looking for information, and how to evaluate what you find.
4-May-2017	Presenting at Academic Conferences	This workshop provides an introduction to presenting at academic conferences.
29/6/2017	Excel: Analysing Data	This course is for students with some knowledge of Excel. It's for those who would like to be able to analyse data in existing spreadsheets.